PSYCHOPHYSICAL INVESTIGATIONS OF HUMAN PERIPHERAL VISION

KEZIAH JANE CAMERON LATHAM

Doctor of Philosophy

THE UNIVERSITY OF ASTON IN BIRMINGHAM

January 1995

The University of Aston in Birmingham

Psychophysical Investigations of Human Peripheral Vision

Keziah Jane Cameron Latham
Doctor of Philosophy
1995

Summary

This thesis investigates various aspects of peripheral vision, which is known not to be as acute as vision at the point of fixation. Differences between foveal and peripheral vision are generally thought to be of a quantitative rather than a qualitative nature. However, the rate of decline in sensitivity between foveal and peripheral vision is known to be task dependent, and the mechanisms underlying the differences are not yet well understood.

Several experiments described here have employed a psychophysical technique referred to as 'spatial scaling'. Thresholds are determined at several eccentricities for ranges of stimuli which are magnified versions of one another. Using this methodology a parameter called the E_2 value is determined, which defines the eccentricity at which stimulus size must double in order to maintain performance equivalent to that at the fovea.

Experiments of this type have evaluated the eccentricity dependencies of detection tasks (kinetic and static presentation of a differential light stimulus), resolution tasks (bar orientation discrimination in the presence of flanking stimuli, word recognition and reading performance), and relative localisation tasks (curvature detection and discrimination). Most tasks could be made equal across the visual field by appropriate magnification. E_2 values are found to vary widely dependent on the task, and possible reasons for such variations are discussed.

The dependence of positional acuity thresholds on stimulus eccentricity, separation and spatial scale parameters is also examined. The relevance of each factor in producing 'Weber's law' for position can be determined from the results.

Keywords: eccentricity; magnification; perimetry; resolution; hyperacuity.

Hope for the best
Expect the worst
Do the possible

Buddhist saying

This thesis is dedicated to my parents, for a lifetime of love and support.

Acknowledgements

I would like to express my gratitude to the Engineering and Physical Sciences Research Council (EPSRC; formerly SERC) for making this thesis possible by providing me with funding for a research studentship.

I have had excellent supervision from Dr David Whitaker. He has always been available for discussion and advice, and has taken great interest in the project all the way through, for which I am most grateful.

For several informative discussions I would also like to thank Dr John Wild, Dr Jyrki Rovamo, Dr David Elliott and Dr Neville Drasdo.

Many people have willingly sat as subjects for the experiments in this thesis, and I would particularly like to thank Pia Mäkelä, the elective studies students, the Postgrads and the '109 Grannies'.

Finally, 'thank you's go to Dad for proofreading; all my family for being brill; John for 'odds and ends'; Parky, Ola and Elaine for being good chums when the going got tough; Mike for bearing the brunt of AOK; and *Adrian for locum work and cream* cakes.

Contents

List of Tables

List of Figures

Chapter 1
Introduction

The human visual system is remarkable in its abilities. Despite its contruction of "leather, water and jelly" (Walls, 1942) the eye allows us to observe minute detail, see tiny quantities of light, judge distances and depths with extreme accuracy, and distinguish colours differing only by a few nanometers in wavelength.

When considering the maximum capabilities of the human eye, for photopic vision in particular, the best achievements in visual performance are made at the fovea, the central point of fixation. When a stimulus is moved away from the fovea onto more eccentric retina performance declines, and it appears that peripheral vision is poorer than that at the fovea.

There has been much research examining the extent to which peripheral vision is poorer than that at the fovea. It may be imagined that peripheral vision is qualitatively worse than that at the fovea, due to differences in mechanisms of neural function. Alternatively, the differences between foveal and peripheral vision might be explained by quantitative variations in neural sampling with eccentricity. A critical question, and one which has run throughout the history of research into peripheral vision, is thus whether the differences between foveal and peripheral vision are of qualitative, or quantitative form.

Early workers studying peripheral vision believed foveal and peripheral vision to be qualitatively different. Aubert and Förster (1857) were among the first to observe that visual acuity is highest in central vision, and that sensitivity declines in an orderly manner with increasing eccentricity from the point of fixation. Wertheim (1891, translated 1980) described the fall in sensitivity with eccentricity as being at first very rapid, and then gradually slower from the centre towards the periphery. He reasoned that variation in acuity with eccentricity must be due to anatomical and functional elements of the retina and their distribution.

In 1958, Weymouth plotted his own and Wertheim's acuity data in the form of the minimum angle of resolution, rather than as sensitivity. By describing the data in this way, as a threshold rather than a sensitivity, resolution was seen to vary approximately linearly with eccentricity. In addition to visual acuity, this observation of linearity held for a wide range of pattern discrimination tasks, including vernier, motion, and stereo

thresholds. Weymouth concluded that the regional distribution of ganglion cells was the basis for the linear relationship of resolution thresholds with eccentricity.

The retinal image received by the ganglion cells is mapped onto the striate cortex in a topographical manner. The linear distance along the visual cortex, in millimeters, corresponding to one degree of retinal visual angle is described as the cortical magnification factor, M (Daniel and Whitteridge, 1961). To estimate human values for the cortical magnification factor, it was initially assumed that M was directly proportional to the square root of the density of ganglion cell receptive fields (Drasdo, 1977; Rovamo and Virsu, 1979). Using such values of M, it was argued that visual thresholds could be made equivalent across the visual field by enlarging peripheral stimuli in proportion to 1/M. Thus, peripheral vision was shown to be equivalent to that at the fovea apart from a change of scale, and that a single scale change could account for all threshold variations with eccentricity.

Many visual thresholds obeyed the concept of M-scaling (eg.Virsu, Näsänen and Osmoviita, 1987; Pointer, 1986; see also Chapter 4), but further work began to find many exceptions which could not be M-scaled (eg. Westheimer, 1982; Pointer, 1986; see also Chapter 4), and it became obvious that such a simple model was not tenable. In addition, anatomical findings in monkey suggested that the foveal representation in the cortex was greatly expanded from that at retinal level (Connolly and Van Essen, 1984; Van Essen, Newsome and Maunsell, 1984; Azzopardi and Cowey, 1993). The choice of a particular *a priori* scaling factor from the possibilities provided from anatomy and physiology began to appear somewhat arbitrary.

Taking into account the new anatomical data, Levi, Klein and Aitsebaomo (1985) argued that two gradients were required to describe eccentricity dependent threshold gradients. They suggested that the decline in grating acuity with eccentricity was due to retinal factors, while the somewhat steeper fall in vernier acuity with eccentricity was compatible with the estimates of cortical magnification which showed foveal cortical over-emphasis (Dow, Snyder, Vautin and Bauer, 1981; Van Essen et al., 1984). Alternatively, Drasdo (1989) suggested that failures in M-scaling might be explained by differences in eccentricity gradients of different classes of ganglion cell. The distribution of magnocellular ganglion cells across the retina appears to be more even than that for parvocellular cells, which are concentrated in central retina (Connolly and Van Essen, 1984; Perry and Cowey, 1985). The eccentricity related gradient of the parvocellular system may thus be steeper than that for the magnocellular system. Following this argument, tasks determined by the parvocellular system are predicted to

follow the steeper eccentricity gradient while thresholds for tasks limited by the magnocellular sytem will show less eccentricity dependence.

In the light of such diversity of anatomical M values, and differing opinions as to why M-scaling did or did not work, subsequent methodologies have made no *a priori* assumptions regarding scaling factors on the basis of anatomy or physiology. Such 'spatial scaling' methods (Watson 1987; see also Chapter 4), have shown that, far from all thresholds falling with eccentricity at the same rate, as purported by cortical magnification theory, threshold gradients in peripheral vision vary over a huge range (eg. Whitaker, Mäkelä, Rovamo and Latham, 1992a).

By whatever means eccentricity dependent gradients are derived, a quantitative description of the gradients is required to allow comparison between methodologies and tasks. Throughout this thesis, eccentricity dependent gradients of visual performance will be described quantitatively by the value E_2 (Levi et al., 1985). The E_2 value is defined as the eccentricity, in degrees, at which stimulus size must double in order to maintain performance equivalent to that at the fovea.

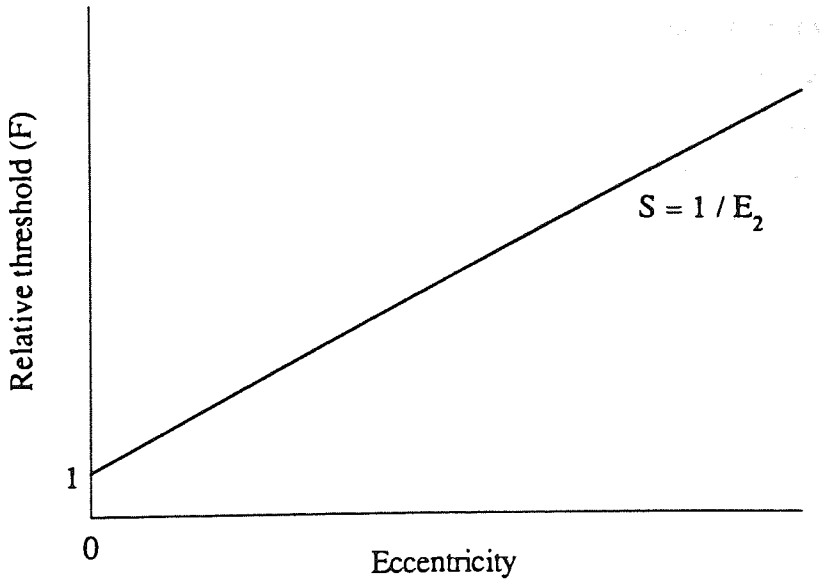

Figure 1.01 shows a linear dependence of some task referenced to its foveal threshold with eccentricity. The linear regression is of the form $F = 1 + E / E_2$.

The graph above (Figure 1.01) shows in schematic form how relative threshold varies with eccentricity (E). The normalised threshold size, or scaling factor (F), depicts

threshold at a peripheral location normalised with reference to the foveal threshold, or can also represent the amount of magnification required to maintain homogeneity at any given peripheral location.

From the definition of E_2: when $F = 2$, $E = E_2$.

Thus, for a linear regression: $2 = 1 + (S \times E_2)$

and, $E_2 = 1 / S$

where S is the gradient of the regression.

Substituting the E_2 value into the equation for the linear regression:

$$F = 1 + E / E_2 \qquad \text{Equation 1.01}$$

The variation in the rate of decline of sensitivity in peripheral vision with different types of stimulus is not surprising from a functional viewpoint. It is easy to understand the benefits of having a peripheral visual system, which, in comparison to the fovea, is devoted much more to movement detection than static positional judgements. Similarly, it makes computational sense to have these fine static judgements concentrated centrally, since these may then be performed optimally via a foveation of the stimulus. However, what is not yet clear are the physiological mechanisms underlying the range of gradients.

Prior studies have shown that for tasks examined using spatial scaling methodologies, foveal and peripheral vision differ by a change of scale, rather than by a change of form. Eccentricity-dependent gradients vary over a huge range of values, and the physiological mechanisms underlying such a large range are not yet well understood. This thesis seeks to further investigate aspects of peripheral visual performance including eccentricity-dependent gradients using spatial scaling methods. The purpose is to gain a better understanding of the mechanisms involved in vision across the visual field, and their regional distributions.

Chapter 2
Visual Thresholds

2.1 Introduction

The limits to vision can be measured in many ways, using a huge range of different visual tasks, each of which has a threshold which is determined on a different physiological basis. Investigation of the visual system using different tasks provides knowledge on how the visual system works. The purpose of this chapter is to introduce the spatial thresholds which are used in this thesis to examine visual function. The term 'threshold' is used throughout to indicate the limit of visual performance, and sensitivity to be the reciprocal of the threshold. A more rigourous explanation of threshold determination is given in Chapter 5.

2.2 Detection

Detection of an object, or the minimum visible, can be described as the ability to distinguish an object from its background. Whilst detection is essentially a light difference discrimination, or brightness threshold, it can be expressed in spatial terms by manipulating contrast through varying the spatial dimensions of the stimulus. However, detection is not in essence a visual acuity, since no spatial differentiations are required in the task.

When the background is dark, the minimum amount of light needed to detect the presence of an object is termed the absolute threshold. In order for it to be observed, the light from the object must exceed the inherent noise in the visual system, and under optimum conditions a light can be observed if as few as 5 quanta fall on the retina (Hecht, Schlaer and Pirenne, 1942).

Detection of a thin line on a uniform background can be expressed in spatial terms by varying the width of the line (Figure 2.01). The image of a narrow line on the retina is spread by the optics of the eye to form a line spread function (Campbell and Gubisch, 1966) which has a width at half height of approximately 1 min arc. If the line is narrower than 1 min arc, its retinal image will have the shape of this line spread function. Variations in line width will manifest as variations in local contrast on the retina, and threshold will be reached when the local brightness difference (ΔI) reaches threshold, shown as the dotted line in Fig 2.01. For a small line (a), the local luminance change is too small to be detectable. A thicker line (b) reduces local luminance to threshold value and will just be detected. The thickest line (c) is clearly suprathreshold. Hecht and Mintz (1939) showed that under ideal conditions a line of

width 0.5 sec arc can be detected. This is equivalent to observing a 1 cm thick telegraph wire at a distance of over 4 km. They then calculated that detection is possible when the light intensity distribution in the retinal image has a dip in its value of less than 1%.

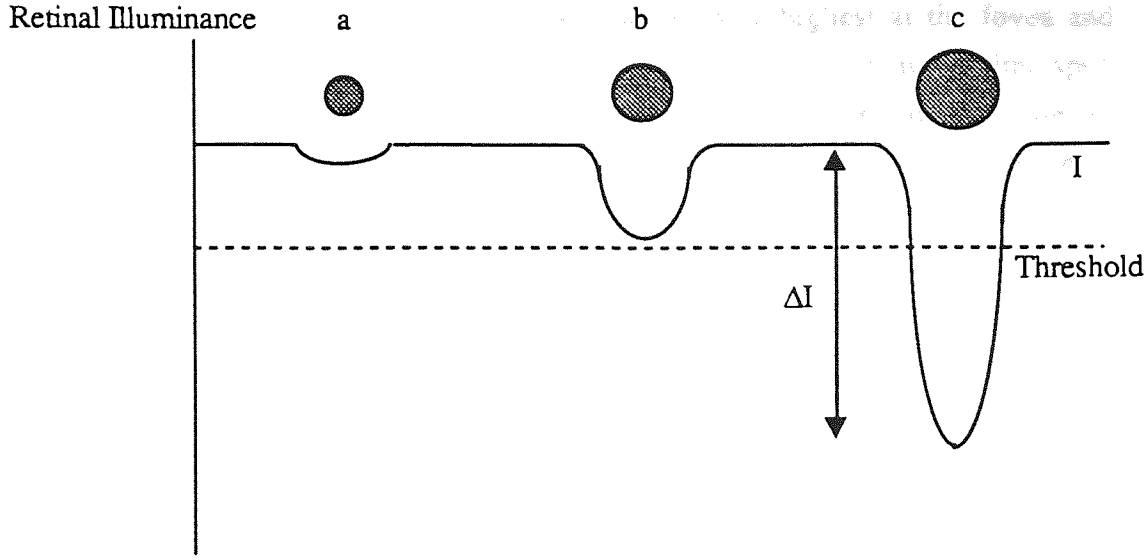

Figure 2.01. Retinal illuminance profiles for three lines of varying thickness, a-c. The dashed line represents the threshold illuminance at which change is detectable. For the small line (a), the local luminance change is too small to be detectable. The thicker line (b) reduces local luminance to threshold value and will just be detected. The thickest line (c) is clearly suprathreshold.

The threshold value of ΔI is dependent on the background luminance upon which a target is presented. The smallest intensity difference (ΔI) which can be detected is directly proportional to the background luminance (I). The units of I are cdm^{-2}. This is stated in Weber's Law (Weber, 1834; Fechner, 1860):

$$\Delta I / I = \text{constant} \qquad \text{Equation 2.01}$$

Hecht and Mintz (1939) showed that as background light intensity falls to very low luminances, the diameter of a wire at threshold increases, and the constant associated with $\Delta I / I$ increases.

2.2.1 Perimetry

The measurement of the differential light threshold ($\Delta I / I$) in the form of perimetry is clinically used to assess visual function. The stimulus for differential light threshold determination is usually a sharp-edged luminance target of specified spatial and temporal parameters. The visual field, or all the space that one eye can observe at any given moment, was characterised by Traquair (1927) as being "an island hill of vision in a sea of darkness". This is depicted in Figure 2.02, where the x and z axes represent

visual field coordinates, while the vertical y-axis shows differential light sensitivity increasing on moving up the axis. The differential light threshold, or intensity of the target, is the reciprocal of the sensitivity. Stimuli presented outside the hill of vision are unseen by the observer, whilst inside the hill of vision is the observer's visible environment. The figure shows that visual sensitivity is highest at the fovea and declines monotonically away from the point of fixation, apart from at the blind spot, shown in the figure as a dark circle. The blind spot is an 'absolute scotoma', or area of no vision, situated at 15 deg in the temporal field, and corresponding to the optic nerve head on the retina. The outer boundaries of the visual field, or the shoreline where the 'hill' meets the 'sea', are at 60 deg eccentricity in nasal and superior fields, 75 deg in inferior field, and 100 deg in temporal field (Anderson, 1992). It should be noted that the hill of vision is constructed from the visibility of stimuli with a constant size at all eccentricities.

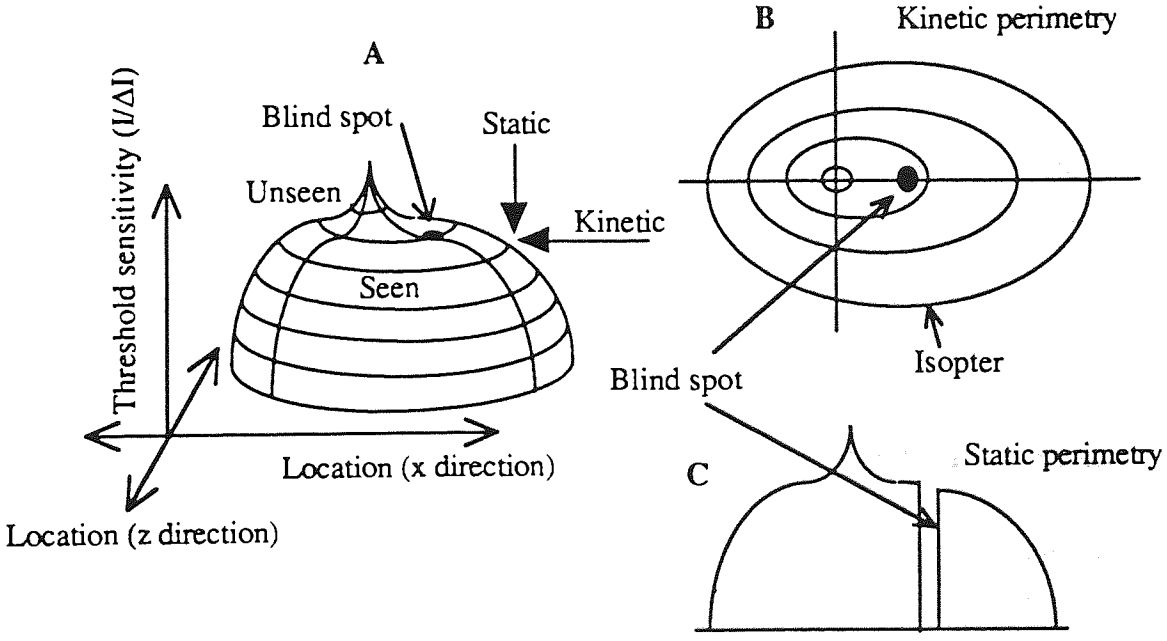

Figure 2.02. (a) Schematic representation of Traquair's "hill of vision". The x- and z- axes represent visual field loci. Differential light sensitivity is shown on the y-axis, with sensitivity increasing up the axis. Thresholds thus decrease on moving up the y-axis. Kinetic perimetry is depicted as a horizontal approach to the hill of vision, whilst static perimetry is shown as a vertical approach.

(b) Isopter plot resulting from kinetic perimetry. Each isopter represents a line of equal sensitivity, and represents the hill of vision as observed from above.

(c) Profile plot resulting from static perimetry. The data plot represents a slice taken through the hill of vision. After Aulhorn and Harms, 1972.

Two methods are available to determine perimetric thresholds, and Figure 2.02 allows the visualisation of both kinetic and static methods. In kinetic perimetry, a target is chosen of specified size and luminance, which is moved across the visual field from outside visibility until it is just observed. Threshold is thus approached in spatial steps, and the locus is found at which a given luminance difference just exceeds threshold. Locations of equal kinetic threshold can be joined together to form an isopter, or line of equal sensitivity. In Figure 2.02 the kinetic target, being of fixed luminance, has a fixed value on the luminance (y) axis. By changing location, the hill of vision is approached horizontally. The resultant isopter plot is also shown, which appears as a cartographer's contour map of the hill of vision.

Using the method of static perimetry, the differential light sensitivity is determined at specific locations with a stationary target of specified size whose luminance is varied. The staircase technique of luminance variation which is used to determine threshold is described in more detail in Chapter 5. Thresholds in static perimetry are therefore approached in luminance steps, a vertical approach to the hill of vision (Figure 2.02). One possible form of data presentation is also shown in the figure, which is that of a retinal profile, or a 'slice' through the hill of vision. With the advent of automated static perimeters, very detailed statistical evaluation of static perimetric results is now possible.

2.2.2 Factors affecting perimetric thresholds

Background luminance

A variety of physiological and physical factors affect perimetric thresholds. One such factor is the background luminance against which the target is presented. From Figure 2.03 it can be seen that at photopic luminances, Weber's Law (Eqn 2.01) applies to perimetric differential light thresholds. At very low luminances approaching absolute threshold, increment sensitivity ΔI is constant. In the transitional phase between these two extremes, a 'scotopic power law' (Schoultes and Bouman, 1977) applies:

$$\Delta I / (I^k) = \text{constant} \qquad \text{Equation 2.02}$$

where k varies between 0 and 1 (Tate, 1985). If k = 0.5, the equation is known as the de-Vries Rose Law. The Humphrey Field Analyser used in this thesis has a background luminance of 31.5 apostilbs, or 10 cdm^{-2} (asb = π cdm^{-2}). The background luminance is at the low end, or possibly below, the limits of Weber's Law. Photopic adaptation is critically dependent on retinal illumination, which is in turn dependent on pupil size. Retinal illumination (in Trolands, Td) equals the product of the background luminance (in cdm^{-2}) and pupillary area (mm^2). A retinal illumination of 100 Td may be sufficient to ensure photopic adaptation (Anderson, 1992). At low

photopic adaptation levels, the Weber fraction is not constant, and variations in pupil size can modify perimetric thresholds (Johnson, Adams and Lewis, 1989). However, it has been noted that once the effects of age are taken into account, pupil size does not influence the mean sensitivity of the visual field on the Humphrey Field Analyser (Brenton and Phelps, 1986; Heijl, 1987).

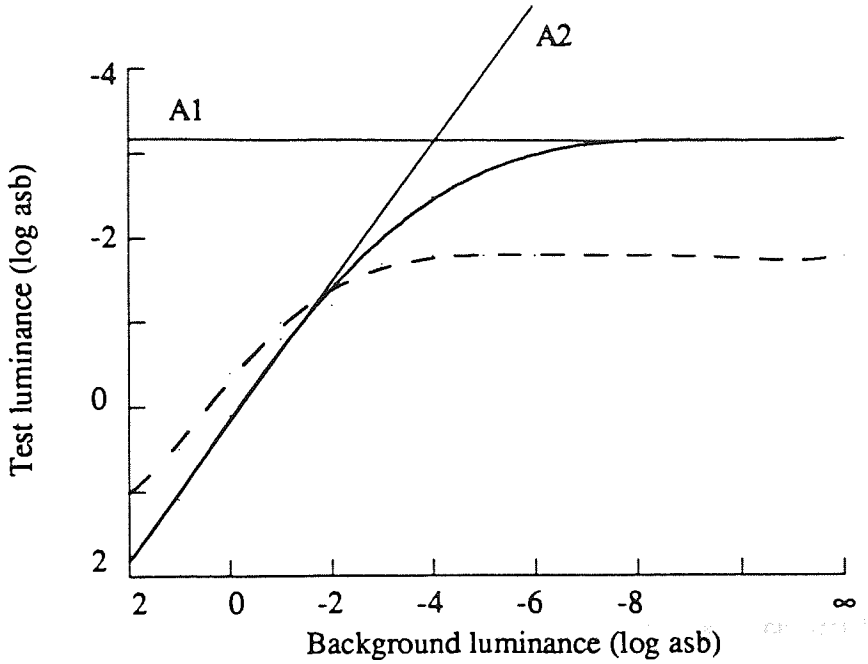

Figure 2.03. Plot of log increment threshold against log background luminance. Dashed curve: central vision; solid curve: 30 deg nasal field. At very low background luminances, threshold (log ΔI) is constant (asymptote A1). At high background luminances, the curves have a slope of 1 (asymptote A2). This means that the Weber fraction (ΔI / I) is constant. Deviation from a constant Weber fraction occurs at higher background luminances centrally than peripherally. After Aulhorn, Harms and Raabe, 1966.

Stimulus size and spatial summation.

Clinical perimetry is generally carried out using the same stimulus size at all visual field locations. Classically, a Goldmann size III stimulus is chosen (subtending 0.431 deg visual angle). Fankhauser and Schmidt (1958) obtained retinal profiles such as those in Figure 2.02c using different stimulus sizes, and demonstrated how thresholds change with eccentricity as a function of stimulus size (Figure 2.04).

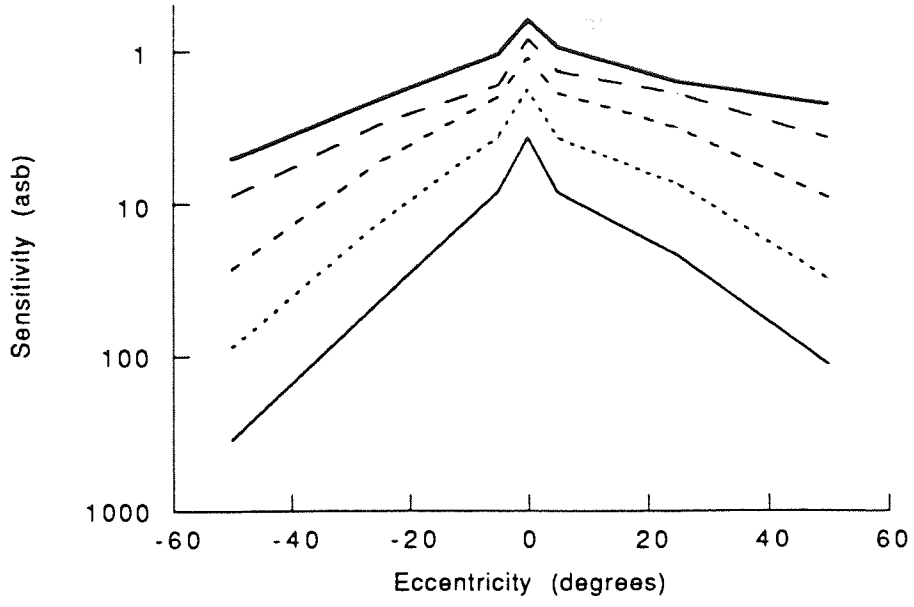

Figure 2.04. From Fankhauser and Schmidt, 1958 (their Figure 8). The x-axis depicts eccentricity (deg) in nasal and temporal visual field. The y-axis shows threshold (asb) decreasing on moving up the axis. Increasing stimulus size improves threshold. This increase is more marked in the periphery than at the fovea. Stimulus sizes used (from the lowest data curve upwards) are Goldmann sizes I-V, subtending 0.108, 0.216, 0.431, 0.864 and 1.724 deg at the eye respectively.

The term 'spatial summation' describes how changes in differential threshold are induced by changes in the size of test stimuli, and therefore stimulated retinal area. In other words, spatial summation is descriptive of the integration of signals across retinal area. The threshold luminance for detection of a small visual stimulus of relatively brief duration on a uniform background is inversely related to its area. ie. the brightness and size of a test object are interchangeable. Mathematically, this is shown by Ricco's Law:

$$LA = c \qquad \text{Equation 2.03}$$

where L is the incremental luminance threshold ($\Delta I / I$), A is stimulus area and c is a constant. In other words, such a stimulus is visible so long as enough light energy arrives at the retina: within limits, the area over which it is spread is immaterial. This is 'complete spatial summation'.

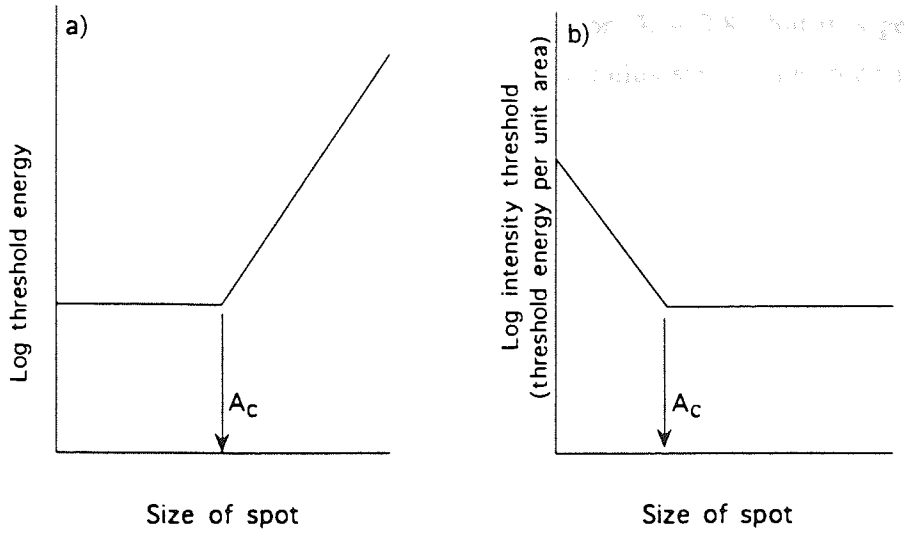

Figure 2.05. Schematic graphs showing spatial summation, where K is 1 or 0. After Haber and Hershenson (1980). (a) Amount of light energy required for threshold as a function of stimulus diameter. Up to a critical area (Ac), the amount of light needed to reach threshold is constant, and the light may occur anywhere within the spot. Beyond the critical diameter, the amount of light needed to reach threshold increases, to ensure that sufficient light falls within the critical spot size. (b) The alternative representation shows threshold luminance (amount of light energy per unit area) as a function of stimulus diameter. The threshold luminance decreases as stimulus size increases up to the limit of the critical area (Ac). Beyond this, threshold remains constant despite any increase in stimulus area.

Complete summation holds up to a certain value of A, generally known as the 'critical area', Ac. The critical area is thus the largest target area at which threshold energy is minimal and constant, as is shown in Figure 2.05a. For targets of greater size than the critical area, the reciprocity between target area and luminance fails, and Ricco's Law takes on a more general form:

$$(L)A^K = c \quad [0<K<1] \qquad \text{Equation 2.04}$$

or $$\log L + K \log A = \log c$$

The exponent K is known as the 'summation coefficient' and has a value between 0 and 1. The value of K indicates the extent of spatial summation. K is unity for stimuli smaller than the critical area, indicating complete summation. As the stimulus increases in size beyond the critical area, K decreases and the summation becomes partial. Under these conditions, as the stimulus area increases so does the total luminance required for threshold to be reached. This is so that the luminance per unit area falling within the critical area remains constant, as is shown in Figure 2.05b. When K falls to 0, Weber's

critical area remains constant, as is shown in Figure 2.05b. When K falls to 0, Weber's Law is obeyed ($\Delta I / I = c$), and an increase in target area has no effect on the threshold. Specific laws of partial summation have been proposed (eg. Piper's Law, K = 0.5; Pieron's Law, K = 0.3; Goldmann's approximation, K = 0.8), but it is generally held that K changes continuously as a function of stimulus size, rather than in a series of specific steps.

The summation coefficient, K, can be calculated from the log derivative of Equation 2.04:

$$\log \Delta I / I = \log c - K \log A \qquad \text{Equation 2.05}$$

Plotted graphically, K is represented by the gradient of the plot of log $\Delta I / I$ against log area. It can be seen in Figure 2.06 that K decreases gradually from 1 to 0 as the target area increases, and also that there is no specific value of the critical area as suggested by the previous schematic graphs, which took no note of partial summation.

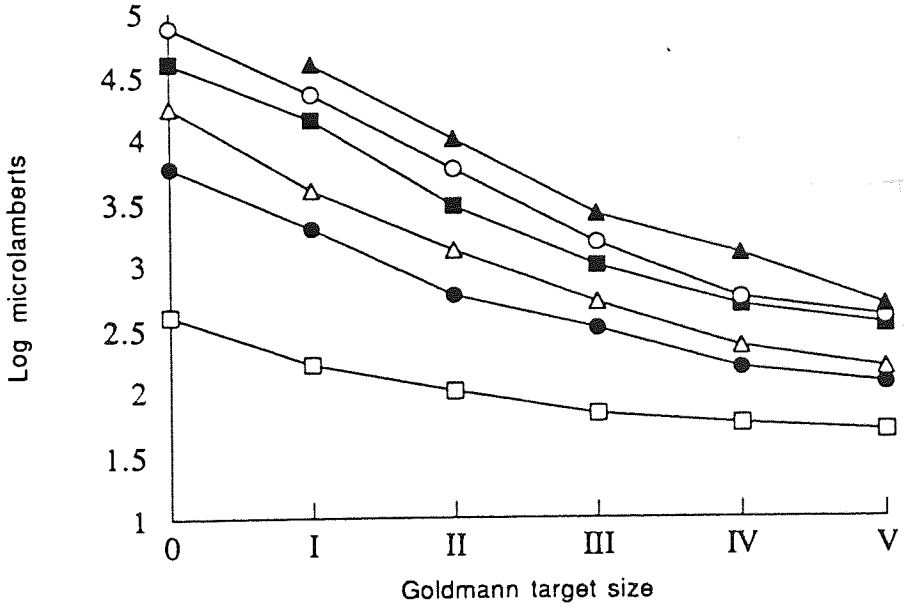

Figure 2.06 shows how the schematic diagram 2.05b actually appears (From Sloan (1961), Figure 4). The curves take the form of Equation 2.05. The gradient of the curves, K, represents the extent of spatial summation under the specific conditions. K increases with eccentricity, and decreases with increasing stimulus size. The graph differs from the schematic diagram in that the transition from full summation (K = 1) to no summation (K = 0) does not occur at a defined 'critical diameter', as the gradient of the function changes steadily between the two extreme values. Symbols represent different eccentricities in nasal visual field: Open squares: 0°; closed circles: 10°; open triangles: 20°; closed squares: 30°; open circles: 40°; closed triangles: 50°.

Several factors affect the amount of spatial summation exhibited by the eye. The state of adaptation affects summation in that the critical area is smaller photopically than scotopically (Barlow 1958; Dunn and Lakowski, 1981; Brown, Peterken, Bowman and Crassini, 1989). The size of the critical area falls as the square root of the increase in background luminance (Glezer, 1965). Weber's Law ($\Delta I / I = c$) holds in the photopic range (Barlow, 1958; Wilson, 1970; Schoultes and Bouman, 1977). At lower luminances the de-Vries Rose Law applies (Schoultes and Bouman, 1977). Increasing stimulus duration reduces spatial summation (Barlow, 1958).

The completeness of spatial summation increases with eccentricity, as is shown by an increase in the value of K (Fankhauser and Schmidt, 1960; Sloan, 1961; Johnson, Keltner and Balestrery, 1978). The size of the critical area also increases with eccentricity, indicating increased spatial summation in the peripheral visual field (Sloan, 1961; Wilson, 1970; Dannheim and Drance, 1971; Greve, 1973; Lie, 1980; Inui, Mimura and Kani, 1981; Wood, Wild, Drasdo and Crews, 1986; Wild, Wood and Flanagan, 1987). The increase is reported to occur linearly with eccentricity (Wilson, 1970; Inui et al., 1981), although Lie (1980) finds that the increase in critical size with eccentricity is interrupted by a plateau of constant size.

Stimulus duration and temporal summation.

Temporal summation describes the integration of luminance signals over time by the retina. To a certain limit, presenting a stimulus for a longer time increases its likelihood of being seen. This is represented mathematically by Bloch's Law:

$$LT = c \qquad \text{Equation 2.06}$$

where L is the luminance threshold ($\Delta I / I$), T is the exposure duration, and c is a constant. Bloch's Law only holds for small targets at short exposures. The critical time (Tc) is dependent on stimulus variables, but may be as low as 0.06 sec, beyond which sensitivity will fail to increase at the same rate with exposure duration (Tate, 1985).

Aulhorn and Harms (1972) found no further decrease in the differential light threshold when exposure duration was extended beyond 0.5 sec. The critical period may be longer in the periphery. Ideally a perimetric stimulus would be presented for longer than the period over which temporal summation occurs. In practice however, since the latency of voluntary eye movements is only 150-250 msec (Tate and Lynn, 1977), fixational problems may become apparent at such an exposure duration.

Defocus

The effect of defocus is to degrade the retinal image quality of a perimetric stimulus, making it dimmer and larger in diameter. This has a relatively greater effect on small targets than large ones (Ogle, 1961a). Blur has been shown to affect thresholds for smaller Goldmann targets (sizes I to III) in the central 30 deg, but has no effect on larger targets (sizes IV and V) (Sloan, 1961; Fankhauser and Enoch, 1962; Atchison, 1987; Herse, 1992). Thresholds are less affected by blur at greater eccentricities (Ogle, 1961b; Sloan, 1961; Maguire, 1971; Tate, 1985; Atchison, 1987). The studies described above use the best foveal correction as the baseline for examining the effects of defocus. Wild, Wood and Crews (1988) found that perimetric sensitivity was not improved by the use of peripheral refractive corrections.

Factors affecting kinetic perimetry

In static perimetry the only variable in a single threshold measurement is that of luminance. In kinetic perimetry, the additional variable of movement is introduced. The fundamental difference between kinetic and static perimetry is to be found in the continuous presentation and movement of the stimulus in kinetic perimetry, on account of which interaction and reaction time influence the threshold measurements (Greve, 1973).

A kinetic perimetric stimulus is continuously present and moving, and the thresholds to such a stimulus will be contaminated by the reaction time of the subject. If automated perimetry is not used, the reaction time of the examiner will also be a factor. As the stimulus is moved from an unseen region of the visual field to a location where it is seen, there is a latent period between observation of the stimulus and reaction to it. The magnitude of simple visual reaction time is approximately 200ms (Keele, 1986). The effect of a subject's reaction time is to reduce the size of an isopter, and this is evident at velocities of more than 4 deg/sec (Johnson and Keltner, 1987). Reaction times to peripheral visual stimuli are slightly slower than to foveal stimuli (Teichner, 1954; Rains, 1963; Ball and Sekuler, 1980; Keele, 1986), but as speed of motion increases, peripheral retinal reaction times improve relative to those for foveal stimuli (Tynan and Sekuler, 1982). Simple reaction times change little from 20 to 60 years of age, and at older ages there is a 'moderate slowing' of reaction time (Teichner, 1954; Keele, 1986).

The continuous presence of a moving kinetic stimulus can also lead to successive lateral summation. In the 500ms (Aulhorn and Harms, 1972) summation period prior to detection of a stimulus, summation of successive infraliminal stimuli can occur. The

effect of successive lateral summation is to enlarge the size of an isopter. With faster stimulus movement, more area is stimulated in the time prior to detection, and more summation can occur. Summation and reaction time become balancing effects in kinetic perimetry, with the effect that threshold loci for slow and fast moving stimuli are often identical (Tate and Lynn, 1977).

The different bases of static and kinetic perimetry, and the factors described above, contribute to differences between kinetic and static perimetric thresholds. The difference is called stato-kinetic dissociation, or SKD. Fankhauser and Schmidt (1960) showed that kinetic sensitivity is slightly higher in periphery, while static sensitivity is higher centrally. In other words, a subthreshold static peripheral spot of light can be made to appear by moving it slowly, whereas close to the fovea, a stationary spot of light which is just visible can be made to disappear by moving it. Hudson and Wild (1992), using automated perimetry with normal observers, also found kinetic sensitivity to be greater than static peripherally, by an average of 4 dB. This was largely independent of age, stimulus size, meridian or eccentricity.

2.3 Spatial Thresholds

2.3.1 Contrast sensitivity

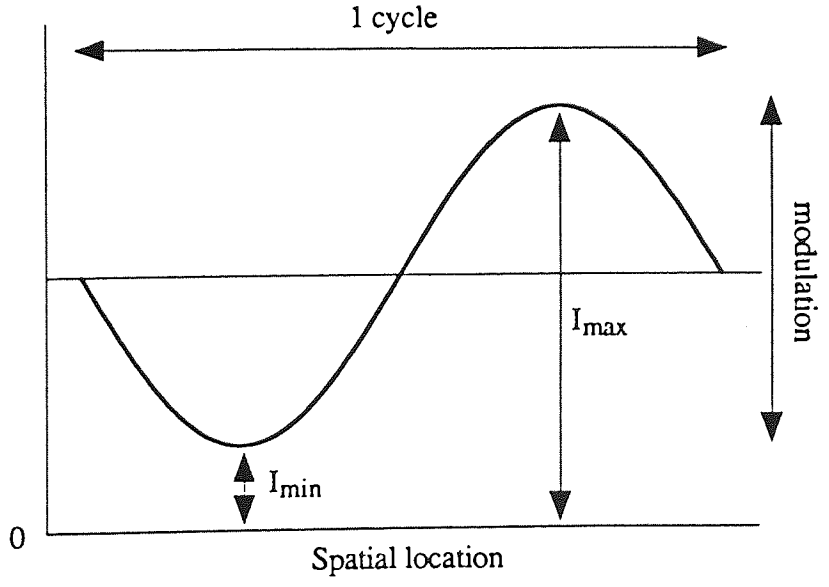

Figure 2.07. Sinusoidal grating. Luminance modulates in space around a mean luminance, producing a contrast grating. The spatial frequency of the grating is the number of cycles (light / dark patches) subtended per degree of visual angle.

An observer's contrast sensitivity describes their ability to detect luminance differences, and as such represents a fundamental measure of visual function. The contrast sensitivity function (CSF) is generally determined using a sinusoidal grating as a stimulus, which is shown in Figure 2.07. The contrast of a grating describes the modulation of its brightness about an average level, defined by the Michelson contrast:

$$\text{Michelson contrast} = (I_{max} - I_{min}) / (I_{max} + I_{min}) \qquad \text{Equation 2.07}$$

The spatial frequency of a grating describes the number of cycles, or light / dark periods, per degree of visual angle at the eye.

Plotting the reciprocal of the threshold contrast, or contrast sensitivity, against spatial frequency on logarithmic coordinates gives a contrast sensitivity function (Campbell and Green, 1965), shown in Figure 2.08. Contrast sensitivity is highest at 3-5 cpd (cycles per degree), and the highest spatial frequency observable is approximately 60 cpd at a contrast of unity, and represents the resolution acuity.

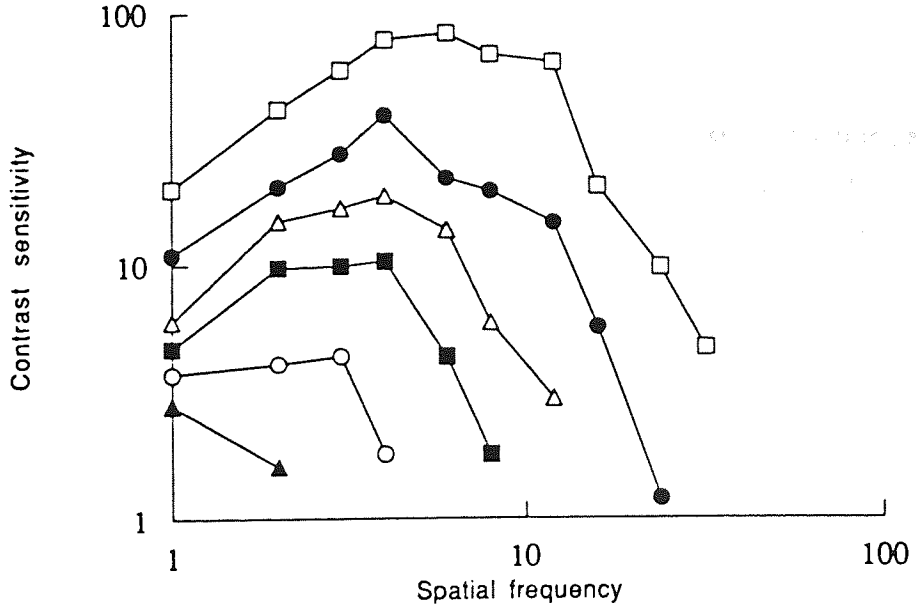

Figure 2.08. Contrast sensitivity as a function of spatial frequency under photopic conditions, at the fovea and various eccentricities in the inferior visual field. The grating stimulus has a constant size at all eccentricities. From Rovamo, Virsu and Näsänen, 1978 (their Figure 1a). Open squares: 0 deg; closed circles: 1.5 deg; open triangles: 4 deg; closed squares: 7.5 deg; open circles: 14 deg; closed triangles: 30 deg.

Contrast sensitivity declines with eccentricity when measured using stimuli of the same size at all eccentricities, the slope of the sensitivity decline being steeper for higher

spatial frequencies (Rijsdijk, Kroon, and van der Vildt, 1980; Wright and Johnston, 1983). The sensitivity decline with eccentricity is faster for vertical than for horizontal meridia (Rijsdijk et al., 1980), and is independent of temporal frequency (Wright and Johnston, 1983). Contrast sensitivity functions obtained using stimuli which are enlarged peripherally in accordance with cortical magnification factors are almost identical at each eccentricity (Koenderink, Bouman, Bueno de Mesquita and Slappendel, 1978; Rovamo et al., 1978; Johnston, 1987; Watson, 1987). This subject is dealt with in greater detail in Chapter 4.

Loss of contrast sensitivity with age is most pronounced at mid to high spatial frequencies, above 4 cpd (Wright and Drasdo, 1985; Elliott, 1987; Elliott, Whitaker and MacVeigh, 1990; Owsley and Burton, 1991) at both central and peripheral (Crassini, Brown and Bowman, 1988) locations. This contrast sensitivity loss appears to be mainly neural in origin, with some optical contribution at high spatial frequencies (Elliott, 1987; Sloane, Owsley and Jackson, 1988).

2.3.2 Resolution

Visual acuity, or the minimum resolvable acuity, represents the spatial limit of visual discrimination. Acuity represents only one small part of visual function, that of resolution of the smallest possible objects at the highest possible contrast, and is part of the fuller picture of visual function provided by the contrast sensitivity function. Resolution capability is defined as the smallest angular separation between two objects that can be resolved as being separate. Figure 2.09 below shows how this is achieved.

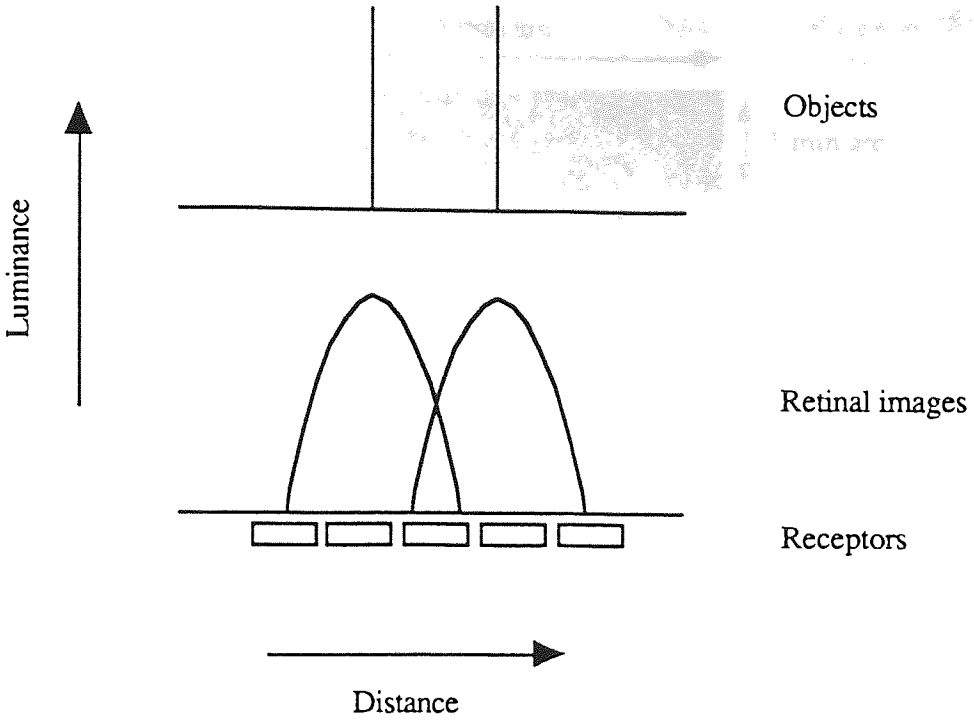

Fig 2.09. Resolution of two point or line images. See text for details.

The objects to be resolved are two bright dots, lines, or stripes of a grating. Their images on the retina are spread by the eye's optics to form two point or line spread functions (Campbell and Gubisch, 1966). In order to be resolved, there must be a detectable difference in the retinal illuminance between the two objects (see also Figure 2.22, top). To be detectable, the light dip must be above the ΔI limit of the system for the prevailing stimulus area and adaptation conditions. Finally, and this is what distinguishes resolution from detection, the differentially stimulated site must have a distinguishable location, ie. the luminance peaks and troughs must fall in separate detecting units (Westheimer, 1979b, 1992; Levi, 1991). The magnitude of the resolution threshold, described as the 'minimum angle of resolution' (MAR), is approximately 0.5-1 min arc.

In clinical settings, MAR is usually measured using symbols such as Snellen letters (Figure 2.10), Llandolt Cs or Illiterate Es. Resolution of these stimuli can be described as the minimum recognisable acuity (Levi, 1991), as factors of form recognition or orientation identification are involved in the task, additional to those factors involved in resolution.

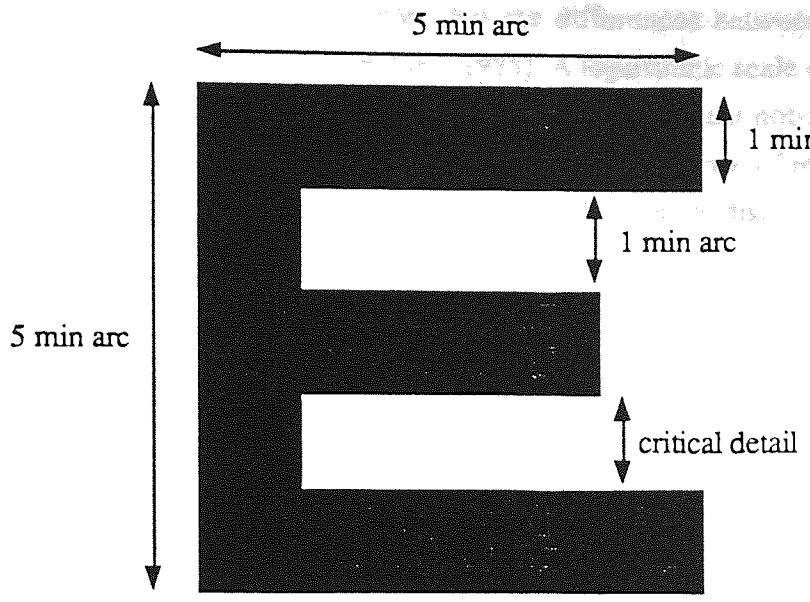

Figure 2.10. Construction of a Snellen 6/6 letter. At 6m, the letter size is 8.73mm high and the gap size, or critical detail, measures 1.75mm. This gap size corresponds to a visual angle of $\tan^{-1}$ (1.75mm / 6m) = 1 min arc. Snellen fractions are defined as the ratio of the distance at which a chart is viewed to the distance at which the critical detail of the letter would subtend 1 min arc at the eye. In the UK, 6 metres is the standard distance for a test chart, and so 6/6 is the standard 'normal' acuity. In the USA, distances are defined in feet, and their 'normal' acuity is quoted as 20/20.

As for the minimum resolvable acuity, MAR for the minimum recognisable acuity is approximately 0.5-1 min arc. However, minimum recognisable acuity differs from minimum resolvable acuity in several ways (Levi, 1991). Firstly, the former stimulus is localised, whereas grating acuities are not. Secondly, Snellen acuities are subject to 'crowding effects' (to be discussed later). Finally, whilst optimum foveal thresholds are very similar, Snellen acuities are more degraded in peripheral vision than grating acuities. Levi (1991) concludes that "while factors limiting resolution acuity and Snellen acuity may be the same in normal foveal vision, the two forms of acuity are differentially sensitive to physiological and pathological degradation."

Measurement of acuity has been described so far in terms of the minimum angle of resolution, MAR. This threshold definition constitutes a linear acuity scale. In contrast, acuity measures are traditionally quoted as Snellen fractions in a clinical setting. The Snellen fraction is defined as the ratio of the distance at which a chart is viewed to the distance at which the critical detail of the letter would subtend 1 min arc at the eye. As it is the reciprocal of the MAR, it constitutes a reciprocal scale (Westheimer, 1979a), and is a measurement of sensitivity. Both the linear and reciprocal scales described are

ordinal, in that they exhibit order, but the differences between pairs of successive points are unequal (Wild and Hussey, 1985). A logarithmic scale of MAR measurement is advocated by Westheimer (1979a). Using this scale, just noticeable differences are approximately equal everywhere on the scale (standard error of repeated measurements / mean logMAR = constant), such that it is a scale of equal discriminability.

2.3.2 Factors affecting resolution

Refractive error

Defocus obviously has a severe effect on resolution thresholds. Any increase in optical defocus widens the retinal point spread function of an object, such that to be identified as separate, two objects need to be further apart than in the fully focussed state. The effect of defocus is reduced with smaller pupil sizes (to a minimum of 2mm) since the depth of focus increases (Westheimer, 1992).

Pupil size

Visual acuity remains constant with pupil sizes in the range 2.5 to 6mm. Below 2.5mm diameter, the retinal image becomes degraded by increased diffraction. Above 6mm diameter, non-paraxial aberrations such as spherical aberrations reduce the retinal image quality.

Luminance

Visual acuity increases with increase in ambient luminance, but remains constant over a large photopic range (Westheimer, 1992), the luminance at which acuity plateaus being higher in foveal than peripheral vision (Kerr, 1971). Light intensity is not as critical a factor in determining peripheral thresholds as foveal acuities, and this applies to scotopic and low photopic luminances (Mandelbaum and Sloan, 1947) as well as photopic luminances (Sloan, 1968).

Stimulus duration

For foveal recognition acuity under photopic conditions, MAR is found to be time dependent over periods much longer than the critical duration for detection under the same observation conditions. The critical detection duration has a maximum value of 100 ms, while acuity thresholds continue to improve up to, and even beyond, 400ms duration (Baron and Westheimer, 1973).

Age

Visual recognition acuity has been shown to decrease with age (see Spear, 1993 for a review), even in the absence of ocular pathology. Although optical changes during

normal aging may cause some decrease in visual resolution, it seems likely that at least some of the acuity loss is due to aging related changes in the retina or cortex. Resolution loss with age is also depicted in studies of contrast sensitivity loss with age (see above), where preferential loss of high spatial frequencies is noted (Wright and Drasdo, 1985; Elliott, 1987; Elliott et al., 1990; Owsley and Burton, 1991).

Eccentricity

Many studies over the years have investigated visual acuity as a function of eccentricity (see Genter, Kandel and Bedell (1981) for a review). Since acuity is a spatial threshold and threshold is generally found by varying the size of the object to be resolved or recognised, thresholds in these studies have been found by a spatial scaling method.

Weymouth (1958) was the first to notice that although sensitivity, as measured by visual acuity, declined with eccentricity in merely an 'orderly manner', visual acuity thresholds, or the minimum angle of resolution, increased with eccentricity in a linear fashion to at least 30 deg. The linear rise of acuity threshold with respect to peripheral location can be quantified using the E_2 parameter described in Chapter 1. If peripheral thresholds are expressed relative to the fovea, then the acuity data may be fitted with a linear regression of the following form:

$$F = 1 + (E / E_2) \qquad \text{Equation 1.01}$$

where F is the minimum angle of resolution at some eccentricity, relative to that at the fovea, ie. MAR / MAR_0; E is eccentricity (deg); and E_2 represents the eccentricity, in degrees, at which the foveal MAR doubles. E_2 therefore quantifies the eccentricity related decline in performance: a small E_2 indicating a rapid decline, and a large E_2 indicating a shallow eccentricity dependent gradient.

If acuity thresholds are expressed as actual values, then Equation 1.01 can be expressed as:

$$MAR / MAR_0 = 1 + (E / E_2)$$

so,
$$MAR = MAR_0 (1 + (E / E_2)) \qquad \text{Equation 2.08}$$

or,
$$MAR = MAR_0 + ((MAR_0 / E_2) E) \qquad \text{Equation 2.09}$$

The equations given above may all be justifiably used if standard errors are provided, such that the regression can be weighted by the inverse of the variance. As has already been noted however, a linear scale of MAR is an ordinal scale, and standard errors increase as the mean value of MAR increases. Using Equations 2.08 and 2.09 to determine E_2 on a linear scale with no standard errors will weight each point equally, although the standard errors would be larger at greater eccentricities if they were known. A more valid procedure under these circumstances is to plot the logarithm of

MAR against eccentricity, and fit a regression to the data which is the logarithmic derivative of Equation 2.08. This will have the form:

$$\log MAR = \log MAR_0 + \log(1 + (E / E_2)) \qquad \text{Equation 2.10}$$

Under these circumstances, the standard error is a constant proportion of the mean (Westheimer, 1979a), and the absence of standard errors from the data will not greatly affect the curve fit or the E_2 value. To illustrate this point, data is shown below taken from Westheimer (1979a). In Figure 2.11a, data is shown for 2 observers for a grating acuity task with MAR plotted against eccentricity on linear axes. The regressions to the data are of the form of Equation 2.08, giving E_2 values of 3.70 ± 0.41 deg for observer 1 and 0.60 ± 1.12 deg for observer 2. Note how the high threshold for observer 2 at 15 deg has steepened the regression, giving a small value of E_2. In Figure 2.11b, the same data has been fitted with a linear regression of the form of Equation 2.08, but this time the data has been weighted in accordance with the inverse variance at each point. E_2 values under these conditions are 3.07 ± 0.06 deg for observer 1 and 2.11 ± 0.05 deg for observer 2. The weighting procedure drastically affects the slope of the regression for observer 2, since the 'rogue' peripheral point has a relatively higher standard error and now has less effect on the overall gradient. In Figure 2.11c, the data are shown plotted on a logarithmic y-axis, and regressions fitted to the data of the form of Equation 2.10, unweighted with standard error. Such a regression gives E_2 values of 3.09 ± 0.30 deg for observer 1, and 1.99 ± 0.56 deg for observer 2. Whilst the E_2 values obtained are not exactly equivalent, they are very similar to those obtained in Fig 2.11b. This is because on a logarithmic scale, standard errors for visual acuity are approximately equal, since standard errors are approximately a constant proportion of the mean. Plotting the data in this way is almost the same as taking the actual standard errors into account in the regression. Thus, if standard errors are not available in the following sets of data, E_2 values are calculated on a logarithmic y-axis, and then shown on linear axes for clarity.

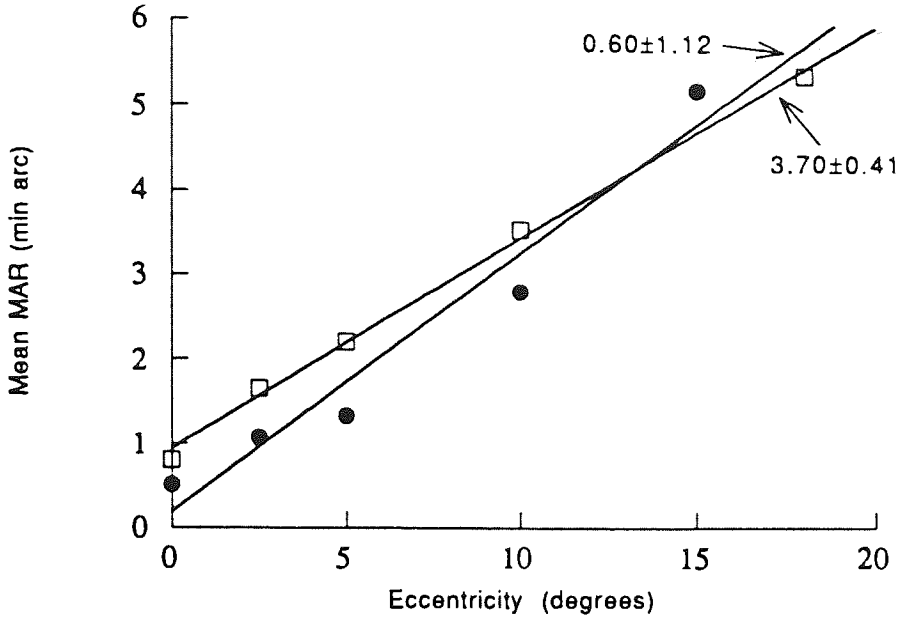
Mean MAR (min arc)
0
1
2
3
4
5
6
0
5
10
15
20
Eccentricity (degrees)
0.60±1.12
3.70±0.41

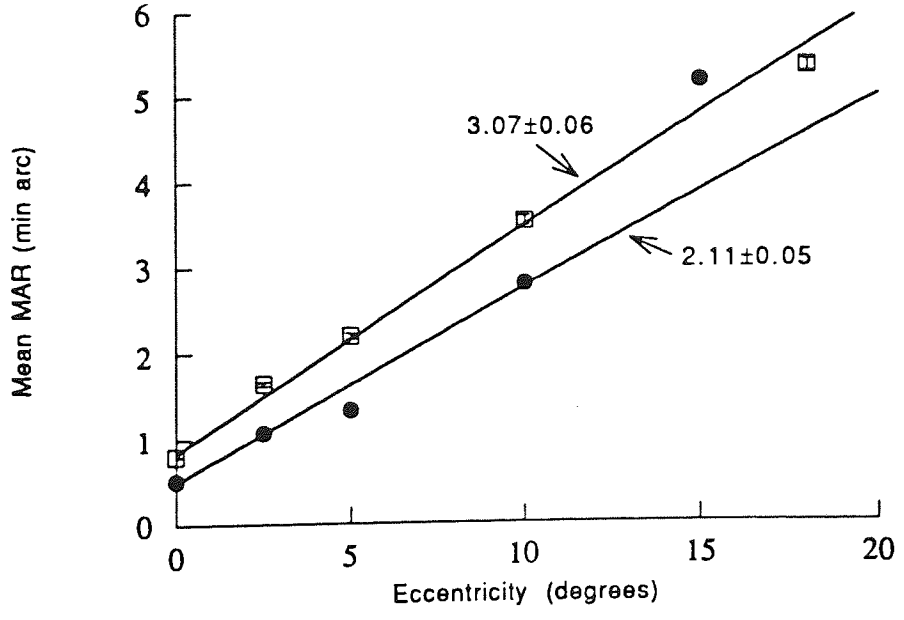
Mean MAR (min arc)
0
1
2
3
4
5
6
0
5
10
15
20
Eccentricity (degrees)
3.07±0.06
2.11±0.05

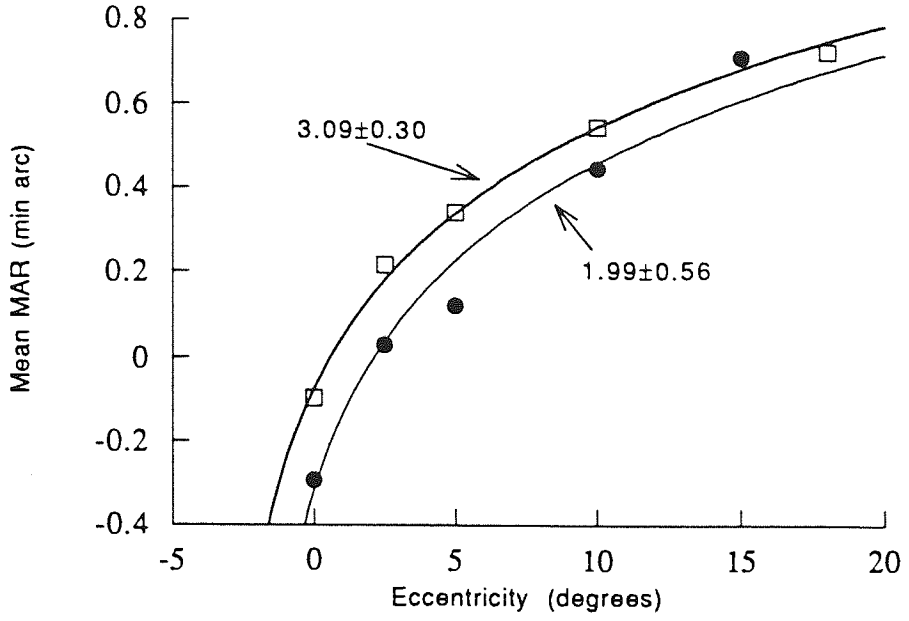

Figure 2.11. Data of Westheimer (1979a). Open squares: observer 1; closed circles: observer 2.

a. Minimum angle of resolution plotted against eccentricity on linear axes. The regressions are from the linear data without weighting the data in accordance with their standard errors. Observer 1: MAR = 0.93 (1 + (E / 3.70)); observer 2: MAR = 0.19 (1+ (E / 0.60)).

b. Data as for Fig a. The regressions are from the linear data, weighted in accordance with standard error. Error bars show standard error: for the closed symbols error bars are smaller than the symbols. Observer 1: MAR = 0.82 (1 + (E / 3.07)); observer 2: MAR = 0.48 (1 + (E / 2.11)).

c. Minimum angle of resolution expressed in logarithmic units plotted against eccentricity, so that standard errors represent a constant proportion of the mean threshold value. Observer 1: logMAR = -0.078 + log(1 + (E / 3.09)); observer 2: logMAR = -0.32 + log(1 + (E / 1.99)).

A number of studies from the literature are now evaluated here in terms of their E_2 values. Since E_2 is a relative comparison of foveal and peripheral data, values of E_2 can be used to compare the eccentricity related decline in performance across studies which differ in several variables, and have different absolute thresholds. The studies examined, whilst all dealing with resolution and recognition acuities, vary greatly in terms of their stimulus type, meridian of presentation, method of data collection, background luminance, and stimulus duration, amongst other factors.

One of the first papers to examine peripheral visual acuity was that of Wertheim (1891), who used square wave gratings consisting of wire grids to examine resolution thresholds at peripheral locations. Wire grids of different thicknesses were employed,

but each was a scaled version of the others as the same number of cycles were present in each. Figure 2.12 shows how thresholds relative to that at the fovea varied as a function of eccentricity.

Figure 2.12. From the data of Wertheim (1891). Acuity thresholds relative to those at the fovea, plotted against eccentricity. Open squares: temporal visual field; crosses: superior visual field. Temporal data is fitted with the regression log F = 0.01 + log (1 + (E / 2.36)) over the range 0-30 deg; superior data is fitted with the regression log F = -0.02 + log (1 + (E / 1.59)) over the range 0-20 deg.

The regression fitted to the restricted data range on a logarithmic acuity axis is of the form of Equation 2.10, from which it is found that E_2 for the temporal field is 2.36 ± 0.08 deg in the range 0-30 deg, and for the superior field E_2 is 1.59 ± 0.19 deg in the range 0-20 deg. Not shown for clarity are the data for nasal and inferior visual field meridians. These meridia have E_2 values of 2.12 ± 0.29 deg (0-30 deg range), and 1.54 ± 0.27 deg (0-20 deg range) for nasal and inferior fields respectively. The variation in E_2 values highlights differences in peripheral visual acuity in each meridian. The eccentricity related decline in performance is greatest for the vertical meridia, while acuity falls off much more slowly with eccentricity in the horizontal meridia, particularly the temporal field. Wertheim produced isoacuity isopters to show this, which are ellipsoidal with the long axis horizontal and extending further into the temporal field.

Low (1951) obtained similar data to that of Wertheim for Llandolt ring acuity from 100 untrained observers in the temporal visual field. While thresholds rise linearly with eccentricity to 30 deg, beyond this acuity thresholds rise faster than a linear increase with eccentricity. The fit to the data in the 0-30 deg range was obtained on a logarithmic acuity axis, with the equation:

$$\text{logMAR} = 0.11 + \log(1 + (E / 2.93))$$

such that E_2 is 2.93 ± 0.50 deg.

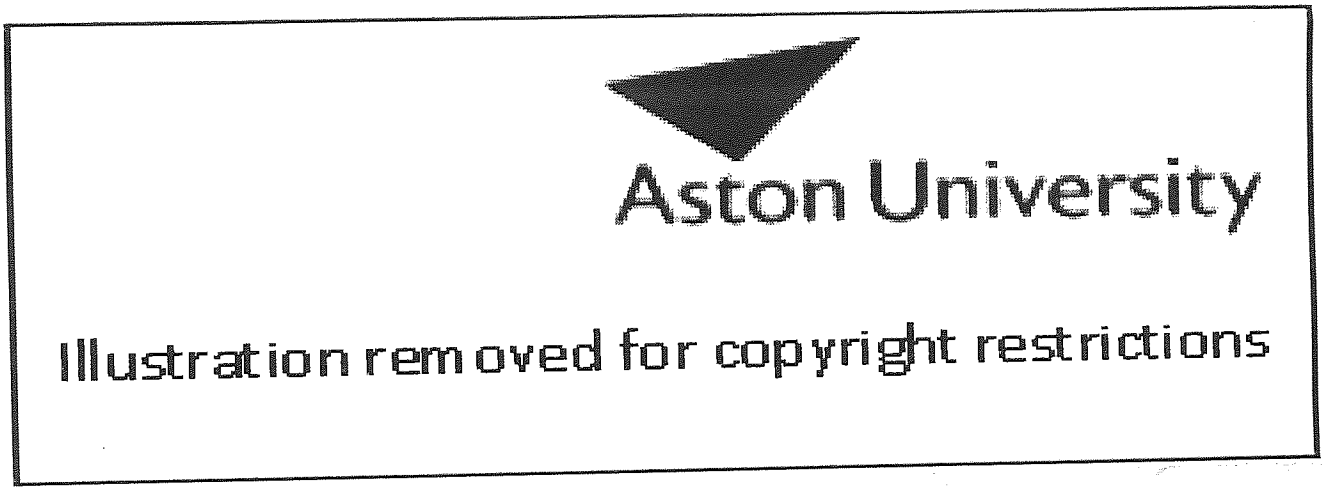

Figure 2.13. Data of Low (1951). The regression fitted to the data in the range 0-30 deg in temporal visual field is: logMAR = 0.11 + log(1+ (E / 2.93)), so that E_2 is 2.93 ± 0.50 deg, and MAR at the fovea is extrapolated to be 10^(0.11) = 1.29 min arc.

The loss of linearity at eccentricities beyond 30 deg shown by the data of Wertheim and Low was noted by Weymouth (1958), but he concluded that a linear fit to acuity data below 30 deg eccentricity was still valid. Weymouth looked at thresholds to Llandolt rings from 0-20 deg eccentricity in a group of 20 students. Both nasal and temporal meridians were examined, but as no systematic differences were observed the data were averaged across meridia.

Eccentricity (degrees)

Figure 2.14. From the data of Weymouth (1958). Average minimum angle of resolution for 20 students in nasal and temporal meridia. The regression fitted to the data, weighted with standard error, is MAR = 1.90 (1 + (E / 1.35)).

The mean results are shown in Figure 2.14: MAR does rise linearly with eccentricity to 20 deg with the regression of the form of Equation 2.08:

$$MAR = 1.90 (1 + (E / 1.35))$$

and so E_2 is 1.35 ± 0.11 deg. The regression is weighted by the inverse of the standard error of the data, which is plotted on the graph. This evaluation is slightly different to that of Weymouth, who describes the data by the form of Equation 2.09: MAR = 1.469 + 1.504 E. E_2 therefore calculates to be 1.469 / 1.504 = 0.98 deg. These values are consistent with fitting the data with a regression without paying heed to the standard errors, which increase with the mean. Several observations may be made about Weymouth's data. His use of untrained students in a laboratory class appears to have resulted in very poor acuity measurements. From the data, the mean foveal MAR is given as 2.06 min arc, corresponding to a Snellen acuity of just over 6/12. Interindividual variation appears to have also played a large part in the results. Weymouth himself says that the average data is not representative of individuals. For example, E_2 for subject K calculates to be 4.633 / 1.731 = 2.68 deg, while for subject M it is 3.285 / 1.816 = 1.81 deg, somewhat different values than those calculated from the mean results.

Randall, Brown and Sloan (1966) investigated peripheral visual acuity with the intention of providing a guide to expected acuities from patients using eccentric retina due to central visual loss. Data is shown below for their 5 normal observers for Llandolt ring acuity of targets of 1 sec duration in nasal visual field. Since standard errors are provided for the data, E_2 is calculated in Figure 2.15 on linear axes by applying Equation 2.08 and weighting the data according to its inverse variance at each point. From the regression, E_2 is calculated to be 1.79 ± 0.07 deg.

Figure 2.15. Data of Randall et al. (1966). Mean minimum angle of resolution from 5 normal observers in nasal visual field is plotted against eccentricity. Error bars show standard error. The regression applied to the data is: MAR = 1.01 (1 + (E / 1.79)), so that E_2 is 1.79 ± 0.07 deg, and the foveal value of MAR extrapolated from the regression is 1.01 ± 0.02 min arc.

The purpose of the study of Sloan (1968) was to examine the effect of luminance on acuity in the photopic range, extending the work of Mandelbaum and Sloan (1947). The acuity data derived from the highest luminance of 314 cdm^{-2} is shown in Figure 2.16. As no standard errors were provided, E_2 has been calculated from a regression on log-linear axes with the form

$$\log MAR = -0.35 + \log(1 + (E / 1.32))$$

from which E_2 is calculated to be 1.32 ± 0.08 deg.

Figure 2.16. Data of Sloan (1968). Minimum angle of resolution in minutes of arc in the nasal visual field is plotted against eccentricity. The regression was calculated on a logarithmic y-axis, and is: logMAR = -0.35 + log(1 + (E / 1.32)). E_2 is calculated to be 1.32 ± 0.08 deg, while the foveal value of MAR extrapolated from the regression is 10^(-0.35) = 0.45 min arc.

Green (1970) examined acuity variation with eccentricity using sine wave gratings and interference fringes. The data for 2 observers with high contrast gratings in the temporal visual field is shown in Figure 2.17. For observer RA, E_2 is 1.32 ± 0.32 deg, and for DG E_2 is 2.53 ± 0.36 deg.

Figure 2.17. Data of Green (1970). Minimum angle of resolution in minutes of arc for resolution of a high contrast sine grating in temporal visual field, plotted against eccentricity. Open squares, and solid line: observer RA. The regression fitted to the data was calculated on a logarithmic y-axis and is: logMAR = -0.13 + log(1 + (E / 1.32)), so that E_2 is 1.32 ± 0.32 deg, and MAR at the fovea is calculated to be 10^(-0.12) = 0.76 min arc. Crosses, and dashed line: observer DG. The regression is fitted in the same way as for observer RA, and the equation is: logMAR = -0.02 + log(1 + (E / 2.53)), so that E_2 is 2.53 ± 0.36 deg, and MAR at the fovea is calculated to be 10^(-0.02) = 0.95 min arc.

Although Wertheim (1891) examined the entire visual field in his study, most studies of peripheral visual acuity have dealt with acuity along the horizontal meridia, the nasal and temporal visual fields. Millodot and Lamont (1974) instead examined the vertical meridia of superior and inferior visual field with Llandolt rings of 220ms duration and 65% contrast on a photopic background. They found acuities to be poorer in superior field than at corresponding locations in inferior visual field. From their data (mean of 3 observers, from 0-15 deg) examined on logarithmic axes, inferior field is described by the values -0.16 ± 0.05 log min arc for $logMAR_0$, so that MAR_0 is 0.69 min arc, and E_2 is 4.7 ± 1.0 deg. For superior field, $logMAR_0$ is -0.2 ± 0.1 min arc, such that MAR_0 is 0.63 min arc, and E_2 is 2.58 ± 0.83 deg.

Anstis (1974) found the eccentricity at which Helvetica typeface letters of various sizes were identifiable binocularly. The data follow a linear pattern from 0-30 deg. However, the regression applied to his data is:

$$MAR = 0.046\ E - 0.031$$

giving an E_2 value (from Equation 2.09) of -0.031 / 0.046 = -0.67 deg. Anstis explains the negative intercept as being due to experimental error. A negative intercept makes no sense however, since a character must have a positive size at the fovea to be detected. If the data is examined on logarithmic axes so that the effect of variation of standard error with eccentricity is accouted for, $\log MAR_0$ is -1.41 ± 0.27 log min arc, giving MAR_0 of 0.04 min arc, and E_2 is 0.91 ± 0.62 deg.

Figure 2.18. Data from Johnson et al. (1978). Scaling factors required to superimpose peripheral spatial summation curves onto foveal data, expressed in terms of diameter, and plotted against eccentricity. The regression fitted to the data is: log F = log(1) + log(1 + (E / 3.11)), so that E_2 is 3.11 ± 0.18 deg for the nasal visual field.

Johnson et al. (1978) obtained resolution thresholds with the same perimetric equipment as they used to examine differential light detection thresholds (Figure 7.05). Their resolution task was to distinguish between circular and diamond shaped targets, and the differential light contrast at which this distinction could be made was taken as threshold. The data were presented as spatial summation curves of log threshold vs log area for each eccentricity (their Figure 6). Shifting the data for each eccentricity along the x-axis to coincide with the foveal data provides scaling factors, which are shown in diameter terms plotted against eccentricity in Figure 2.18. A regression was fitted to the data on a logarithmic axis of the form :

$$\log F = \log (1) + \log (1 + (E / 3.11))$$

so that E_2 is 3.11 ± 0.18 deg for the nasal visual field. This compares with the E_2 value found for detection under the same conditions of 1.94 deg.

The study of Lie (1980) which examined detection thresholds across the visual field (Figure 7.06) also examined recognition thresholds, with the subject's task being to distinguish between squares of incremental luminance presented as squares, or on their sides as diamonds. The differential light threshold for a range of target sizes was found from 0 to 45 deg in nasal and temporal retina, and were plotted as spatial summation curves. As for the detection thresholds, the area-threshold functions for the recognition data were invariant in shape with retinal locus, varying only in their position on the size axis. In Figure 2.19, scaling factors have been determined by eye as the amount of shift along the x-axis the peripheral data curves require to superimpose them on the foveal data. The shift is expressed in terms of relative size for their respective eccentricities.

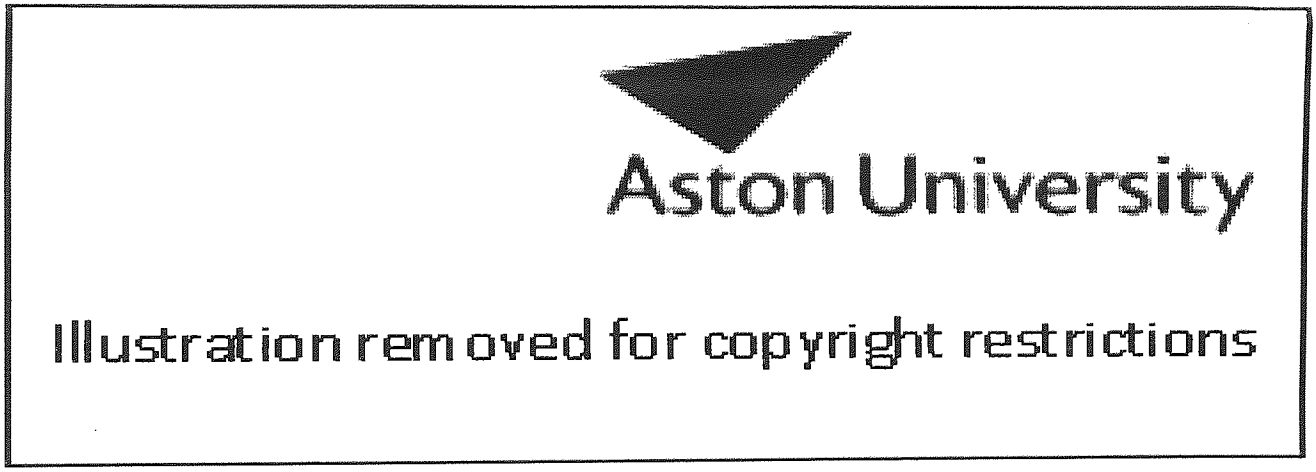

Figure 2.19. From Lie (1980). Scaling factors for resolution data in nasal visual field, expressed in terms of relative size shift, and plotted against eccentricity. The regression fitted to the data is log F = log (1) + log (1 + (E / 8.03)).

The regression fitted to the data is of the form of Equation 2.10, and is:

$$\log F = \log (1) + \log (1 + (E / 8.03))$$

so that E_2 is 8.03 ± 0.61 deg for the nasal visual field. Lie noted an isosensitivity plateau in his data between 12 and 21 deg eccentricity, as for the detection data. Lie's data for detection in the same meridian gives an E_2 of 8.79 deg, a similar value. One

point of note is that Lie's resolution task, discriminating between a square and a diamond, is rather different to the other types of resolution task detailed in this review and may contribute to the rather high E_2 value found.

The task in the study of Farrell and Desmarais (1990) was that of digit recognition of stimuli presented for a short time (10 ms), with a Michelson contrast of 72%. From their data, target size giving 50% threshold has been calculated for four observers. Mean threshold target size is shown as a function of eccentricity in Figure 2.20. The E_2 value found by this method is 0.27 ± 0.04 deg. This value is small in comparison to other estimates of the eccentricity related decline in recognition thresholds. Relevant factors may be the very short duration of their stimulus, and the uncertainty produced by the absence of a foveal data set.

Figure 2.20. From Farrell and Desmarais (1990). Mean threshold target size as a function of eccentricity. The regression fitted to the data is log (size) = 0.20 + log (1 + (E / 0.27). E_2 is 0.27± 0.04 deg.

Strasburger, Harvey and Rentschler (1991) also used the task of digit recognition in their examination of peripheral visual acuity. However, rather than varying size at high contrast to find acuity, contrast thresholds were found for targets of varying size. One experiment involved presentation of single digits binocularly in the left visual field at eccentricities 0-12 deg. The authors plotted their contrast vs size data on log-linear axes, from which they found that the functions had similar shapes, shifted towards

larger sizes at greater eccentricities, but that maximum sensitivity reduced with increasing eccentricity. This led them to conclude that 'the relative inferiority of peripheral vision could not be fully compensated for by making alphanumeric targets larger'. However, Figure 2.21a shows the data of their observer MB replotted on log-log axes. Plotting the data in this way shows that the series of functions for different eccentricities are merely displaced from one another along the size axis. The various eccentricities may be scaled relative to the data at 0 deg in the same manner as for the data of Lie (1980), and Johnson et al. (1978) shown above. A regression relating the resultant scaling factors to eccentricity (not shown) is of the form $\log F = \log (1) + \log (1 + (E / 1.57))$, and so E_2 is 1.57 deg. In Figure 2.21b, the data of 2.21a has been scaled at each eccentricity by dividing the size by a scaling factor derived from the equation:

$$SF = 1 + E / (1.57)$$

This collapses the data to a single function, removing the majority of the eccentricity dependence from the data. Similar evaluation for observer KZ results in an E_2 value 1.31 deg.

Table 2.01 summarises the E_2 values found for various resolution and recognition tasks. The values found vary between 0.27 and 8.03 deg, but the majority of values lie between 1 and 2.5 deg. Several obvious sources of variation may help to explain the inter-study variability. The use of different meridia will result in different E_2 values (Wertheim, 1891). The number of observers varies between single subjects (eg. Green, 1970) and large groups (eg. Low, 1951). Exposure duration varies from 10ms (Farrell and Desmarais, 1990) to unlimited viewing time (Lie, 1980). The target stimuli used vary considerably from squares (Lie, 1980), to Llandolt rings (eg. Weymouth, 1958), to letters (Anstis, 1974). Given these variables, it is perhaps unsurprising that the values calculated span such a large range.

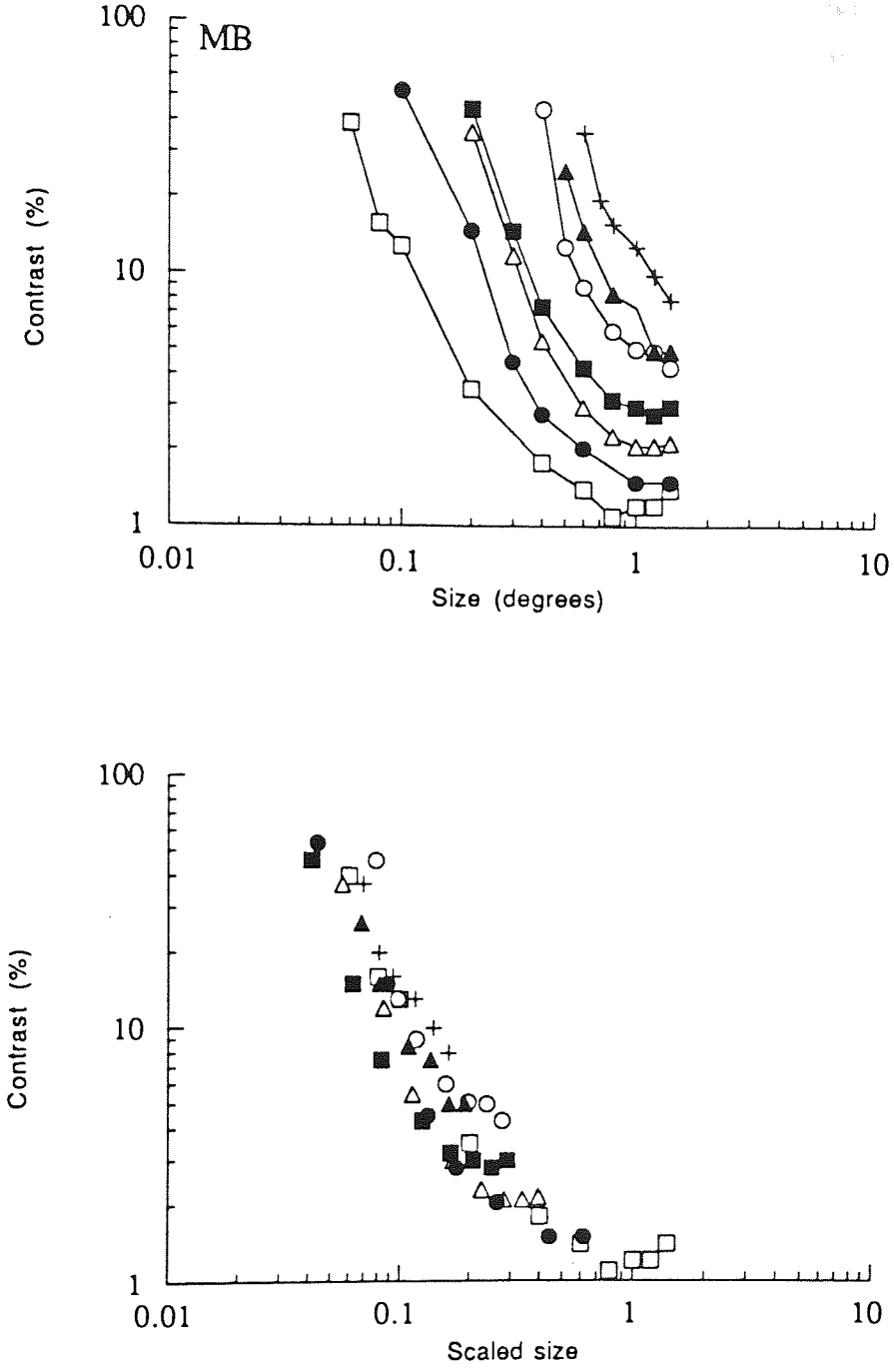

Figure 2.21. Data from Strasburger et al. (1991), observer MB, left visual field. a. Contrast thresholds for digit recognition, plotted against digit size. Open squares: 0 deg; closed circles: 2 deg: open triangles: 4 deg; closed squares: 6 deg; open circles: 8 deg; closed triangles: 10 deg; crosses: 12 deg. b. Data of a, scaled on the x-axis according to the equation: SF = 1 + (E / 1.57).

Authors	Target type	E_2	Ecc range	Meridian	Notes
Wertheim (1891)	Square grating	2.36 2.12 1.59 1.54	0-30 0-30 0-20 0-20	Temporal Nasal Superior Inferior	
Low (1951)	Llandolt ring	2.93	0-30	Temporal	
Weymouth (1958)	Llandolt ring	1.35	0-20	Nas/Temp	
Randall et al. (1966)	Llandolt ring	1.79	0-20	Nasal	
Sloan (1968)	Llandolt ring	1.32	0-10	Nasal	
Green (1970)	Sine wave grating	1.32 2.53	0-8	Temporal	subject RA subject DG
Anstis (1974)	Letters	0.91	4-28		Binocular
Millodot & Lamont (1974)	Llandolt ring	4.7 2.58	0-15	Inferior Superior	
Johnson et al. (1978)	Incremental squares/ circles	3.11	0-20	Nasal	
Jacobs (1979)	Llandolt ring	1.15	0-10		
Westheimer (1979a)	Grating	3.07 2.11	0-18 0-15	Binocular	subject 1 subject 2
Lie (1980)	Incremental square orientation	8.03	0-45	Nasal	
Farrell & Desmarais (1990)	Digit recognition	0.27	1.9-8.1		
Strasburger et al. (1991)	Digit recognition (contrast threshold)	1.57 1.31	0-12	Left visual field	subject MB subject KZ
Toet & Levi (1992)	Letter orientation	2.04	0-10	Inferior	

Table 2.01. E_2 values for resolution.

2.4 Localisation and hyperacuity

Relative localisation acuities represent the ability to assign location to a feature. Under optimal conditions, the relative positions of two features can be judged with a precision substantially smaller than the size of a foveal cone, and are the most precise spatial discriminations that the human eye can make.

In order to achieve localisation precision of greater accuracy than the underlying receptor mosaic, responses are weighted from the photoreceptors on which the retinal

image distribution falls. A certain amount of blur of the retinal image is therefore necessary to spread the image over a number of receptors, allowing weighting of the responses and interpolation of location. If the retinal image were to fall completely within one receptor, interpolation between receptors would be impossible, and localisation would be limited by the size of the receptors. However, the optics of the eye are such that the retinal image of even a very thin line or point of light is spread to form a 'line spread function' (Campbell and Gubisch, 1966). The line spread function has a width at half height of about 1 min arc, enough to cover several photoreceptors. The accuracy of positional judgements is also aided by a high degree of regularity in the arrangement of photoreceptors.

Thresholds for relative localisation tasks under optimal conditions may be 4-10 sec arc: far less than the resolution limit of approximately 30 sec arc set by optical and retinal qualities. Due to the exceptional sensitivity of the visual system to such tasks, they have been termed 'hyperacuities' (Westheimer, 1975). The original definition of hyperacuity was based on threshold magnitude. However, localisation tasks which give hyperacuity thresholds under optimum conditions may give significantly poorer thresholds, more akin to those of resolution, if the stimulus parameters change. For example, detection of the offset of two abutting lines (vernier acuity) has a foveal threshold of about 5 sec arc (Westheimer and Hauske, 1975; Westheimer and McKee, 1977b). However, offset discrimination for lines which are separated by some amount, or positioned in peripheral visual field (Westheimer, 1982) rise dramatically. Under the original definition, these thresholds would not be considered to be hyperacuities although the same localisation mechanism is used to determine threshold in each case. In this thesis, the term hyperacuity is used to define those spatial configurations where threshold is determined by a relative localisation mechanism, even though the absolute threshold may be no better than the optimum resolution acuity. This enables the term to be applied to spatial judgements across the visual field.

To highlight the differences between resolution and localisation, Figure 2.22 illustrates both tasks for horizontal separation of two features which decreases on moving from left to right in the figure. Resolution soon becomes impossible, but the relative offset can be detected long after resolution has failed.

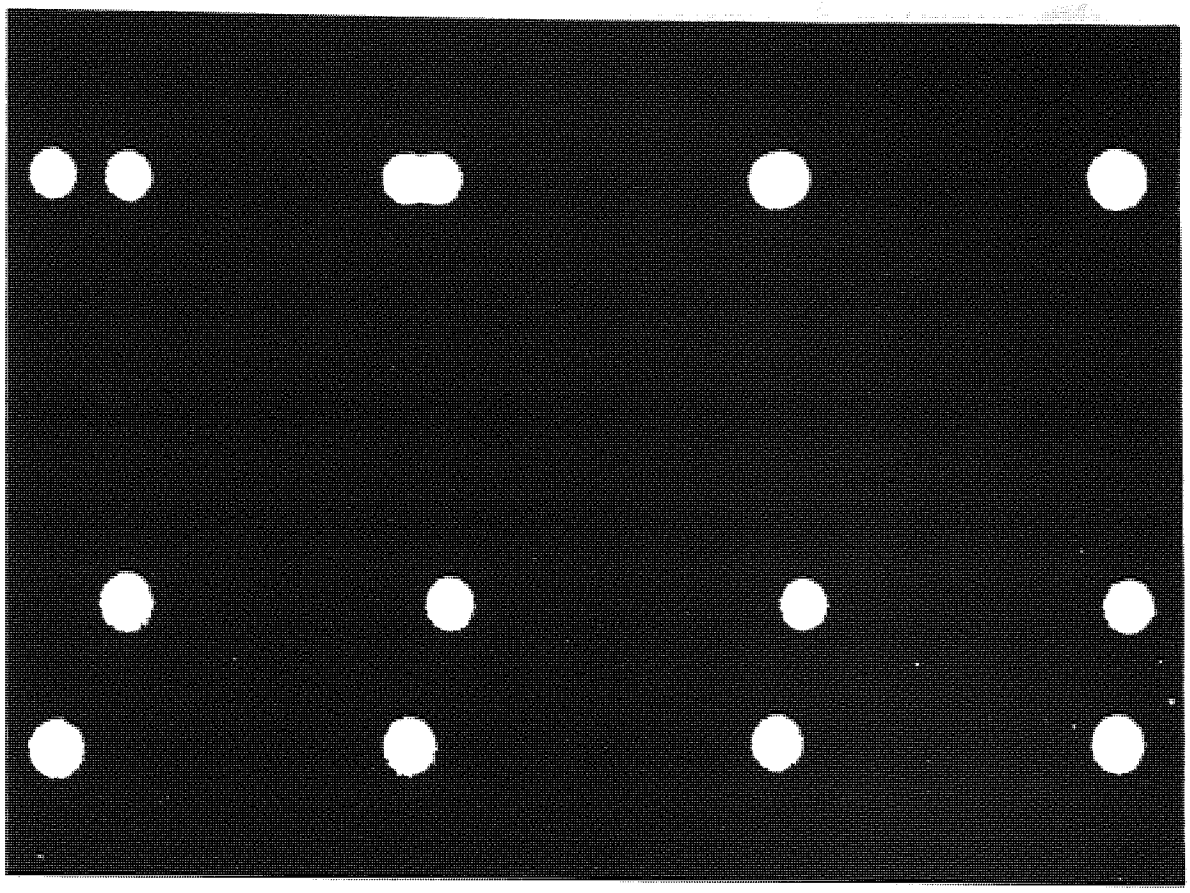

Figure 2.22. A resolution stimulus (upper row) and a localisation stimulus (lower row), pictured with the separation between the elements decreasing on moving from left to right in the picture. The reduction in separation soon makes resolution impossible, yet the offset of the localisation stimulus is still apparent at separations for which resolution is not achieved.

Many types of target configuration can be used to measure hyperacuities. The most common types are shown in Figure 2.23 (after McKee, 1991). For the vernier target, the observer judges whether the upper line or dot lies to the left or the right of the lower feature. For orientation, the observer judges if the line is tilted to the left or right. For curvature, the judgement is whether the curve is more or less curved than some mean value. In spatial interval discrimination, the choice is whether the separation is larger or smaller than some mean value. In bisection acuity, the observer judges whether the test line is closer to the left or right reference line. For displacement, the judgement is whether the test target has moved left or right with respect to the reference. In stereoacuity, the observer judges whether the test line is in front of or behind the reference. Some of the factors affecting hyperacuity thresholds are now discussed.

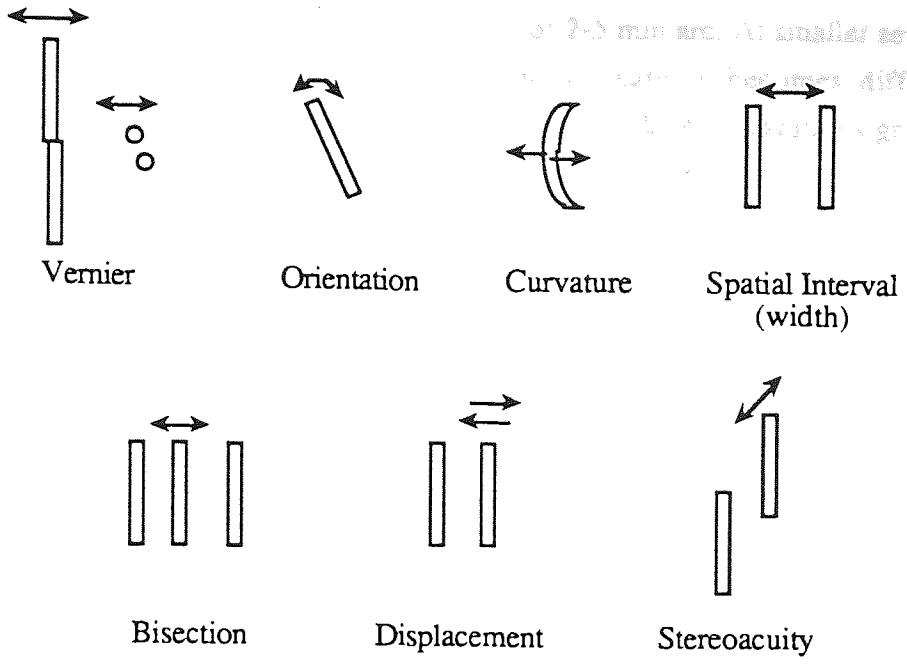

Figure 2.23. Hyperacuity configurations. After McKee, 1991.

2.4.1 Factors affecting localisation

Stimulus features

The choice of features to be compared in relative localisation tasks has little effect on thresholds. For vernier stimuli, alignment thresholds are similar whether the comparison is made between dots, lines, or locations implied by a gap in a long line. The features do not even need to have the same orientation, with comparable thresholds obtained for alignment of a line and a chevron (Westheimer and McKee, 1977b). Further, thresholds are independent of the length of abutting line vernier stimuli once the length is longer than 5 min arc. Thresholds are higher for shorter lines. However, introduction of an appropriate gap of 2-5 min arc between the two stimulus elements results in thresholds which are equally good for all line lengths (see Figure 2.24). In other words, alignment acuity can be as good with two dots as with two lines (Westheimer and McKee, 1977b). In spatial interval discrimination tasks, the interval can be demarcated by two dark or bright dots, lines, bars or edges. The choice of feature has no effect on thresholds (Westheimer and McKee, 1977b), unless the test and reference are of opposite polarities (Levi and Westheimer, 1987).

Separation

The separation between two objects which are to be localised can affect thresholds. Vernier alignment thresholds for stimuli of different lengths are shown as a function of separation in Figure 2.24 (from Westheimer and McKee, 1977b). Regardless of line length, thresholds yield an optimum value of around 5 sec arc provided that the

separation between the elements is in the order of 2-5 min arc. At smaller separations, separating the stimulus elements into individual features becomes difficult and thresholds rise, representing a resolution limit to the task. At separations greater than the optimum, alignment thresholds increase, giving rise to an overall U-shaped function.

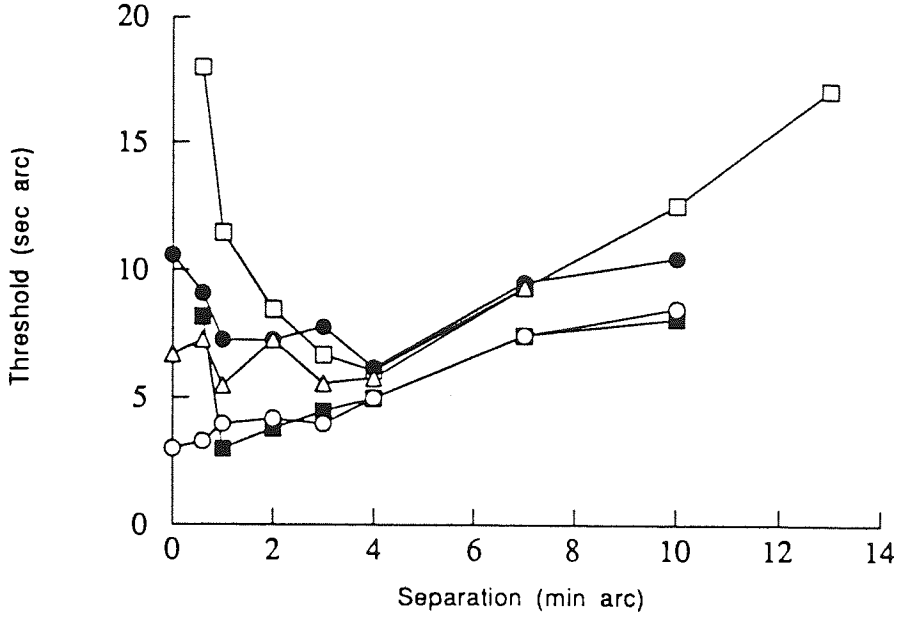

Figure 2.24. From Westheimer and McKee, 1977b; their Figure 2. Vernier alignment thresholds for stimuli of different length as a function of feature separation. Symbols: open squares: observer LK, line length 30 sec arc (dots); closed circles: LK, 2 min arc; open triangles: LK, 4 min arc; closed squares: observer SM, 30 sec arc (dots); open circles: SM, 8 min arc.

A similar dependence of thresholds on feature separation is shown for spatial interval discrimination tasks (eg. the closed circles of Figure 2.26). Above a certain optimum separation, the just noticeable difference in separation rises in proportion to the separation itself. In other words, thresholds obey 'Weber's law' (Equation 2.01) for position. For spatial interval stimuli centred on the fovea, neither stimulus element actually falls on the fovea, but at some eccentricity defined by the separation of the features. Is the noted increase in threshold due to increased separation, or to the inevitably associated increase in eccentricity? Several studies have examined this question (Levi, Klein and Yap, 1988; Levi and Klein, 1989, 1990a, 1992; Morgan and Watt, 1989; Burbeck and Yap, 1990b; Hess and Hayes, 1993), which is discussed in greater detail in Chapter 11.

'Weber's law' goes further than just having relevance to the separation between independent objects. It also relates to size judgements, since the impression of the size of an object may be gained by estimating the separation of its edges. Consider two objects which can just be discriminated in size at a given viewing distance. If the viewing distance changes, 'Weber's law' predicts that the size of the objects will still be just discriminable, since both the absolute size and the difference in size of the two objects have changed by the same proportion. This situation is known as 'scale invariance' (Jamar and Koenderink, 1983; Toet, Snippe and Koenderink, 1988b) and its effect is to allow us to maintain a subjectively stable world irrespective of our position within it.

Eccentricity

Leaving aside for a moment the confounding effects of stimulus separation, the effects of eccentricity on hyperacuity thresholds are now considered. This topic is covered in greater detail in Chapter 4, and also Chapter 6. It is well documented that localisation thresholds rise with eccentricity at a faster rate than do resolution thresholds (eg. Westheimer, 1982; Levi et al., 1985; Whitaker et al., 1992a,b).

Levi et al. (1985) established an E_2 value for repetitive vernier stimuli (ie. alignment of grating stimuli) in the order of 0.6-0.8 deg (see Chapter 4), which correlated well with analyses of other hyperacuities such as stereoacuity and phase discrimination. Their findings suggested that all localisation acuities might vary with eccentricity in a similar manner. The small E_2 values obtained, indicating a relatively rapid rise in thresholds with eccentricity, compare with E_2 values for grating acuity which have been shown earlier in this chapter to be in the order of 1.5-3 deg. The conclusion of Levi et al. (1985) was that the rate of change of performance for grating acuity reflected retinal limitations, while the change in hyperacuity thresholds represented cortical limitations.

Toet, Snippe and Koenderink (1988a) compared thresholds across eccentricities for a three blob alignment task using Gaussian stimuli (see Figure 11.03) at contrast detection threshold. The three stimuli were arranged vertically with the separation of the two outer blobs being proportional to their spatial spread, or blur parameter. Eccentricity was varied by moving the stimulus arrangement along the horizontal meridian, and at each eccentricity thresholds were obtained for a series of blur parameters. Thresholds could be made equal across the visual field with an E_2 value of approximately 0.1 deg.

McKee, Welch, Taylor and Bowne (1990) examined the effect of eccentricity on various hyperacuity tasks using similar stimuli. Results are shown in Figure 2.25 for stereoacuity, for abrupt motion displacement in the presence of a reference, and for a 'paired width' task, or spatial interval task in the presence of a reference standard with a small standard separation (less than 10 min arc). All types of threshold can be seen to rise in approximately the same way with eccentricity. Averaging this data, an E_2 of 0.94 deg was derived for this subject, consistent with Levi et al.'s (1985) hypothesis.

Figure 2.25. From McKee et al., 1990; their Figure 5. Hyperacuity thresholds as function of eccentricity. Observer WAM. Symbols: open squares: stereoacuity; closed circles: motion displacement; open triangles: paired width discrimination.

Whitaker et al. (1992a,b) have since demonstrated differences in the rate of decline of hyperacuity performance between different tasks. Values vary from 0.07 deg for bisection acuity to 1.95 deg for orientation discrimination. These differences are detailed in Chapter 4.

Hess and McCarthy (1994) compared resolution acuity with that for a spatial order localisation task across eccentricities. The spatial order task involved discrimination of one of three bars which had previously been labelled by a contrast or flicker variation. The acuity for spatial order was comparable to that for resolution at the fovea, but fell more sharply with eccentricity. The authors argued that the acuity for spatial order was set by the fidelity of the ordering of detectors in the projection from retina to cortex,

while resolution was determined by the sampling density of the detectors. Their results therefore suggest that topological disorder increases with eccentricity, limiting localisation ability but not resolution.

Contrast

Variation in contrast appears to affect localisation thresholds in one of two ways. For some tasks, thresholds improve with increasing contrast over most of the visible range, following a power law with an exponent of -0.4 to -0.5 (McKee, 1991). Tasks falling into this category include vernier acuity for abutting stimuli or having a separation of around 6 min arc (Watt and Morgan, 1983; Morgan and Regan, 1987; Wehrkahn and Westheimer, 1990; Waugh and Levi, 1993b), curvature detection (Hess and Watt, 1990), and stereoacuity (Legge and Gu, 1989). For other tasks, thresholds improve with increasing contrast only to approximately 2-3 times their contrast detection threshold, and then become invariant of any further increase in contrast. Tasks falling into this latter category include orientation discrimination for gratings (Regan and Beverley, 1985), spatial frequency discrimination (Regan, 1985), vernier acuity for widely separated targets (Waugh and Levi, 1993b), and spatial interval discriminations (Morgan and Regan, 1987).

Morgan and Regan (1987) directly compared the effects of contrast between 10 and 75% on a vernier task and a spatial interval task, using Gaussian line stimuli. They showed that vernier thresholds were contrast dependent to an approximate square root relationship both for abutting stimuli and those separated by a 6 min arc gap. Interval discrimination thresholds for 5 or 10 min arc standard intervals showed very little dependence on contrast.

Waugh and Levi (1993b) examined the effects of contrast on vernier targets as a function of target separation. For targets separated by more than 4 min arc, thresholds were contrast independent above 3 times detection threshold. For abutting lines and separations of only 2 min arc, thresholds decreased with increasing contrast to 30 times the detection threshold.

These studies suggest that the mechanisms underlying position acuity at close and wide separations are different. Possible mechanisms and further evidence regarding the dependence of position thresholds on contrast are examined in Chapter 11.

Blur

The effect of blur on resolution thresholds is obviously detrimental. With relative localisation tasks, the effect of blur is not so clear cut. Williams, Enoch and Essock (1984) examined the effects of blur on vernier thresholds. For abutting lines, or two dots separated by a small amount, blur degraded thresholds. Note that small separations are the conditions under which hyperacuities are generally optimum, and blur does degrade performance here. For two dot acuity at relatively wide separations however, thresholds were independent of blur. Williams et al. (1984) argued that since these thresholds were blur resistant, the stimulus configuration could be used to identify post-optical defects in the presence of media opacities.

Toet, van Eekhout, Simons and Koenderink (1987) measured three blob displacement and alignment thresholds using Gaussian blob stimuli at their contrast threshold. At contrast threshold, the blobs activate only a small range of spatial frequency mechanisms, and therefore provide a precise measure of the resolution of the stimuli. Localisation thresholds were found to increase in proportion to blur, when the separation of the outer blobs of the stimulus was maintained at a constant ratio of ten times the blur parameter. When both blur and separation were varied, results depended on the separation. At separations less than 25 times the blur parameter, alignment thresholds were independent of separation but dependent on blur, while bisection thresholds increased with increasing separation. At separations greater than 25 times the blur parameter, both types of threshold exhibited Weber behaviour with respect to stimulus separation. The results for the alignment task concur with the observations of Williams et al. (1984). It was concluded that the mechanisms computing localisation are independent of the level of feature resolution, or scale-invariant. It also appeared that thresholds are computed on a different basis at large and small separations, regardless of the blur parameter.

Duration

For highly visible vernier stimuli, increasing exposure duration does not improve thresholds (Westheimer and McKee, 1977a). However, low contrast vernier stimuli do benefit from increased exposure duration, since temporal summation improves their visibility (Waugh and Levi, 1993a).

Westheimer and Hauske (1975) showed that so long as the two elements of a vernier stimulus are presented together, an exposure duration of as little as 50 msec can give thresholds in the order of 6 sec arc. At this short exposure duration however, thresholds were susceptible to interference from items presented after the stimulus. At

longer exposure durations, thresholds were free of temporal interference effects. If the two lines of the vernier stimulus were presented with onset asynchrony, at least 250 msec of simultaneous exposure was required to maintain thresholds.

Manipulation of exposure duration has been used by Burbeck and her colleagues to examine the processing time required by various hyperacuity configurations, leading to a better understanding of the mechanisms involved. For spatial interval tasks, exposure duration effects are separation dependent. For separations greater than 25 min arc, exposure durations of longer than 150 ms have little effect on thresholds. At smaller separations, increasing exposure duration improves thresholds at least up to 400 ms duration (Burbeck, 1986; Burbeck and Yap, 1990b). The effect of exposure duration is not primarily due to object separation however, but to the spatial frequency content of the objects (Burbeck, 1986). It was shown that for large separations, the use of high spatial frequency stimuli makes thresholds again dependent on duration to 400 ms. Similarly, Burbeck and Yap (1990a) showed that interval discrimination thresholds for a widely separated pair of bars were independent of duration from 100-500 ms. By addition of flanking bars, thresholds were raised more for 100 ms duration than for 500 ms. This effect was explained by proposing that under cluttered conditions, higher spatial frequency filters determined thresholds than when the bars were isolated. From these studies it appears that around 150 ms of processing time is required to achieve hyperacuity performance. Increasing exposure duration above this level will only improve high spatial frequency responses.

Manipulation of exposure duration has been shown to have a different effect on bisection thresholds to that for spatial interval discrimination (Burbeck and Yap, 1990c). Bisection thresholds improve more with increase in exposure duration, which supports a description of bisection discrimination in which the two separations in the bisection task are encoded separately and then compared.

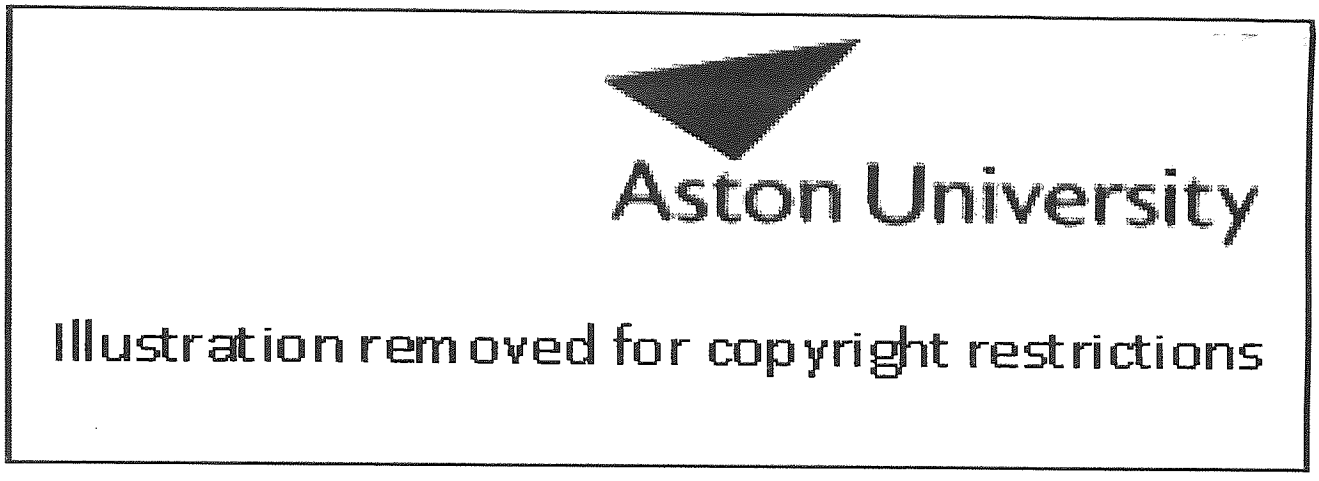

Figure 2.26. After Westheimer, 1979b. Spatial interval discrimination thresholds as a function of baseline separations for three modes of stimulus presentation. Open squares: sequential presentation of reference and test lines; closed circles: single presentation with internal standard; open triangles: sequential presentation of entire stimulus with no temporal delay.

The importance of temporal factors in the mode of presentation of a spatial interval discrimination task was highlighted by Westheimer (1979b), shown in Figure 2.26. The two features comprising the stimulus may be presented sequentially in that only the reference line is shown for defined period, which then disappears and is replaced by the test stimulus. Using this configuration, thresholds rise markedly when the baseline separation of the features is more than 2 min arc. Alternatively, an 'internal standard' may be built up by the observer. In this case an indication can be made from a single simultaneous presentation of reference and test line whether a test gap was smaller or larger than that of the standard (Westheimer and McKee, 1977b; Westheimer, 1979b; Burbeck, 1986; Levi and Westheimer, 1987; Morgan and Regan, 1987). Such internal standards are easy to develop (Westheimer and McKee, 1977b). Under such conditions, discrimination thresholds are optimum for separations of 2-8 min arc, but are higher at larger and smaller separations, displaying a characteristic U-shaped function. As another alternative, the entire standard stimulus can be displayed prior to the test stimulus, either with (Levi and Westheimer, 1987; Morgan and Regan, 1987; Burbeck and Yap, 1990b) or without (Westheimer, 1979b) a temporal delay between the successive presentations. If there is no delay between presentation of the standard

and the test stimulus, then the task can be considered to be an instantaneous movement displacement task with references. Under these conditions, thresholds remain low over a wide range of separations.

Spatial Interference

For foveal abutting vernier stimuli, thresholds are raised if other features are placed within 8 min arc of the stimulus, with maximum interference caused when flanks are between 2 and 4 min arc from the target (Westheimer and Hauske, 1975; Levi et al., 1985). Additionally, maximum interference occurs in the direction of vernier offset (Levi et al., 1985). These interference effects are not determined at the retinal level, since they occur even under dichoptic conditions where target and flanks are presented to different eyes (Westheimer and Hauske, 1975; Levi et al., 1985).

In an exhaustive set of data, Levi et al. (1985) extended the basic observations above to several locations in the visual field. At any eccentricity, the extent of interference was shown to be the same relative to the unflanked vernier threshold: maximum interference occurs at 25-30 times the unflanked threshold, while complete isolation occurs at 50-60 times the threshold distance. The results were explained in terms of psychophysical processing modules or 'perceptive hypercolumns', which have a constant cortical extent. At each eccentricity, vernier thresholds are 1/40th of a perceptive hypercolumn. Spatial interference occurs when flanks fall in the same, or adjacent, perceptive hypercolumns as the target.

Consistent with the data of Westheimer and Hauske (1975) are the findings of Toet and Koenderink (1989) who examined spatial displacement thresholds for alignment of three Gaussian blobs in the presence of interfering stimuli. The flanking elements did not affect thresholds except at very small spreads of the Gaussian blobs, when stimuli placed within ten times the blur parameter of the Gaussian envelope severely affected thresholds.

Practice

The effects of practice on hyperacuity tasks can have a profound effect on thresholds. McKee and Westheimer (1978) showed that for foveal vernier acuity, thresholds improve with practice until 2000-2500 responses have been made. Similarly, at locations of 0-10 deg eccentricity, Fendick and Westheimer (1983) found that stereoacuity thresholds and standard errors decrease with practice over about 3000-4000 trials. The magnitude of the peripheral threshold improvement was between 60 and 80%.

2.5 Summary

In this chapter the rich variety of stimuli available with which to investigate vision have been introduced, along with some of the factors which affect them. In this thesis, examples of detection, resolution and hyperacuity stimuli have all been used to examine visual performance with eccentricity.

Chapter 3
The Visual Pathway

3.1. Introduction

The purpose of this chapter is to provide an overview of the visual pathway, and to identify those anatomical and physiological factors which may limit foveal and peripheral vision at various stages.

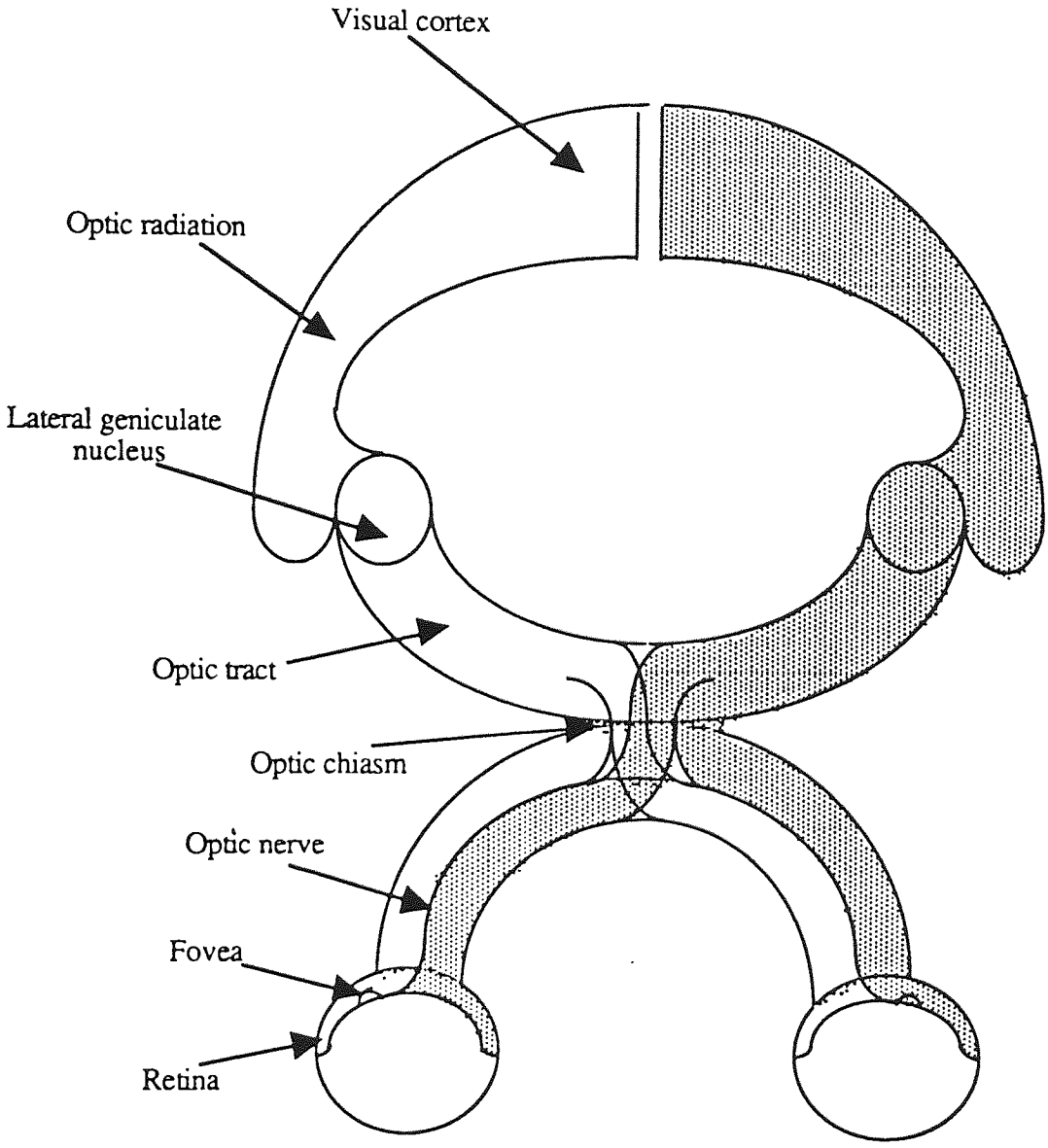

Figure 3.01 is a schematic diagram of the geniculo-striate visual pathway. Note that the fibres from nasal retina decussate at the optic chiasm, such that each cortical hemisphere receives input from the contralateral visual field.

The geniculo-striate pathway is followed by 90% of axons leaving the eye (Perry, Oehler and Cowey, 1984) and is shown in Figure 3.01. Light enters the eye through the cornea, and is focussed to a clear image at the retina in the emmetropic eye. Light energy is transformed to a neural signal by the photoreceptors, and this signal passes to the ganglion cells. The signal continues up the optic nerve to the optic chiasm and on to the lateral geniculate nucleus (LGN). The signal passes up the optic radiation to the striate cortex. From the visual cortex, signals pass to many other extra-striate cortical areas. The preceding structures are dealt with in more detail in the following sections. The remaining 10% of cells follow a path to the cortex via the superior colliculus (Perry et al., 1984).

3.2 Retina

The retina forms the inner coat of the eye, and contains the image plane of the eye's optical system. Its purpose is to translate light into nerve signals, which are transmitted to the brain for interpretation. The efficiency of this process, or the resultant spatial resolution, varies greatly with retinal location.

3.2.1 Retinal sampling

Sampling is an operation whereby a continuous signal is measured only at a finite number of separated points. Any signal can be represented as a combination of sine waves, often described by decomposing the waveform into its constituent sinusoids by Fourier analysis. In the case of the visual system, the array of sampling points might be considered to be the photoreceptors, or any subsequent array of neurons in the visual pathway.

In order to unambiguously reconstruct a sine wave, there must be at least one sampling point for every half-cycle of the sine wave (Williams, 1985). The highest frequency which can be unambiguously reconstructed is known as the Nyquist limit (Nyquist, 1919). A sine wave sampled at the Nyquist limit is shown in Figure 3.02a. At frequencies higher than the Nyquist limit, a sine wave is undersampled by the array. Such a situation is shown in Figure 3.02b. The resultant waveform is seen as a sine wave of lower frequency than that of the signal, and is called an alias.

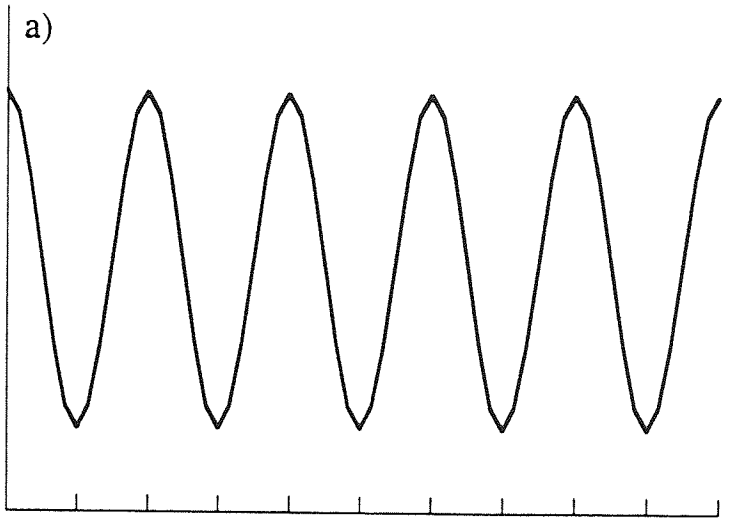

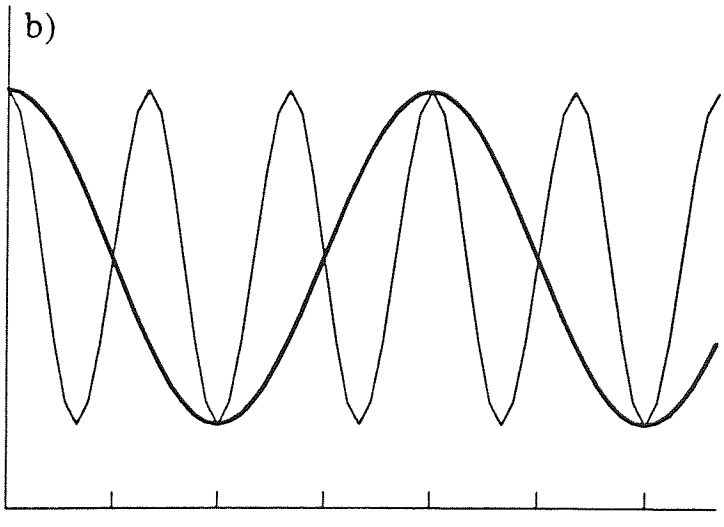

Figure 3.02. Sampling of a sine wave by a one dimensional sampling array. a. A sine wave sampled veridically at its Nyquist limit. b. The same sine wave sampled by a coarser array such that the frequency of the sine wave is greater than the Nyquist limit. A waveform of lower spatial frequency than that of the signal is observed (heavier line).

The above description assumes that the sampling array is regularly spaced. Irregularity in the sampling array compromises its resolution by the introduction of white noise and demodulation of the signal.

3.2.2 Optical quality of the eye

In order to produce an image on the retina which can be sampled, a luminance signal must pass through the optical system of the eye. The process of forming such an image inevitably results in a retinal stimulus which is degraded in comparison to the external stimulus. Aberrations which decrease retinal image quality include spherical and chromatic aberrations along the optic axis, and additionally oblique astigmatism, coma and distortion in the periphery (Charman, 1991).

Image quality can be quantitatively described by the modulation transfer function (MTF) which describes the percentage of contrast actually present in an incoming luminance signal which is retained in the retinal image, as a function of spatial frequency (eg. Campbell and Green, 1965). Under optimal conditions for images formed along the optic axis, all contrast is maintained in the image at low spatial frequencies, but the amplitude of the MTF declines with increasing spatial frequency, and is zero by approximately 60 cycles per degree. In other words, at the fovea the eye acts as a low pass filter with a high frequency cutoff of 60 cpd (Campbell and Gubisch, 1966; Williams, 1985).

Optical quality away from the optic axis remains essentially constant with a high frequency cutoff of 50cpd within 30 deg of the fovea, and then decreases to 40cpd at 40 deg (Jennings and Charman, 1981). Other factors of increasing importance to image quality with eccentricity include increased light scatter (Gorrand, 1979) and increased oblique astigmatism. Refractive correction of peripheral oblique astigmatism does not improve peripheral visual acuity (Millodot, Johnson, Lamont and Liebowitz, 1975), although it has been reported that motion thresholds (Liebowitz, Johnson and Isabelle, 1972) may be improved by peripheral correction. Such improvement was not found by McKee and Nakayama (1984) however.

It should be noted that image quality is highest along the optic axis. The fovea is placed on the visual axis, some 5 deg temporal to the optic axis. Therefore, in nasal retina image quality is superior to that in temporal retina. Additionally, anatomical retinal cell densities are higher in nasal retina (see below), and psychophysical observations show a naso-temporal asymmetry in performance (eg. Wertheim, 1891; Fahle and Schmidt, 1988).

3.2.3 Laminar retinal organisation

Under light microscopy, the retina can be seen to consist of ten distinct layers, the basic structure being a layer of photoreceptors, leading to three layers of nerve cell bodies, separated by two plexiform layers containing synapses made by the axons and dendrites of these cells. A further layer of ganglion cell axons carries the resultant nerve fibres out of the eye (Figure 3.03). Notice that the photoreceptors are the deepest layer, pointing backwards, and that light has to pass through all the preceding layers before stimulating the receptors. Figure 3.03 shows the retinal structure in the near periphery (after Polyak, 1957). In man, this laminar arrangement is interrupted in the central retina to form the fovea. The fovea is a shallow rounded depression of 1.5mm diameter (Davson, 1990) lying on the visual axis, from which all internal retinal layers are laterally displaced from the central 350μm (Davson, 1990). This allows light to fall directly onto the photoreceptors, which is of critical importance in this area of finest form vision.

3.2.4 Photoreceptors

The photoreceptor mosaic provides all the spatial information available to higher levels of visual processing and imposes fundamental limits on the range of spatial frequencies available to the retina. The human eye contains two types of photoreceptor: rods are sensitive to very low light levels and are the receptors of scotopic vision, while cones are involved in photopic vision. Each photoreceptor consists of an outer segment containing photopigment, an inner segment, a cell body and a synaptic terminal. The photopigment of each photoreceptor is visual purple, or rhodopsin, which is bleached on exposure to light, and becomes reformed as a photochemical response. In rods the rhodopsin is maximally sensitive to light of 496nm wavelength. There are three types of cones, each containing photopigment maximally sensitive to 420, 530, or 565 nm (Dartnall, Bowmaker and Mollon, 1983; Bowmaker, 1991), and thus allowing the retina to be spectrally sensitive.

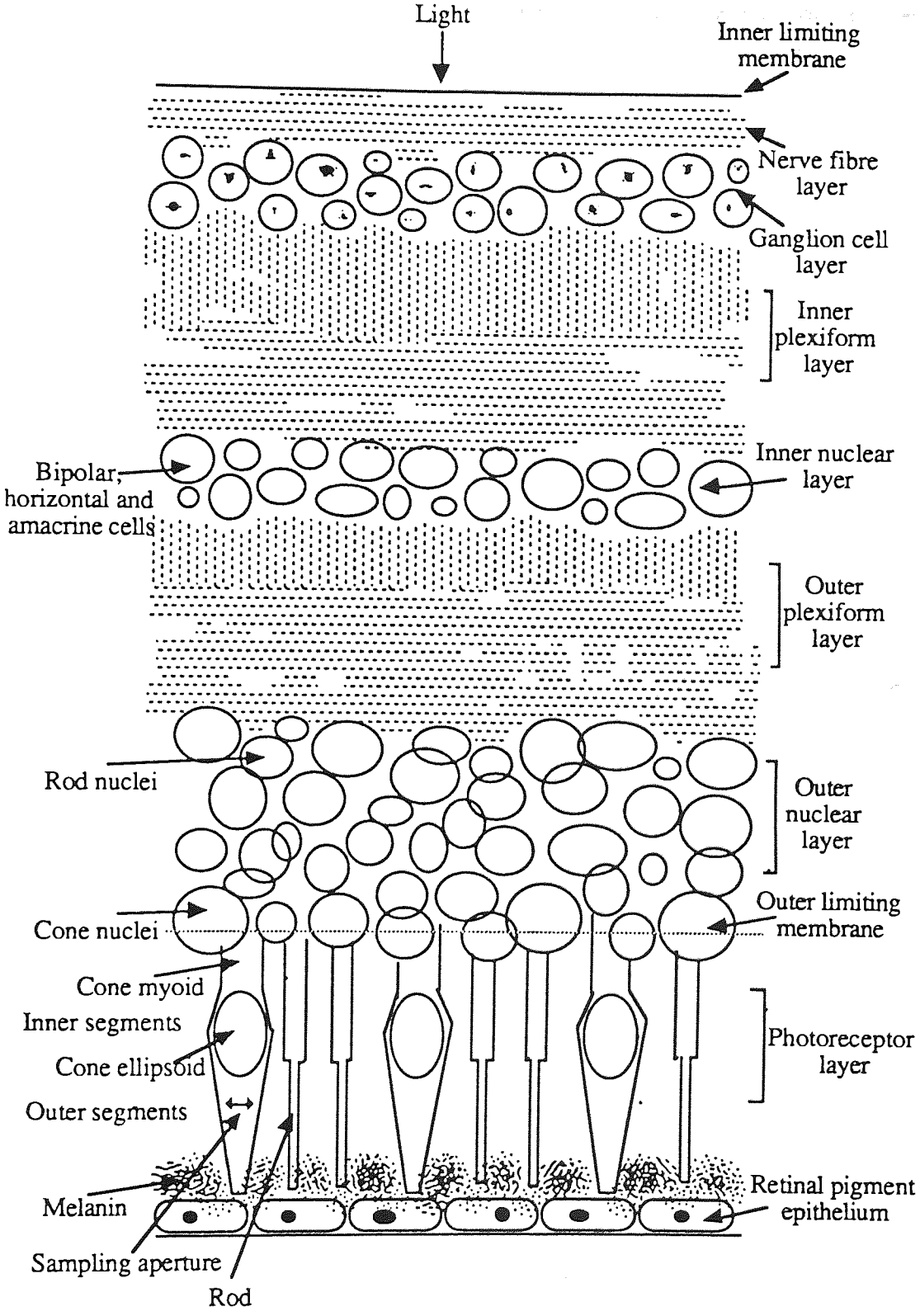

Figure 3.03. Laminar construction of the retina in a parafoveal region. After Polyak (1957).

As mentioned above, photoreceptors form the innermost layer of the retina, and for light to reach them, it must first pass through all the other layers of the retina, except in the central fovea where the other layers are displaced. The refractive index of the outer segment is significantly higher than that of the surrounding medium, and so light is guided down the photoreceptors towards the photopigments by total internal reflection. The photoreceptors thus act as optical waveguides to capture as much incoming light as possible (Enoch, 1961; Rowe, 1991).

There are approximately 100 million photoreceptors in each human retina. Their topographical distribution was first described in detail by Østerberg (1935), and more recently an extensive study has been reported by Curcio, Sloan, Kalina and Hendrickson (1990). The average total number of cones in the eye is 4.6 million. The peak cone density is found at the centre of the foveal area, with an average value of 199,000 mm^{-2}. The cones are arranged in a regular two dimensional lattice with an approx. spacing between rows of 0.5 min arc, and an observed cone Nyquist limit, of 66.3cpd. In other words, foveal cones adequately sample all spatial frequencies passed by the optics (Rowe, 1991; Anderson, Mullen and Hess, 1991). Peak cone density values are highly variable, varying over 3 fold between individuals. However, within the central 5mm, all retinas have approximately the same number of cones, which are distributed differently. This is thought to reflect variability in the migration of cones during development, and ties in with the variation in peak psychophysical resolving power of the eye between individuals (Hirsch and Curcio, 1989; Rowe, 1991).

Moving away from the fovea, cone density initially declines precipitously, falling by an order of magnitude within 1mm of the foveal centre. The decline is fastest in vertical rather than horizontal meridia. Within the central millimetre, nasal and temporal retinal cone densities fall at the same rate. Further into the periphery, as the fall in cone density becomes less steep, nasal retinal cone densities are 40-45% higher than for equivalent eccentricities in temporal retina, resulting in a 'cone streak'. Differences in cone density between superior and inferior retina are variable between individuals, such that average results show a weak asymmetry with inferior retina having slightly higher density than superior. Cone density declines with eccentricity at a much faster rate than the optical quality of the retinal image, such that peripheral cones significantly undersample the image. In other words, spatial frequencies are passed by the eye's optics which cannot be veridically sampled by the photoreceptors. Aliasing phenomena can be demonstrated in peripheral vision under normal viewing conditions (Smith and Cass, 1987), generally appearing without form as visual noise. Such broadband noise is a predicted effect of an irregular lattice array where the Nyquist limit is not sharply defined (Yellott,

1982). If the separation between elements of the sampling array is not constant, then the Nyquist limit reflects the range of sampling separations. With increasing eccentricity the regularity of the cone lattice is reduced, both by the intrusion of rods and blue cones, and by an increase in the random positional jitter of the location of the cones (Hirsch and Miller, 1987). An increase in disorder degrades the sampled image by demodulation and distortion (Hirsch and Miller, 1987). Such 'positional uncertainty' therefore represents a further limitation to vision in the periphery.

The topography of rod density follows quite a different pattern from that of cones (Curcio et al., 1990). In the average human eye, there are approximately 92 million rods, so rods outnumber cones by 20:1. There are no rods present in the central 350μm of retina, which is therefore known as the 'rod-free zone', and subtends 1.25 deg of visual angle (equations of Drasdo and Fowler, 1974). Peak rod density occurs in an elliptical "rod ring" at the eccentricity of the optic disc. The actual point of highest rod density, or the rod 'hot spot', is generally found on the rod ring in superior retina and average peak density is approximately 160,000 mm^{-2}. With increasing eccentricity from the rod ring, density declines, remaining highest in nasal and superior retina.

3.2.5 Ganglion cells

Neural signals from the photoreceptors are passed via bipolar cells to the ganglion cells. Visual information leaves the eye in the ganglion cell axons, and so ganglion cells limit the proportion of information from the photoreceptors that can be transmitted to the brain. On average, there are 1.07 million ganglion cells in the eye, with a twofold range from 0.7 to 1.5 million between individuals (Curcio and Allen, 1990). In comparison, there are approximately 100 million photoreceptors in each eye (Curcio et al., 1990), and so at this level of the visual pathway there has to be a great deal of convergence of information.

The topography of human ganglion cell distribution shows several distinct basic features (Stone and Johnston, 1981; Curcio and Allen, 1990). Firstly, a high concentration of cells is found near the fovea. Since ganglion cells are displaced away from the central fovea to allow direct access of light to foveal cones, the peak density of ganglion cells is found in a elliptical ring 0.4-2.0 mm from the fovea. Peak ganglion cell density is, on average, 35,100 mm^{-2} (Curcio and Allen, 1990). From their peak density, cell density falls initially sharply (by an order of magnitude in the first 4mm of retina) and then more slowly (another order of magnitude between 4mm eccentricity and the ora serrata). However, density falls more sharply in the vertical meridia than in the horizontal. This results in the appearance of a 'visual streak', the second basic

feature of ganglion cell distribution. Finally, a naso-temporal asymmetry is observed, with cell density higher in nasal than temporal retina by up to 300% (Curcio and Allen, 1990). There is also a slight and variable vertical asymmetry, with superior retina showing higher cell densities than inferior retina. These asymmetries result in isodensity contours which are elliptical about the fovea, and displaced supero-nasally.

Cone and ganglion cell distributions differ in that the central to peripheral cell density gradient is much steeper for ganglion cells than that for cones (Perry and Cowey, 1985; Curcio and Allen, 1990). Reflecting this, Drasdo (1991) quotes E_2 values of 3.0 deg for cones and 1.29 deg for ganglion cells. Such differences in gradients reflect the increased convergence of cones through bipolars to ganglion cells with increasing retinal eccentricity. In the central fovea the ratio of ganglion cells to cones is now generally accepted to be 2:1 or slightly greater (Schein, 1988; Drasdo, 1989; Wässle, Grünert, Röhrenbeck and Boycott, 1989, 1990; Curcio and Allen, 1990), maintaining the fineness of central vision. Convergence of photoreceptors onto ganglion cells forms a receptive field (Kuffler, 1953). A receptive field can be defined as the locus of all points in the visual field at which light stimuli elicit a response from the cell (Hartline, 1940). Ganglion cell receptive fields have an antagonistic centre/surround arrangement, the purpose of which is to suppress steady state information and enhance edges. It would appear that there are also meridional differences in convergence, with ganglion cell: cone ratios lowest in nasal retina (Curcio and Allen, 1990), suggesting that receptive fields are potentially smaller along this meridian. In addition, the convergence of photoreceptors onto ganglion cells increases with eccentricity, so that the average size of receptive fields increase (Perry et al., 1984), and receptive field density decreases (Drasdo, 1977). Since convergence increases with eccentricity, the ability to resolve decreases in peripheral retina, but the potential for spatial summation increases.

3.2.6 Retinal limitations to vision

Much of the variation in visual performance with eccentricity can be explained on the basis of the retinal properties discussed above. At the fovea, photoreceptors and optics are reasonably well matched in the frequencies that they can observe veridically (Campbell and Gubisch, 1966; Williams, 1985). For naturally imaged stimuli, detection and discrimination contrast sensitivity functions are identical in the fovea and significant undersampling does not occur for eccentricities up to 8 deg (Anderson and Hess, 1990). Aliasing phenomena can be observed at the fovea, but occur only with the use of interference fringes which pass spatial frequencies higher than those of the eye's optics (Williams, 1985).

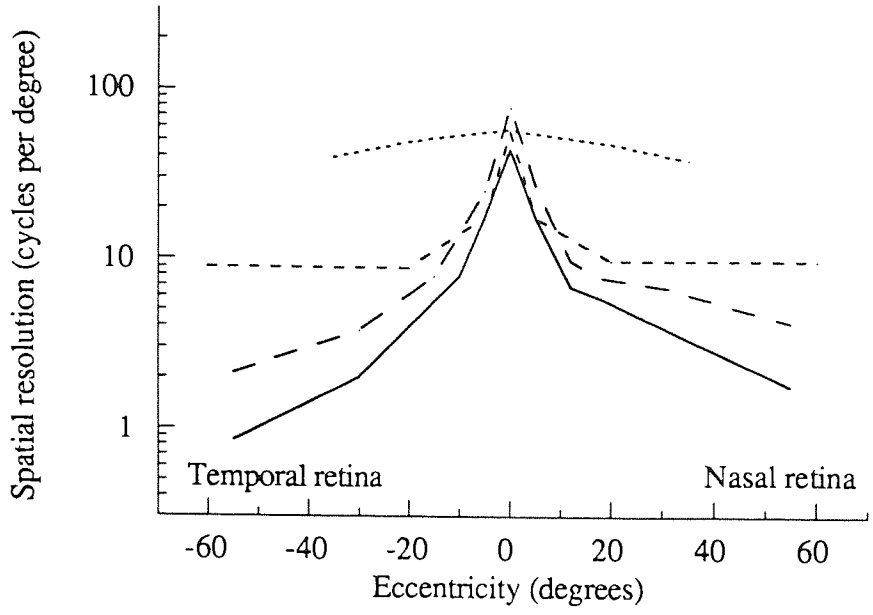

Figure 3.04. Retinal limitations to spatial resolution across the visual field. Dotted line indicates the optics of the eye; short dashed lines represent cone density; long dashed lines show ganglion cell density (all types); solid line depicts psychophysical spatial resolution acuity. Redrawn from Anderson et al. (1991).

In the retinal periphery, the optical quality of the image is not a limiting factor to spatial resolution (Millodot et al., 1975; Jennings and Charman, 1981), and spatial frequencies are passed by the optics of the eye which are undersampled by the retina. Spatial resolution thresholds measured with unaliased, naturally imaged stimuli decline with eccentricity faster than any optical or receptoral retinal parameter. This is depicted in Figure 3.04, redrawn from Anderson et al., 1991. Such Nyquist limits for spatial resolution determined psychophysically thus reflects a post receptoral limitation. Acuity is also poorer than for the population of the ganglion cells taken as a whole, but qualitatively reflects its naso-temporal asymmetry. It is speculated that resolution might be specifically determined by a subset of ganglion cells (see below), but the anatomical eccentricity dependencies of ganglion cell subset densities are not yet known. Thibos, Cheney and Walsh (1987) suggested from comparisons with macaque data that resolution might depend on the spacing of P cells. Banks, Sekuler and Anderson (1991) suggest that the apparent superiority of the fovea for contrast sensitivity and resolution might be explained purely on the grounds of optical and retinal specialisations, and that postretinal mechanisms are equally efficient across the visual field.

It has been suggested that variations in the optical quality of the eye might explain the faster rate of threshold rise with eccentricity for hyperacuities as opposed to resolution tasks (Deeley and Drasdo, 1987; Toet, Snippe and Koenderink, 1988b). At the fovea, the effects of the optical spread function dominate those of 'neural blurring', improving hyperacuity performance as the image is spread over several receptors, and limiting resolution performance. In the periphery, where 'neural blurring' due to sampling limitations is of greater importance than optical blurring, hyperacuity performance is more degraded than that of resolution.

It has also been suggested (Hess and McCarthy, 1994) that at a post-receptoral level, the topological fidelity of the sampling array decreases with eccentricity, in that the probability of swaps occuring in the ordering of retinal projections increases. The effect of the increased topological disorder is to reduce localisation accuracy without affecting resolution capabilities, and can therefore also help to explain the sharper rise in thresholds with eccentricity for hyperacuities as compared to resolution tasks.

3.2.7 Magnocellular and Parvocellular divisions

The discussion of ganglion cells up to this point has been with regard to ganglion cells as an entire group. There are several types of ganglion cell, and a number of classification systems have arisen to describe them. I shall refer to the two main types of ganglion cell of the geniculostriate pathway as M and P (Shapley and Perry, 1986). These constitute 10 and 80% respectively of the retinal ganglion cells, and project to the magnocellular and parvocellular layers of the LGN (Perry et al., 1984). These are thought to correlate to the parasol and midget cells found anatomically in human retina (Rodieck, Binmoeller and Dineen, 1985; Dacey and Petersen, 1992), to the Pα and Pβ cells of monkey (Perry and Cowey, 1981) and possibly to the Y and X cells of the cat (Enroth-Cugell and Robson, 1966). The remaining 10% of retinal ganglion cells project to the superior colliculus, and thence to extrastriate areas 18 and 19.

There are several major distinctions between cells of the M and P pathways. M cells show either linear or non-linear spatial summation (Kaplan and Shapley, 1982; Derrington and Lennie, 1984), short latencies and transient responses, large receptive fields, and are sensitive to low contrasts although responses saturate at 10-15% contrast. Their centre-surround receptive fields are broadband colour insensitive, with cones of all types contributing to centres and surrounds (Livingstone and Hubel, 1988b). The major properties of M cells are thus low acuity, high temporal and contrast sensitivity, and lack of wavelength selectivity (DeYoe and Van Essen, 1988; Bassi and

Lehmkuhle, 1990). P cells, on the other hand, show linear spatial summation (Kaplan and Shapley, 1982; Derrington and Lennie, 1984), longer latencies and sustained responses, and have low sensitivity to contrast but do not saturate at high contrasts. Although the receptive field sizes of both M and P cells increase with eccentricity, at any given eccentricity P cell receptive field centres are 2-3 times smaller than those of M cells. The centres and surrounds of P cell receptive fields consist of different cone classes so that they are colour opponent (Livingstone and Hubel, 1988b). The major properties of P cells are thus their high acuity, wavelength selectivity, low contrast and temporal sensitivity.

There has been much debate in the literature as to whether the relative proportions of M and P cells vary with eccentricity. Several authors have found from anatomical studies that P cells are more concentrated in the fovea, whereas the M cells appear to be more evenly distributed across the visual field. De Monasterio (1978) found that the ratio of P to M ganglion cells was 9:1 from 1-10 deg eccentricity, but more peripherally (11-20 deg) was 7:3. P cells were also found to predominate in central retina by Perry and Cowey (1981). In the human retina, Dacey and Petersen (1992) examined the midget and parasol ganglion cells and calculated that the midget to parasol cell density ratio is approximately 30:1 at 3 deg eccentricity, and 3:1 in the periphery. At the level of the LGN, Connolly and Van Essen (1984) found an even greater foveal emphasis on P cells with P:M ratios being 40:1 at 1 deg, and 4:1 at 80 deg. Perry and Cowey (1985) also showed an increased representation of foveal P cells in the LGN, with no corresponding expansion of M cell representation. Daniel, Kerr, Seneviratne and Whitteridge (1961) found the representation of the fovea in P layers of the LGN to be greater than that of M layers, and Derrington and Lennie (1984) found no M cells in the LGN with foveal receptive fields. Drasdo (1989) calculated that the sampling densities of M and P ganglion cells change linearly with eccentricity, and have E_2 values of 6.4 deg, and 1.6 deg respectively. These estimates were later revised (Drasdo, 1991) to be 4.76 deg for M cells, and 1.21 deg for P cells.

Psychophysical evidence also points to differences in M and P eccentricity gradients. From examination of reaction times to suprathreshold grating stimuli, Harwerth and Levi (1978) suggested that 'sustained' channels, which may correlate to the P pathway found anatomically, were concentrated foveally. Drasdo and Thompson (1989) examined the perimetric threshold criteria for coloured stimuli of 'visibility' and 'colour recognition' as a function of eccentricity. The threshold gradient was found to be steeper with eccentricity for colour recognition than for detection. The difference between these gradients approximately represented the difference in M and P cell

gradients found by Drasdo (1989). Similarly, Drasdo, Thompson and Deeley (1991) measured thresholds for square wave gratings under contrast and duration characteristics designed to separate M and P responses. E_2 values were found to approximate 6 deg for the magno task and 2 deg for the parvo task, and they conclude that the M and P distributions with eccentricity may well be different.

In contrast, whilst not ruling out some change in ratio with eccentricity, Livingstone and Hubel (1988a) found no evidence that in the cortex there is a large difference between fovea and far periphery in the relative mapping densities of magno and parvo systems. From cell counts throughout the ganglion cell layer, Perry and Silveira (1988) found that M cells were numerous in the central region, and that any variation in P:M ratio with eccentricity was not as great as had been suggested. Perry et al. (1984) also found that M cells constituted a constant 8-12% of retinal ganglion cells from 10-50 deg. This findings have been extended by Silveira and Perry (1991) who found, using a retrograde stain selectively marking M cells, that M cells constitute 6-10% of retinal ganglion cells from 1mm from the fovea to peripheral retina. The only deviation from this is beyond 7 mm eccentricity in nasal retina, where the proportion of M cells rises to approximately 20% of ganglion cells.

The evidence appears more persuasive that there is some difference in the relative proportions of M and P cells across the field, with P cells making up a greater proportion of the cells in central vision, and M cell distribution being more even across the field. If this is the case then the distribution of psychophysical thresholds in peripheral vision might be partly determined by the division of labour between M and P systems on the basis of stimulus qualities (Drasdo, 1989; Drasdo and Thompson, 1989) as magno and parvo streams will not usually operate in isolation (DeYoe and Van Essen, 1988; Zeki and Shipp, 1988). It has also been predicted that cortical magnification in visual area 1 (V1) reflects the eccentricity variation of P cells alone (Schein and de Monasterio, 1987; Drasdo, 1989; Dacey and Petersen, 1992). Additionally, at the fovea where there may be relatively few M cells, the low contrast portion of the contrast sensitivity function may be determined by probability summation across ten or more P cells (Derrington and Lennie, 1984; Dacey and Petersen, 1992).

3.3 Lateral Geniculate Nucleus

Ganglion cell axons leave the retina and pass up the optic nerve to the optic chiasm (see Fig 3.01). At this point nerve fibres from the temporal retina, representing nasal visual field, continue to the ipsilateral lateral geniculate nucleus (LGN). Fibres from the nasal retina cross at the chiasm to travel to the contralateral LGN. From the geniculate level

onwards each cortical hemisphere thus deals with the processing of the contralateral visual field.

The LGN consists of six cellular layers in a horseshoe-like shape. The apical angle of the horseshoe is called the hilum. The ventral layers, 1 and 2, receive axons of retinal M cells, while the dorsal layers, 3 to 6, receive input from retinal P cells (Perry et al., 1984). Information is segregated into monocular layers which alternate between ipsi- and contralateral eyes, so that each eye is represented in the LGN by two parvo- and one magnocellular layer. Receptive fields in the LGN are of the centre-surround type like those of ganglion cells. Although information leaves the LGN in the same form as it is input, the LGN is not merely a relay station. Feedback is received from the cortex and the brainstem reticular formation, and local synapses occur within the LGN, suggesting some sort of information modification at this level.

3.4 Striate cortex

Beyond the LGN, nerve fibres continue up the optic tract to the striate cortex, also known as visual area 1 (V1), Brodmann's area 17, or the primary visual cortex. It is found occupying most of the occipital lobe. The striate cortex is so named because of its distinct layering: six main layers are identified, with some subdivision of the layers (shown in Fig 3.05). Cortical input arrives in layer 4C, with magnocellular axons synapsing primarily in layer 4Cα, and parvocellular in 4Cβ. At the entry level of layer 4, cortical cells have concentric receptive fields like those of the retina and LGN, receiving information from one eye only and with no preference for orientation. Beyond this layer, receptive fields become progressively more complicated and are termed simple, complex, and hypercomplex or endstopped cells (Hubel and Wiesel, 1968). The receptive fields of simple cells show elongated, spatially distinct areas of excitation and inhibition. The optimum stimulus is a bar, edge or slit at the correct orientation and visual field location. Most simple cells are monocular. Complex cells are the most common in V1, and are found in all layers apart from 4B and C. Receptive fields for these cells are again elongated and are most sensitive to lines within 10-15 deg of a specific orientation. To elicit the best response, the stimulus must move across the receptive field in a direction perpendicular to the long axis of the field. Many complex cells are directionally sensitive and only respond to one direction of movement. Endstopped cells, originally termed hypercomplex cells, show the same properties as simple or complex cells but with the additional constraint that they are specific to stimulus length. If a stimulus extends beyond the limit of the receptive field, the stimulus ends are strongly inhibited, and the response reduced. For cells endstopped at one end only, a corner is the ideal stimulus, while for cells endstopped at

both ends, the optimum stimulus is a short line or a curve (Dobbins, Zucker and Cynader, 1987).

Whilst the increasing complexity of successive layers represents a hierarchical progression, segregation of pathways is maintained in the cortex. Figure 3.05 shows the projections of the M and P streams in the geniculostriate pathway. Although the information is based mainly on work in primates, there are many similarities between the findings in monkey and those observed in man (Bassi and Lehmkuhle, 1990). While the magno and parvo pathways remain segregated as far as V1, there is a great deal of reciprocal cross connection between the processing streams in striate cortex and beyond; only the major connections are shown. The amount of connectivity between cortical visual areas is thought to approach 40% of the maximum possible connections (Felleman and Van Essen, 1991). The two cellular classes (magno- and parvo-) give rise to three major processing streams in the cortex. In the magno-stream projections from the magnocellular layers of the LGN pass via layer 4B of V1 to the thick stripes of V2 and thence to areas MT and V3, and on to parietal cortical regions. The parvo-interblob stream receives projections from parvocellular layers of the LGN, which pass to the interblobs of V1, to interstripes of V2, and then to V4 and the inferotemporal cortex. The parvo-blob stream also receives parvocellular input, which passes from cytochrome oxidase rich blobs in V1 to thin stripes in V2, and then on to V4 and inferotemporal cortex (DeYoe and Van Essen, 1988).

Figure 3.05 on the following page shows the projections of Magnocellular (M) and Parvocellular (P) streams in the geniculo-striate pathway. Sources of information: DeYoe and Van Essen, 1988; Livingstone and Hubel, 1988b; Zeki and Shipp, 1988.

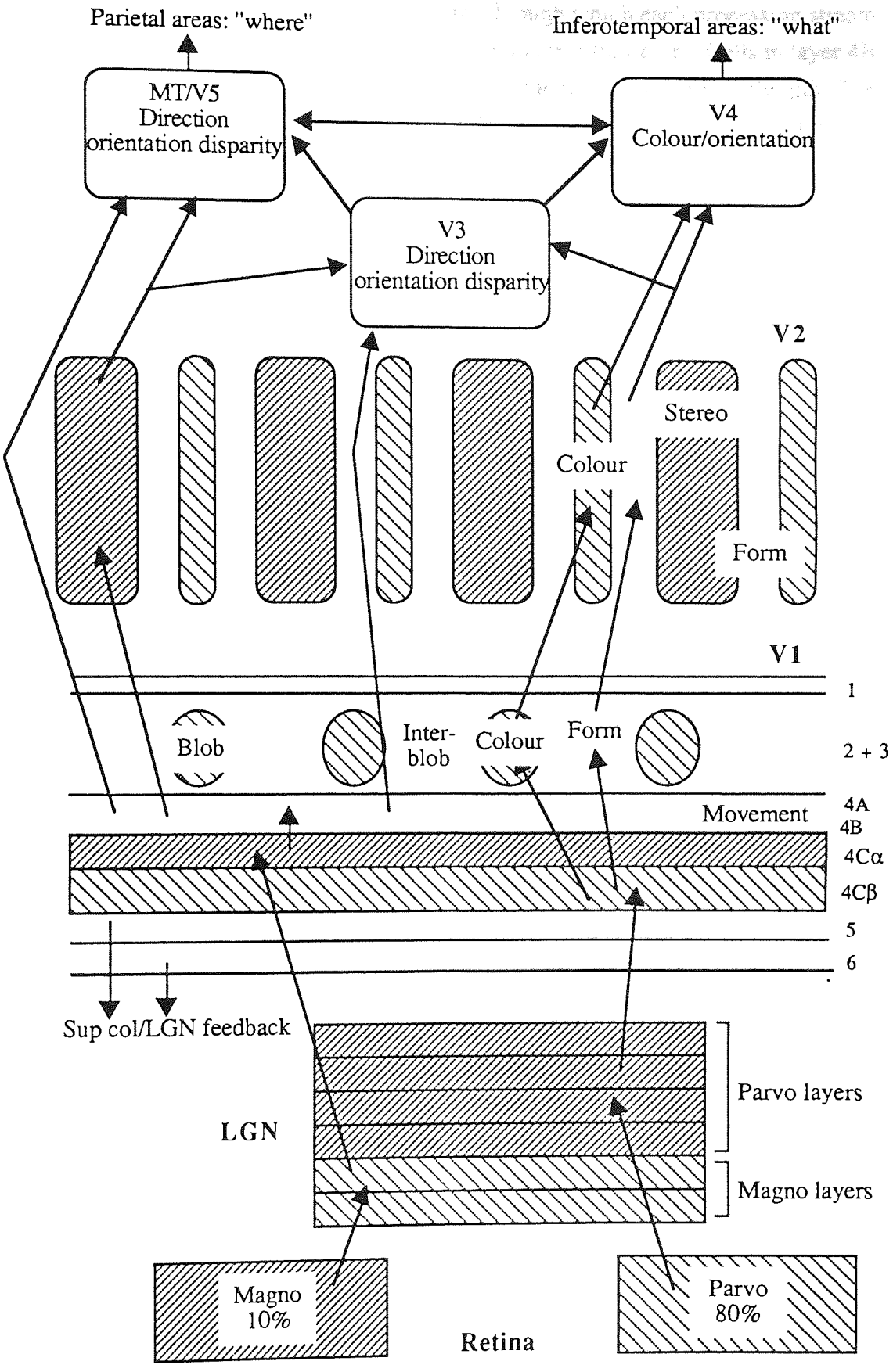
Parietal areas: "where"
Inferotemporal areas: "what"
MT/V5
Direction
orientation disparity
V4
Colour/orientation
V3
Direction
orientation disparity
V2
Stereo
Colour
Form
V1
1
Blob
Inter-
blob
Colour
Form
2 + 3
Movement
4A
4B
4Cα
4Cβ
5
6
Sup col/LGN feedback
LGN
Parvo layers
Magno layers
Magno
10%
Parvo
80%
Retina

As can be seen from Figure 3.05, the structures through which each processing stream pass are specialised in the kinds of visual information that they carry. Cells in layer 4B are selective to orientation and direction of movement, but not to wavelength. The interblobs have cells with small receptive fields, endstopping, are not directionally sensitive and can detect colour edges. Cells in the cytochrome oxidase rich blobs have double opponent colour receptive fields, or are broadband cells with large fields and inhibitory surrounds. These layers are thus thought to primarily be for processing movement and stereopsis (4B), form (interblobs), and colour and brightness (blobs) respectively (Livingstone and Hubel, 1988b). It seems that the magno system is involved with movement perception, depth perception by stereopsis and other depth cues, and linking features. Thus the function of the magno system appears to be that of figure / ground discrimination, providing a transient global interpretation of spatial organisation. Conversely, the parvo system is involved with form and colour discrimination. Its function appears to be analysis of scenes in greater local detail for a more sustained period, allowing visual identification and association (Livingstone and Hubel, 1988b; Bassi and Lehmkuhle, 1990).

In addition to its vertical organisation, the cortex has a horizontal topography. In a vertical section, cells have the same orientation or eye preference. Moving horizontally across the cortex, the eye of dominance changes every 400μm. This is clear cut in monocular layer 4, and a continuous progression from favouring one eye through binocularity to favouring the other eye in the binocular layers. The pattern of ocular dominance columns has been observed (Hubel and Freeman, 1977) and appear as irregular parallel 'zebra-stripes'. Orientation preference of cells also varies with horizontal movement across the cortex. For every 25-50μm movement, orientation preference changes by about 10 deg (Hubel and Wiesel, 1974). A complete 180 deg rotation of orientation columns, or a left plus right eye set of dominance columns, are named 'hypercolumns' and are approximately 1mm in extent (Hubel and Wiesel, 1977). However, ocular dominance and orientation groupings are not closely related. Horizontal movement across the cortex also changes the location in the visual field of the cortical receptive fields. This is now discussed below in some detail.

3.4.1 Cortical magnification

The visual world projected from the retina is laid out in the visual cortex in a topographical map. Topographic representations give emphasis to the fovea. In the retina, as we have seen, this is manifested in the regional variation in ganglion cell density. Post-retinally, cell density is reasonably constant with eccentricity, but there is an increase in the volume and surface area devoted to central visual fields (Polyak,

1957). The quantitative description of how the extent of cortical processing varies with eccentricity is given by the cortical magnification factor, M. The cortical magnification factor is defined (Daniel and Whitteridge, 1961) as the linear extent of visual cortex, in millimetres, devoted to each degree of visual field.

There have been many attempts to measure M in various species, which are discussed in the following sections. The variation of M with eccentricity tends to linearity, as in Figure 1.01. As in Equation 1.01, we can say that:

$$M_0 / M = 1 + E / E_2 \qquad \text{Equation 3.01}$$

where M_0 is the foveal value of M.

Thus, $1 / M = 1 / M_0 (1 + E / E_2)$ Equation 3.02

and, $1 / M = 1 / M_0 + (E / (M_0 E_2))$ Equation 3.03

Equation 3.03 indicates that a plot of 1 / M as a function of eccentricity should have a gradient of $1 / (M_0 E_2)$ and a y-intercept of $1 / M_0$.

As in Chapter 2, the above equations may all be justifiably used if standard errors are provided and used to to weight the regression by the inverse of the variance. In the absence of standard errors, it is more appropriate to use the logarithmic derivative of Equation 3.02, ie:

$$\log (1 / M) = \log (1 / M_0) + \log (1+(E / E_2)) \qquad \text{Equation 3.04}$$

In the review below, where Equation 3.04 is used to derive values of M_0 and E_2 the data are shown on linear axes. This is done to highlight the approximately linear rise of 1 / M with eccentricity, even though the regression is given in logarithmic terms.

3.4.1.1 Direct estimates of M in monkey

Polyak (1932) first suggested that the retinal projection to the cortex could be described by a fixed mathematical relationship. Talbot and Marshall (1941) made the first experimental observations of the topographical map of the striate cortex and showed Polyak's suggestion to be correct. By recording the action potentials evoked on the visible posterolateral cortical surface to light spots presented in the visual field, the field of six rhesus monkeys was mapped. They found that at the fovea, 1mm of cortex corresponded with 2 min arc in the visual field. At 5 deg eccentricity, 1mm of cortex represented 18 min arc. From these figures, it would appear that:

M_0 = 1mm / 2min = 30 mm/deg

and since M_5 = 1mm / 18min = 3.33 mm/deg;

from Equation 3.01: $M_0 / M = 1 + E / E_2$

and, $30 / 3.33 = 1 + 5 / E_2$

Thus, $E_2 = 0.62$ deg.

It is also possible, although somewhat more complicated, to use integrals to find linear distances on the cortex for any point in the visual field. In the example of Talbot and Marshall's (1941) data described above, integrals can be used to find simultaneous equations for the two known locations, from which E_2 can be solved. From Equation 3.01:

$$M = \frac{M_0}{\left(1 + \left(\frac{E}{E_2}\right)\right)}$$

$$\int_a^b M\,dE = \int_a^b \left(\frac{M_0}{\left(1 + \left(\frac{E}{E_2}\right)\right)} \right) dE$$

$$\int_a^b M\,dE = M_0 \int_a^b \left(\frac{1}{1 + \left(\frac{E}{E_2}\right)} \right) dE$$

$$\int_a^b M\,dE = M_0 \left[\ln\left(1 + \left(\frac{E}{E_2}\right)\right) \right]_a^b \qquad \text{Equation 3.05}$$

Centrally, 1mm of cortex is associated with 2 min arc of visual field. Therefore:

$$1\text{ mm} = M_0 \left[\ln\left(1 + \left(\frac{E}{E_2}\right)\right) \right]_0^{\frac{2}{60}}$$

$$1\text{ mm} = M_0 \left[\ln\left(1 + \frac{2}{60\,E_2}\right) - \ln(1 + 0) \right]$$

$$1\text{ mm} = M_0 \ln\left(1 + \frac{2}{60\,E_2}\right)$$

At 5 deg eccentricity, 1mm of cortex represents 18 min arc of visual field, ie. the region 5 deg ± 9 min arc. Therefore:

$$1\text{ mm} = M_0\left[\ln\left(1+\left(\frac{E}{E_2}\right)\right)\right]_{\frac{291}{60}}^{\frac{309}{60}}$$

$$1\text{ mm} = M_0\left[\ln\left(1+\frac{309}{60\,E_2}\right)-\ln\left(1+\frac{291}{60\,E_2}\right)\right]$$

$$1\text{ mm} = M_0\left[\ln\frac{\left(1+\frac{309}{60\,E_2}\right)}{\left(1+\frac{291}{60\,E_2}\right)}\right]$$

$$1\text{ mm} = M_0\left[\ln\left(\frac{60\,E_2+309}{60\,E_2+291}\right)\right]$$

Combining the two simultaneous equations derived gives:

$$\ln\left(1+\frac{2}{60\,E_2}\right)=\ln\left(\frac{60\,E_2+309}{60\,E_2+291}\right)$$

$$1+\frac{2}{60\,E_2}=\frac{60\,E_2+309}{60\,E_2+291}$$

$$\left(1+\frac{2}{60\,E_2}\right)(60\,E_2+291)=60\,E_2+309$$

$$(60\,E_2+2)(60\,E_2+291)=60\,E_2\,(60\,E_2+309)$$

$$3600\,E_2^2+120\,E_2+17460\,E_2+582=3600\,E_2^2+18540\,E_2$$

$$960\,E_2=582$$

$$E_2=0.61\text{ deg}$$

The value for E_2 derived in this way is the same as that calculated previously by simple regression between the two given points.

Using the integral of Equation 3.05, the general projection of the visual field on the cortex can be determined, enabling the construction of cortical maps. However, it should be noted that the calculations do not account for any anisotropic or meridional variations in the cortical map.

Figure 3.06 shows the data of Daniel and Whitteridge (1961) depicting 1 / M (deg/mm) as a function of eccentricity (deg). The regression is log(1/M) = log(1/9.52) + log(1 + E/1.14), so that M_0 is 9.52±2.37 mm/deg, and E_2 is 1.14±0.38 deg.

Daniel and Whitteridge (1961) also used electrophysiological techniques to map the cortices of a variety of monkey and baboon species. They were able to extend their measurements on the calcarine cortex to 60-70 deg in the visual field. Their results were described in terms of the cortical magnification factor, M, as defined above. The results of Daniel and Whitteridge (their Figure 4) are replotted to 15 deg in Figure 3.06.

The regression fitted to the data points is of the form:

$$\log(1 / M) = \log(1 / 9.52) + \log (1 + (E / 1.14))$$

So that from Equation 3.04, $M_0 = 9.52 \pm 2.37$ mm/deg.

and, $E_2 = 1.14 \pm 0.38$ deg.

It should be noted that beyond 15 deg, the data does not rise linearly with eccentricity. It was observed that the inverse magnification factor for monkey varied in approximately the same way with eccentricity as the human visual acuity data of Weymouth (1958). Also, by comparison with macaque acuity, it was deduced that the foveal minimum angle of resolution (MAR) occupies 67 μm of cortex. Thus at any eccentricity, the cortical resolution distance is 67 μm, and two sensations must be separated across this cortical distance in order to be resolved.

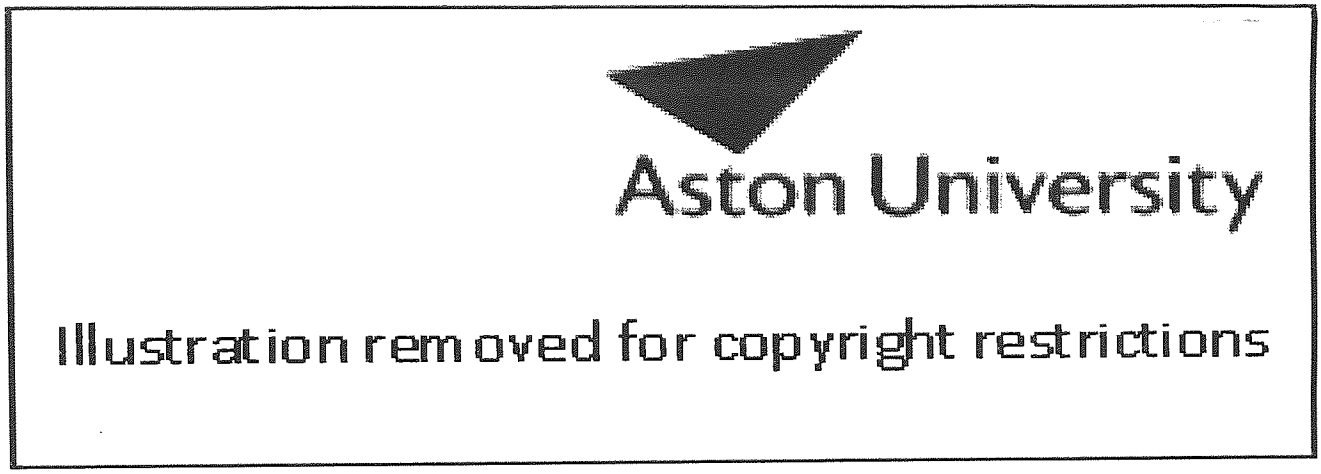

Figure 3.07 shows the data of Rolls and Cowey (1970) depicting 1 / M (deg/mm) as a function of eccentricity (deg), for macaque (open squares) and squirrel (open circles) monkeys. The regression for the average of both types (filled triangles) is $\log(1/M) = \log(1/6.42) + \log(1 + E/2.38)$, so that M_0 is 6.42±0.66 mm/deg, and E_2 is 2.38±0.38 deg.

Rolls and Cowey (1970) compared foveal MAR values, ganglion cell and cone counts with cortical magnification values for macaque and squirrel monkeys. The data of Cowey (1964) was used for squirrel monkeys, while that of Daniel and Whitteridge (1961) was used for the macaques. The cortical magnification data for the two types of monkey are shown in Figure 3.07 (their Figure 7 replotted).

For macaque monkeys:
$M_0 = 8.90 \pm 1.32$ mm/deg, and $E_2 = 1.99 \pm 0.44$ deg.
For squirrel monkeys:
$M_0 = 5.05 \pm 0.67$ mm/deg, and $E_2 = 2.65 \pm 0.57$ deg.
For an average of the two species:
$M_0 = 6.42 \pm 0.66$ mm/deg, and $E_2 = 2.38 \pm 0.38$ deg.

Rolls and Cowey found the cortical magnification factors to be approximately proportional to ganglion cell densities from 10 - 50 deg eccentricity. Below 10 deg, ganglion cell displacement prevented accurate comparisons, but cone density is approximately proportional to magnification factors. They thus concluded that 'retinal

topography, and the cortical magnification of the visual field, are closely related to visual acuity'.

Hubel and Wiesel (1974) found that a block of cortex of 2 x 2 mm surface extent comfortably contains the cortical machinery required to analyse a visual field region covering the aggregate receptive field size. Aggregate field size is the average size of the cortical receptive field plus its associated scatter. The size of each cortical module is independent of eccentricity, but the area of visual field that it subserves increases with eccentricity according to 1 / M, and is proportional to the aggregate receptive field size. The authors concluded that the cortex is remarkably uniform in both its anatomy and physiology. Figure 3.08 below (based on their Figure 6A, and Hubel and Freeman (1977) Figure 2) shows the increase in 1 / M with eccentricity.

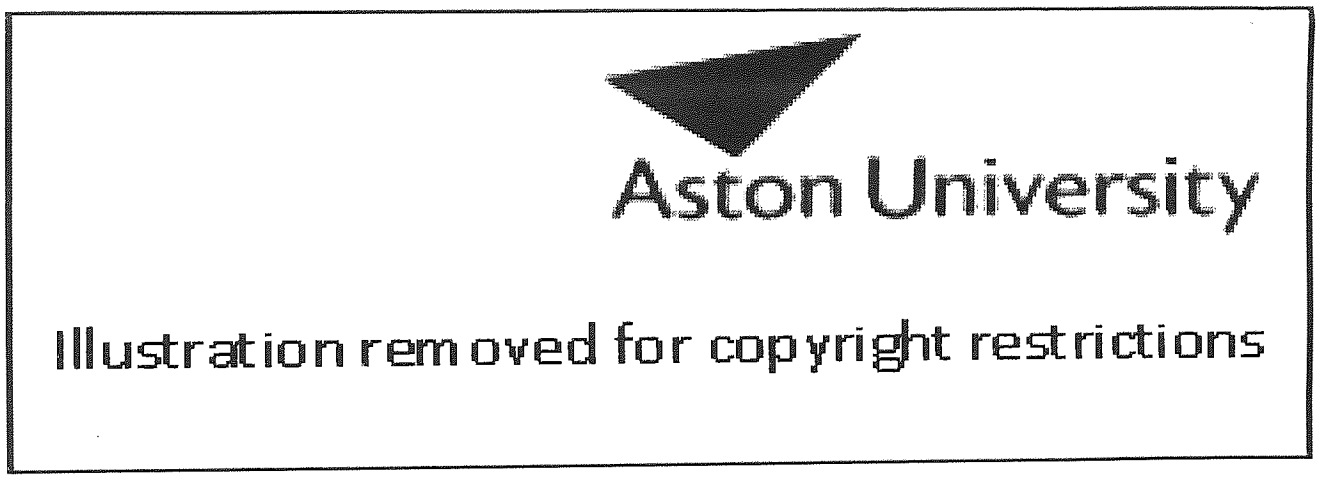

Figure 3.08 shows the data of Hubel and Wiesel (1974) depicting 1 / M (deg/mm) as a function of eccentricity (deg). The regression is $\log(1/M) = \log(1/5.76) + \log(1 + E/3.22)$.

From the regression applied to the data, which is of the form of Equation 3.04, M_0 is found to be 5.76 ± 0.83 mm/deg, and E_2 is 3.22 ± 0.66 deg.

Studies up to this point had extrapolated foveal M_0 values from parafoveal data. Dow, Snyder, Vautin and Bauer (1981) made single cell recordings close to the fovea (5-160 min arc eccentricity) in two awake, behaving rhesus monkeys, and measured receptive field sizes and magnification values. For the combined data of the two monkeys, a plot

of 1 / M against eccentricity is fitted with a linear regression (their Figure 5, not shown) which in the form of Equation 3.03 is:

$$1 / M = 0.040 + 0.116E$$

Thus, $M_0 = 1 / 0.04 = 25$ mm/deg.

Also, $1 / (25 \times E_2) = 0.116$, and $E_2 = 0.34$ deg.

The authors themselves quote M_0 as 'approaching 30 mm/deg.' They also find that, contrary to Hubel and Wiesel (1974), mean receptive field size is not proportional to 1 / M. Receptive fields do not decrease in size sufficiently towards the fovea to match the magnification change, and thus foveal receptive fields are more overlapped than peripheral ones. They suggest that there is no constant 'cortical acuity distance' with eccentricity, as observed by Daniel and Whitteridge (1961) and Hubel and Wiesel (1974). The cortical distance required to resolve two objects increases with eccentricity, and they conclude that the fovea has a greater cortical representation than it has at the retina.

The study of Dow et al. (1981) has been reevaluated and criticised by several authors because of the exceedingly high value found for M_0. Levi et al. (1985) reanalysed the data for each monkey separately, giving M_0 of 12-17 deg, and E_2 of 0.8 deg. Van Essen et al. (1984) also suggest that 30 mm/deg is an artificially high value caused by averaging the data from two individuals with different M_0 values. They suggest that 15-20 mm/deg is more representative of the data. However, Drasdo (1991), while confirming that the data reflects an M_0 of 30 mm/deg, questions the use of the intensive foveal training of the monkeys. He argues that prolonged training combined with cortical plasticity may have enhanced the foveal projection, contributing to the high M_0 value.

Visual experience is mentioned as a possible factor determining M_0 in a later publication by Dow, Vautin and Bauer (1985). In this paper, further data on the two monkeys studied in the 1981 paper are given. Values for 1 / M are plotted in Figure 3.09 for the monkey 'Luke'. The regression fitted to the data is of the form of Equation 3.04, and gives values of 25.76 ± 1.64 mm/deg for M_0 and 0.32 ± 0.03 deg for E_2.

Figure 3.09 shows the data of Dow et al. (1985) depicting 1 / M (deg/mm) as a function of eccentricity (deg) for 'Luke'. The regression is $\log(1/M) = \log(1/25.76) + \log(1 + E/0.32)$, so that M_0 is 25.76±1.64 mm/deg, and E_2 is 0.32±0.03 deg.

Tootell, Silverman, Switkes and De Valois (1982) used the method of labelled 2-deoxyglucose (2DG) mapping to investigate cortical magnification, in contrast to the previous electrophysiological studies. Anaesthetised macaques were injected with 2DG and positioned to observe a counterphasing black and white target consisting of concentric circles and radial spokes for approximately 30 minutes. The 2DG is taken up by areas of activity in the cortex, allowing cortical localisation of each part of the visual target. For two monkeys, at eccentricities 0-10 deg, magnification was found to observe the linear regression:

$$1 / M = 0.077 + 0.082E$$

Thus, $M_0 = 1 / 0.077 = 13$ mm/deg, and $1 / (13 \times E_2) = 0.082$, so that $E_2 = 0.94$ deg.

Van Essen et al. (1984) examined striate representation by electrophysiological methods in six macaques. They found that beyond 2.5 deg eccentricity, 1 / M is reasonably proportional to eccentricity. This relationship breaks down somewhat in the fovea, where M has a steeper gradient. Examination of their experimental results for areal magnification factor (Ma), where $Ma = 103\ (0.82 + E)^{-2.28}$, gives a value for M_0 of 12.6 mm/deg. The square root of this power function, giving linear magnification values, does not have an exponent quite equal to -1, but to a first order approximation,

E_2 can be calculated to be 0.6 deg. Additionally, the authors provide a 'standard' map of macaque striate to allow for the large inter-individual variations observed. This has an equation for areal magnification of $Ma = 140\ (0.78 + E)^{-2.20}$. With the same reservations as above, a linear M_0 can be calculated to be 15.6 mm/deg, and E_2 to be 0.6 deg. They conclude that the cortical emphasis on the fovea is greater than that in the retina.

Tootell, Switkes, Silverman and Hamilton published further results of 2DG mapping in 1988. The value for M_0, averaged over several specimens, was found to be 14-16 mm/deg. Variations in cortical magnification with eccentricity were plotted for horizontal and vertical meridia. The linear regressions quoted for these results are:

Horizontal meridian: $1 / M = 0.108 + 0.066E$

Therefore, $M_0 = 1 / 0.108 = 9.26$ mm/deg.

Also, $1 / (9.26 \times E_2) = 0.066$, so $E_2 = 1.64$ deg.

Vertical meridian: $1 / M = 0.070 + 0.052E$

Therefore, $M_0 = 1 / 0.070 = 14.3$ mm/deg.

Also, $1 / (14.3 \times E_2) = 0.052$, so $E_2 = 1.35$ deg.

The results suggest that even at the fovea, some local anisotropy occurs, in that M is dependent on the direction of measurement. This had previously been suggested to be the case in the periphery (Van Essen et al., 1984).

Authors	M_0 (mm/deg)	E_2 (deg)	Comments
Talbot & Marshall (1941)	18.7	0.6	
Daniel & Whitteridge (1961)	9.5	1.1	Not linear beyond 15 deg
Rolls & Cowey (1970)	6.4	2.4	Average of two species
Hubel & Wiesel (1974)	5.8	3.2	
Dow et al. (1981)	25	0.3	Intensive foveal training
Dow et al. (1985)	25.9	0.3	Intensive foveal training
Tootell et al. (1982)	13	0.9	
Van Essen et al. (1984)	15.6	0.6	'Standard' map; non linear
Tootell et al. (1988)	14-16	1.5	Average of meridia

Table 3.01. Summary of estimates of M_0 and E_2 in monkey calculated by and for various studies in the literature.

As can be seen from Table 3.01, the values found for M_0 and E_2 are somewhat variable. Several possible reasons have been suggested for the observed variations in

cortical magnification values. Firstly, while most studies have used macaque monkeys, several different species have been investigated. As an example, Van Essen et al. (1984) used the smaller *M. fasicularis*, while the studies of Tootell et al. (1982, 1988) featured *M. arctoides*, a larger creature. Even within species, individuals can have very different cortical shapes (Tootell et al., 1988) and sizes (Van Essen et al., 1984). Tootell et al. (1988) suggested that many differences in cortical magnification could be explained by variations in brain size. Drasdo (1991) suggested that the cortex might be fairly plastic, allowing cortical magnification to reflect visual experience. Also, the measurement of M_0 is fraught with problems. For the direct foveal measurements of 2DG mapping, M_0 depends critically on the area of cortex over which the value is averaged. For the electrophysiology studies which constitute the majority of data, actual foveal measurements are not possible, and values of M_0 are extrapolated from parafoveal data. It is interesting to note that the study which got closest to the fovea using electrophysiology (Dow et al., 1981) also gives the highest M_0 value. In summary, recent results in monkey are in relative agreement that M_0 is in the region of 13-16 mm/deg. E_2 is probably somewhere in the range 0.6-1.5 deg.

3.4.1.2 Direct estimates of M in man

The relevance of monkey data to cortical magnification factors in man depends on how good a model the monkey cortex is for that of the human. Tolhurst and Ling (1988) suggest that the human striate cortex is a linearly scaled up version of that of macaque, being stretched by approximately 1.6 times. Even if this is the case, it is still important to have data from humans. Despite the extreme difficulties in recording from humans, a few attempts have been made to estimate M directly in man.

Brindley and Lewin (1968) implanted electrodes onto the occipital pole of a patient blinded by glaucoma, as a prototype prosthetic device for the visually impaired. Stimulation of these electrodes elicited discrete localised phosphenes, appearing as small spots of light in central visual field, and somewhat larger 'clouds' more peripherally. It was noted that a cortical separation of 2.4mm resulted in easily resolvable phosphenes.

The results of Brindley and Lewin as evaluated by Cowey and Rolls (1974) have been used in several studies estimating M (Drasdo, 1977; Rovamo and Virsu, 1979; Tolhurst and Ling, 1988). Cowey and Rolls (1974) used the data of Brindley and Lewin (1968) to calculate M by relating the interelectrode distance at the cortex of 53 electrode pairs to the angular separation of the resultant phosphenes in the visual field. M was found to be approximately 4 mm/deg at 2 deg, falling to 0.5 mm/deg at 25 deg.

As no electrodes gave phosphenes closer than 1.6 deg to the fovea, a value for M_0 was extrapolated to be 15.1 mm/deg. Figure 3.10 below replots the data for 1 / M at various eccentricities (their Figure 3a).

The regression from data in the eccentricity range 1-30 deg is of the form of equation 3.04. This gives values of 6.14 ± 1.57 mm/deg for M_0, and 2.90 ± 0.95 deg for E_2. Note how the use of the logarithmic regression gives less emphasis to the values at higher eccentricities, which are likely to have higher standard errors associated with them. The regression gives a lower value for M_0 than that derived by the authors.

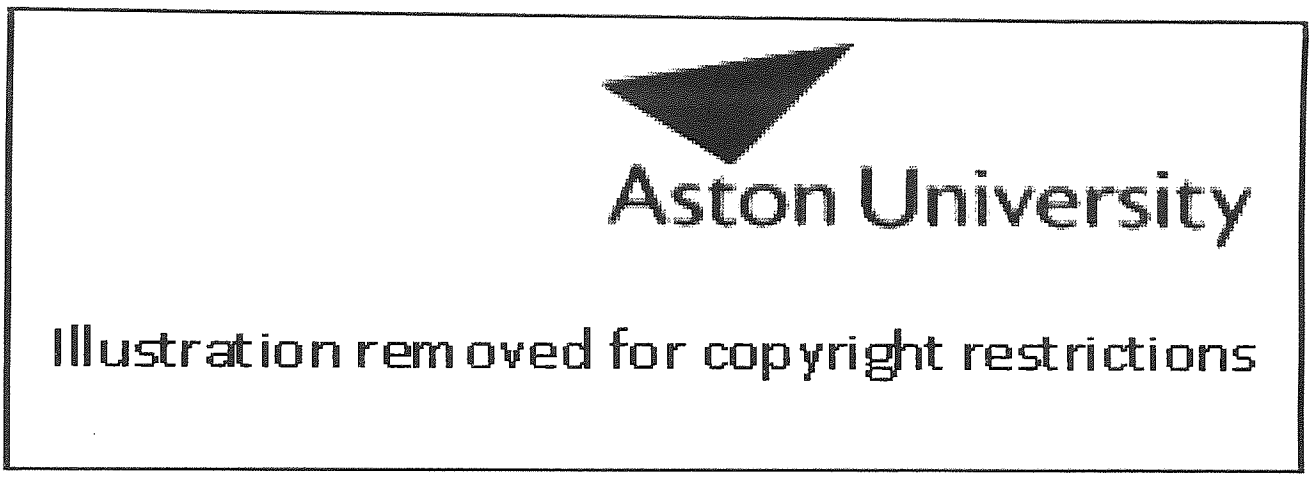

Figure 3.10 shows the data of Cowey and Rolls (1974) depicting 1 / M (deg/mm) as a function of eccentricity (deg). The regression is $\log(1/M) = \log(1/6.14) + \log(1 + E/2.90)$, so that M_0 is 6.14±1.57 mm/deg, and E_2 is 2.90±0.95 deg.

By comparison with the acuity data of Wertheim (1891), 1 / M was shown to be proportional to MAR. The minimum angle of resolution thus has a constant cortical extent at any eccentricity, and they estimated this distance to be 84 μm. This value agrees well with the 67μm proposed by Daniel and Whitteridge (1961) in their comparison of monkey M and MAR, but is contrary to later monkey studies (Dow et al., 1981; Van Essen et al., 1984) which suggests that cortical MAR increases with eccentricity.

Dobelle, Turkel, Henderson and Evans (1979) repeated a similar experiment to that of Brindley and Lewin (1968) by implanting an electrode array into a blind volunteer. The results from this study are shown in Figure 3.11 (their Figure 6 replotted). Fitting a regression of the form of Equation 3.04 to the data gives a value for M_0 of 4.45 ± 2.33 mm/deg, and E_2 of 3.34 ± 2.36 deg. The rather large standard errors can be attributed to the scattered data.

Figure 3.11 shows the data of Dobelle, Turkel, Henderson and Evans (1979) depicting 1 / M (deg/mm) as a function of eccentricity (deg). The regression is log(1/M) = log(1/4.45) + log(1 + E/3.34), so that M_0 is 4.45±2.33 mm/deg, and E_2 is 3.34±2.36 deg.

The technique of positron emission tomography (PET) was employed by Fox, Miezin, Allman, Van Essen and Raichle (1987) to map the striate cortex in normally sighted human volunteers. The subjects were injected with $^{15}O_2$-labelled water whilst observing red and black checked annular stimuli. Measurements of the tracer in the cerebral blood flow allowed the detection of focal functional brain activity. Three different annular stimuli were presented to the six subjects over the course of the experiment. Values of M were calculated for three locations, and are shown in Figure 3.12 (data from their Table 3).

The square symbols represent M at the mean eccentricity of the two annuli being compared. The resulting data does not appear linear with respect to eccentricity. The annuli presented to the subjects were not very localised, extending over the ranges 0.1-

1.5 deg, 0.5-5.5 deg, and 5.5-15.5 deg. The solid horizontal lines on the graph represent the distance from the mean eccentricity of one annulus to that of the one it is compared with. Obviously, these span a large range, and the values for M thus derived could be applicable anywhere within this range.

Figure 3.12 shows the data of Fox et al. (1987) depicting 1 / M (deg/mm) as a function of the mean eccentricity of two annuli (deg).

3.4.1.3 Indirect estimates of M in man

Given the relatively few attempts to measure M in man by direct means, several indirect methods have been applied to estimate cortical magnification on the basis of monkey data, and human anatomical and physiological observations. Richards (1971) mapped the visual disturbances caused by migraine headaches in a single subject. These disturbances begin as a central scotoma, which spreads gradually into the peripheral field, taking the appearance of zig-zag lines or fortifications. These fortification lines appear to increase in length as the disturbance travels peripherally. Figure 3.13 shows the results found when his subject drew their fortification illusions, and shows how the extent of the line increases with increasing eccentricity.

The data is fitted with a regression of the form:

$$\log(\text{angular size}) = \log(0.033) + \log(1 + E / 0.35)$$

Therefore, E_2 is 0.35 ± 0.25 deg, and the angular extent of the illusion at the fovea is 0.033 ± 0.024 deg. Richards states that each fortification line occupies 1.2mm of

cortical distance, although unfortunately, details of the calculations are not provided. Assuming that the cortical distance of each line is 1.2mm, then:

$$M_0 = 1.2 / 0.033 = 36.4 \text{ mm/deg.}$$

Figure 3.13 shows the data of Richards (1971) depicting the angular size of migraine fortifications (deg) as a function of eccentricity (deg). The regression is log(illusion extent) = log(0.033) + log(1 + E/0.35).

Drasdo (1977) estimated M across the visual field in man using ganglion cell data. Previous studies (Daniel and Whitteridge, 1961; Cowey and Rolls, 1974) had already suggested that cortical magnification was inversely proportional to linear ganglion cell density ($M \propto 1 / \sqrt{D_C}$). However, using ganglion cell density to deduce M is fraught with difficulties due to the displacement of ganglion cells in the central part of the retina. Instead, Drasdo calculated receptive field densities of ganglion cells (D_r = receptive fields per solid degree) across the visual field by interpolation and correction of available ganglion cell density data. The derived values compared well with other estimates of M in man (Richards, 1971; Cowey and Rolls, 1974). Thus 1 / M is found to be proportional to $1 / \sqrt{D_r}$, and M^2 is proportional to D_r. From a foveal estimate of $1 / \sqrt{D_r} = 0.0055$, foveal ganglion cell receptive field density was calculated to be 33,058 fields mm^{-2}, and M_0 was given as 11.5 mm/deg. A general equation was proposed to relate $1 / \sqrt{D_r}$ to eccentricity. This takes the form:

$$V = k [1 + SE (1 + 3E^2 \times 10^{-5})] \qquad \text{for } E < 70 \text{ deg}$$

or in a more simplified form:

$$V = k\,(1 + SE) \qquad \text{for } E < 20 \text{ deg}$$

where E is eccentricity, V might be a spatial threshold, 1 / M, or $1/\sqrt{D_r}$ at any eccentricity, k is the corresponding foveal value, and S is the gradient of the normalised function. Substituting cortical magnification terms, and since we know that $S = 1 / E_2$ (Equation 1.01), the equation becomes:

$$1 / M = 1 / M_0\,(1 + E / E_2) \qquad \text{Equation 3.02}$$

which has been used throughout this chapter. Since Drasdo suggests a figure for S of 0.59 averaged over meridia for eccentricities less than 30 deg, $E_2 = 1 / 0.59 = 1.69$ deg. It was also recognised that the decline of retinal ganglion cell receptive field density with eccentricity, and thus that of M, was not radially symmetric. The following table gives values of S proposed for the four major meridia separately, along with the eccentricity to which the simplified equation may be applied, and the corresponding E_2 value.

Meridian	S	E_2 (deg)	Eccentricity range (deg)
Nasal	0.50	2.00	0-20
Superior	0.62	1.61	0-10
Temporal	0.46	2.17	0-35
Inferior	0.66	1.52	0-20

Table 3.02. E_2 values from Drasdo (1977)

Rovamo and Virsu (1979) estimated M across the visual field in a similar manner to that employed by Drasdo (1977). By comparison with published data, M^2 was assumed to be proportional to D. Values for M were derived by using ganglion cell densities for eccentricities beyond 10 deg. In contrast to Drasdo's study, Rovamo and Virsu used cone densities at eccentricities below 10 deg to represent ganglion cells, due to the displacement of ganglion cells. The use of central cone densities assumes a cone to ganglion cell ratio of 1 in the fovea, which under-represents the fovea with respect to Drasdo's evaluation, and is questioned by more recent anatomical data (Wässle et al., 1989; Curcio and Allen, 1990). M_0 was given as 7.99 mm/deg. M can be found from the following equations, representing each of the principle meridia. The cubed term of the equations below are insignificant when the eccentricity (E) is small, and the E_2 values given have therefore been determined by omitting this value.

Meridian	Equation	E_2 (deg)	Eccentricity range (deg)
Nasal	$M_N = (1 + 0.33E + 0.00007E^3)^{-1} M_0$	2.97	0-60
Superior	$M_S = (1 + 0.42E + 0.00012E^3)^{-1} M_0$	2.32	0-45
Temporal	$M_T = (1 + 0.29E + 0.000012E^3)^{-1} M_0$	3.43	0-80
Inferior	$M_I = (1 + 0.42E + 0.000055E^3)^{-1} M_0$	2.35	0-60

Table 3.03. Cortical magnification equations of Rovamo and Virsu (1979).

Tolhurst and Ling (1988) reviewed the cortical magnification data on monkey and man. Whilst they conclude that the macaque is a reasonable model for man, the human striate cortex being a linearly stretched version of 1.6 times that of macaque, they question the assumptions made in previous estimates (Cowey and Rolls, 1974; Drasdo, 1977; Rovamo and Virsu, 1979) that M is proportional to the square root of ganglion cell density, or to visual acuity, in the light of more recently available anatomical evidence. From their own evaluation and scaling up of recent monkey data (Dow et al., 1981; Tootell et al., 1982; Van Essen et al., 1984) they suggest that human values of M_0 should be approximately 20-25 mm/deg, and from the equations given, E_2 approximates 1.1-1.3 deg.

In his comprehensive review paper, Drasdo (1991) reexamined his previous evaluations of M with regard to ganglion cell receptive field densities (Drasdo 1977, 1989). A value for M_0 of 12.86 mm/deg is suggested, on the basis of the following equation:

$$M_0^2 = (A_{cort} / N_g) \times D_r$$

where A_{cort} = total area of striate cortex (5000mm^2), N_g = total number of geniculostriate ganglion cells (1,080,000), and D_r = foveal receptive field density of geniculostriate ganglion cells (35,720deg^{-2}). A_{cort} / N_g thus represents the cortical area devoted to any geniculostriate ganglion cell (4.63×10^{-3} mm^2). Alternatively, on the basis of recent monkey data suggesting M_0 to be in the region of 10 mm/deg (Drasdo, 1991), it is suggested that in human this would correspond to an M_0 of 14.4.mm/deg. E_2 values are also proposed for various anatomical structures: for V1, 1.14 deg; magnocellular ganglion cells, 4.76 deg; parvocellular ganglion cells, 1.21 deg; and all ganglion cells taken together, 1.29 deg.

Authors	M_0 (mm/deg)	E_2 (deg)	Comments
Richards (1971)	36.4	0.4	Migraine scotoma dimensions
Cowey & Rolls (1974)	6.1	2.9	Data of Brindley & Lewin ('68)
Drasdo (1977)	11.5	1.69	Various sources
Dobelle et al. (1979)	4.5	3.3	Electrode implant
Rovamo & Virsu (1979)	7.99	2.32-3.43	Various sources
Tolhurst & Ling (1988)	20-25	1.1-1.3	Various sources
Drasdo (1991)	12.86-14.4	1.14	Various sources

Table 3.04. Estimates of M_0 and E_2 in man.

Table 3.04 shows the different estimates obtained for M_0 and E_2 in man. As in the monkey studies, there is a great deal of variation in the results found. Whilst it is accepted that the foveal representation is large throughout the topographic mapping of the visual system, it is still a matter of debate whether all the foveal enhancement occurs at ganglion cell level, or whether there is further foveal magnification at the LGN and / or cortical level. Does the topographic cortical map directly and exactly transpose retinal information from the ganglion cells, such that M is proportional to ganglion cell density? Or, as others have suggested, does the fovea gain extra representation from that at ganglion cell level during its passage through the LGN and into the cortex? If this is the case, eccentricity gradients for cortical magnification will be steeper than those for ganglion cell density and E_2s will be smaller for cortical than ganglion representations.

Early work on monkeys (Talbot and Marshall, 1941; Daniel and Whitteridge, 1961) suggested that cortical magnification was proportional to the square root of ganglion cell density. This assumption was made by several studies estimating M indirectly in man (Drasdo, 1977, 1989; Rovamo and Virsu, 1979). Rovamo and Virsu's estimation made the additional assumption that foveally the ganglion cell: cone ratio was 1:1. Conversely, Drasdo's calculation of foveal receptive field densities indicated a higher value than that found anatomically for cone density. This observation has been borne out by subsequent anatomical studies which find that rather than a foveal ganglion cell : cone ratio of 1:1 (Polyak, 1941), the ratio may be 2:1 (Schein, 1988; Perry and Cowey, 1988) or even greater (Wässle et al., 1989, 1990; Curcio and Allen, 1990). Such high foveal ganglion cell densities are consistent with expansion of the foveal representation occurring only at the ganglion cell level, with no further expansion of the fovea required at subsequent processing stages in the LGN (Schein and de Monasterio,

1987; Schein, 1988) or striate cortex (Wässle et al., 1989, 1990; Curcio and Allen, 1990).

Several authors have claimed that the relative representation of the fovea increases from that at the retina in both the LGN (Malpeli and Baker, 1975; Connolly and Van Essen, 1984; Perry and Cowey, 1988) and the cortex (Dow et al., 1981; Van Essen et al., 1984; Perry and Cowey, 1985; Levi et al., 1985; Tolhurst and Ling, 1988; Silveira, Picanço-Dinaz, Sampaio and Oswaldo-Cruz, 1989; Azzopardi and Cowey, 1993). To quantify this difference it has been noted (Connolly and Van Essen, 1984) that the central 5 deg of visual field is processed by 20% of layer 6 of the LGN, and by 42% of the striate cortex. While central ganglion cells outnumber those at 80 deg eccentricity by a factor of 50 (Rolls and Cowey, 1970), 100 (Curcio and Allen, 1990) or 300 (Perry and Cowey, 1985), the equivalent ratio for LGN cell density is 870 (Connolly and Van Essen, 1984), and that for areal cortical magnification is 4400 (Van Essen et al., 1984). Tolhurst and Ling (1988) suggested that Rovamo and Virsu's estimate (1979) of 8 mm/deg for M_0 might be accurate for ganglion cells, whilst the foveal emphasis of the cortex was best represented by a higher M_0 of 20-25 mm/deg. Levi et al. (1985) also suggested that since the emphasis on central vision appeared to be greater in the cortex than at the retina, separate retinal and cortical eccentricity gradients exist. These were proposed to have E_2 values of 2.5 deg for retinally limited resolution tasks, whilst cortically limited positional acuities would correspond to the cortical gradient, with an E_2 of 0.8 deg.

Additionally, some evidence suggests that foveal overrepresentation might differ for magnocellular and parvocellular pathways. Several studies suggest that the majority of overrepresentation in the P pathway occurs in the retino-geniculate projection (Connolly and Van Essen, 1984; Perry and Cowey, 1985; Azzopardi, 1994), whereas that for the M pathway occurs in the geniculo-cortical projection (Connolly and Van Essen, 1984; Azzopardi, 1994).

Whilst there is considerable evidence that the emphasis on central vision is greater in the cortex than in the retina, such expansion may be smaller than suggested. Estimates of foveal ganglion cell density are difficult to make in the face of ganglion cell displacement and the presence of displaced amacrine cells. Early estimates may have underestimated foveal ganglion cell receptive field density (Drasdo, 1991) by underestimating the number of geniculostriate ganglion cells and overestimating the contribution of displaced amacrine cells. Additionally, some monkey studies of the cortex appear to have overestimated M_0 (Dow et al., 1981). Both underestimating

ganglion cell density and overestimating M_0 will appear to make any foveal overrepresentation larger than it is. An interesting point to note is that while we assume the macaque to be a good model for human visual function (Tolhurst and Ling, 1988), the hilum of the LGN in macaque is more pointed (60 deg apical angle) than that of man (90 deg). It seems reasonable that this angle might reflect the amount of parvocellular expansion in the LGN, as the topographies remain in register across the thalamic layers. If this is the case man may have less foveal expansion, at least at LGN level, than the macaque demonstrates. Drasdo (1991) suggests that the E_2 value for retinal ganglion cells is 1.29 deg (or 1.21 deg for P ganglion cells alone), while that for the striate cortex is 1.14 deg, reflecting a small foveal overemphasis in the cortex.

3.5 Summary

Limitations are placed on foveal and peripheral vision at every level of the visual pathway, from photoreceptors and retinal ganglion cells to the visual cortex and beyond. Whilst much anatomical data has been obtained, there is still much that is not known. The topographies of human photoreceptors and ganglion cells are well documented, but the relative distributions of ganglion cell types, particularly M and P projecting cells, are not known with certainty. The visual cortex has been extensively mapped in macaque monkey, but results vary considerably between studies, and there is little information available regarding humans. In the light of such discrepancies, it is unsurprising that there is little consensus as to whether ganglion cell and cortical topographies are identical, or whether the foveal representation expands along the visual pathway. In summary, assumptions made on the basis of anatomical and physiological data should be viewed with caution. Psychophysical observations made without the need for such *a priori* assumptions may be able to tell us much about the workings of the human visual system.

Chapter 4
Psychophysical studies of peripheral vision

4.1 Introduction

Cortical magnification equations derived from anatomical measurements and estimates were discussed in the previous chapter. The use of these equations in the psychophysical procedure of M-scaling is now discussed as a means used to attempt to equate foveal and peripheral visual performance. Studies using spatial scaling, the method used in this thesis, are then examined.

4.2 Cortical magnification

From Chapter 3 we know that M, the linear amount of cortex representing 1 deg of visual field, declines with eccentricity. According to the theory of cortical magnification (Virsu and Rovamo, 1979), enlarging peripheral stimuli by M_0 / M_E (where M_0 is the foveal value of M, and M_E is the value of M at eccentricity E) will equalise the cortical representation of all stimuli, and result in equivalence of thresholds at all points in the visual field. This procedure, known as M-scaling, has been applied to a variety of tasks with varying degrees of success. The following studies have employed prechosen magnification factors of some kind, such as those defined by cortical magnification theory.

4.2.1 Studies in which M-scaling was successful

Rovamo et al. (1978) first proposed their invariance principle for static grating detection in nasal and inferior fields. With gratings of a constant size, contrast sensitivity reduced with eccentricity, and the peak spatial frequency shifted to lower spatial frequencies. This data is shown in Figure 2.08. For gratings scaled in size according to the magnification factor of Cowey and Rolls (1974), with a value of M_0 of 7.75 mm/deg, and a prechosen E_2 of 2.2 deg, the contrast sensitivity functions collapsed to an apparently single function, as shown in Figure 4.01.

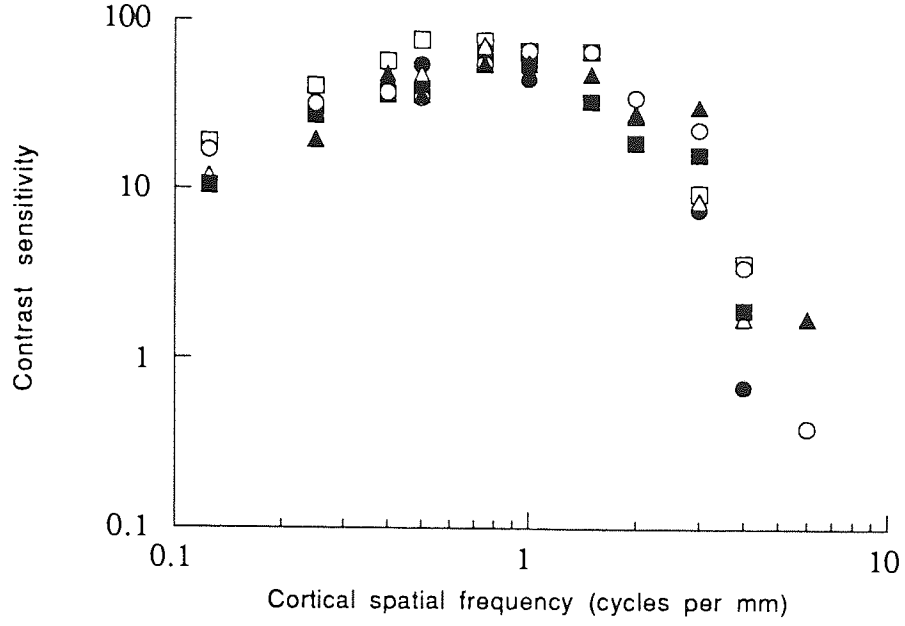

Figure 4.01. From Rovamo et al (1978). Their Figure 1b replotted. Contrast sensitivity measured with M-scaled stimulus gratings in inferior visual field. Open squares: 0 deg; closed circles: 1.5 deg; open triangles: 4 deg; closed squares: 7.5 deg; open circles: 14 deg; closed triangles: 30 deg.

Detection of sine wave gratings moving at 4Hz was examined from 0-50 deg in the nasal field by Koenderink et al. (1978). Detection thresholds could be made as good as those foveally if the targets used were large enough, the only difference being a shift to lower spatial frequencies at greater eccentricities. The data was scaled with respect to the 'just resolvable distance', and Figure 4.02 shows how detection thresholds vary in terms of the just resolvable distance at any eccentricity. After scaling, a small systematic trend still exists, but the authors were able to conclude that "instead of a sensitive fovea and an almost blind periphery, we have to reckon with a visual field that is more or less equally sensitive anywhere." The authors noted that their just resolvable distance correlated well in the periphery with retinal interganglion cell distance (Drasdo, 1977).

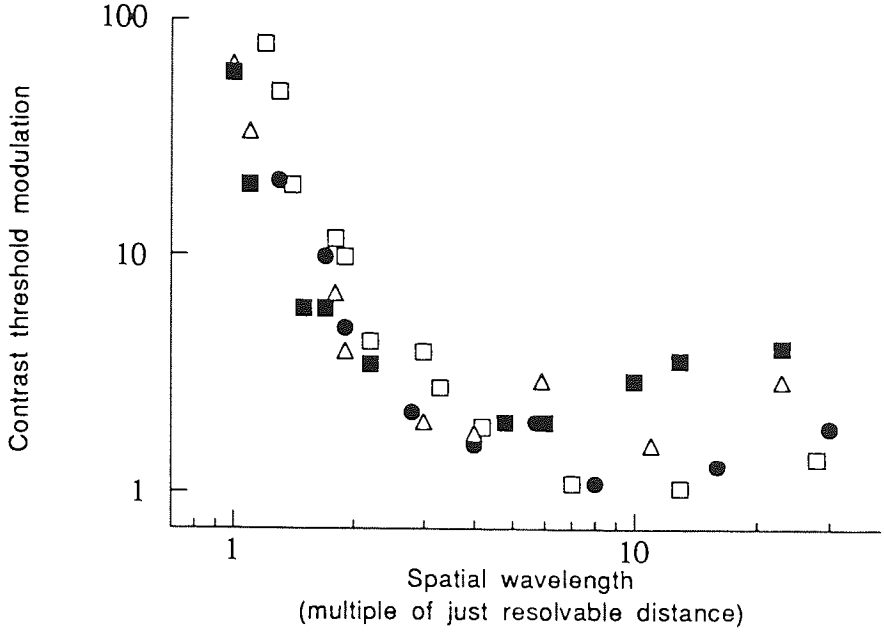

Figure 4.02. From Koenderink et al. (1978). Their Figure 7 replotted. Contrast modulation thresholds plotted against spatial wavelength in units of just resolvable distance at any eccentricity. Open squares: 0 deg; closed circles: 6 deg; open triangles: 21deg; closed squares: 50 deg.

Virsu and Rovamo (1979) first introduced the term 'M-scaling'. Contrast thresholds were obtained for grating detection, grating orientation discrimination and discrimination of direction of movement in the inferior visual field. The target in all cases was a semicircular grating with a radius of 8 cm and the straight edge closest to fixation. Enlargement of peripheral stimuli was achieved by changing the viewing distance, and the magnification factors used were those used in Rovamo et al. (1978) (M_0 7.75 mm/deg, E_2 2.2 deg). With the magnified stimuli providing 'equivalent cortical projections', contrast sensitivity functions became similar at all locations, but showed a systematic shift to lower spatial frequencies at greater eccentricities. If spatial frequency was expressed in cycles per cortical mm, rather than in cycles per degree, all differences disappeared and the peak spatial frequencies became similar. The scaling breaks down slightly at high spatial frequencies, but this is attributed to optical attenuation.

In their subsequent paper, Rovamo and Virsu (1979) derived equations for application to M-scaling in man (see Table 3.03). Using these equations, contrast thresholds were found for 25 locations along all four major field meridia, with peripheral stimuli scaled in size according to the appropriate equation. Contrast sensitivity plotted against cortical

spatial frequency (spatial frequency / M_E) was similar at all locations, except for an increase in variance at the highest spatial frequencies again. The introduction of Rovamo and Virsu's equations for cortical magnification prompted a spate of studies of peripheral vision to which the equations were applied.

Virsu, Rovamo, Laurinen and Näsänen (1982) repeated the study of Rovamo and Virsu (1979) for spatiotemporal contrast sensitivity in nasal visual field. Stimuli were M-scaled for area, spatial frequency, and translational velocity. M-scaling normalised thresholds for movement, counterphase flicker and on-off flicker from 0-25 Hz, and for thresholds of grating detection, orientation discrimination and discrimination of direction of motion. They concluded that central and peripheral vision are qualitatively similar for spatiotemporal visual performance. Another study by Rovamo, Leinonen, Laurinen and Virsu (1984) found that the dependence of contrast sensitivity on exposure duration was independent of eccentricity, so long as the stimuli were M-scaled.

Kelly (1984) examined spatiotemporal contrast sensitivity from 0-12 deg. His stimuli were annuli of sinusoidal gratings, with the annuli increasing in size with eccentricity with an equivalent prechosen E_2 of 1.6 deg. Under these conditions, spatial contrast sensitivity was measured for temporal modulations of 0.5 and 10 Hz. With a temporal modulation of 0.5 Hz, the resulting contrast sensitivity functions (shown in Figure 4.03) were bandpass and of the same form at each eccentricity, the only difference being a shift to lower spatial frequencies with increasing eccentricity. The change in peak spatial frequency with eccentricity agreed well with the cortical magnification equations of Rovamo and Virsu (1979).

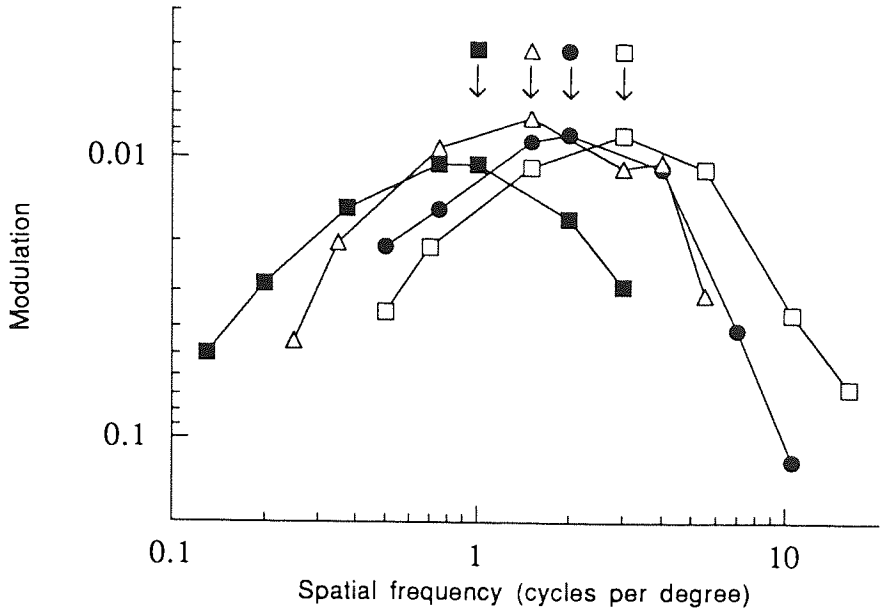

Figure 4.03. From Kelly (1984), his Figure 5. Spatial contrast sensitivity at 0.5 Hz for annular stimuli of different nominal eccentricities. Open squares: 0 deg; closed circles: 3 deg; open triangles: 6 deg; closed squares: 12 deg. The upper arrows show estimated spatial frequencies for maximum sensitivity at each eccentricity (1, 1.5, 2 and 3 cycles per degree). These values were used for the temporal contrast sensitivity function shown in Figure 4.04.

Using stimuli having been shown to have peak spatial frequency at each eccentricity, Kelly then measured temporal contrast sensitivity. Scaling the spatial frequencies with eccentricity in this way gave a single low pass temporal contrast sensitivity function, independent of eccentricity, as shown in Figure 4.04. Temporal contrast sensitivity measured with lower spatial frequencies, but which had given identical contrast thresholds with eccentricity in the previous experiment, resulted in a band pass function. The only deviation from scaling here was a greater sensitivity for high temporal frequencies in the periphery.

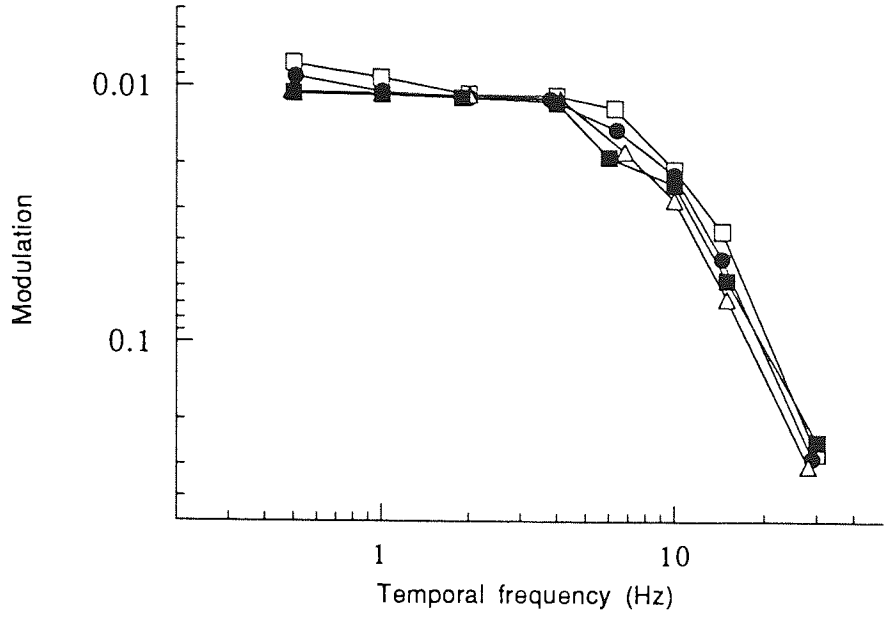

Figure 4.04. From Kelly (1984), his Figure 7. Contrast sensitivity as a function of temporal frequency for annular stimuli of various nominal eccentricities. Symbols as in Fig 4.03. Measurements are made at the peak spatial frequency for each eccentricity, as indicated by the arrows in Fig 4.03.

Movement

The fine-grain movement illusion was investigated by Foster, Thorson, McIlwain and Biederman-Thorson (1981). Brief peripheral presentation in rapid sequence of two luminous point stimuli too close together to be resolved gives the illusory impression that a single dot moves over a path of considerable extent. This study showed that the apparent extent of the illusion increased with eccentricity, at a rate described by the equation:

$$\text{Illusion extent} = 0.28 + 0.23E$$

Since this is of the form of Equation 2.09, $E_2 = 0.28 / 0.23 = 1.2$ deg. The authors noted that if the extent of the illusion was expressed in terms of cortical length, by multiplying the illusory extent by M at that eccentricity (Cowey and Rolls, 1974), a relatively constant cortical extent of 3 mm was observed. Note that the authors' analysis of the data of Cowey and Rolls (1974) gives a regression of the form:

$$1 / M = 0.091 + 0.067E$$

so that from Equation 2.09, $E_2 = 0.091 / 0.067 = 1.36$ deg, comparable with their findings of illusion extent, and $M_0 = 1 / 0.091 = 10.99$ mm/deg.

Van de Grind, van Doorn and Koenderink (1983) examined detection of coherent motion for different velocities in moving random dot patterns. Eccentricities of 0-48 deg in temporal visual field were examined, and stimuli were scaled according to the equations of Drasdo (1977) (M_0 11.5 mm/deg; E_2 2.17 deg). The cortical coherent motion for such stimuli was found to be similar at all eccentricities, although it was noted that some eccentricity dependence remained which might be eliminated by the use of a slightly different scaling factor.

McKee and Nakayama (1984) measured differential motion detection and velocity discrimination thresholds for stimuli in the inferior field. Differential motion stimuli were scaled by a prechosen E_2 of 3 deg according to Weymouth's (1958) acuity data, and were measured by different means at the fovea (random dots) and in the periphery (line stimuli). Thresholds expressed relative to the foveal threshold were linear with eccentricity, with a gradient steeper than that for visual acuity. The relevance of this finding is limited since foveal and peripheral thresholds were determined differently. Velocity discriminations of 6% could be achieved at all eccentricities, but this was achieved at higher velocities (deg per sec) for greater eccentricities. Expressing velocity in resolution units per second, in other words by scaling according to MAR, resulted in the data conforming to an approximately single function.

Short range apparent motion perception was investigated with eccentricity by Baker and Braddick (1985). This percept induces a sensation of motion, produced by discontinuous presentation with a short interstimulus interval of two successive positions with a small displacement. It is thus similar to the fine grain movement illusion studied by Foster et al. (1981). The minimum displacement for apparent motion, d_{min}, increased with eccentricity in a manner compatible with cortical magnification (Rovamo and Virsu, 1979). The maximum displacement producing apparent motion, d_{max}, increased at a rate faster than that predicted by M-scaling.

The lower threshold of motion (LTM) is the rate of movement at which a drifting grating can just be distinguished from a stationary one. LTM, expressed as a temporal frequency (Hz) and measured from 0-7.5 deg in inferior visual field, increases with eccentricity and is dependent on spatial frequency (cycles per deg). If spatial frequency is defined in cortical terms (cycles per mm), LTM still increases with spatial frequency, but is independent of eccentricity. Further, if expressed as a cortical velocity (mm/s) using the equations of Rovamo and Virsu (1979), LTM is invariant of eccentricity and spatial frequency, having a constant cortical velocity of 0.15-0.16 mm/s (Johnston and Wright, 1983, 1985). The motion aftereffect represents apparent movement of a

stationary grating in the opposite direction to a previously presented pattern moving in a given direction. The motion aftereffect (MAE) can be measured as the temporal frequency of drift required to cancel the illusory motion percept (Johnston and Wright, 1983; Wright and Johnston, 1985b). Using this method, similar results to those for LTM were found, with MAE in terms of cortical velocity measuring 0.78-1.2 mm/s. A similar effect has also been found for threshold amplitude for detecting square wave oscillatory motion of a sinusoidal grating (Wright and Johnston, 1985a). When M-scaled in accordance with the M-scaling equations of Rovamo and Virsu (1979) a constant cortical threshold distance of 0.03 mm was observed. It was concluded that 'in the analysis of visual motion, the near periphery is not qualitatively different from foveal vision'.

Colour Vision

Traditionally, colour vision of the peripheral retina has been thought to be poorer than at central retinal locations. This opinion has been derived from many experiments, not least the work of Moreland and Cruz (1959) who found, using an asymmetric colour matching technique, that the retina appears to change from trichromatic centrally to dichromatic by 25-30 deg, and monochromatic by 40-50 deg eccentricity. In all early studies, target size remained constant with increasing eccentricity. Some studies concluded that the peripheral retina was tritanomalous (Moreland and Cruz, 1959; Abramov and Gordon, 1977) while others found evidence of peripheral deutanomaly (Moreland, 1972; Wooten and Wald, 1973; Obstfeld, 1981). However, Wooten and Wald (1973) showed that all three cone mechanisms were present to 80 deg in peripheral retina. Gordon and Abramov (1977) used large peripheral targets and concluded that "it is misleading to term the peripheral retina colour blind, or even colour deficient. The quality of colour vision in the periphery depends crucially on stimulus size." A fully saturated range of colours is only observable to 20 degrees, however (Abramov, Gordon and Chan, 1991).

More recent studies of peripheral colour vision have included stimulus size as a variable and have shown that colour vision in peripheral retina can be made as good as that at the fovea if peripheral target sizes are M-scaled. Noorlander, Koenderink, den Ouden and Edens (1983) assessed spatiotemporal colour contrast at several retinal locations as a function of target size. They could find no retinal locale that was either red-green or blue-yellow blind, provided the stimulus used was "suitably" enlarged. The peripheral sensitivities for chromatic contrast could be brought up to foveal levels simply by reducing the spatial frequencies of equiluminant chromatic gratings, and spatiotemporal colour discrimination was practically constant as a function of eccentricity if the target

size was scaled according to Drasdo's (1977) estimate of the cortical magnification factor or the reciprocal of the interganglion cell distance.

Van Esch, Koldenhof, van Doorn and Koenderink (1984) found spectral sensitivity measured by flicker photometry at 20 Hz to be independent of eccentricity between 0 and 80 deg in temporal visual field, if target size was scaled according to the cortical magnification factor of Rovamo and Virsu (1979), and foveal performance was corrected for macular pigment absorption. Wavelength discrimination could also be made approximately independent of eccentricity by magnification, but only from 8 to 80 deg. Foveal discrimination performance remained considerably better than that in the periphery.

Other tasks

Ransom-Hogg and Spillmann (1980) analysed perceptive field sizes from 0-70 deg in temporal visual field using the Westheimer paradigm. The perceptive field is a hypothetical psychophysical correlate of the receptive field, representing the centre-surround antagonism of receptive fields. The Westheimer paradigm (Westheimer, 1965) shows perceptive fields by measurement of increment thresholds for a small test spot on steady background discs of varying diameter. With increase of background diameter, thresholds first rise to a peak representing the size of the perceptive field centre. Thresholds then fall, and finally begin to plateau. The total size of the perceptive field is represented as the background size at which the plateau starts. Under photopic conditions both centre and total field sizes increase with eccentricity. The rise in total perceptive field size with eccentricity relates to the inverse of cortical magnification as calculated by Cowey and Rolls (1974). A constant amount of cortical space was seen to be devoted to a perceptive field, irrespective of retinal eccentricity.

Meredith and Celesia (1982) examined the effects of eccentricity on localised pattern evoked visual potentials (pattern VEPs). The smallest field size required to evoke a potential was measured from 0-18 deg in horizontal, vertical and oblique meridia. When these field sizes were expressed in terms of cortical extent by M-scaling, the equations of Cowey and Rolls (1974) gave a constant cortical area with eccentricity. The equations of Rovamo and Virsu (1979), however, underrepresented the fovea.

Scobey (1982) examined orientation discrimination thresholds for a line on an unstructured background, as a function of line length and eccentricity to 10 deg. Thresholds improved with line length to a critical value and then plateaued. The critical line length was longer at greater eccentricities, but equivalent optimum thresholds

occured at each location. The increase in critical line length with eccentricity correlated well with Hubel and Wiesel's (1974) estimates of monkey cortical receptive field size, from which the authors derived an E_2 of 4.3 deg and successfully applied this to the data.

Hampton and Kertesz (1983a) measured the horizontal extent of Panum's area by presenting a single vertical line to each eye, which was scaled with eccentricity according to the M-scaling equations of Rovamo and Virsu (1979). The maximum disparity giving a single percept was taken to represent the extent of Panum's area, and was found for various locations in the visual field. The increase in size of Panum's area with eccentricity was found to correlate well with the cortical magnification factor, although some meridional variation was noted.

The tilt after effect (TAE) represents the apparent tilt of a line or grating following inspection of a line or grating of slightly different orientation. Calvert and Harris (1985) found that M-scaling abolishes the eccentricity related increase in TAE observed with stimuli of constant retinal size. Both the retinal size and spatial frequency of the stimuli need to be M-scaled to achieve isosensitivity.

The purpose of Nothdurft's study (1985) was to compare sensitivity for line orientation with the ability to discriminate texture areas on the basis of different structure orientation. Thresholds for both tasks were found as a function of line length for eccentricities up to 30 deg in nasal visual field. The minimum line length required for accurate assignation of orientation increased with eccentricity, but was consistently shorter than the line length required to make texture discriminations. Using these results, line length was set at 5 times the texture discrimination threshold at all eccentricities. When texture discrimination thresholds were then measured as a function of the orientation difference between texture areas, thresholds did not vary markedly with eccentricity. This was taken to support the concept of magnification scaling (Virsu and Rovamo, 1979).

Swanson and Wilson (1985) obtained contrast detection thresholds at 0 and 8 deg, and found that the results could be made equal by scaling the peripheral data by a factor of 2, so that E_2 was therefore 8 deg. This scaling factor was incorporated into a foveal model of spatial vision by scaling the peak spatial frequencies of the model's filters with eccentricity. The adapted model was found to provide good fits to suprathreshold data for contrast matching and oblique masking.

Saarinen, Rovamo and Virsu (1987) successfully M-scaled the task of texture discrimination. Their stimulus consisted of two random dot patterns of equal dot density, but varying in the smallest interdot distance in the pattern. Thus, while the first order characteristics of the texture were identical, the second order statistics were different. The task of the observer was either to detect dissimilarity between the two texture patterns, or to detect the locations of the two textures. The foveal stimulus measured 2.5 deg on each side, and peripheral stimuli were M-scaled from this according to the equations of Rovamo and Virsu (1979) by reducing viewing distance. Under these conditions, texture discrimination became practically independent of eccentricity between the fovea and 25 deg nasal field.

Virsu et al. (1987) defined an M-scaling success as one where less than 10% of the original eccentricity dependent variation remained after scaling. Using this criterion, four visual acuity tasks could be made to M-scale. These were grating acuity, Snellen E acuity, discrimination of mirror symmetric stimuli consisting of three dots, and discrimination of three abutting dots from three separated dots. Llandolt ring acuity could not be made to M-scale. Two hyperacuity tasks were additionally investigated. Two-dot vernier acuity was measured from 0-20 deg in the left visual field with binocular viewing. The stimulus elements were two dots of constant size (1 min arc square) with eccentricity. When vernier offset was expressed as the angular orientation of threshold offset as a function of dot separation, thresholds were found to scale according to the equations of Rovamo and Virsu (1979). M-scaling did not remove eccentricity dependence from a bisection task however.

Higgins, Arditi and Knoblauch (1992) examined the ability to detect and discriminate lower case letters 'b' and 'd' to 7.5 deg eccentricity. These letters have almost identical spatial frequency content, but differ in their relative phase: the odd spatial frequency components differ by 180 deg in phase angle. Peripheral stimulus sizes were scaled according to Rovamo et al. (1978) (M_0 7.75 mm/deg, E_2 2.2 deg). The proportion of correct responses as a function of contrast then had identical slopes at each eccentricity. This successful M-scaling result is in contrast to several other studies of phase discrimination (see below).

4.2.2 Studies in which M-scaling was unsuccessful

Whilst an impressive range of stimuli can be successfully scaled by the inverse of the cortical magnification factor, a substantial number have been found which do not scale according to 1 / M. These stimuli fall into the general categories of temporal

discriminations, binocular interactions, perimetry, and processing of spatial relationships.

Temporal discriminations

Westheimer (1983) determined thresholds for detection of temporal order of onset of adjacent stimuli. Thresholds were measured for a range of stimulus separations in the left and inferior visual fields, with binocular viewing. Stimulus line length was increased from 12 min arc at the fovea to 60 min arc at 20 deg, although line length is not a critical parameter in this task, at least at the fovea. Optimum threshold remained constant with eccentricity at around 4 ms. The separation required to attain optimum threshold increased from 0 to 2.5 deg, but then remained fairly constant with further increase in eccentricity, thus changing far more slowly with eccentricity than visual acuity or cortical magnification would suggest.

Detectability of amplitude modulation and spatial frequency modulation of suprathreshold sine wave gratings were investigated by Jamar, Kwakman and Koenderink (1984). Data were obtained with unlimited viewing times for 0-30 deg in nasal visual field. Stimuli were size scaled in order to equate contrast thresholds, correlating well with the values of Rovamo and Virsu (1979). Despite M-scaling, thresholds for both tasks were worse for peripheral than for foveal vision. The authors concluded that while central and peripheral vision could perform equally well for contrast detection, peripheral vision was much less able to utilise information presented in suprathreshold gratings for discrimination tasks.

Critical flicker frequencies (CFF) were found to increase with eccentricity even after M-scaling with respect to retinal area (Rovamo and Raninen, 1984). If M-scaled with respect to retinal illuminance, thresholds fell with eccentricity. This procedure was later named F-scaling (Raninen and Rovamo, 1986), and its intention is to make the amount of luminous flux collected by ganglion cells invariant across the visual field, assuming that photopic Ricco's area estimates the area of the ganglion cell receptive field area. CFF thresholds could, however, be made independent of visual field location, but only by M-scaling both retinal area and illuminance, or MF-scaling. However, as Drasdo (1991) observed, it seems anomalous to apply F-scaling only to those tasks which do not M-scale, since all thresholds change with illuminance to some extent.

Binocular interactions

Fendick and Westheimer (1983) examined stereoacuity thresholds between 0 and 10 deg. Stimuli were scaled with a prechosen E_2 value of 2.5 deg according to acuity

considerations. Optimum stereothresholds occured at greater separations with eccentricity. Optimum thresholds increased with eccentricity with an E_2 of approximately 0.4 deg, a steeper increase with eccentricity than that found for acuity or cortical magnification.

Hampton and Kertesz (1983b) examined binocular fusion capabilities across the visual field. At meridia every 45 deg and eccentricities of 0-20 deg, dichoptic horizontal convergent disparities were presented to observers, which were M-scaled (Rovamo and Virsu, 1979) in size and disparity. The motor component of binocular fusion, vergence eye movements, were measured in response to stimulus presentation. Vergence movements had greater latency and duration in peripheral vision, and compensated for a lower proportion of the disparity with greater eccentricity. Variations in the size of the motor fusional response with eccentricity could not be explained by M-scaling.

Perimetry

By the time Rovamo, Raninen and Virsu (1985) reviewed their work on the cortical magnification factor to date, it had become obvious that M-scaling, as such, was incomplete. M-scaling could not equate thresholds at different field locations for CFF (Rovamo and Raninen, 1984) or for positional acuities (see below). Their suggestion was that M-scaling compensates only for the decrease in sampling density of retinal ganglion cells, and that F-scaling was also required for some tasks to compensate for the increase in receptive field size with eccentricity. Such a position assumes that all retinotopic differences could be explained at the retinal level by changes in density, size and overlap of sampling apertures. The visibility of perimetric stimuli was suggested to be a task suitable for MF-scaling. The equations given with which to MF-scale a task give an equivalent E_2 value of 10.72 deg for nasal visual field. They described the resultant isosensitivity profile as a 'perimetrogram' in which visual field defects would be readily observed as pits.

Wild, Wood and Barnes (1986) looked at perimetric thresholds with the Friedmann Visual Field Analyser. This perimeter gives an essentially isosensitive perimetric profile by the use of stimuli which increase in size with eccentricity in an experimentally determined manner, at a low photopic luminance of 1 asb. The stimulus diameters employed in the perimeter were compared with those calculated by M-scaling (Rovamo and Virsu, 1979) to result in equivalence of cortical projection with eccentricity. The M-scaled diameters were found to be larger than those used to achieve isosensitivity, a difference which increased with eccentricity to up to 3.5 times the diameter of the Friedmann stimuli. It was suggested that the reason for the for the M-scaling failure

was that sensitivity to perimetric spot stimuli does not depend solely on ganglion cell density, but additionally on the spatial summation exhibited by ganglion cells, which increases with peripheral angle, and decreases with increasing luminance.

Wood et al. (1986) extended their examination of M-scaling perimetric stimuli by use of the Octopus perimeter. This instrument has a background luminance of 4 asb, a stimulus duration of 100 ms, and employs stimuli subtending 0.054 to 1.724 deg visual angle. As before, perimetric sensitivity with M-scaled stimulus sizes increased with eccentricity and did not provide an isosensitive profile. Target sizes were calculated which would result in an isosensitivity profile. From these stimuli, E_2 can be calculated to be 5.6 deg for nasal visual field (0-35 deg range), and 8.5 deg for temporal field (0-45 deg range). It was again concluded that perimetric sensitivity is dependent upon both ganglion cell density and on spatial summation. Anatomically, the product of these two factors (dendritic field area and cell density) is defined as the coverage factor (Perry and Cowey, 1985).

Wild et al. (1987) then examined perimetric thresholds on the Humphrey Field Analyser (HFA), a perimeter with a higher background luminance (31.5 asb) and longer stimulus duration (200 ms) than the Octopus perimeter- both conditions favouring reduced spatial summation. Thresholds were measured to 60 deg with stimulus sizes 0.108-1.724 deg. M-scaled stimulus diameters were calculated using the equations of Rovamo and Virsu (1979) to equate sensitivity at all locations, relative to a 0.108 deg foveal stimulus. The actual sensitivity found with such stimulus sizes at the relevant locations was then interpolated. It was found that M-scaling in this way did not result in an isosensitive profile. A paracentral reduction in sensitivity to approximately 12 deg was seen, beyond which sensitivity increased monotonically with further increase in peripheral angle. It was noted that scaling with Drasdo's (1977) equations gave less paracentral sensitivity reduction. The authors concluded that under these conditions of reduced spatial summation, an underrepresentation of the fovea in M-scaling equations was revealed.

Figure 4.05a shows the data of Wild et al. (1987) (their Fig 2a) replotted to 30 deg for the superior visual field. The data curves for successive eccentricities are of the same form but displaced to larger sizes with increasing eccentricity. By determining the amount of shift along the size axis required to superimpose each data curve onto the foveal data, scaling factors are derived. These scaling factors, when plotted as a function of eccentricity, can be used to find a value for E_2 using an equation of the form of Equation 2.10. E_2 for superior field found in this way is 3.64 ± 0.10 deg, while that

for inferior field (not shown) is 5.98 ± 0.55 deg. In comparison, E_2 for the superior visual field, according to Rovamo and Virsu (1979), is 2.32 deg. In Figure 4.05b, the data has been scaled with respect to the E_2 value of 3.64 deg by shifting the peripheral curves by a scaling factor (SF) derived from the E_2 value according to the equation, $SF = 1 + (E / E_2)$. This procedure removes the majority of the eccentricity dependence from the data.

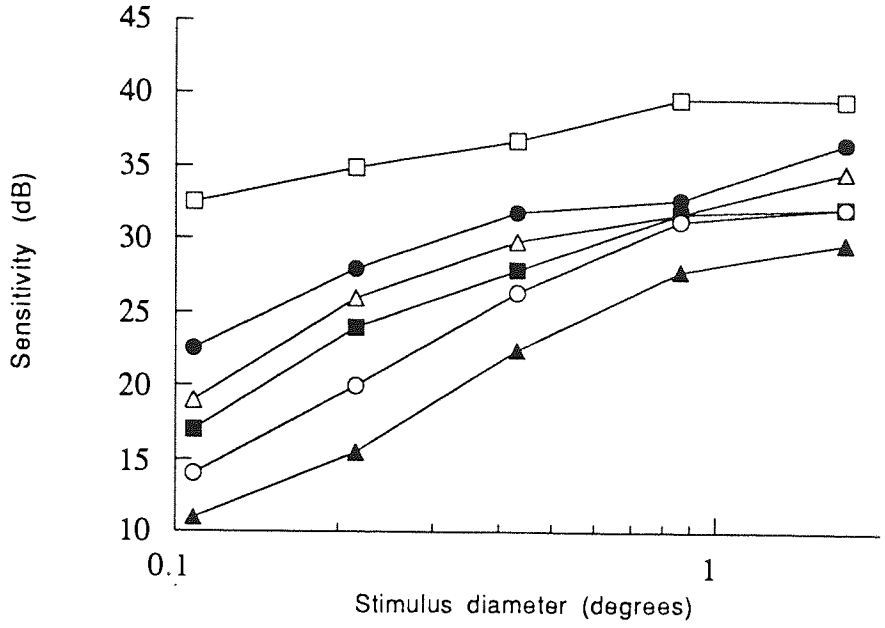

Figure 4.05a. From Wild et al. (1987). Their Figure 2a replotted. Perimetric sensitivity for static stimuli on the Humphrey perimeter measured as a function of stimulus size for a number of eccentricities in superior visual field. Open squares: 0 deg; closed circles: 6 deg; open triangles: 12 deg; closed squares: 18 deg; open circles: 24 deg; closed triangles: 30 deg.

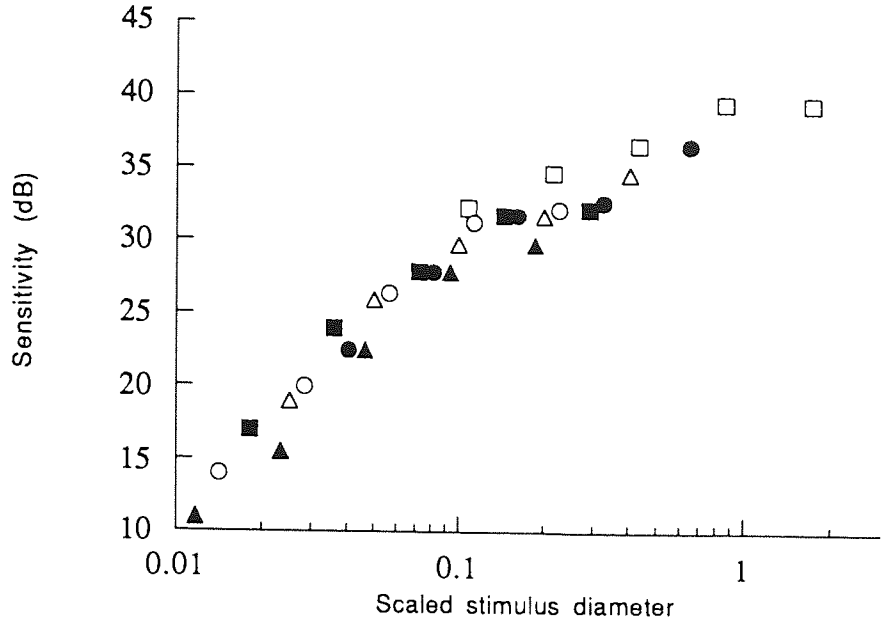

Figure 4.05b. The data of Figure 4.05a scaled at each eccentricity according to the equation: SF = 1 + (E / 3.64). Symbols as in 4.05a.

One study has however noted an M-scaling success in perimetry, as noted by Wild et al. (1987). Drum, Armaly and Huppert (1986) investigated photopic and scotopic perimetric thresholds in normal observers and glaucoma patients. Under photopic conditions (40 asb), and with stimuli size scaled according to retinal ganglion cell densities of Perry et al. (1984), sensitivity was essentially constant from 5 to 15 deg eccentricity.

Spatial relationships

Westheimer (1982) examined 2-dot vernier acuity and orientation discrimination as a function of eccentricity. In the vernier experiment, stimuli consisted of two squares, each of 1 min arc side length, which remained fixed in size with eccentricity. Vernier and orientation thresholds were seen to rise far more steeply with eccentricity than the minimum angle of resolution or cortical magnification. However, the feature separation at which optimum thresholds were achieved rose more slowly than MAR with eccentricity.

Levi, Klein and Aitsebaomo (1984) examined unreferenced motion thresholds to 20 deg eccentricity, with stimulus sizes scaled according to a prechosen E_2 of 2.5 deg. The rise in thresholds in the periphery was represented by the x-intercept value of a plot of

normalised threshold against eccentricity. This value indicates at what peripheral angle foveal thresholds will double, and its positive value was later (Levi et al., 1985) termed the E_2 value. E_2 for unreferenced motion was found to be 5.6 deg for a normal observer's detection thresholds, and 5.8 deg for the same observer's discrimination thresholds. Since these values compared with E_2s for grating acuity of 2.5 deg, and 1.0 deg for vernier or Snellen acuity, the authors concluded that a single magnification factor does not exist. Different acuities might be processed in different cortical regions, or cortical and retinal factors might impose different limitations on different tasks.

The theme of different scaling factors was expanded by Levi et al. (1985) in their study of vernier acuity in the periphery. In this instance, the abutting repetitive vernier stimuli were scaled according to an E_2 of 0.77 deg. This value was based on an analysis of the data of Dow et al. (1981). Using such stimuli, peripheral and foveal vernier acuity could be equated with an E_2 value of 0.62 ± 0.08 deg, for the same observer as participated in the motion study (Levi et al., 1984). It was concluded that the scaling factor for grating acuities reflected that the task was limited by retinal processes, while that for position acuities was due to cortical limitations on the task. E_2 values of 0.8 deg for cortical processing and 2.5 deg for retinal processing were given. Such a position contradicts the assumption (Rovamo and Virsu, 1979) that cortical magnification is proportional to mean interganglion cell spacing, and implies an increase in foveal representation from retina to cortex (see Chapter 3).

Paradiso and Carney (1988) used the cortical magnification factor of Levi et al. (1985), where E_2 is 0.8 deg, with respect to their orientation discrimination data. M-scaling in this way was successful to 20 deg. Beyond this eccentricity, thresholds were better in temporal than in nasal visual field, suggesting that the magnification factor must decrease faster in nasal than in temporal field. Mäkelä, Whitaker and Rovamo (1993) suggest that an E_2 of 1.95 deg provides a better representation of this data.

Deeley and Drasdo (1987) investigated the effects of optical degradation on contrast sensitivity, to see if this factor might explain some of the differences becoming apparent between threshold gradients for grating acuity and hyperacuity. Contrast sensitivity functions were measured for annular stimuli subtending 0.5 deg at the fovea, and spanning eccentricities 0.5-1 deg, 1-2 deg and 2-4 deg. With hindsight, Drasdo (1991) observes that the extent of these annular stimuli was somewhat arbitrary, affecting the gradients in 'an imponderable manner'. The increase in the spatial frequency of peak contrast sensitivity ($1 / SF_{max}$) with eccentricity corresponded to an E_2 of 1.33 deg. When a correction was applied for optical degradation based on the modulation transfer

function (MTF), the threshold gradient steepened and E_2 became 0.41 deg. This was consistent with the idea that grating acuity and hyperacuity show the same steep decline in performance with eccentricity, but this is masked for grating acuity by the effects of optical degradation. Hyperacuities, on the other hand, often demonstrate considerable resistance to optical degradation (Westheimer, 1979b, Williams et al., 1984).

Stephenson and Braddick (1983), and Stephenson, Knapp and Braddick (1991) compared compound grating detection and phase discrimination thresholds for gratings consisting of a fundamental spatial frequency with a third harmonic either added to or subtracted from the peak. Discrimination thresholds rose more sharply with eccentricity than detection thresholds over a range of spatial frequencies, and differences still occured when the stimuli were M-scaled. The authors concluded that foveal and peripheral vision are qualitatively different.

Rentschler and Treutwein (1985) also examined phase discrimination for compound gratings at the fovea and at 2 deg eccentricity. Test and comparison gratings consisting of a fundamental frequency and a third harmonic were presented at the same location in sequence, with the observer's task to decide whether the two gratings differed. When the two gratings differed in phase by 0 or 180 deg, such that they were mirror images of one another, no contrast differences exist apart from in the relative position of local contrast regions. Even when these stimuli were M-scaled (Rovamo and Virsu, 1979) performance declined to chance level at 2 deg eccentricity. For stimuli of an intermediate phase shift with local contrast differences between the gratings, thresholds could be equated at 0 and 2 deg by M-scaling the stimuli. It was concluded that while contrast detection could be made equal at the two locations, peripheral vision was qualitatively poorer than the fovea at spatial localisation. In response, Livingstone and Hubel (1985) suggested that spatial localisation might merely decline faster with eccentricity than contrast detection, rather than representing a qualitative deterioration of peripheral vision. Livingstone and Hubel argued that spatial localisation might depend on cortical complex cell responses, for which the V1 magnification factor used by Rentschler and Treutwein was not necessarily appropriate.

Bennett and Banks (1987) also examined spatial phase discrimination as a function of eccentricity. The stimuli to be discriminated were gratings consisting of a fundamental and a second harmonic, with phase shifts between the gratings of 0 and 180 deg, or 90 and 270 deg. These grating pairs represented even- and odd-symmetric mechanisms respectively of encoding phase. Peripheral stimuli were scaled by changing viewing distance so that the peak spatial frequency of the contrast sensitivity function at that

eccentricity was subtended at the eye, in order to make the stimuli equally detectable. Under these conditions, thresholds for the even-symmetric measurement rose only slightly with eccentricity, but the thresholds for the odd-symmetric mechanism rose 'dramatically and monotonically'. Repeating the data for the odd-symmetric mechanism at different spatial frequencies did not improve thresholds, implying that this task could not be scaled across the visual field.

Saarinen (1988) investigated observers' ability to detect mirror symmetry within a pattern of random dots. Random dot patterns were presented at eccentricities 0-20 deg in nasal visual field, and the task was to decide whether the stimulus exhibited symmetry about its horizontal midline. The detectability of symmetry for constant retinal sized stimuli fell markedly with eccentricity. Although the decline was not so rapid, performance also fell with eccentricity for stimuli M-scaled according to Rovamo and Virsu (1979).

4.3 Spatial scaling

The previous section highlights some of the difficulties involved in peripheral scaling according to prechosen magnification factors. In the application of M-scaling, the value of M has to be chosen before data is collected, such that the peripheral stimuli can be enlarged by the appropriate amount. The assumption is made that all tasks vary with eccentricity at the same rate. If the value chosen fails to remove eccentricity dependency from the task, it may either be that the magnification factor chosen was inappropriate or that the task cannot be equated across eccentricities by simple magnification scaling. The successful scaling of a task depends critically on the choice of magnification factors. For example, vernier acuity cannot be scaled by the cortical magnification estimates of Rovamo and Virsu (1979) (Westheimer, 1982; Levi et al, 1985) but can be scaled by the estimates of Dow et al. (1981) (Levi et al., 1985). At the other extreme, critical flicker frequency cannot be scaled by the equations of Rovamo and Virsu (1979), while including a compensatory (F-scaling) factor allows thresholds to be equated (Rovamo and Raninen, 1984).

In Chapter 3, it was observed that assumptions made on the basis of anatomical and physiological data should be viewed with caution, since large discrepancies exist between studies. The equations of Rovamo and Virsu (1979) are most often used in M-scaling procedures. Their data assumes a ganglion cell: cone ratio of 1: 1, and a direct relationship between ganglion and cortical cells. Both these assumptions have been questioned in the light of more recent anatomical evidence (see Chapter 3). The effect of these assumptions is to give a low M_0 value and high E_2 value in comparison to other

estimates. Drasdo (1989) suggested that Rovamo and Virsu's (1979) underestimation of foveal representation results in a gradient that lies midway between the shallow normalised eccentricity gradient of the magnocellular system and the steeper gradient of the parvocellular system. Such a position may explain its approximate relationship to many 'average' psychophysical tasks, which breaks down when stimuli are used which activate one system rather more selectively. The equations of Drasdo (1977) have a steeper gradient, lying closer to estimates of the parvocellular gradient, and might be expected to equate tasks activating primarily the parvo-system, eg. colour contrast sensitivity (Noorlander et al., 1983).

In view of the problems associated with M-scaling, a better alternative is to be able to compare performance at various visual field locations without the need for *a priori* assumptions with regard to the appropriate magnification factors. Spatial scaling is such a method. Thresholds for a sequence of stimuli which are all magnified versions of each other are measured at the fovea and at various eccentric locations. Thresholds are then plotted against stimulus size for each eccentricity, and the amount by which peripheral data is offset from the foveal data is found. This shift reveals the rate at which stimulus size must increase in order to maintain performance at the foveal level. Since the data is scaled by shifting along a logarithmic size axis, the error associated with each scaling factor is a constant proportion of its value on a logarithmic scale. As in Chapter 2, E_2 values are therefore best calculated on a log-linear plot, with the value of E_2 derived from an equation of the form:

$$\log SF_E = \log SF_0 + \log (1+(E / E_2)) \qquad \text{Equation 2.10}$$

where SF_E is the scaling factor at some eccentric location, and SF_0 is the value of the foveal scaling factor. The scaling factor at the fovea is always unity, since the data needs no magnification to be scaled relative to itself. Therefore:

$$\log SF_E = \log 1 + \log (1+(E / E_2))$$

$$\log SF = \log (1+(E / E_2)) \qquad \text{Equation 4.01}$$

The early studies of Wilson (1970) and Lie (1980), amongst others, which examined spatial summation with eccentricity, used an implicit method of spatial scaling since thresholds were found at a number of locations for a range of stimulus sizes. Wilson's (1970) data did not include foveal thresholds, making derivation of an E_2 value for the data difficult. The data of Lie (1980) provided E_2 values of 8.79 deg for increment spot detection, and 8.03 deg for distinction between incremental diamonds and squares. These studies are discussed further in Chapters 2, 7 and 8.

Studies of visual acuity in peripheral vision are, by their nature, experiments following a spatial scaling methodology. Threshold in this task is defined as the size of stimulus at which consistent resolution or recognition is achieved. Threshold at each location is a scaling factor which can relate foveal and peripheral performance. A detailed examination of the behaviour of acuity with eccentricity has been given in Chapter 2.

Johnston and Wright (1986) obtained thresholds for lower thresholds to motion (LTM) and apparent velocity for gratings as a function of eccentricity and viewing distance. At each eccentricity, thresholds were obtained for a series of viewing distances, such that while the grating always consisted of the same number (13.5) of cycles, its spatial frequency and size varied according to viewing distance. Eccentric locations examined were 0-25 deg in nasal visual field. The temporal frequency thresholds are shown as a function of spatial frequency for observer MW in Figure 4.06.

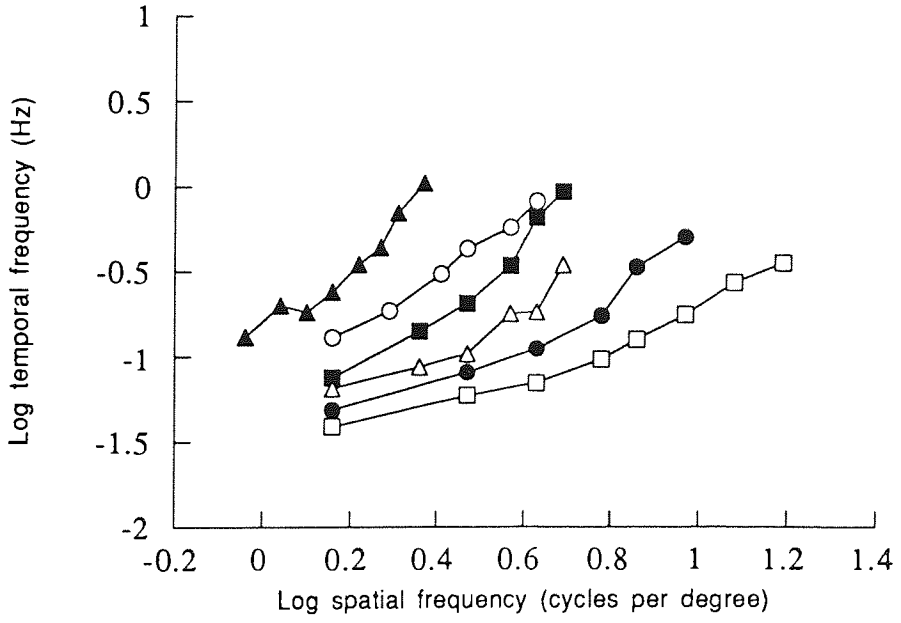

Figure 4.06. From Johnston and Wright (1986). Their Figure 1a replotted. Lower threshold of motion expressed as temporal frequency, plotted as a function of spatial frequency, for a number of eccentricities. Nasal visual field. Observer MW. Open squares: 0 deg; closed circles: 3 deg; open triangles: 6 deg; closed squares: 10 deg; open circles: 16 deg; closed triangles: 25 deg.

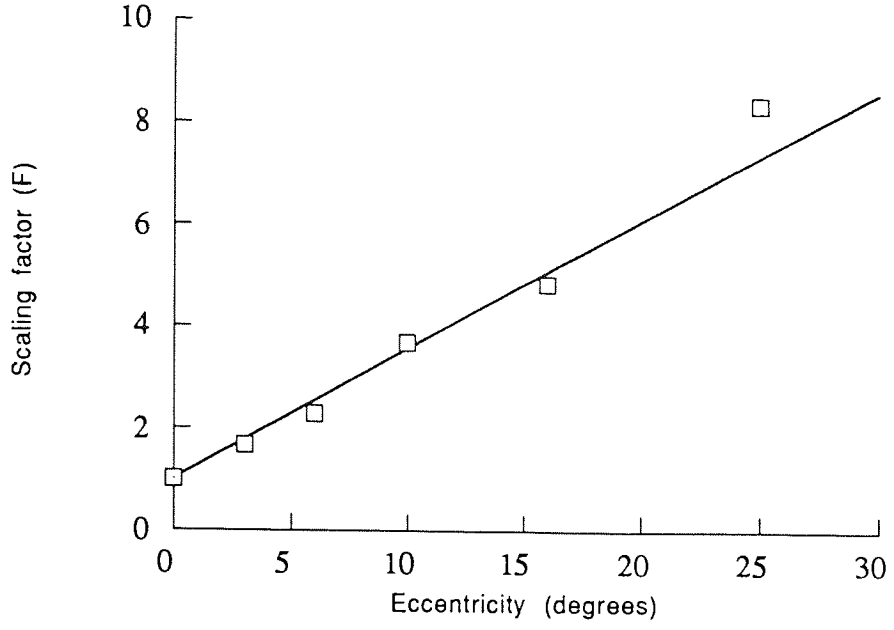

Figure 4.07. Scaling factors derived from Figure 4.06 to superimpose peripheral data onto the foveal data curve by horizontal shift along the spatial frequency axis. The points are fitted with an equation of the form: log F = log (1 + (E / 3.86)) such that E_2 is 3.86±0.21 deg.

The translation along the log spatial frequency axis required to match the foveal and peripheral data is shown for each eccentricity in Figure 4.07. These values were determined by eye from inspection of the data. A regression passed through these scaling factors has the equation:

$$\log F = \log (1 + (E / 3.86))$$

such that E_2, from Equation 4.01, is 3.86 ± 0.21 deg. Scaling the data according to this E_2 value resulted in data as shown in Figure 4.08. The scaling factors derived here were also found to be applicable to the velocity matching task, over a range of standard temporal (1-7 Hz) and spatial (1-9 cpd) frequencies. A spatial transformation can therefore match foveal and peripheral motion perception with the temporal parameters kept constant.

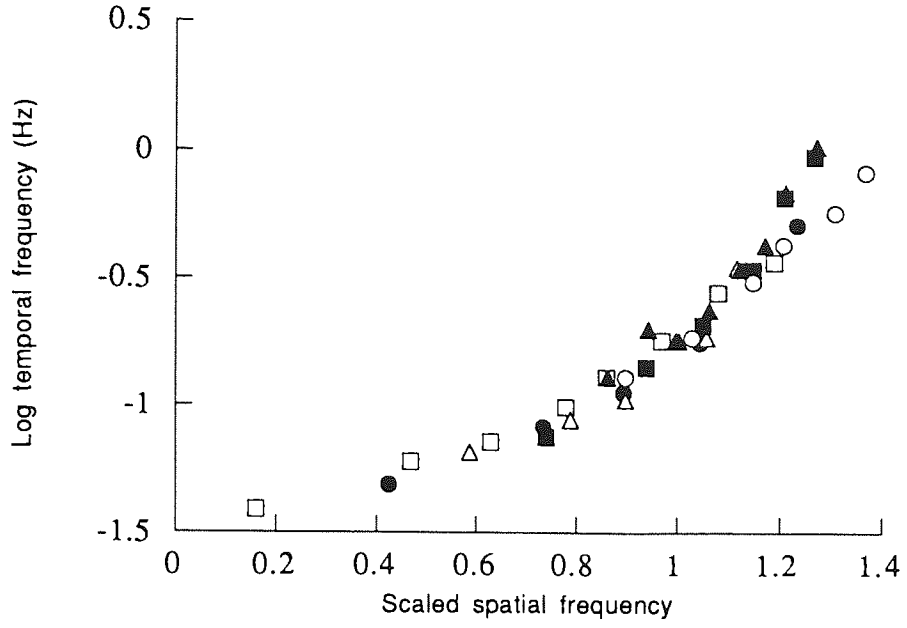

Figure 4.08. The data of Figure 4.06 are scaled by multiplying the peripheral data by scaling factors derived from the E_2 value of 3.86 deg. The effect is to shift the peripheral data curves rightwards along the spatial frequency axis, removing most of the eccentricity dependence from the data.

Whilst the E_2 value derived by this method is of the same order as that of Rovamo and Virsu (1979) for the nasal visual field (2.97 deg), the correspondence is not exact. That the scaling factors are similar is shown by the observation that LTM had previously been successfully scaled using the Rovamo and Virsu (1979) equations (Johnston and Wright, 1983, 1985).

Watson (1987) formally presented a method for examining local scale independently of prior physiological assumption, and used the following experiment to illustrate the method. A series of Gabor patches were used as stimuli, in which each stimulus was a magnified version of the previous one by a factor of two. As the stimuli enlarge, the number of grating cycles in the stimuli remains constant, but the spatial frequency halves for each doubling of stimulus size. Contrast detection thresholds were measured at 0 and 3 deg using stimuli with spatial frequencies 0.25 - 16 cpd, and the results are shown in Figure 4.09.

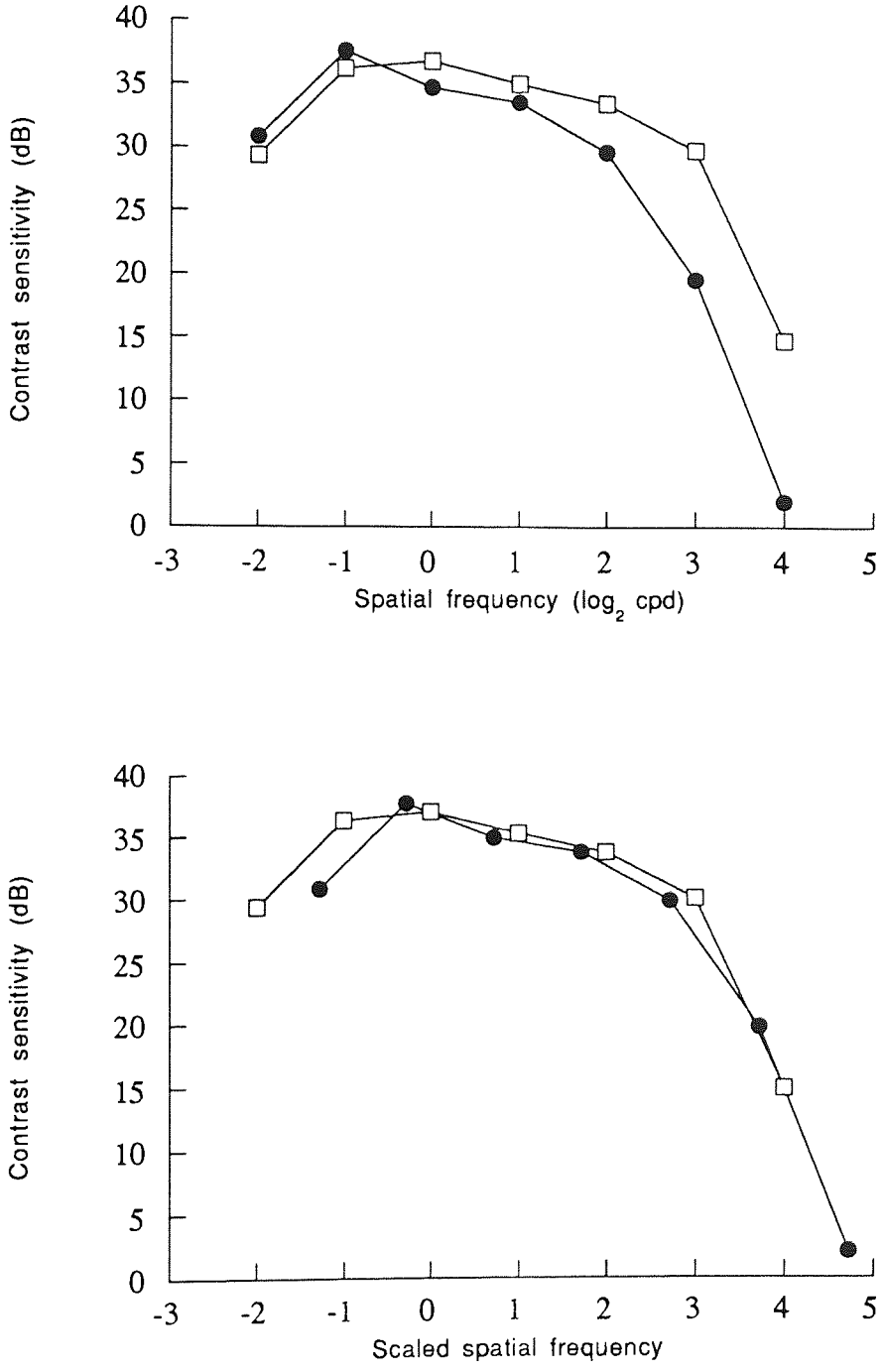

Figure 4.09a & b. From Watson (1987), his Figures 3 and 4 replotted. (a) Contrast detection thresholds for size scaled Gabor stimuli. Open squares: 0 deg; closed circles: 3 deg. (b)

The data of a, with the peripheral data shifted rightwards by a scaling factor of 1.72, equivalent to an E_2 value of 4.2 deg.

A 'shift rule' was applied to the contrast detection data, in that shifting the peripheral data horizontally to the right superimposes the functions obtained at each location. The shift required is a direct estimate of the ratio of the local scales for the two points, and in this case was 1.72. From Equation 1.01: $1.72 = 1 + (3 / E_2)$, so that $E_2 = 3 / 0.72 = 4.2$ deg. Whilst scaling removed most of the eccentricity dependence from the data, it was noted that the data for the lowest spatial frequencies failed to coincide. This was explained by noting that larger targets are less localised to a specific eccentricity, and measure average sensitivity over a spatial region. In 1990, however, Valeton and Watson claimed that for contrast detection of Gaussian blobs and gratings, both horizontal and vertical shifts were required to scale the data, and the concept of local scale did not hold for these tasks.

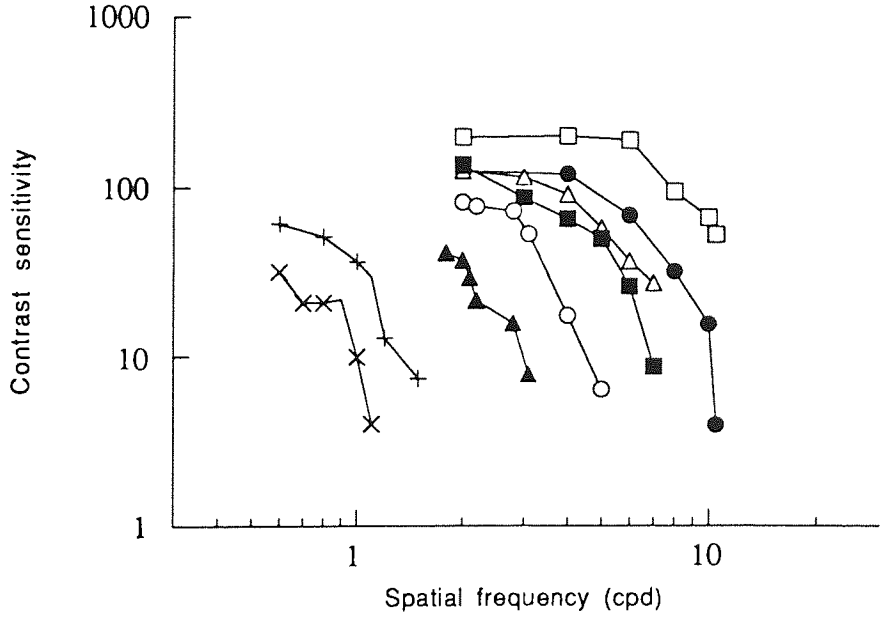

Figure 4.10. From Johnston (1987). His Figure 3a replotted. Contrast sensitivity as a function of spatial frequency for spatially scaled gratings at a number of eccentricities in nasal visual field. Observer AJ. Open squares: 0 deg; closed circles: 3 deg; open triangles: 8 deg; closed squares: 10 deg; open circles: 16 deg; closed triangles: 20 deg; ordinal crosses: 30 deg; oblique crosses: 40 deg.

Johnston (1987) also examined contrast sensitivity using a spatial scaling technique. Thresholds were found for a range of spatial frequencies at several locations by changing viewing distance. Varying viewing distance altered the spatial frequency and size of the grating without changing the number of grating cycles (12) in the stimulus. Results for vertical gratings in the nasal visual field of observer AJ are shown in Figure 4.10. Scaling factors derived from this figure by shifting peripheral curves to

superimpose onto the foveal data are non-linear with eccentricity beyond 16 deg. In the range 0-16 deg, E_2 is 5.96 ± 0.34 deg.

Johnston concluded that while the high frequency limb of the contrast sensitivity function could be scaled with eccentricity by simple magnification, lower frequencies did not scale so well, with peripheral functions flattening at lower maximum contrast sensitivities. Adopting a 'surface scaling' approach resulted in better superimposition of contrast sensitivity curves. In this case, surface scaling involves presenting stimuli along a surface at 9 deg to the line of sight in nasal visual field.

The surface scaling approach relates to the hypothesis of Johnston (1989). He suggests that the global geometry of the striate cortical map can be understood with reference to a conic surface in visual space with its base in the plane of the eye, and its axis along the line of sight. This mapping is such that if the ground plane is viewed at an angle equal to the apical half angle of the cone, equal distances along the surface will map to equal distances along the inferior meridian of the striate topographical map, and receptive fields measured with respect to the surface would have the same mean size at each eccentricity. Such uniform processing of the ground plane has obvious benefits for locomotion. Values of M_0 using this model are smaller than those extrapolated by linear regression, being in the region of 5-8 mm/deg.

Wright (1987) found minimum displacement thresholds for the detection of oscillatory motion of gratings with eccentricity. A spatial scaling technique was used in that displacement thresholds were found for a range of grating frequencies, and spatial frequency was varied by changing viewing distance. Results are shown for a standard oscillation of 2 Hz and contrast 0.4 for observer MW in Figure 4.11.

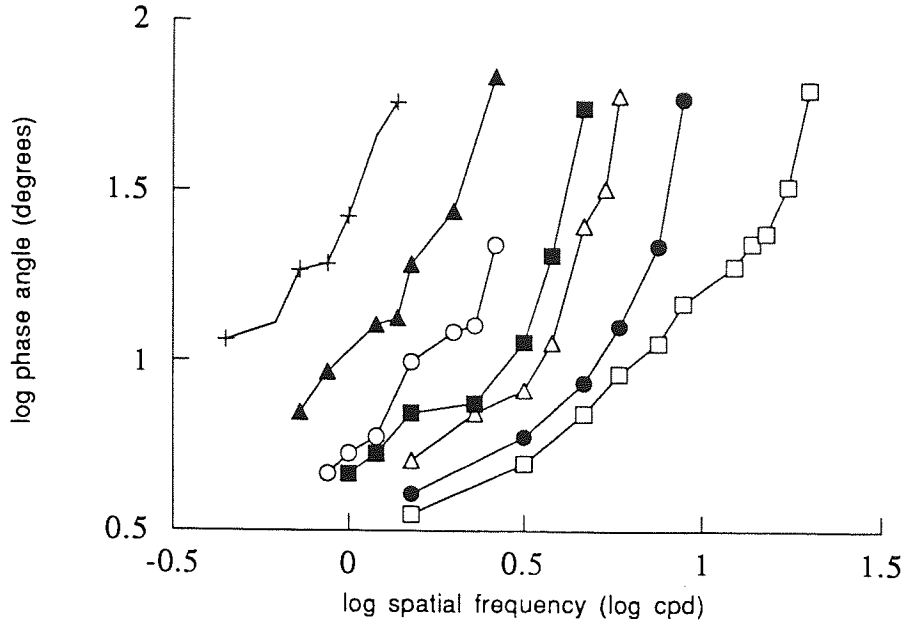

Figure 4.11. From Wright (1987). His Figure 1 replotted. Oscillatory motion displacement thresholds expressed as phase angle, plotted against spatial frequency. Standard oscillation 2Hz, observer MW. Open squares: 0 deg; closed circles: 3 deg; open triangles: 6 deg; closed squares: 10 deg; open circles: 16 deg; closed triangles: 25 deg; crosses: 40 deg.

Displacement sensitivity is shifted to lower spatial frequencies with eccentricity, and a simple translation along the spatial axis produces an approximate general scaling of the data from different eccentricities. However, the increase in scaling factors with eccentricity is not linear over the entire 0-40 deg eccentricity range, as shown in Figure 4.12. In the range 0-16 deg, scaling factors do rise linearly with eccentricity, with an E_2 value of 6.23 $\pm$ 0.42 deg. An additional problem of scaling is that the foveal curve differs in shape at high spatial frequencies from the peripheral functions. Thus, as Wright notes, a single scaling factor cannot be taken as accurate for all spatial frequencies.

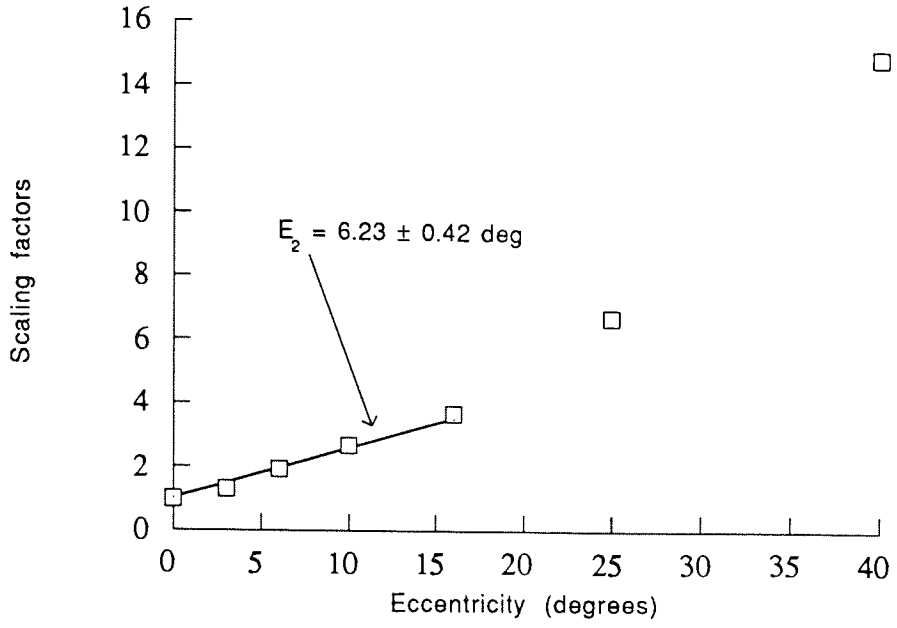

Figure 4.12. Scaling factors derived from superimposition of peripheral data onto the lower frequency limb of the foveal data curve. The regression is of the form log F = log (1 + (E / E_2)). E_2 in the range 0-16 deg is 6.23 ± 0.42 deg.

Despite the lack of a single scaling factor with which to scale the data, for a standard foveal spatial frequency, the viewing distances can be determined from Figure 4.11 which would give the same threshold at a peripheral location. Gratings were spatially scaled in this way, and displacement sensitivity was then measured as a function of temporal frequency for different eccentricities. The scaling factors used were 4.4 at 16 deg and 12.5 at 40 deg. The equivalent E_2 can therefore be calculated to be 3.61 ± 0.24 deg. The low temporal frequencies and peak sensitivities of the resulting temporal frequency functions were equated by spatial scaling in this way, but the periphery was seen to be more sensitive than the fovea to high temporal frequencies. The conclusions of the study were that the primary scaling of motion sensitivity with eccentricity is spatial, with a small but significant residual temporal inhomogeneity. The periphery remains relatively more sensitive to high temporal frequencies, even after spatial scaling.

Saarinen, Rovamo and Virsu (1989) looked at the analysis of spatial relationships, which had been so problematic with M-scaling, using a spatial scaling technique. The stimuli, shown in Figure 4.13, were two S-shaped patterns consisting of short line segments. The subject's task was to decide whether the simultaneously shown patterns

were identical or mirror symmetric about the horizontal axis. At each eccentricity, the discrimination ability for a range of pattern sizes was found, from which the threshold for 75% correct discrimination was calculated. For observer JS, these thresholds were 0.11, 0.65, 1.5 and 2.5 deg for eccentricities 0, 4, 8 and 12 deg respectively. From an equation of the form:

$$\log (\text{size}) = \log (\text{foveal size}) + \log (1 + (E / E_2)) \qquad \text{Equation 2.10}$$

E_2 is calculated to be 0.64 ± 0.14 deg. The authors noted that thresholds rise at a similar rate to the cortical magnification factor suggested by Levi et al. (1985), where E_2 was 0.8 deg.

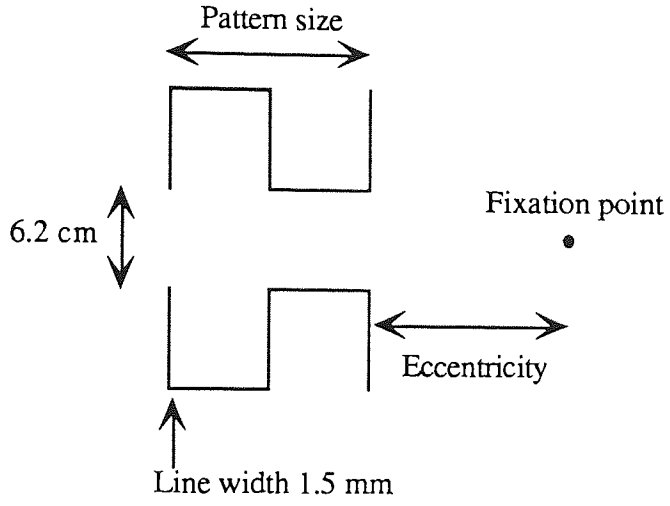

Figure 4.13. Stimulus arrangement used by Saarinen et al. (1989). The task of the observer was to determine whether stimulus patterns on each trial were identical or mirror symmetric. The distance between the two patterns was a constant 6.2 cm.

Drasdo and Thompson (1989) noted that while foveal visibility and colour recognition thresholds were identical for a small red target, the photochromatic interval between the two criteria increased steadily with eccentricity. The photochromatic interval describes the eccentricity range over which a target can be observed, but is not yet seen as coloured. Using a Zeiss Jena bowl perimeter, foveal thresholds were determined by finding the viewing distance at which a small red stimulus could just be detected, or its colour recognised. Thresholds were the same for each criterion. Peripheral thresholds were found for each criterion using a kinetic perimetric technique. For stimuli of 0.108 deg angular subtense moving at 1 deg/sec, and 0.216 deg moving at 2 deg/sec, the eccentricity at which the stimulus was just seen, or just seen as red, was determined. Stimulus velocities were chosen so that each target moved at a constant relative rate of 8 target diameters per second. The stimuli were thus magnified versions of one another, and spatially scaled. Peripherally, a target could be seen at a greater eccentricity than at which its colour was recognisable. The rate of change of performance with eccentricity

was therefore greater for the colour task than for the luminance task. Applying a regression of the form of Equation 2.10 to the data gives E_2 values of 2.20 ± 0.19 deg for visibility, and 0.88 ± 0.20 deg for colour recognition.

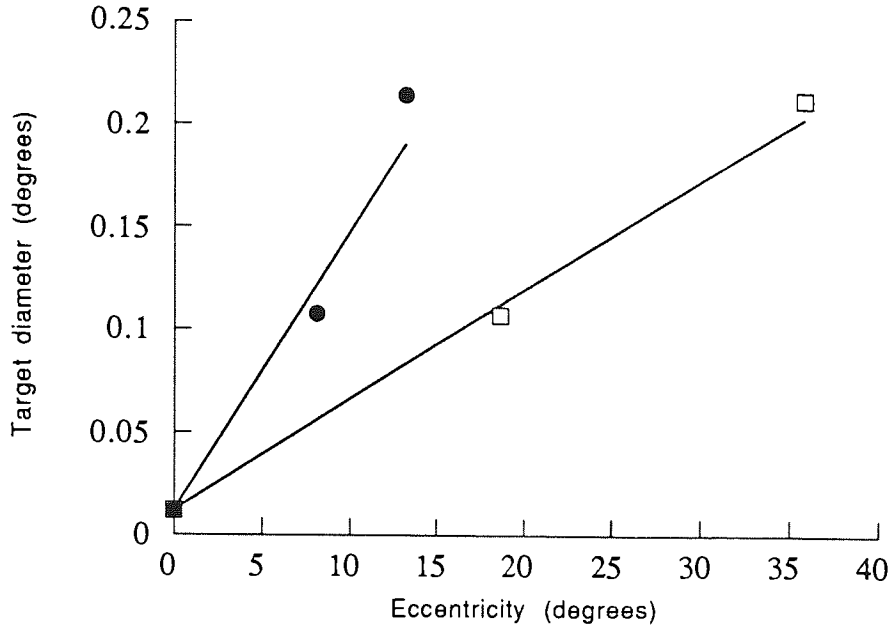

Figure 4.14. From Drasdo and Thompson (1989), their Figure 2 replotted. Open squares represent eccentricity thresholds obtained for the visibility criterion, whilst closed circles are for colour recognition. The regressions are of the form: log (diameter) = log (foveal diameter) + log (1+ (E / E_2)), from which E_2 for visibility is calculated to be 2.20 ± 0.19 deg, and for colour recognition E_2 is 0.88 ± 0.20 deg.

The gradients associated with the visibility and colour recognition criteria seemed to approximately reflect the proposed gradient differences between magno- and parvo-cellular processing systems (see Chapter 3). The authors felt that the data was in agreement with the hypothesis of Drasdo (1989) who suggested that the variation of threshold gradients in peripheral vision might be largely determined by the division of labour between magno and parvo systems, which would be dependent on stimulus attributes such as their spatial, temporal and chromatic qualities.

Drasdo et al. (1991) further investigated this line of argument using spatially scaled grating stimuli presented again as kinetic perimetric stimuli. The eccentricity at which a particular sized grating could be resolved represented threshold. In order to psychophysically stimulate the magnocellular system, grating stimuli were brief (90 ms) and of low contrast (10%). To preferentially stimulate the parvocellular system,

gratings of long duration (400 ms) and high contrast (80%) were used. E_2 values (derived from polynomial functions) were 6.4 and 1.8 deg for the 'M' and 'P' stimuli respectively. In a second similar experiment, the spatial period for peak sensitivity was found with eccentricity for 8 Hz counterphasing gratings, representing a magnocellular stimulus, and for static gratings, representing a parvocellular stimulus. E_2 values were similar to the first experiment, being 6 deg for the 'M' stimulus and 2.1 deg for the 'P' stimulus.

Diameter threshold functions for circular stimuli with Gaussian luminance and temporal profiles were determined by Bijl, Koenderink and Kappers (1992). Contrast thresholds were determined as a function of stimulus size (as in the study of Wilson (1970)) for eccentricities 0-42 deg in nasal and temporal visual fields. As shown in Figure 4.15, the shape of the curves is approximately independent of location. In the temporal field (Fig 4.15a), curves for successive eccentricities can be made coincident with a horizontal shift. The amount of shift required increases rapidly between 0 and 12 deg, after which it is somewhat constant. There is a slight difference in shape between the curves at different locations however, in that large foveal stimuli show lower thresholds than their eccentric counterparts. In the nasal field (Fig 4.15b), a horizontal shift cannot make the curves coincident, since the constant threshold level for large stimuli increases with eccentricity. An additional vertical (or gain) shift is required to achieve coincidence of the data.

The authors propose a model which assumes that spatial scale is proportional to the diameter of the smallest receptive field centre. Additionally, gain is proportional to the overlap factor, or the number of ganglion cells sampling a single point in visual space. The overlap factor is the product of ganglion cell density and mean receptive field area. Such a model predicts their peripheral results well.

Whitaker et al. (1992b) applied the spatial scaling method to the task of vernier acuity, another of the tasks for which M-scaling had generally been unsuccessful (Westheimer, 1982; Levi et al., 1985). Offset thresholds were found for two line abutting stimuli as a function of line length for eccentricities 0-15 deg in nasal visual field. Line length was varied by changing viewing distance so that the series of stimuli were magnified versions of one another. The results are shown in Figure 4.16.

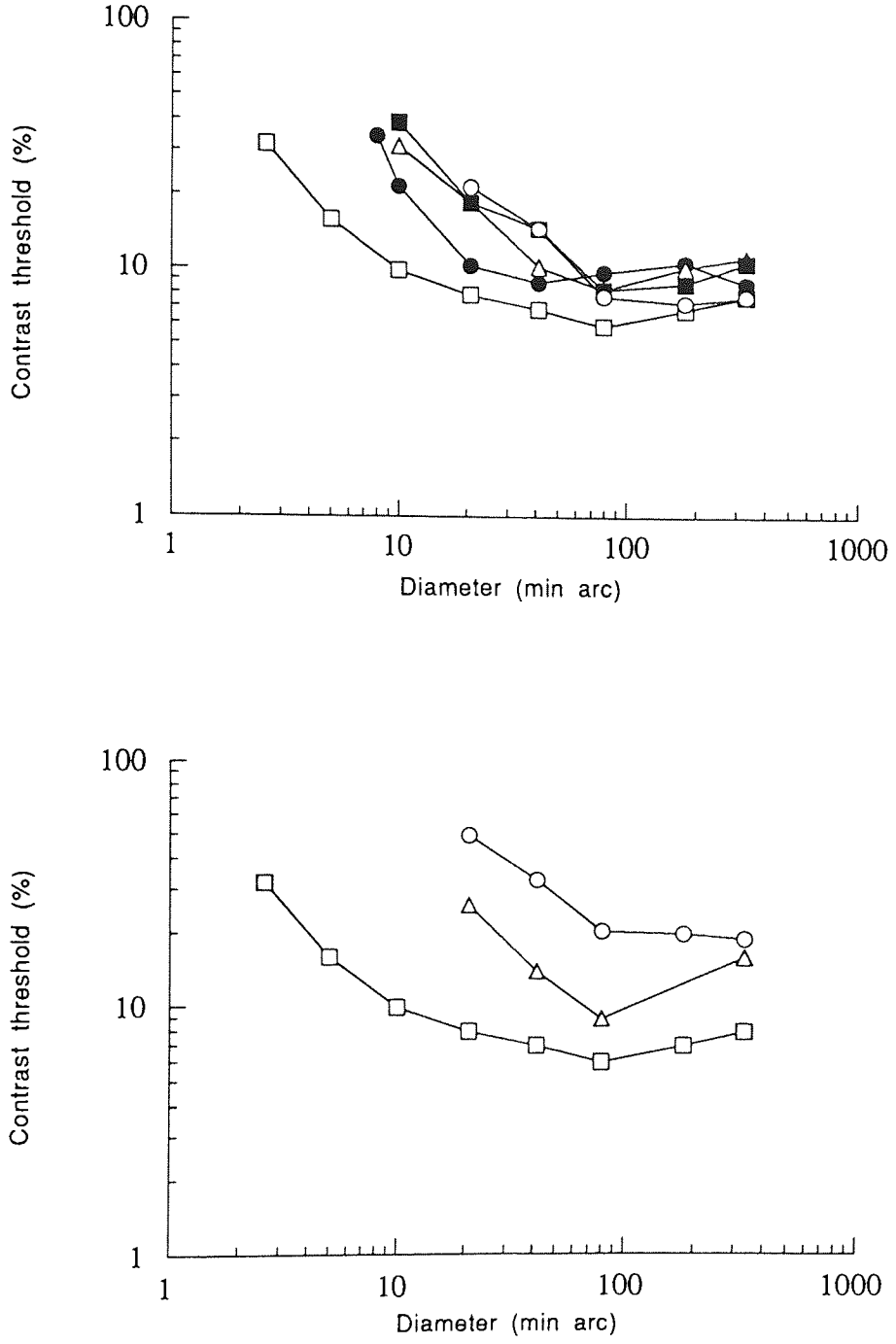

Figure 4.15. From Bijl et al (1992). Their Fig 1 replotted. Contrast thresholds as a function of stimulus diameter for Gaussian blobs. (a) Temporal field. (b) Nasal field. Open squares: 0 deg; closed circles: 6 deg; open triangles: 12 deg; closed squares: 24 deg; open circles: 42 deg.

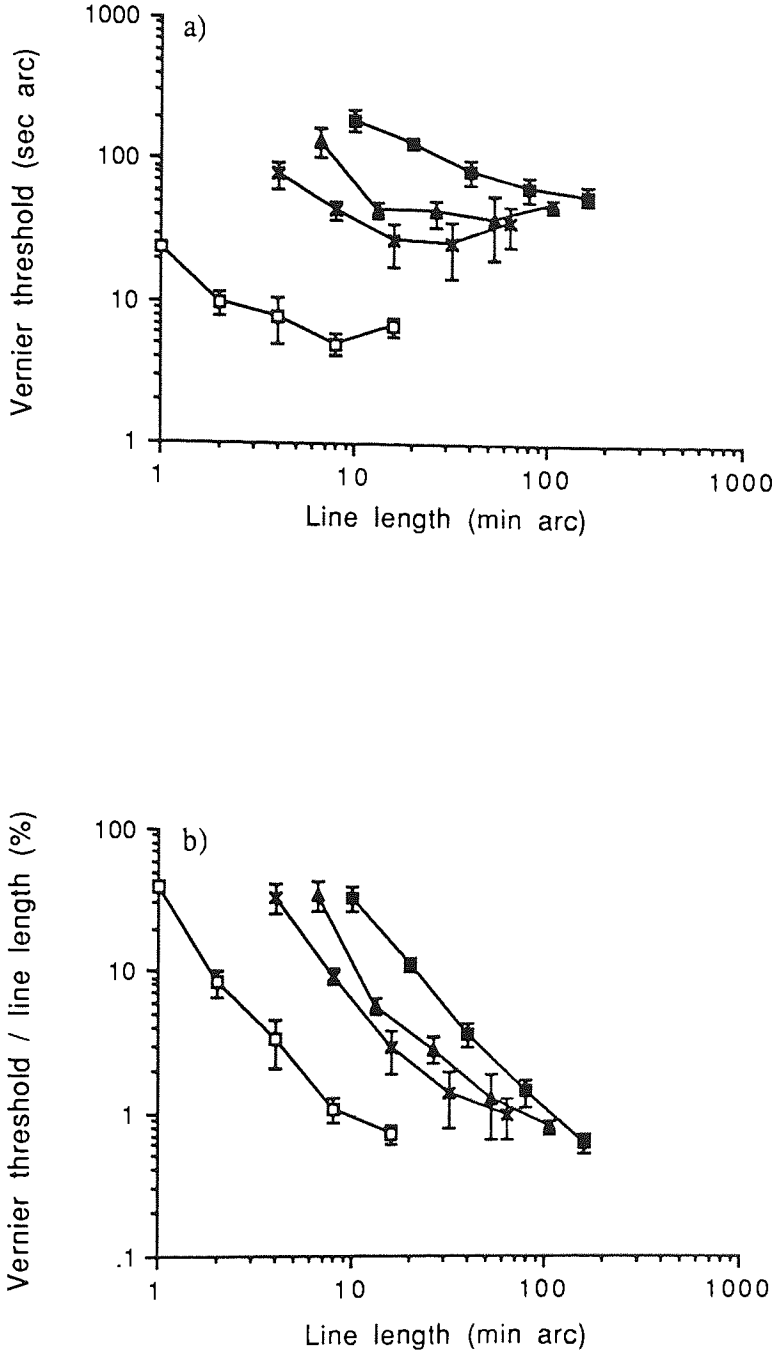

Figure 4.16. See following page for legend.

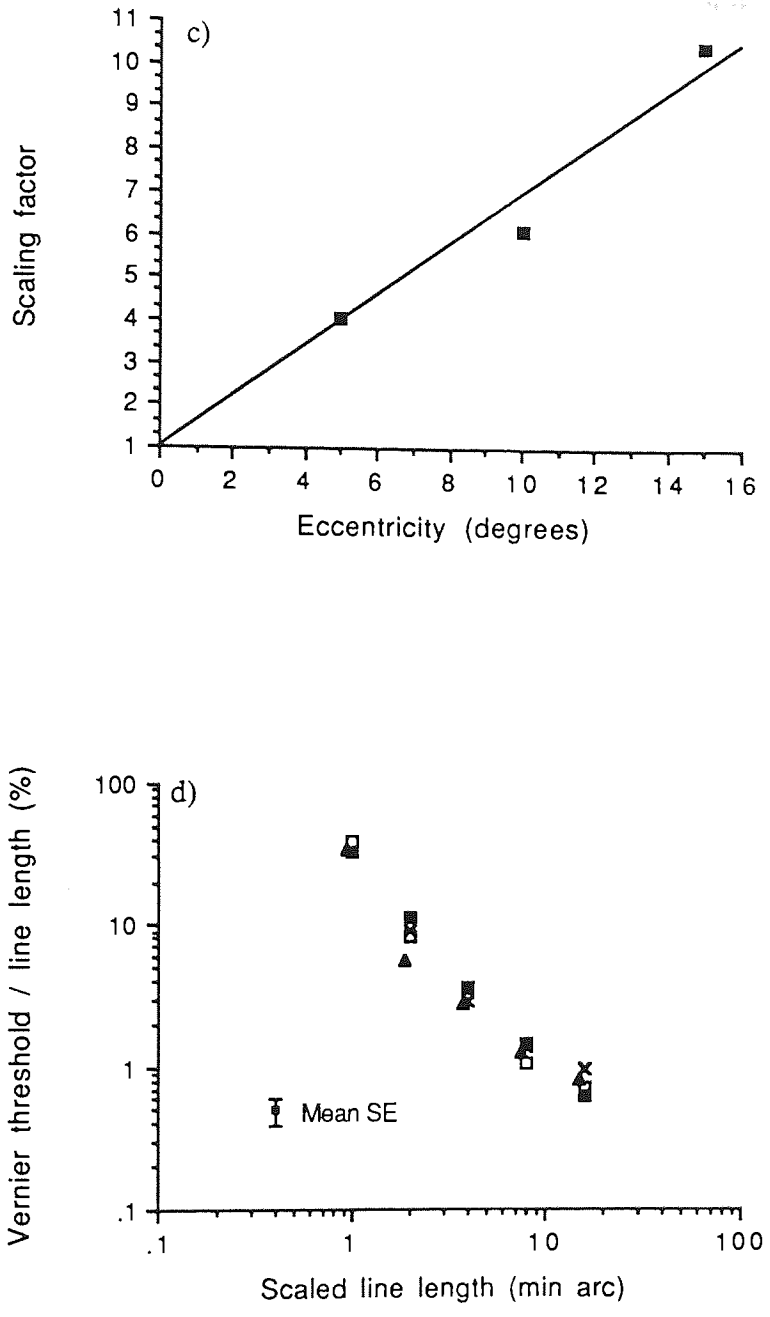

Figure 4.16a-d. After Whitaker et al. (1992b). (a) Abutting line vernier thresholds as a function of line length for a number of eccentricities in nasal visual field. Observer DW. Open squares: 0 deg; closed circles: 5 deg; open triangles: 10 deg; closed squares: 15 deg. (b) Vernier thresholds expressed as a fraction of line length. (c) Scaling factors required for coincidence of peripheral and foveal data curves in b. The linear regression has the form: $F = 1 + (E / 1.66)$. (d) The data of b, scaled according to the E_2 value derived from c.

Since vernier offset is itself a spatial measurement, the resultant functions for each eccentricity were displaced relative to one another along both the horizontal and vertical axes (Figure 4.16a). Vernier data was therefore expressed as a percentage of line length, in order to make the y-axis scale invariant (Figure 4.16b). The transformation results in data curves displaced from one another along the x-axis only. The shift required to superimpose peripheral data curves onto the foveal data can be read from the transformed graph, and is shown in Figure 4.16c. The foveal data is given a scaling factor of unity, since all scaling factors are determined relative to this data. The resultant E_2 values were found to be 1.66 ± 0.14 deg for DW (data shown in Figure 4.16), and 1.78 ± 0.13 deg for DM (not shown).

Two dot vernier stimuli examined in the same way as above did not scale with eccentricity. The optimum gap size increased with eccentricity at a slower rate than the thresholds themselves, reminiscent of the data of Westheimer (1982). The experiment was repeated with the stimuli presented on an iso-eccentric arc, in order to dissociate the effects of dot separation and eccentricity, particularly at the fovea. Repeating the experiment in this way gave data from which the eccentricity dependence could be removed by spatial scaling, with E_2 values of 1.66 ± 0.13 deg for DW and 1.88 ± 0.22 deg for DM.

In subsequent papers, Whitaker et al. (1992a) and Mäkelä et al. (1993) extended the spatial scaling methodology applied to vernier acuity and examined a variety of position and movement acuities. Table 4.01 gives the E_2 values of two observers found for the range of tasks observed.

Task	E_2 PM	E_2 DW	Notes
Spatial interval discrimination	0.17±0.03 0.22±0.01	0.19±0.05 0.07±0.01	Isoeccentric arc. 50ms ISI. Isoeccentric arc. 500ms ISI.
Bisection acuity	0.07±0.03 -0.10±0.01	0.08±0.04 -0.03±0.02	All points on isoeccentric arc Outer points on isoecc. arc
Referenced displacement detection	1.06±0.23	1.35±0.18	Instantaneous displacement
Unreferenced displacement detection	6.3±0.7 18.5±2.7	11.1±1.4 13.5±1.1	Instantaneous 'stop-go-stop' Gradual 'stop-go-stop'
Orientation discrimination	1.95±0.11		Mean of 3 observers

Table 4.01. E_2 values found for various position and movement acuities (Whitaker et al., 1992a; Mäkelä et al., 1993).

The table highlights the dramatically different rates of decline in performance with eccentricity, dependent on the spatial and temporal characteristics of the task itself. There is well over 100-fold difference in the eccentricity related rate of performance change in these results.

4.4 Summary

The original concept of M-scaling was beautifully simple, and inspired a great deal of interest. However, a single magnification rate determined by sampling density, such as that purported by cortical magnification theory, is not sufficient to equate all thresholds across the visual field. Likewise, theories suggesting two rates of magnification change with eccentricity (Rovamo and Raninen, 1984; Levi et al., 1985) cannot account for the variations observed in these results. Possible factors involved in the determination of peripheral threshold gradients, additional to the effects of sampling density, include a division of labour between magno and parvocellular channels, and differences in retinotopic distributions within various cortical areas. Additional factors include the effects of spatial summation, eye movements, and optical degradation (Drasdo, 1991). Such differences as are observed (Whitaker et al., 1992a) in eccentricity dependent gradients are difficult to reconcile with any single one of the factors mentioned above, since the range of E_2 values observed psychophysically is so great, and as such the physiological processes underlying eccentricity related threshold gradients are still largely unclear.

Chapter 5
Psychophysical methods and apparatus

5.1 Threshold

Measurement of a psychophysical threshold is not as straightforward as finding the single intensity of a stimulus parameter where a stimulus is 'seen' as opposed to 'not seen'. If an observer is shown a stimulus at a number of levels and has to report the occasions on which the stimulus is seen, the proportion of 'seen' responses increases gradually as a function of stimulus level, as is shown in Figure 5.01.

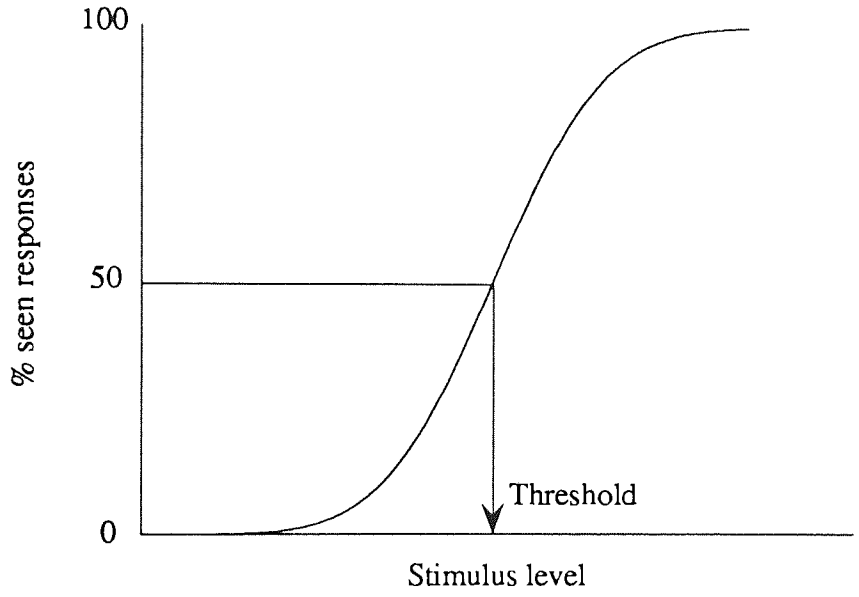

Figure 5.01. Psychometric function. The proportion of correctly seen responses rises gradually as a function of stimulus level. Threshold can be taken as the stimulus level corresponding to any proportion of correct responses, and is often taken as the 50% point.

The frequency-of-seeing curve, or psychometric function, shown in Figure 5.01 is of a sigmoid, or ogive shape. At low values of the variable stimulus parameter, which might be any physical variable such as contrast, duration or length, the stimulus is correctly seen on no, or few, occasions. As the stimulus level increases, the stimulus is seen on a greater percentage of trials, until it is clearly seen on 100% of trials. Threshold can be defined as any value of correct responses, but is generally taken as the stimulus level corresponding to 50% correctly seen. The slope of the curve is greatest at this point, giving most information as to the location of the curve (Pentland, 1980).

The experiment described above is of the 'yes-no' type. The observer is presented with a stimulus, and their task is to reply whether they observed the stimulus or not. This method is open to 'criterion dependency', or the observer's willingness to report a stimulus as seen. Psychological factors involved in setting an observer's criterion include their desire to perform well, the instructions as given and as understood, and their knowledge of the experimental procedure. If an observer is very willing to report stimulus observation even when unsure, thresholds will be lower than for a cautious observer who is unwilling to report a stimulus as seen until they are certain of its presence. If 'catch trials' are introduced where, for example, no stimulus is presented, the risky observer is likely to report that a stimulus is seen, which is termed a false positive response. A cautious observer may not respond to a visible stimulus, a false negative response.

Instead of asking an observer to report the presence or absence of a stimulus, an alternative method is to use a 'forced-choice' technique. A number of alternatives (commonly 2), delineated spatially or temporally, are presented to the observer, whose task is to identify the correct interval, by guessing if necessary. For example, a grating may be placed in one of two temporal intervals, and the observer has to decide in which interval the stimulus appeared. Alternatively, in a vernier acuity task, the observer might have to report whether the upper line of a two line vernier stimulus was offset to the left or to the right of the lower line. Forced choice methods reduce the effects of criterion, since the observer places the same value on all the alternatives, as opposed to a yes-no procedure where the choices have intrinsically different values (Green and Swets, 1966). Taking the 2-alternative forced choice (2AFC) method as an example, the psychometric function varies between 50 and 100% correct (Figure 5.02). Even with their eyes closed, an observer will guess the correct interval on one in two presentations on average, given a large number of trials.

Instead of plotting the psychometric function as the percentage of correct responses, an alternative is to plot the percentages of one type of response, for example, the proportion of 'leftwards' responses in the vernier example used above. This gives a psychometric function with responses ranging from 0 to 100%, as shown in Figure 5.03a.

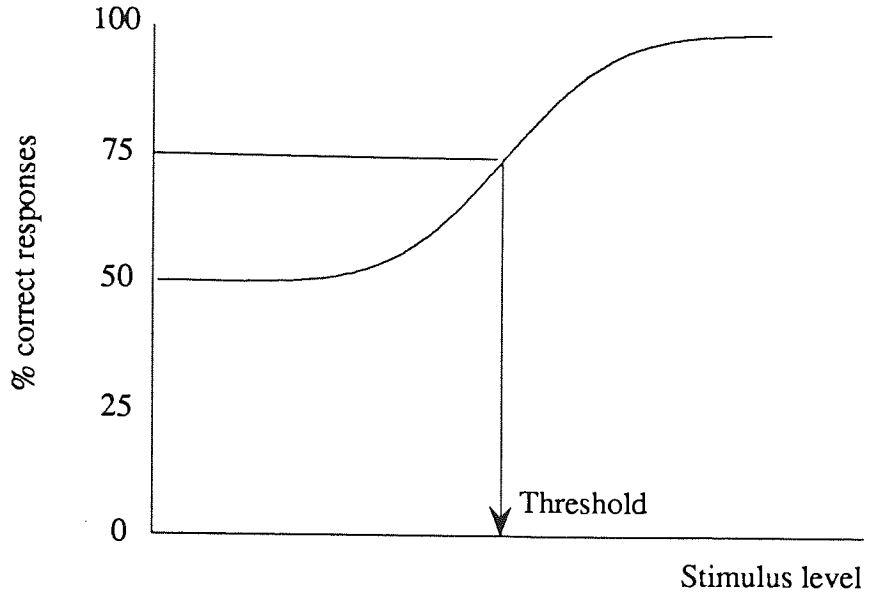

Figure 5.02. Psychometric function for the 2AFC method. Since the observer has two alternative responses, they will be correct on 50% of trials, even if guessing. In this case therefore, correct responses rise as a function of stimulus level from 50 to 100%. Threshold is often taken as the 75% correct point.

In this case, two parameters of the psychometric function are of interest for its description. Firstly, the location of the curve, defined by the stimulus level at which 50% of responses are 'leftwards'. This point represents the 'point of subjective equality' where an observer is as likely to make a 'leftwards' response as a 'rightwards' one. In other words, this is the point at which the observer sees the vernier stimulus as aligned, although this is not necessarily the point at which the stimulus is actually aligned. The difference between the actual and observed alignment is called the bias, and can seriously affect thresholds if not taken into consideration.

The second point of interest on the psychometric function is the spread of the curve, given by the difference in stimulus level between two percentile points equidistant from the point of subjective equality. In other words, threshold is represented by the difference from subjective equality which is deemed just noticeable. Often the threshold is taken as half the distance between the 25% and 75% correct points.

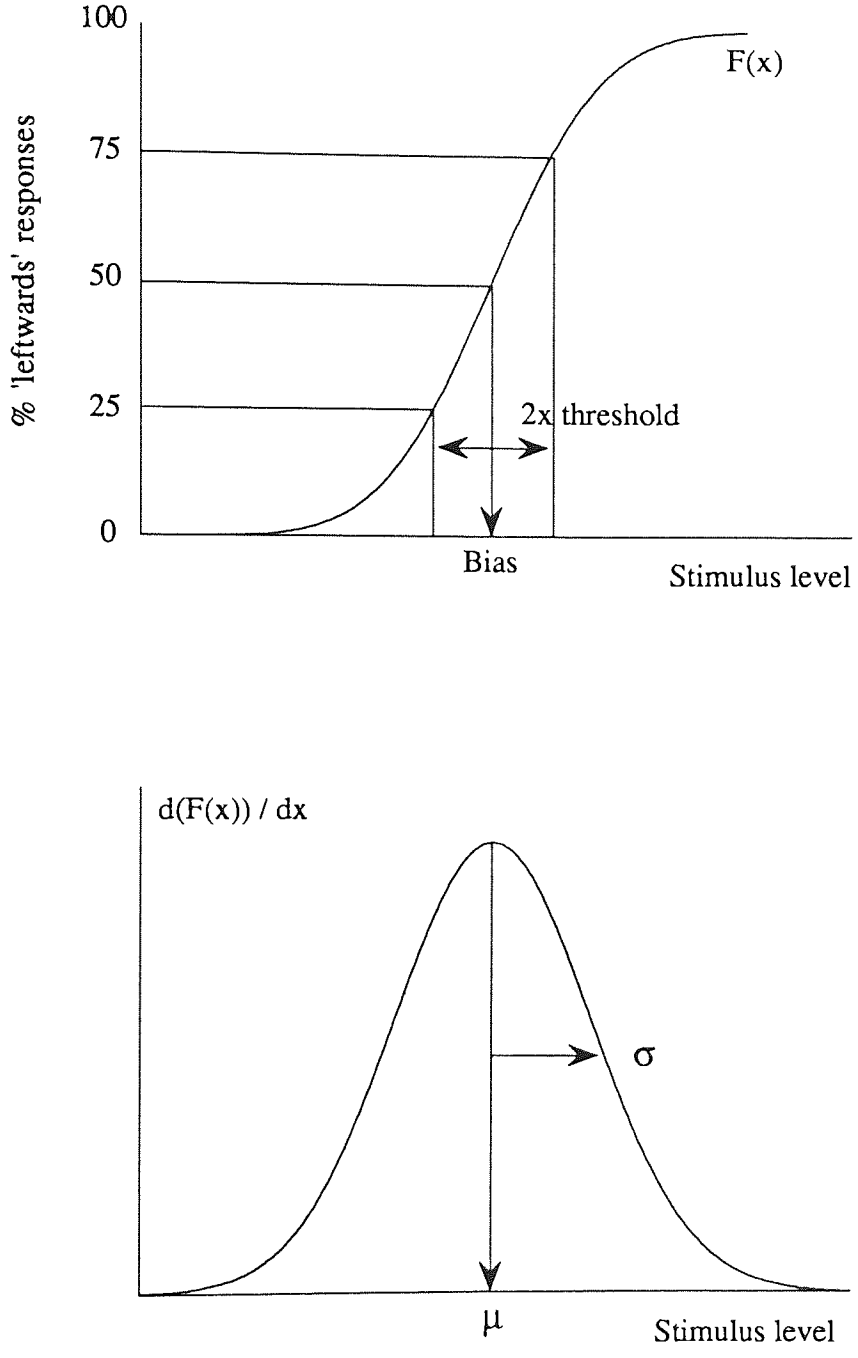

Figure 5.03. (a) Psychometric function of a 2AFC method plotted as number of 'leftwards' responses vs stimulus level. (b) The underlying frequency distribution of (a) derived by differentiation of the function. The parameter μ represents the 'point of subjective equality', where the observer is as likely to give a 'leftwards' response as a 'rightwards' one. The parameter σ, the standard deviation of the distribution, defines the just noticeable difference detected as a change, or the threshold.

In Figure 5.03b, the underlying frequency distribution of the psychometric function is shown, assuming that the psychometric function has a cumulative normal distribution. In this case the parameters μ and σ, the mean and standard deviation of the normal distribution, are of interest. The parameter μ defines the point of subjective equality, while σ describes the threshold.

5.2 Methods of threshold determination

Several methods are available with which to determine thresholds using the yes-no and forced choice responses described above. Each have their own advantages and disadvantages making them suitable for different types of experiment. No single method is ideal for all experimental circumstances.

Method of adjustment

In this method, the observer is presented with a sub-threshold stimulus. Stimulus intensity is adjusted by the observer on a continuous basis until the stimulus can just be correctly seen, at which point the estimate of threshold is made. The procedure is repeated several times, and generally also combined with threshold estimates made by reducing the intensity of a clearly seen stimulus until it can no longer be correctly observed. This method is very simple and quick, but suffers from several drawbacks. Only a yes-no stimulus response is applicable, and there is no control of the observer's criterion.

Method of limits

This method is similar to that of the method of adjustment, only the experimenter changes the stimulus level, and in incremental steps rather than continuously. Since stimulus presentation follows a sequence, an observer can anticipate the next stimulus, and manipulate the point of threshold.

Method of constant stimuli

As in the method of limits, several stimulus levels are chosen before data collection begins for the method of constant stimuli. These are presented to the observer in random order so that no sequence of stimulus presentation is apparent. Stimulus levels are chosen across the whole range of the psychometric function, and a series of responses is obtained at each level. The choice of appropriate stimulus values is essential to maximise the usefulness of the data (Laming, 1991). A complete psychometric function can then be constructed from the data. Threshold is found by probit analysis applied to the data (Finney, 1971), which fits a curve to the data points and interpolates values for threshold and bias. The method of constants is ideal for the

use of forced-choice stimuli, in addition to yes-no responses. However, data collection is time consuming, particularly if only one point on the psychometric function is of interest (Levitt, 1970). A large number of trials are required to accurately construct a psychometric function. Also, a large number of points are examined at some distance from the point of interest, making the procedure inefficient.

Staircase procedures

Staircase procedures are adaptive tests where stimulus level is determined by the preceding stimuli and responses (like the method of limits). Data collection is concentrated on one point of the psychometric function as opposed to the whole function determined with the method of constant stimuli.

The simplest staircase technique is the Up-Down Rule (UD Rule) introduced by Dixon and Mood (1948), and can be considered to be an extension of the method of limits. The staircase is often started at a clearly suprathreshold stimulus level, in order to give the observer initial encouragement. Instead of ending the test after the first reversal of response, as in the method of limits, stimulus presentation continues. If the subject responds correctly, stimulus level decreases, while an incorrect response raises the stimulus level. The point at which the observer's response changes from correct to incorrect, or vice versa, is termed a 'reversal'. The procedure continues either until a set number of presentations have been completed, or a certain number of response reversals, often 6-8 (Levitt, 1970) have occured. Threshold can be calculated as the average level of the reversals, often discarding the first few reversals. This method is relatively efficient for finding the 50% correct threshold, as long as the correct step size is used. Too big a step size gives inaccurate thresholds, and too small a step size prolongs the test (Cornsweet, 1962). Step sizes should be chosen along some scale yielding approximately equal sensory intervals, and generally logarithmic steps suffice (Cornsweet, 1962). As with the method of limits, if a yes-no response is required observers can follow the stimulus sequence and manipulate the data responses if they choose, without apparently making the data meaningless.

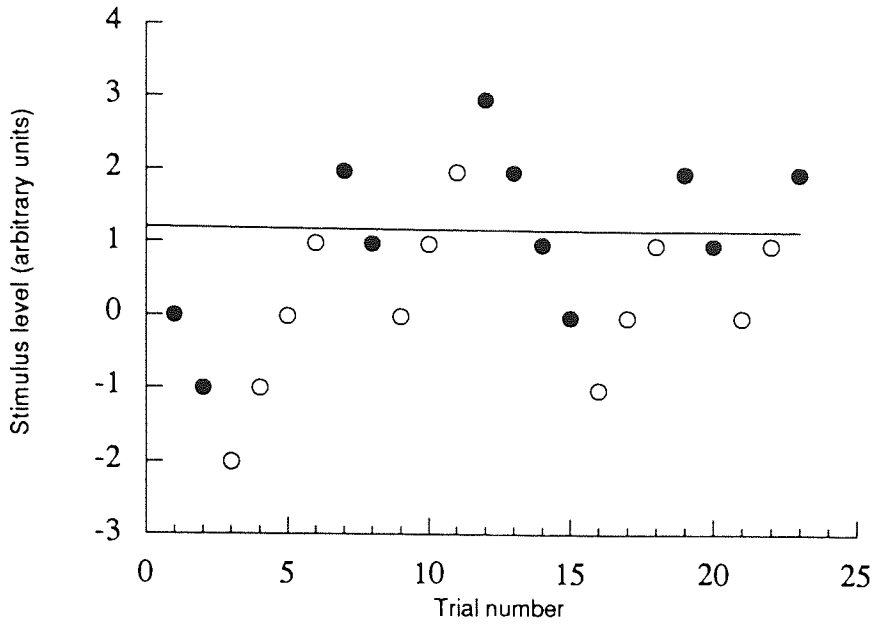

Figure 5.04. Staircase sequence with the UD rule. Filled circles represent 'seen' responses, while open circles represent 'unseen' responses.

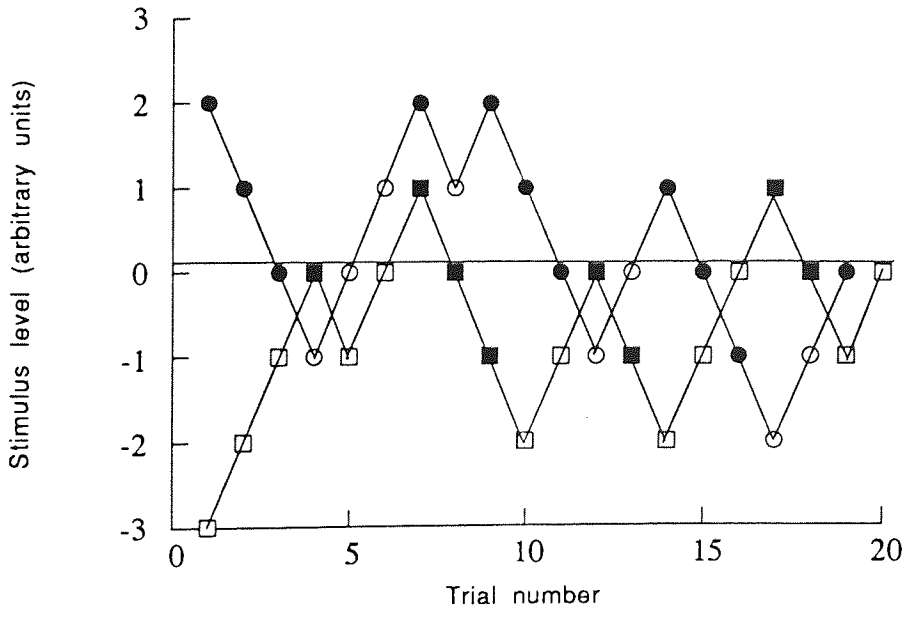

Figure 5.05. Sequence of interleaved staircases. Squares represent a series of stimuli starting below threshold, while circles are for a series starting above threshold. Filled symbols show 'seen' or 'correct' responses, and open symbols represent 'unseen' or 'incorrect' responses.

To reduce an observer's ability to manipulate the data, Cornsweet (1962) suggested randomly interleaving two series of staircase stimuli, one starting from below threshold and the other from above. This makes it difficult for the observer to track the stimulus sequence, and reduces bias in the data.

The 50% correct point as measured by the UD rule is inappropriate as a threshold estimate for a forced choice procedure since this level of accuracy can be achieved purely by guesswork. In order to investigate points on the psychometric function other than 50% correct responses, Wetherill and Levitt (1965) introduced the Up-Down Transform Rule (UDTR). Rather than changing stimulus level after every response, the level is changed only after a certain number of successive correct responses. The percentile points estimated can be varied according to the number of correct responses required before moving down a level. Table 5.01 shows the number of responses required to change level for a number of points on the psychometric function.

Consecutive correct (to decrease stimulus level)	Consecutive incorrect (to raise stimulus level)	Estimated percentile point on psychometric function
1	1	50.0
2	1	70.7
3	1	79.4
4	1	84.1
5	1	87.0
1	2	29.3
1	3	20.6

Table 5.01. Stimulus responses for the UDTR method (Wetherill and Levitt, 1965).

For example, to estimate the 79% point, three consecutive correct responses are required before stimulus level is reduced. The chance for such a sequence at the 50% level is $3\sqrt{0.5} = 0.79$, or approximately 79%, and the sequence will converge to this point on the psychometric function.

Staircases can again be interleaved using the UDTR method. By interleaving staircases measuring percentile points an equal and opposite amount from the 50% correct point, 2 separate points on the psychometric function are determined which can then be used to measure the standard deviation of the the normally distributed psychometric function. Taking the vernier acuity example again, running two concurrent strategies for 29.3%

and 70.7% leftwards responses gives data concentrated 0.54σ either side of μ, from which threshold and bias can be determined (Levitt, 1970).

As further improvement to adaptive procedures, PEST (parameter estimation by sequential testing) was introduced by Taylor and Creelman (1967). As with the UDTR, PEST defines a set of rules for changing the testing level of an embedded psychophysical procedure, coupled with rules determining the stimulus level corresponding to a desired level of performance. PEST consists of a decision rule determining when to change stimulus level, a stepping rule to decide where to set the next level, and an estimator of the final target level (Taylor, Forbes and Creelman, 1983). The rule deciding when to change the testing level is based on a Wald sequential probability ratio test (SPRT) to determine whether the responses at the current testing level are within the range expected for the target probability. Supposing that a target probability of 75% correct is aimed for, then the range of permissable correct responses is given by:

$$N_{corr} = (N_{tot} \times 0.75) \pm W \qquad \text{Equation 5.01}$$

where W is a constant called the deviation limit of the sequential test. If the number of correct responses (N_{corr}) made after a total number of trials (N_{tot}) is compatible with this range, then the next trial will occur at the same level as the previous one. If the number of correct responses is outside the permissable range, then the testing level of the next trial is altered in the appropriate direction. Small values of W give a threshold quickly, but not very accurately. Conversely, large values of W give accurate thresholds, but take more trials to determine threshold. When the testing level is altered, the step size halves on every response reversal. For sequential steps in the same direction, the second step is the same size as the first, the fourth and subsequent steps are double the first, and the third sequential step may, or may not, be double the first according to the previous reversals. Threshold is given as the level called for when the procedure makes a step size of a predetermined minimum value.

Findlay (1978) suggested revisions to improve the PEST technique. These included altering the way in which levels are changed by varying the constant W throughout the test. At the start of the procedure, W is small and threshold is approached quickly, but not very accurately. As the test progresses, the value of W is increased, making thresholds more accurate at the cost of speed.

In this thesis, two alternative forced choice methods have been used in most of the experiments, with the use of the method of constant stimuli (Chapters 9 and 11), Up-Down staircase techniques (Chapter 10), and PEST procedures (Chapter 6). In

contrast, the perimetric experiments (Chapters 7 and 8) involved the use of yes-no stimuli with the method of limits or a simple staircase technique.

5.3 Apparatus

Several pieces of apparatus were used in the collection of data for this thesis, and details of the equipment are given below. The conditions of use of the equipment, in terms of the luminance and contrast conditions, observers used, etc. varied between experiments and are detailed in the relevant chapters.

5.3.1 Humphrey Visual Field Analyser

A Humphrey 640 Visual Field Analyser (Humphrey Inc., San Leandro, CA) was used with commercially available software (Version 6.3) for the perimetric experiments in Chapters 7 and 8. This is an automated projection perimeter employing a photopic bowl luminance of 31.5asb. Sensitivity is expressed in decibels (dB) relative to a maximum stimulus luminance of 10,000asb (=0dB), where 1dB corresponds to a 0.1 log unit step in stimulus luminance. The minimum stimulus luminance employed is 51dB, or 0.08 asb.

The relationship between dB and asb measurements of stimulus intensity is given by the equation:

$$\Delta L \text{ dB} = 40 - 10 \log (\Delta L \text{ asb}) \qquad \text{Equation 5.02}$$

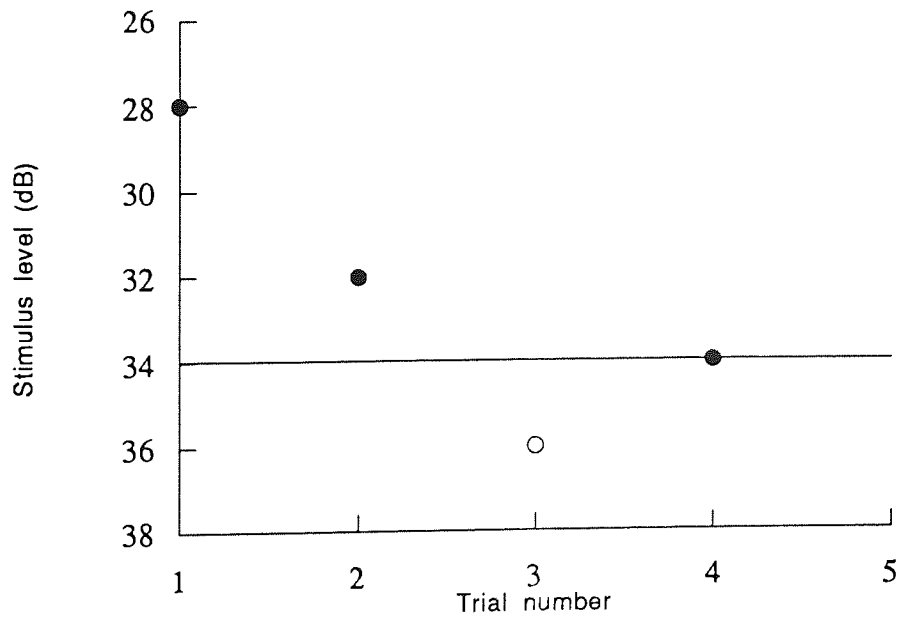

Figure 5.06. Staircase procedure for threshold determination by the Humphrey Field Analyser. Filled circles show 'seen' stimuli, and open circles represent 'unseen' stimuli.

Threshold determination is made using a staircase method. Starting from a luminance above threshold (as estimated from the threshold determinations of adjacent points), luminance is reduced in 4dB steps until the stimulus is reported not seen. Luminance is then incremented in 2dB steps until the stimulus is again seen. The last seen value is taken as a determination of threshold.

The perimeter employs Goldmann stimulus sizes I-V which, according to the manufacturers, have projected diameters of 0.108 deg, 0.216 deg, 0.432 deg, 0.864 deg and 1.724 deg; each increment therefore represents a doubling of stimulus diameter. The sizes of the Goldmann stimuli were verified at a position 5 deg above the central fixation target by photographing the projected stimuli under identical conditions. Rather than being circular, all stimuli were found to be elliptical with their long axis approximately 20% larger than the short axis. The long axis was oriented approximately 15 deg clockwise from vertical. The mean diameter was calculated as (short axis diameter x long axis diameter)$^{0.5}$. In this way the mean diameters of the manufacturer's size II-V stimuli were verified as being accurate to within 1% of the true Goldmann sizes. The actual size of the smallest stimulus was, however, found to be inaccurate, being approximately 9.5% larger than the designated Goldmann I. Taking this discrepancy into account, the Goldmann target sizes expressed in terms of their diameter relative to that of the smallest stimulus are thus 1.00, 1.82, 3.66, 7.30 and 14.62.

In order to increase the number of available stimulus sizes, intermediate stimuli were constructed in order to approximate to 3 and 6 times the Goldmann size I. These were made by making holes in opaque black plastic which were then superimposed onto the aperture wheel of the perimeter. The relative sizes of these stimuli were 2.81 and 5.36 times the actual size of the smallest (Goldmann I) stimulus.

Figure 5.07. Projected stimuli of the Humphrey Field Analyser, photographed to verify the stimulus sizes, are shown on the following page. Right hand row (top to bottom): relative diameters 1.00, 1.82, 3.66, 7.30 and 14.62 (the standard HFA targets). Left hand row: relative diameters 2.81 and 5.36 (constructed stimuli).

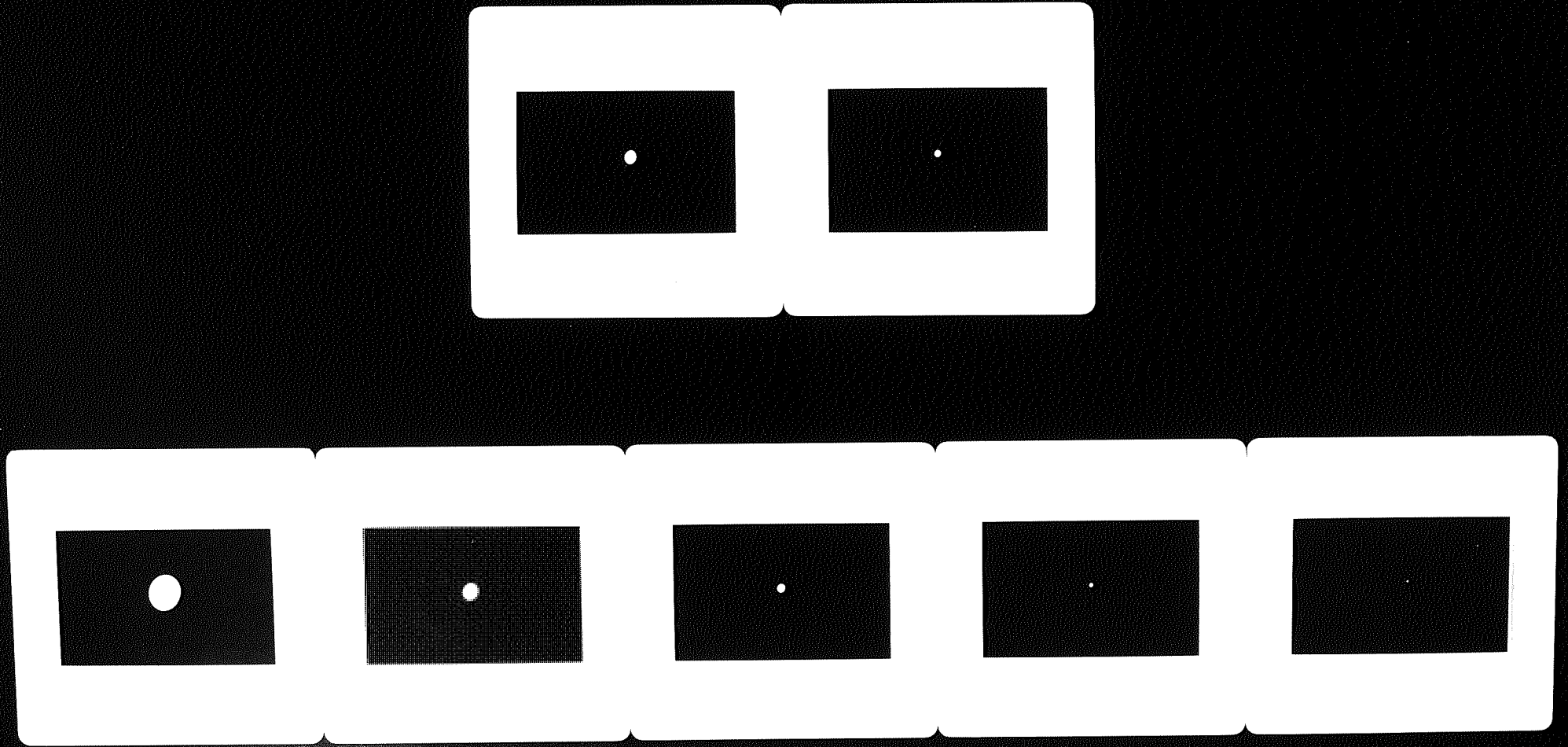

For the static presentation of perimetric stimuli, a number of reliability indices were available. These included 'false positive' responses, or responses made when no stimulus was presented; 'false negative' responses, or responses not made when a stimulus was presented above threshold; and fixation losses, where presentation of a stimulus in the previously mapped blind spot area gave a response (Heijl-Krakau blind spot monitoring technique).

5.3.2 Research Machines Nimbus AX microcomputer

In the experiments of Chapters 6 and 9, a Research Machines Nimbus AX microcomputer was used for stimulus generation. The computer is an IBM clone with a 32Mb internal hard drive. Programs were written in Research Machines Basic. Stimuli were presented on a 14 inch high resolution RGB Eizo 8060S monitor. Pixel separation was 0.32mm in the horizontal and 0.7mm in the vertical direction. Frame rate was 60 Hz. Stimulus size was varied by changing viewing distance from the monitor. Working distances were chosen so that threshold was substantially greater than the pixel size. For working distances less than 2m the monitor was viewed directly. For working distances greater than 2m the monitor was viewed via a mirror. The maximum working distance available was 28m. Responses were made via the keyboard.

5.3.3 Macintosh Centris 650 PC

For the experiments of Chapters 10 and 11, a Macintosh Centris 650 PC was used as the host computer for a Macintosh M1212 colour display with a 50Hz refresh rate. Pixel separation was 0.365mm in the horizontal and 0.359mm in the vertical. In Chapter 10 the stimuli were produced by programs written and compiled in Microsoft Basic. Again, stimulus size was changed by varying viewing distance, and the maximum working distance was 20m. In Chapter 11 the stimuli were generated with 8-bit resolution using the macro capabilities of NIH Image™ 1.52. Stimuli were viewed via a mirror for working distances over 2m. Responses were made via the keyboard or the mouse.

Chapter 6
Curvature detection and discrimination

6.1 Introduction

As was seen in Chapter 4, spatial scaling techniques have shown there to be many different eccentricity-related threshold gradients, which span an enormous range of values (Whitaker et al., 1992a,b). However, the physiological means by which these markedly different gradients are achieved is far from understood. As an example of the application of the spatial scaling method, curvature detection and discrimination thresholds are examined here. Thresholds under optimum conditions are such that curvature thresholds are considered to be hyperacuities (Watt and Andrews, 1982).

In the examination of peripheral gradients, it seems logical that different visual tasks which are performed on the basis of the same physiological characteristics might be expected to demonstrate similar peripheral gradients. For example, the emphasis given to orientation selectivity within the neural system may underlie not just orientation discrimination, but also vernier acuity and curvature detection (Sullivan, Oatley and Sutherland, 1972; Wilson, 1985, 1986; Wilson and Richards, 1989). If these subjectively different tasks behave similarly with respect to eccentricity, this would then lend support to the idea that different groups of peripheral gradients reflect eccentricity-related changes in various neural characteristics, just one of which is orientation selectivity. One purpose of this study, therefore, was to quantify the rate of decline in curvature detection with increasing eccentricity in order to compare it with other tasks.

In order to discriminate curvature, a subject may have to decide whether a test curve is more or less curved than a reference stimulus. The test and reference lines may be presented simultaneously (Watt and Andrews, 1982; Watt, 1984), or sequentially (Wilson, 1985; Wilson and Richards, 1989), generally with some temporal delay between the two presentations. Discriminations of this type may be made over a large range of baseline curvatures. If the reference has a curvature of zero, ie. it is a straight line, then the task may be thought of as curvature detection (Della Valle, Andrews and Ross, 1956; Ogilvie and Daicar, 1967; Andrews, Butcher and Buckley, 1973). Do both types of tasks (detection and discrimination) behave similarly with respect to eccentricity? If these similar tasks do not show similar eccentricity dependencies, then the concept of peripheral gradients being task-dependent may need to be categorised further into the type of threshold discrimination made. A further goal of the study was therefore to compare curvature detection and discrimination in peripheral vision.

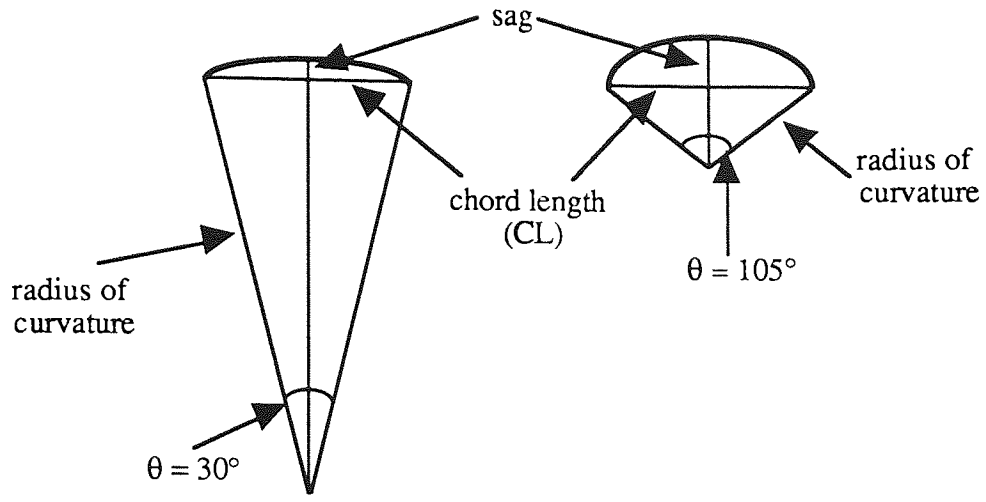

Figure 6.01. Orientation range shown for two curves (heavy lines), having the same chord length (CL). The steeper curve (defined in terms of the sag) has a larger orientation range, θ.

Curvature discrimination, as mentioned above, can be studied over a range of baseline curvatures. Watt and Andrews (1982) examined curvature thresholds for different baseline curvatures at the fovea, and found that the visual system is efficient at processing curvature only within a 40 deg orientation range. Orientation range, depicted in Figure 6.01, is defined as the product of stimulus curvature and length, and represents the range of tangent orientations to the curved contour. Another goal of the study was to examine the eccentricity dependency of curvature discrimination with standard stimuli having different orientation ranges, in order to examine the effect of variation of this parameter with eccentricity.

6.2 Methods

Subjects

Three observers (PM, DW and KL) obtained data for the study. All were pre-presbyopic, moderately myopic (<4.50DS) and wore their distance refractive correction throughout. Corrected acuities were 6/5 or better and viewing was monocular using the dominant eye.

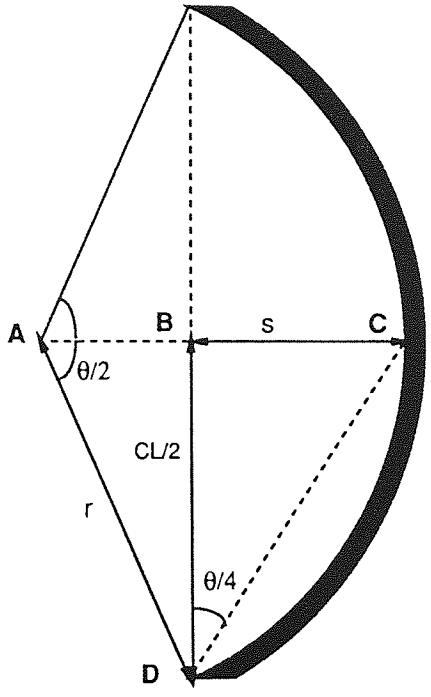

Figure 6.02. Schematic diagram of a typical stimulus as viewed by the observers. Only the curve itself was visible. In peripheral vision, fixation would be to the right of the curve. Symbols have been added to define the geometry of the curve as follows: r, radius of curvature; s, sag; CL, chord length; θ, orientation range.

Stimuli

Stimuli were generated by a Research Machines AX microcomputer and presented on the face of a 14" colour CRT (see Chapter 5 for details). The stimuli consisted of bright (90 cd m^{-2}) curves, formed from part of a circle, and were presented in complete darkness so that neither the edges of the monitor nor any other references were visible within the laboratory. The orientation of the curves was such that their chord lengths were vertical. The width of the line forming the curves was a constant fraction (1.6%) of the chord length. The terms defining the curve are shown in Figure 6.02. Curvature thresholds were defined in terms of the sag of the curve, s. Since

$$AB = r\text{-}s$$

the sag is related to the chord length, CL, and the radius of curvature, r, by the formula

$$r^2 = (CL/2)^2 + (r\text{-}s)^2$$

so that

$$s = r - (r^2 - (CL/2)^2)^{0.5} \qquad \text{Equation 6.01}$$

The geometry of the curve may be defined by its orientation range, θ.
Since

$$AD=AC=r$$

then, because of the equilaterality of the triangle,

$$\angle ACD = \angle ADC = (180-\theta/2)/2 = 90-\theta/4$$

but

$$\angle ADC - \angle BDC = \angle ADB = 90-\theta/2.$$

Hence,

$$\angle BDC = \theta/4$$

so that

$$\theta = 4 \tan^{-1} (2s/CL) \qquad \text{Equation 6.02}$$

In the detection experiment the observer was shown a single 500msec presentation of a curve and was required to respond via the keyboard as to the direction of curvature (mid-point displaced rightward or leftward from vertical). The magnitude of the offset (the sag of the curve) was controlled by two randomly interleaved PEST routines, one designed to concentrate presentations around the 75% rightward response level, the other 75% leftward. 'Rightward' responses tended to make subsequent presentations more 'leftward' and vice versa. Initial presentations were clearly suprathreshold and step size reduced after each successive reversal until it reached the minimum allowed by the resolution of the monitor, after which it remained constant. This minimum was 3.69 sec arc at the foveal viewing distance of 20m. The sequence terminated after 200 trials, following which a psychometric function was derived from the percentage of 'rightward' responses at each stimulus level tested. Psychometric functions were analysed by a probit analysis. Threshold was taken to be half the distance between the 25% and 75% 'rightward' stimulus response levels whilst the stimulus level resulting in a 50% response represented bias. Results were obtained for a series of chord lengths, achieved by a combination of changing the size of the stimulus on the monitor and by changing viewing distance. Foveal viewing distance was 20m for chord lengths of 4, 8, 16 and 32 min arc but had to be reduced to 10m to obtain the 64 min arc size. Thresholds were also measured at eccentricities of 5, 10 and 15 deg in the nasal visual field for which viewing distances were 4m (5m for DW), 3m and 2m respectively. For eccentric viewing, fixation was controlled by a small LED. All stimuli were simply magnified or minified versions of one another in every dimension.

In the discrimination experiments, the observer was shown two curves, each for 500msec with a 250msec inter-stimulus interval. The first was a standard comparison

curve whose orientation range was decided upon before the experiment commenced. The second presentation consisted of a curve whose sag was either slightly greater or slightly less than that of the standard curve. The subjects' task was to decide whether the second stimulus was more or less curved than the first. As in the detection experiments, two interleaved PEST routines concentrated stimulus presentation around the 75% 'more curved' and 75% 'less curved' response levels. Following probit analysis of the data, threshold was defined as half the distance between the 25% and 75% 'more curved' response level whilst the 50% location represented bias. Chord lengths were varied by changing viewing distance within the range 28 to 0.31 metres. Again, therefore, all stimuli were magnified or minified versions of one another. It should be noted that the orientation range of the curve is independent of viewing distance (magnification). Eccentricities of 0, 2.5, 5 and 10 deg in the nasal visual field were investigated. The direction of curvature of peripheral stimuli was always such that the open ends of the curve were directed away from the fixation, in order to be more comparable with the foveal situation. Eccentricities were measured from the mid-point of the curve to fixation. Data sets were collected for two orientation ranges, 30 deg and 105 deg. These were chosen since one lies within and the other lies clearly outside the orientation range (40 deg) thought to be used most efficiently in curvature discrimination (Watt and Andrews, 1982).

Since the stimuli were all magnified or minified versions of one another, they were not all of equal visibility (intensity factor above threshold). Hess and Watt (1990) have demonstrated that intensity affects curvature thresholds, and it appears that the effect is slightly greater at the fovea than in the periphery. The visibility of the shortest, thinnest stimuli was measured by introducing neutral density filters in front of the eye until the presence of the stimuli became undetectable. This required at least 1.1 log units for each observer. Hess and Watt's data indicate that curvature thresholds remain approximately constant at all eccentricities once visibility exceeds threshold by 1 log unit. Hence, visibility differences are unlikely to have seriously affected the results.

6.3 Results

Figures 6.03-05a shows curvature thresholds (expressed in terms of the angular subtense of the sag) plotted against chord length for the detection task. At each eccentricity, thresholds decrease with increasing chord length but begin to reach a plateau for longer lines. This tendency is well established for foveal curvature thresholds (Andrews et al., 1973; Watt and Andrews, 1982) and also for periodic vernier acuity provided the number of cycles is low (Tyler, 1973). At still longer chord

lengths thresholds would be expected to rise (Andrews et al., 1973). However, the use of very large stimuli was avoided since, as stimulus size grows, it becomes more and more inappropriate to assume that a purely foveal visual response is being obtained. This assumption is crucial since visual performance is being compared at other eccentricities relative to that at the fovea.

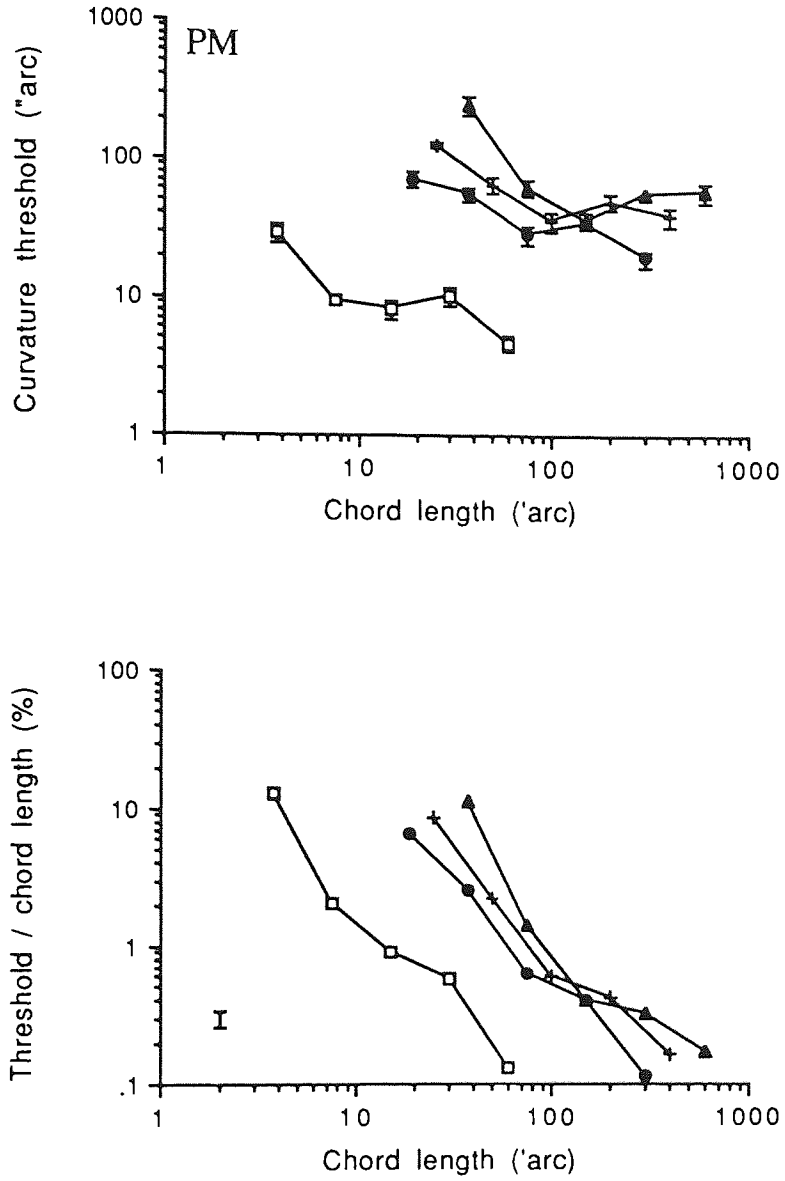

Figure 6.03. (a) Thresholds for the detection of curvature, expressed in terms of the angular subtense of the minimum detectable sag, plotted against chord length, for subject PM. Symbols represent different eccentricities as follows: open squares, 0°; circles, 5°; crosses, 10°; triangles, 15°. Standard errors are shown for each data point.

(b) Thresholds are expressed as a percentage of chord length and plotted against chord length itself. This renders the y-axis scale invariant. Symbols as for Figure 6.03a. Mean standard error is shown.

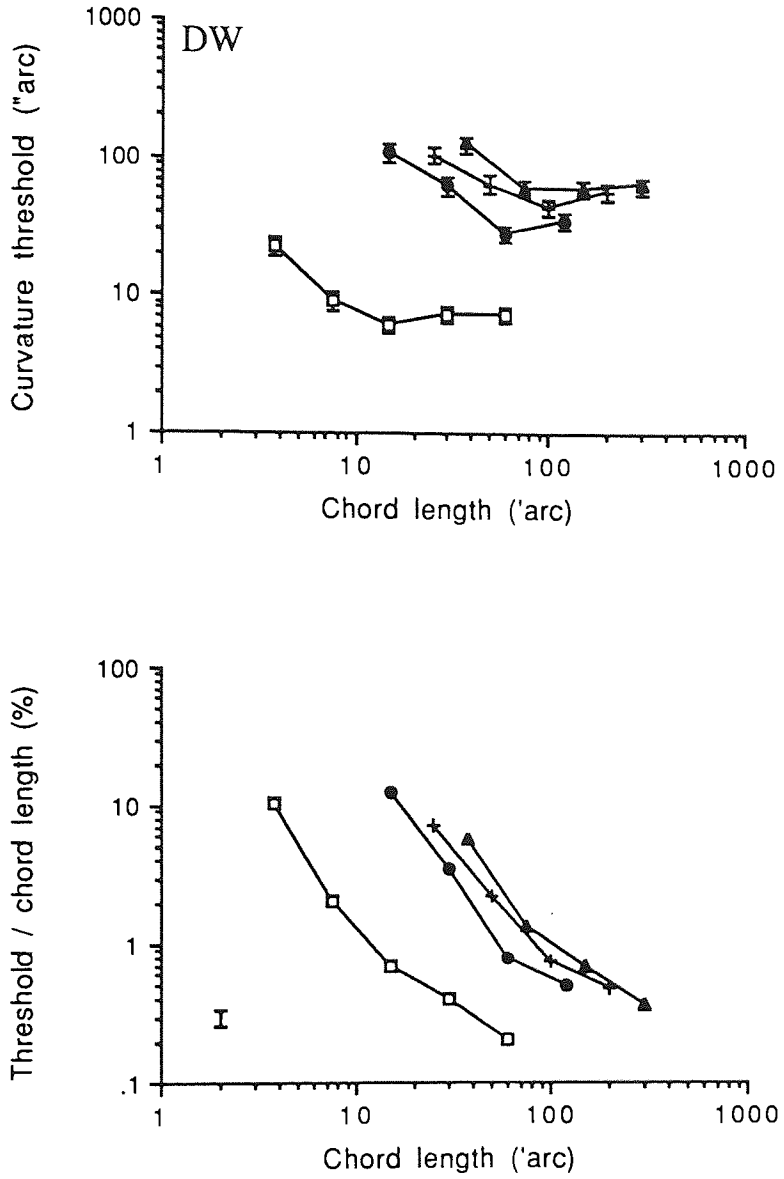

Figure 6.04. (a) Thresholds for the detection of curvature, expressed in terms of the angular subtense of the minimum detectable sag, plotted against chord length, for observer DW. Symbols and errors as for Figure 6.03a.

(b) Thresholds are expressed as a percentage of chord length and plotted against chord length itself. As for Figure 6.03b, but for subject DW.

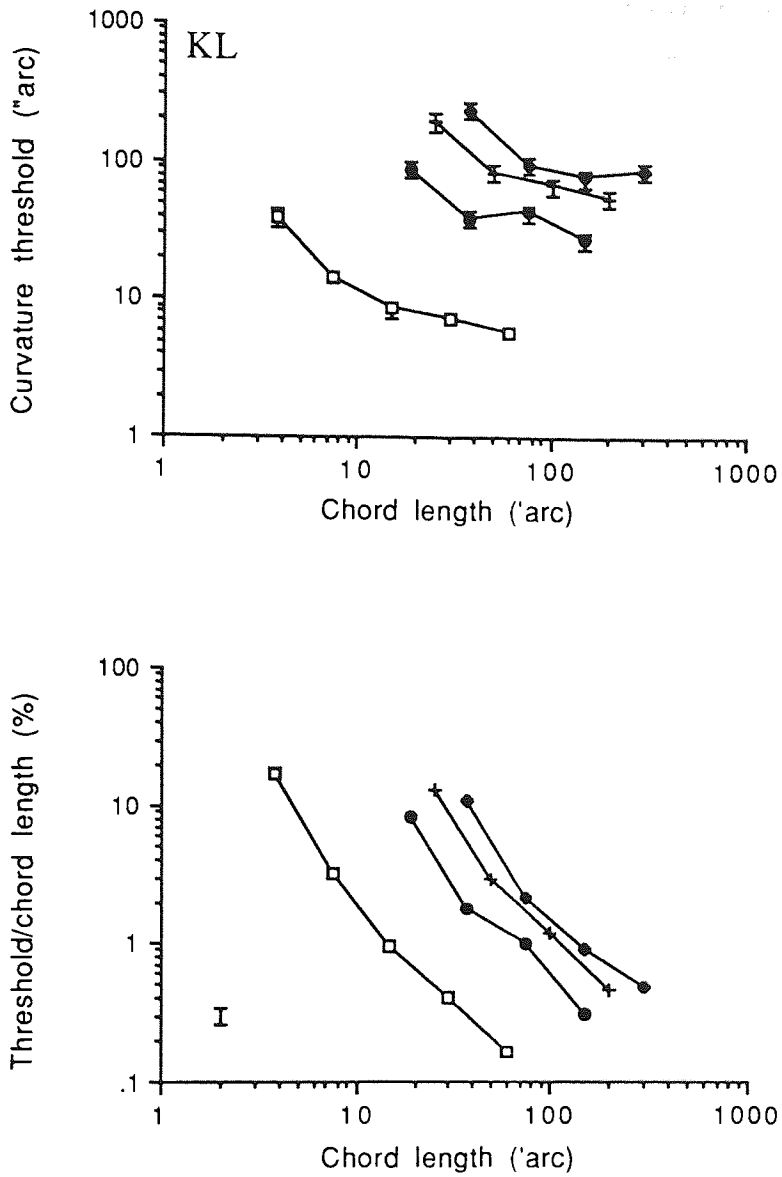

Figure 6.05. (a) Thresholds for the detection of curvature, expressed in terms of the angular subtense of the minimum detectable sag, plotted against chord length, for observer KL. Symbols and errors as for Figure 6.03a.

(b) Thresholds are expressed as a percentage of chord length and plotted against chord length itself. As for Figure 6.03b, but for subject KL.

In Figures 6.03-05a, peripheral thresholds are displaced from the foveal data along both ordinate and abcissa, since both axes represent spatial measures. In Figures 6.03-05b, thresholds have been expressed as a percentage of the chord length, which renders the y-axis scale invariant. If peripheral visual performance differed from that at the fovea simply by a change of scale one would expect functions for successive eccentricities to be shifted horizontally along the size (the x-) axis. This is exactly what is found. The rate at which stimulus size must increase in order to result in performance equivalent to that at the fovea is reflected in the magnitude of this shift. Curves for successive eccentricities were therefore shifted leftwards until an optimum fit to the foveal data, as estimated by eye, was obtained. The amount of shift gave a scaling factor (F) for each eccentricity, and these scaling factors are plotted as a function of eccentricity in Figures 6.06-08a. These data points were fitted with a regression, constrained to pass through a scaling factor of 1 at 0 degrees eccentricity, since the foveal data scaled relative to itself results in a scaling factor of unity. The regression is of the form:

$$\log F = \log (1 + (E / E_2)) \qquad \text{Equation 4.01}$$

from which values (± standard error) for E_2 were found to be 1.85 ± 0.15 deg for PM, 1.68 ± 0.18 deg for DW, and 1.81 ± 0.06 deg for KL.

Figures 6.06-08b show the data from each eccentricity after dividing chord lengths at each eccentricity by a scaling factor derived from the individual E_2 values, using Equation 6.03:

$$\text{scaled chord length} = \text{chord length} / (1 + (E / E_2) \qquad \text{Equation 6.03}$$

This has the effect of collapsing the curvature data from each eccentricity onto a single function and demonstrates that, for the task of curvature detection, the periphery behaves in a manner identical to the fovea except for a simple change of scale or magnification.

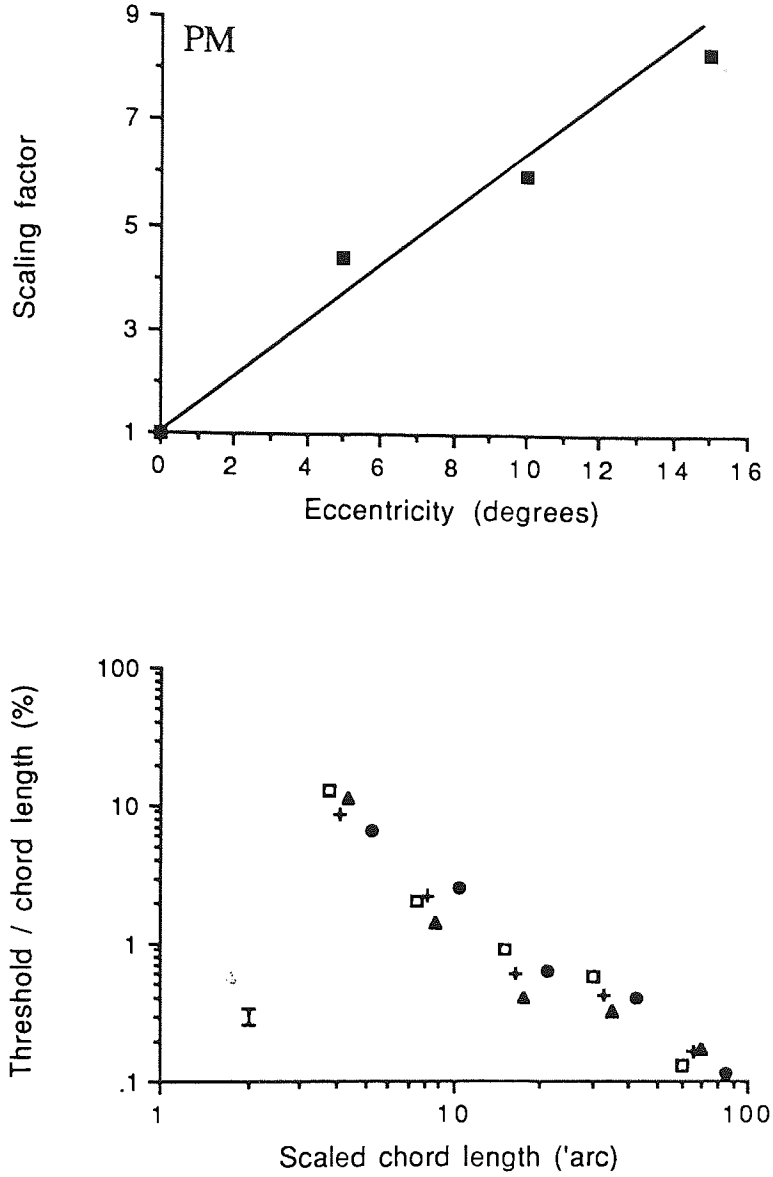

Figure 6.06. (a) Scaling factors for subject PM, derived from Figure 6.03b as described in the text, plotted against eccentricity. Scaling factors represent the extent to which data sets for each eccentricity in Figure 6.03b are shifted rightwards along the x-axis relative to the foveal data set. The scaling factors have been fitted with a regression of the form: $\log F = \log (1 + (E / E_2))$. E_2 is 1.85 ± 0.15 deg.

(b) The data of Figure 6.03b after shifting each of the peripheral data sets leftwards along the x-axis according to scaling factors predicted by the regression of Figure 6.06a. Different symbols represent different eccentricities as described previously. Note how the eccentricity dependence of the data is removed in this way. Mean standard error is shown.

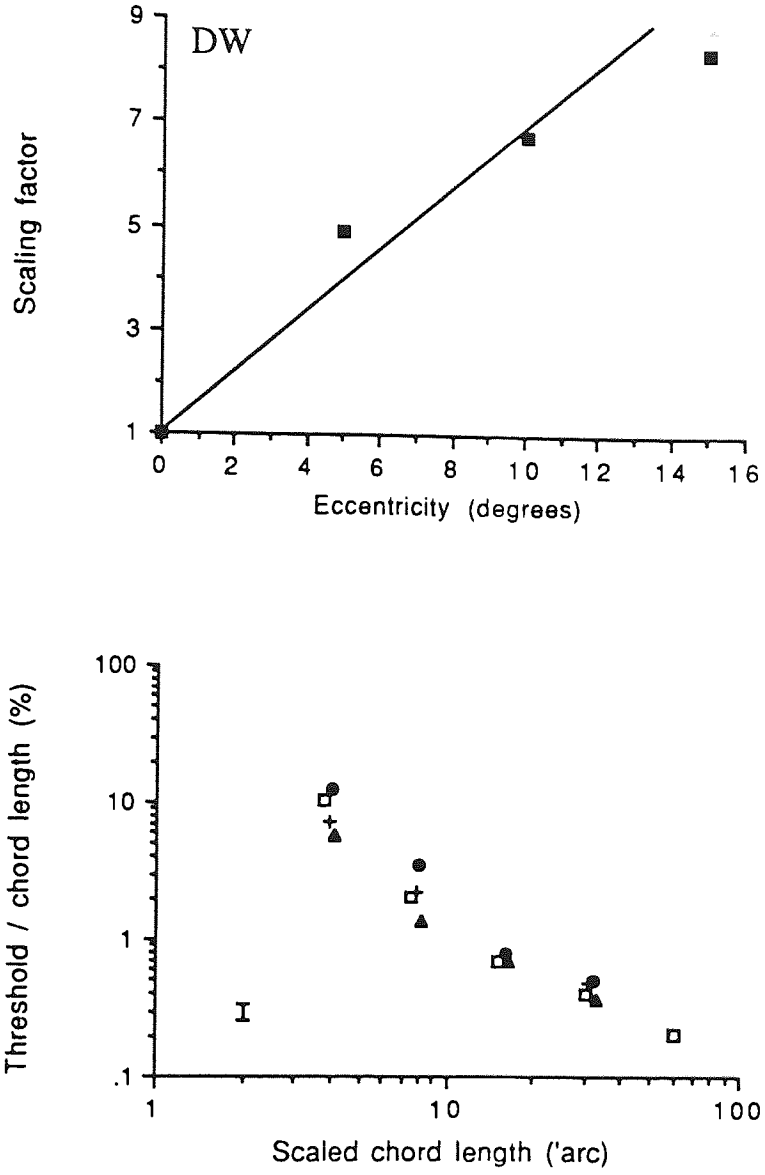

Figure 6.07. (a) As for Figure 6.06a, but for subject DW. Scaling factors are derived from Figure 6.04b. E_2 is 1.68 ± 0.18 deg.

(b) The data of Figure 6.04b, scaled according to the E_2 value found from Figure 6.07a.

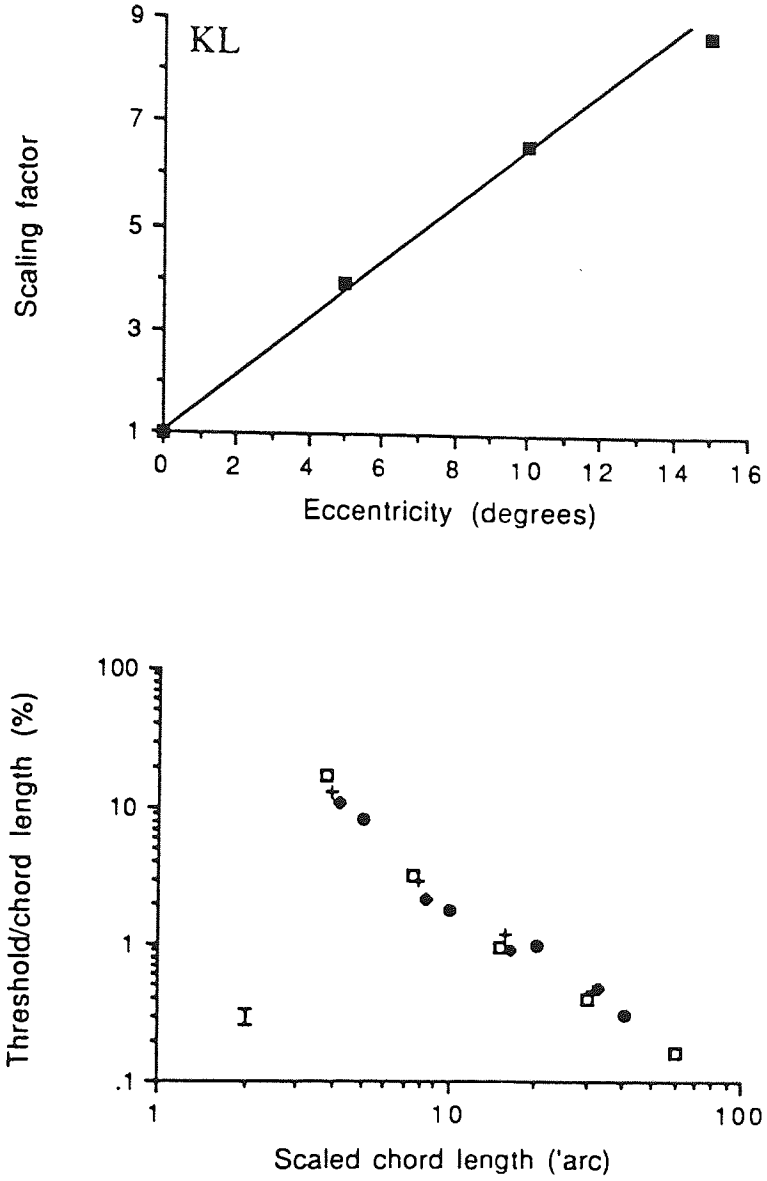

Figure 6.08. (a) As for Figure 6.06a, but for subject KL. Scaling factors are derived from Figure 6.05b. E_2 is 1.81 ± 0.06 deg.

(b) The data of Figure 6.05b, scaled according to the E_2 value found from Figure 6.08a.

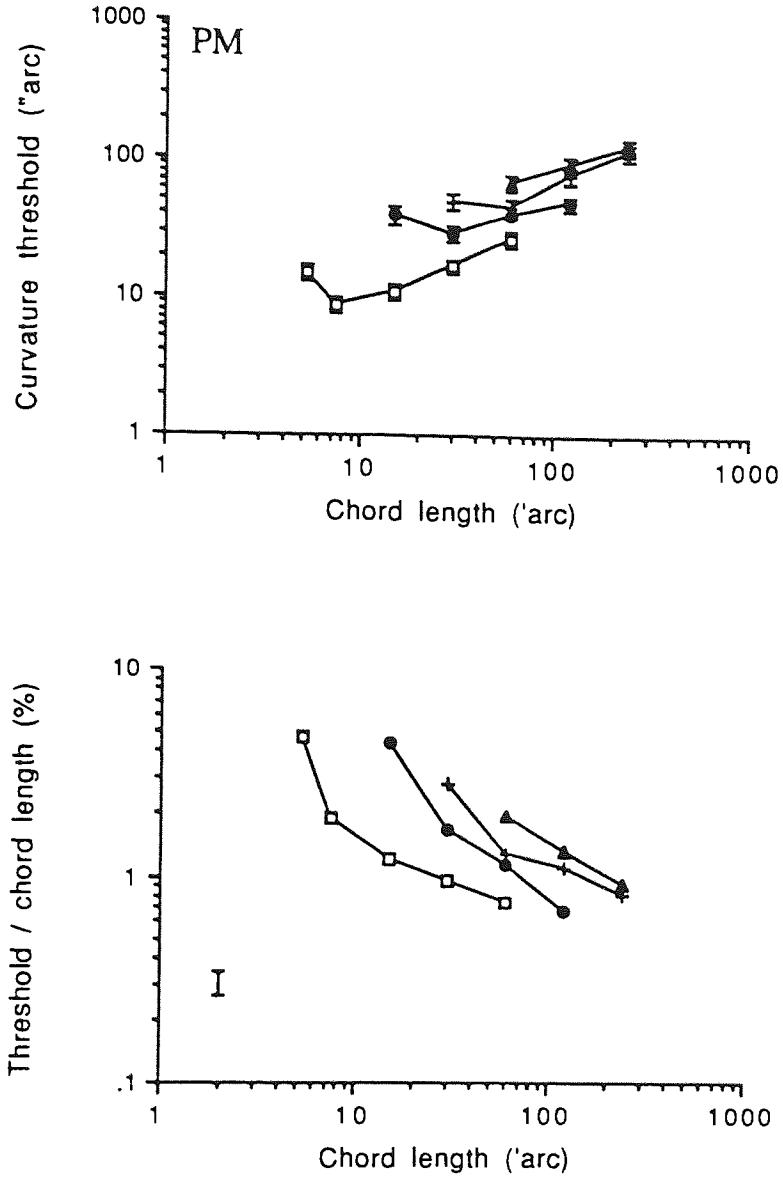

Figure 6.09. (a) Thresholds for curvature discrimination, expressed in terms of the angular subtense of the minimum discriminable change in sag, plotted against chord length for subject PM. Baseline orientation range of the standard curve was 30°. Symbols represent different eccentricities as follows: open squares, 0°; circles, 2.5°; crosses, 5°; triangles, 10°. Standard errors are shown for each data point. (b) Thresholds are expressed as a percentage of chord length and plotted against chord length itself. This renders the y-axis scale invariant. Symbols as for Figure 6.09a. Mean standard error is shown.

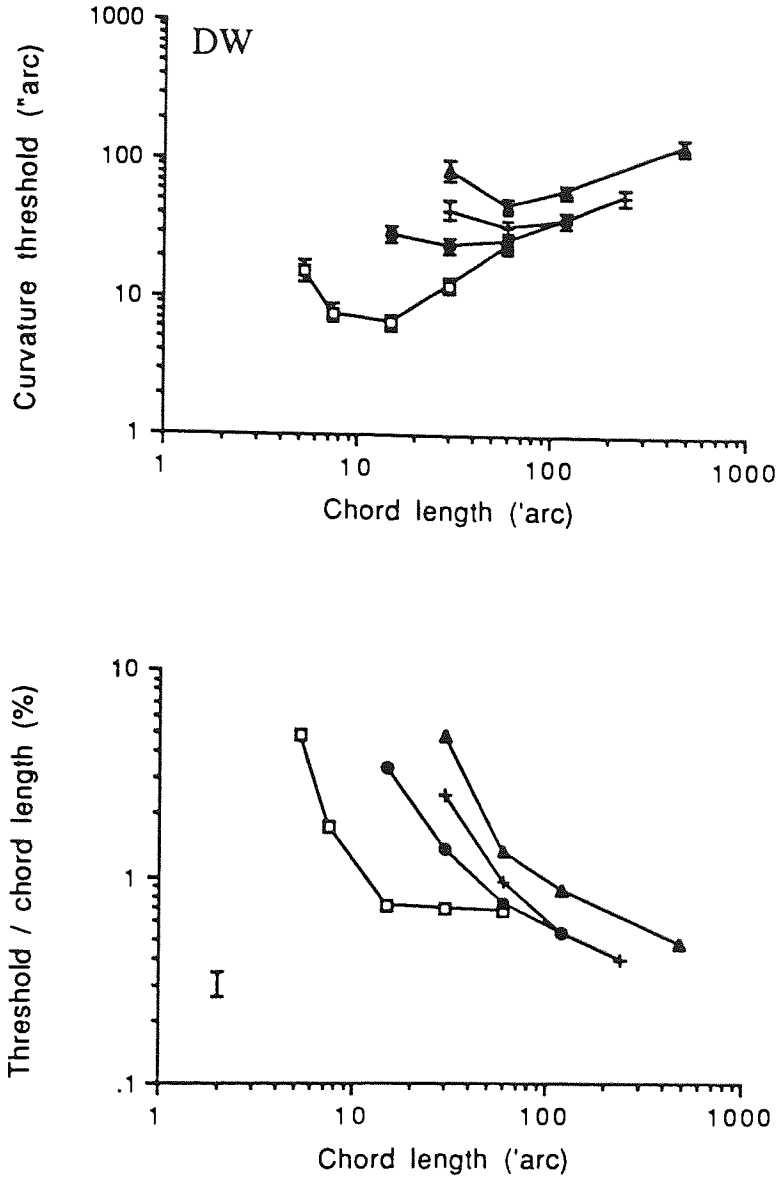

Figure 6.10. (a) Thresholds for curvature discrimination, expressed in terms of the angular subtense of the minimum discriminable change in sag, plotted against chord length, for observer DW. Baseline orientation range of the standard curve was 30 deg. Symbols and errors as for Figure 6.09a.
(b) Thresholds are expressed as a percentage of chord length and plotted against chord length itself. As for Figure 6.09b, but for subject DW.

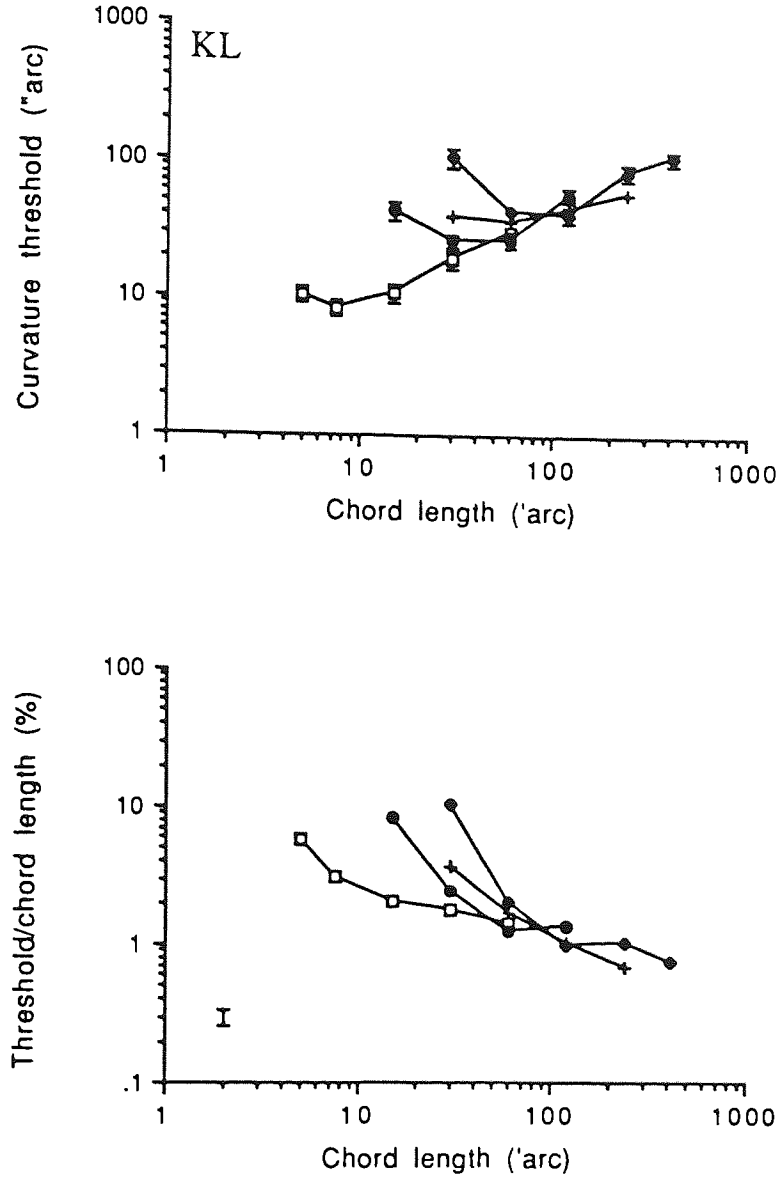

Figure 6.11. (a) Thresholds for curvature discrimination, expressed in terms of the angular subtense of the minimum discriminable change in sag, plotted against chord length, for observer KL. Baseline orientation range of the standard curve was 30 deg. Symbols and errors as for Figure 6.09a.
(b) Thresholds are expressed as a percentage of chord length and plotted against chord length itself. As for Figure 6.09b, but for subject KL.

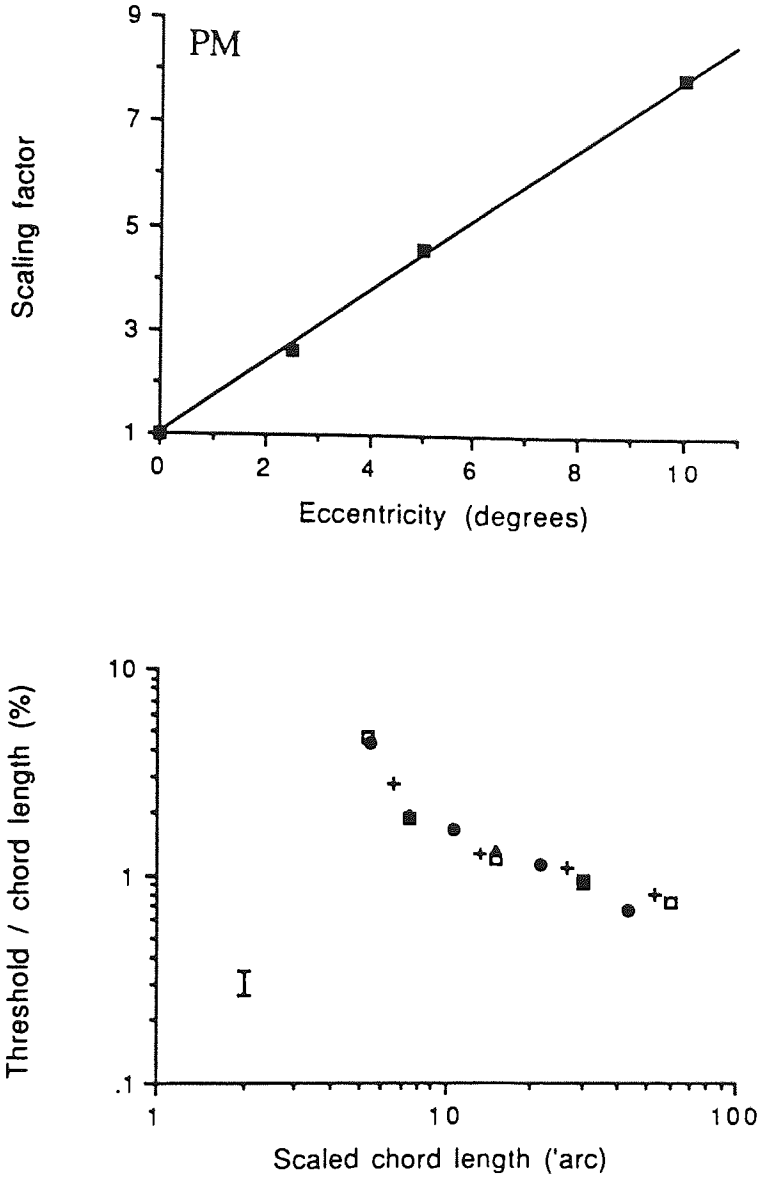

Figure 6.12. (a) Scaling factors for subject PM, derived from Figure 6.09b as described in the text, plotted against eccentricity. Scaling factors represent the extent to which data sets for each eccentricity in Figure 6.09b are shifted rightwards along the x-axis relative to the foveal data set. The scaling factors have been fitted with a regression of the form: $\log F = \log (1 + (E / E_2))$. E_2 is 1.44 ± 0.04 deg.

(b) The data of Figure 6.09b after shifting each of the peripheral data sets leftwards along the x-axis according to scaling factors predicted by the regression of Figure 6.12a. Different symbols represent different eccentricities as described previously. Mean standard error is shown.

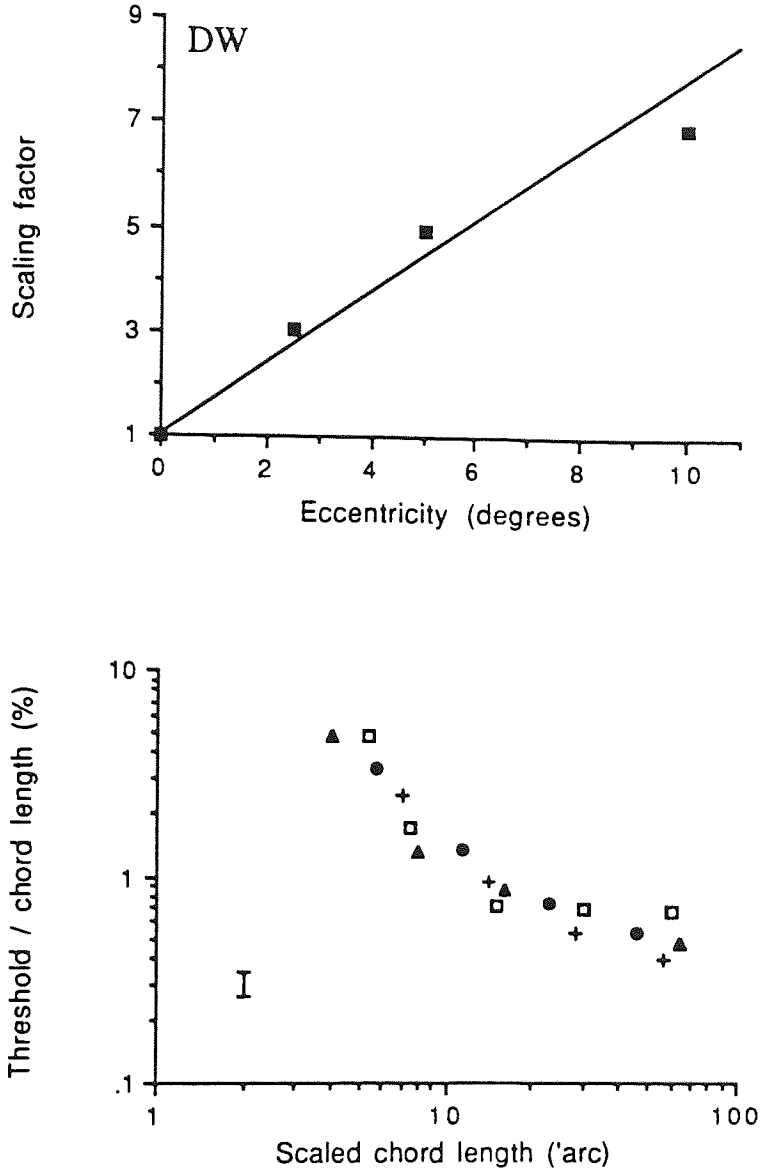

Figure 6.13. (a) As for Figure 6.12a, but for subject DW. Scaling factors are derived from Figure 6.10b. E_2 is 1.40 ± 0.12 deg.

(b). The data of Figure 6.10b, scaled according to the E_2 value found from Figure 6.13a.

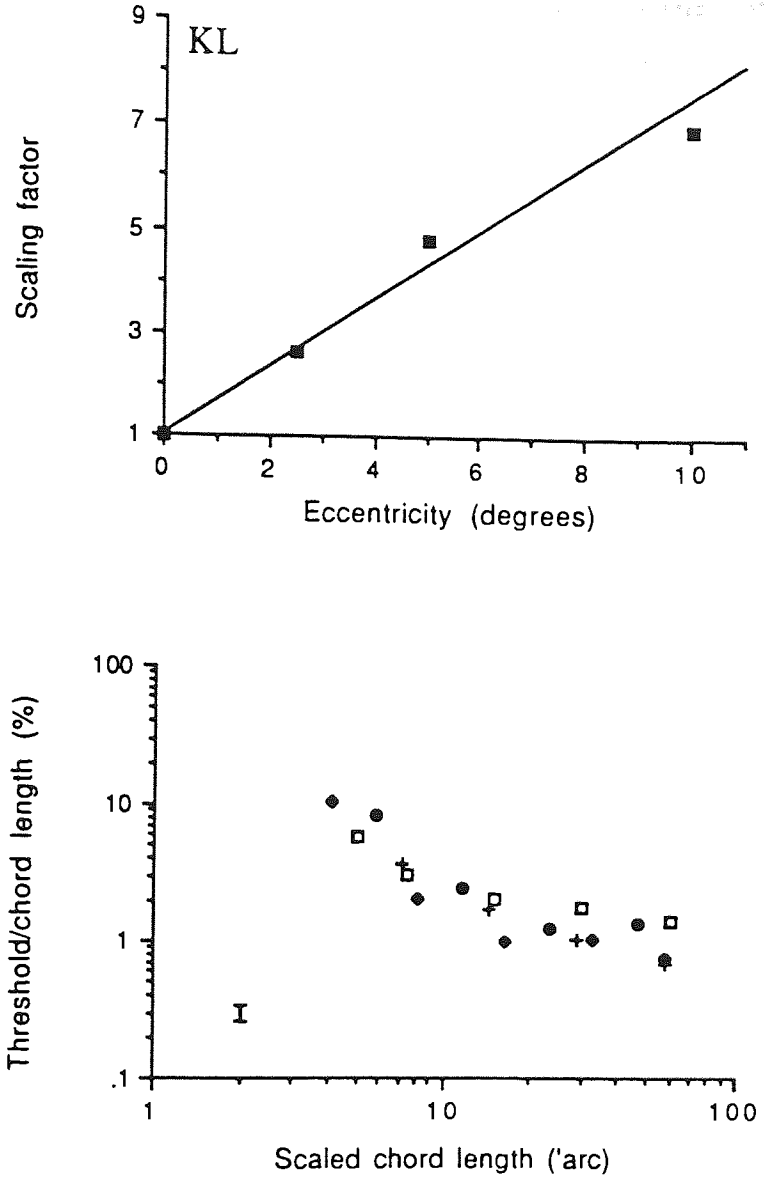

Figure 6.14. (a) As for Figure 6.12a, but for subject KL. Scaling factors are derived from Figure 6.11b. E_2 is 1.51 ± 0.09 deg.

(b). The data of Figure 6.11b, scaled according to the E_2 value found from Figure 6.14a.

Curvature discrimination thresholds for a baseline orientation range of 30 deg are shown in Figures 6.09-11a. Thresholds are expressed in terms of the just discriminable change in sag. In contrast to the detection data, discrimination thresholds are optimum at an intermediate chord length and thereafter increase steadily as chord length increases. Thresholds are plotted as a fraction of chord length in Figures 6.09-11b. Note that the curves are similar in shape apart from KL and DW's foveal data which demonstrate a plateau (representing Weber's law) as chord length grows, whilst the eccentric data continue to decrease slightly. Observer PM shows no such difference between foveal and peripheral conditions.

The peripheral data functions were shifted leftwards in order to produce the best fit to the foveal data. These scaling factors are shown plotted in Figure 6.12-14a and E_2 values derived from the regression analyses were 1.44 ± 0.04 deg for PM, 1.40 ± 0.12 deg for DW and 1.51 ± 0.09 deg for KL. The chord lengths at each eccentricity were scaled according to these E_2 values as before and are shown in Figure 6.12-14b. Much of the eccentricity-dependence of the data is removed in this way, although the slight difference between the foveal and extrafoveal data is evident at greater chord lengths for DW and KL.

Similar data, but for a stimulus with a baseline orientation range of 105 deg, are shown in Figures 6.15-20. Again, Figure 6.15-17a shows that discrimination thresholds increase with increasing chord length. Horizontal superimposition of the curves in Figure 6.15-17b resulted in the scaling factors shown in Figure 6.18-20a. E_2 values were 1.90 ± 0.15 deg for PM, 2.25 ± 0.24 deg for DW and 1.53 ± 0.21 deg for KL. The scaled data are shown in Figure 6.18-20b.

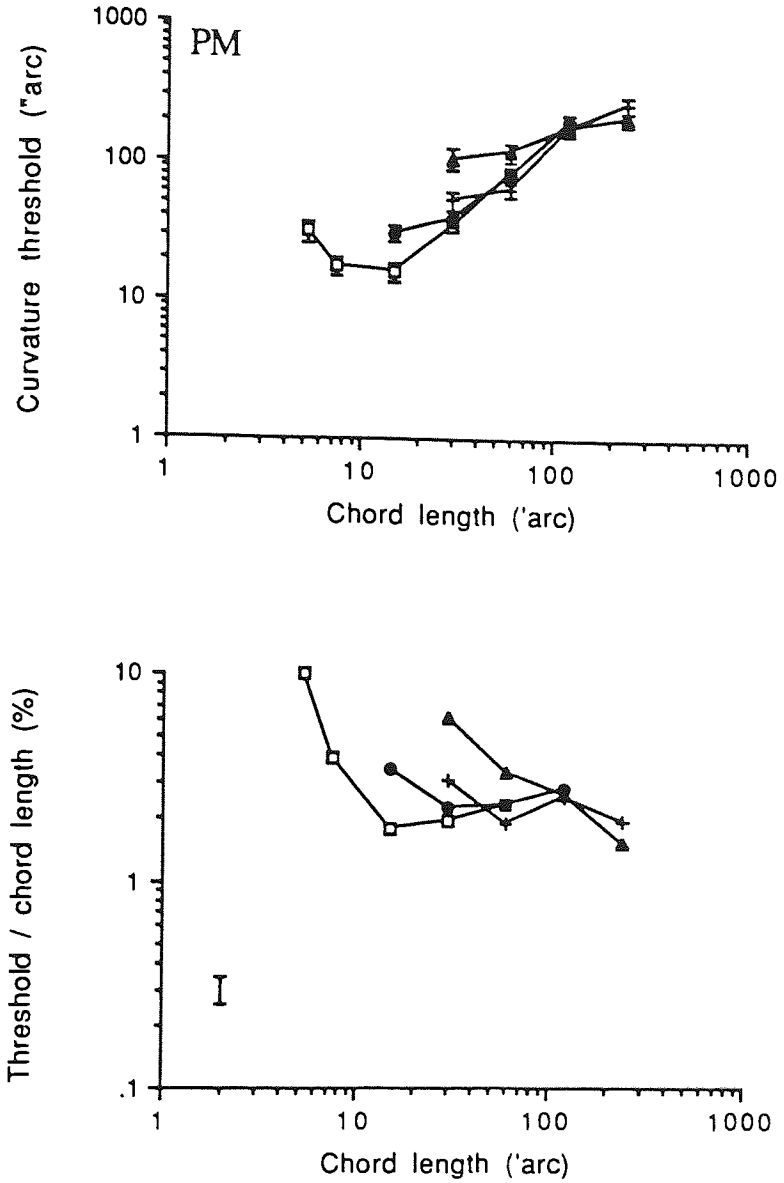

Figure 6.15. (a) As for Figure 6.09a but the baseline orientation range of the standard curve was 105 deg. Subject PM.

(b) As for Figure 6.09b for an orientation range of 105 deg.

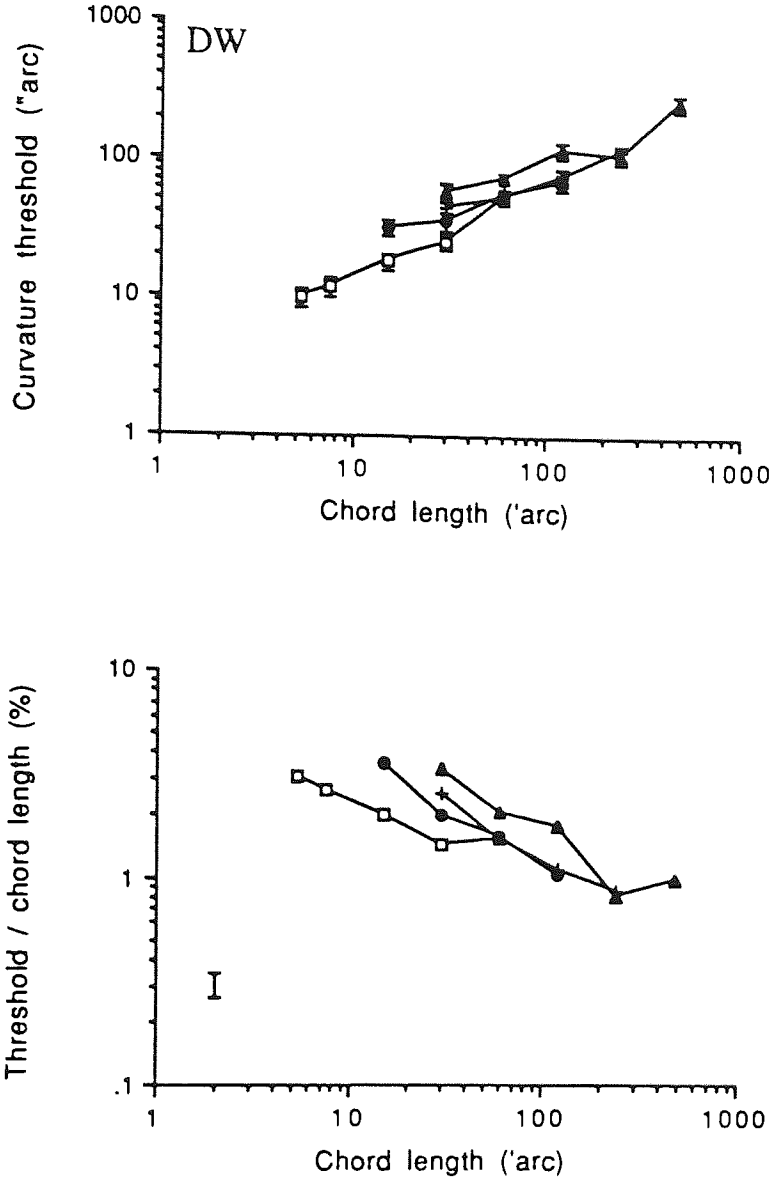

Figure 6.16. (a) As for Figure 6.10a, but the baseline orientation range of the standard curve was 105 deg. Subject DW.

(b) As for Figure 6.10b for an orientation range of 105 deg.

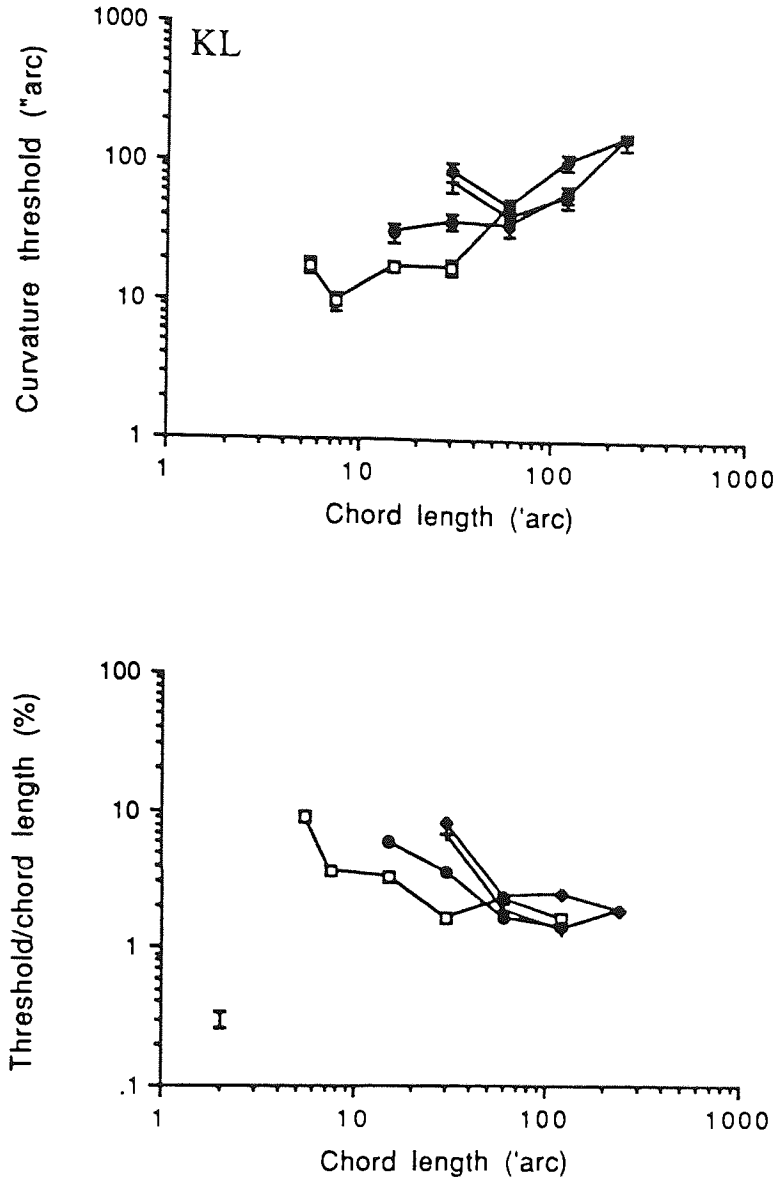

Figure 6.17. (a) As for Figure 6.11a but the baseline orientation range of the standard curve was 105 deg. Subject KL.

(b) As for Figure 6.11b for an orientation range of 105 deg.

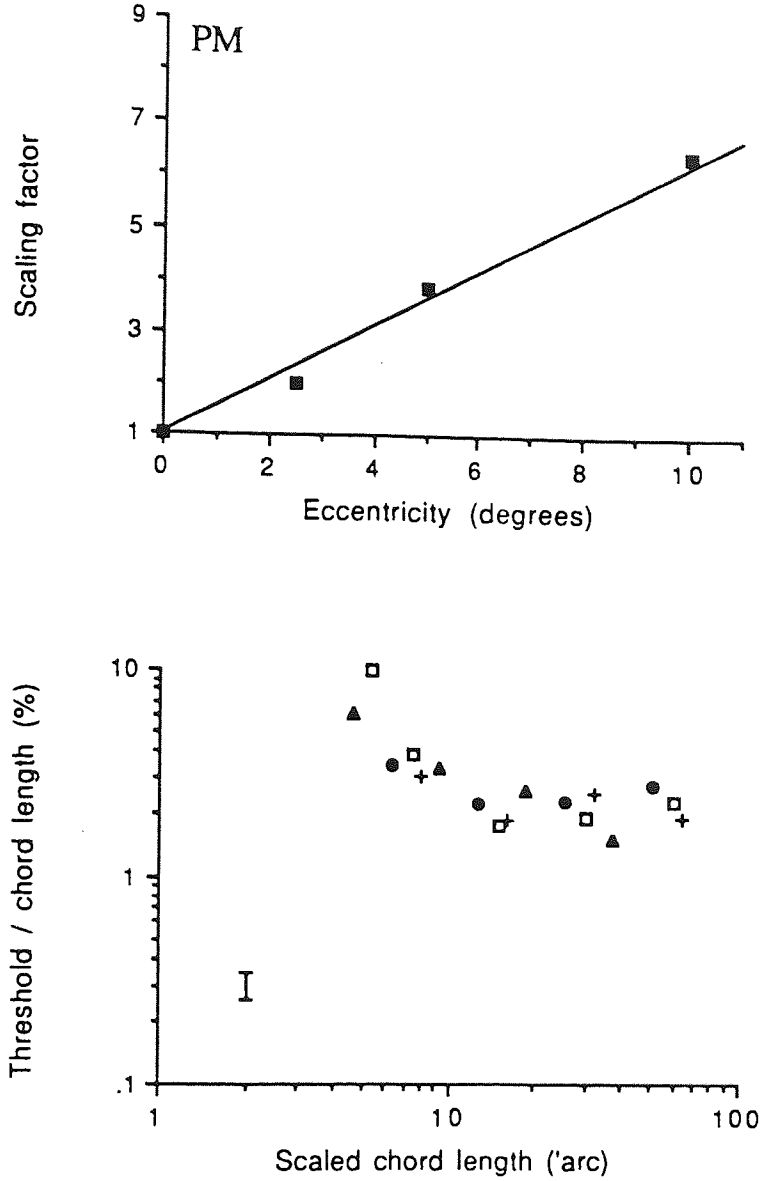

Figure 6.18. (a) As for Figure 6.12a, but with scaling factors derived from Figure 6.15b. E_2 is 1.90 ± 0.15 deg. Subject PM.

(b) The data of Figure 6.15b after shifting each of the peripheral data sets leftwards along the x-axis according to scaling factors predicted by the regression of Figure 6.18a. Different symbols represent different eccentricities as described previously. Mean standard error is shown.

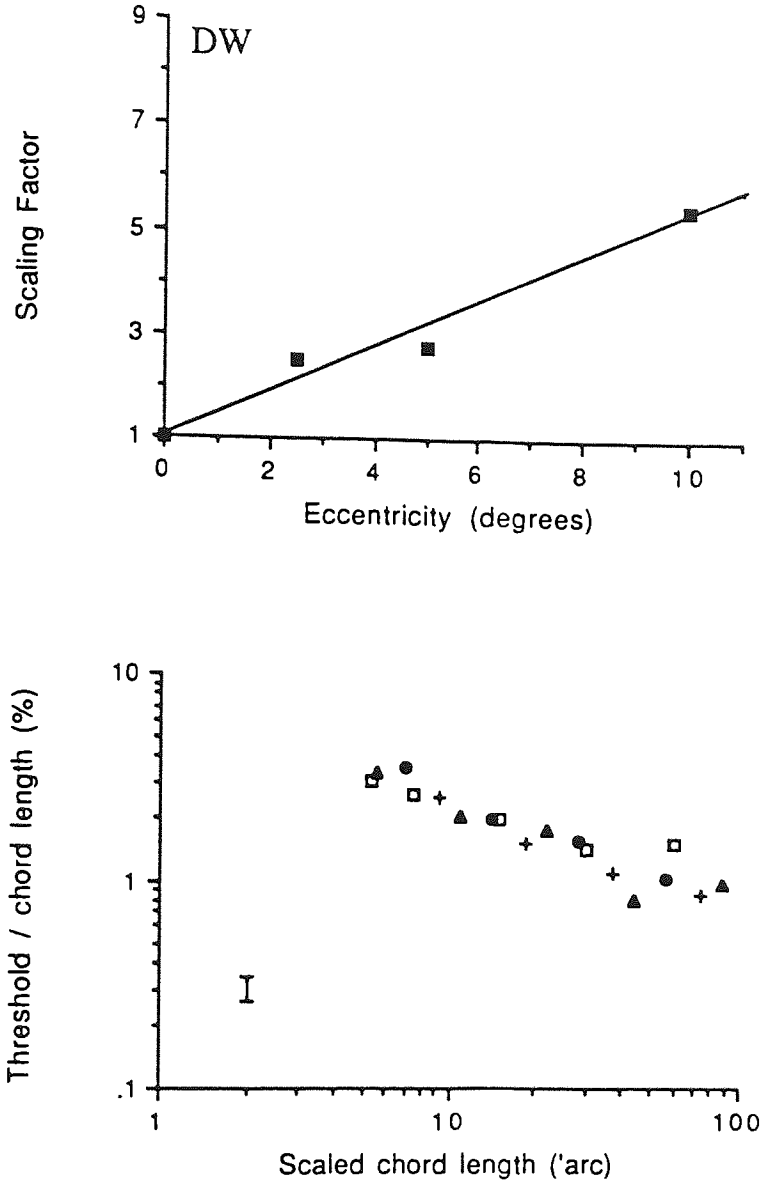

Figure 6.19. (a) As for Figure 6.13a, but with scaling factors derived from Figure 6.16b. E_2 is 2.25 ± 0.24 deg. Subject DW.

(b) The data of Figure 6.16b after shifting each of the peripheral data sets leftwards along the x-axis according to scaling factors predicted by the regression of Figure 6.19a.

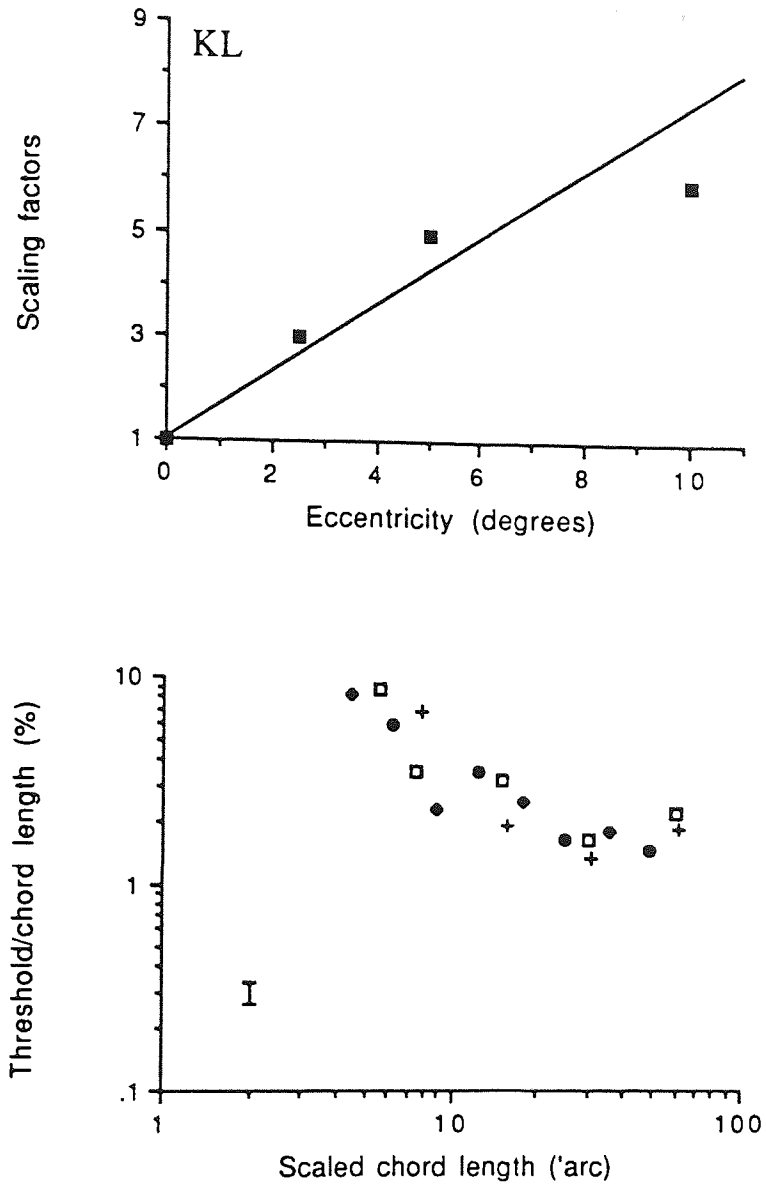

Figure 6.20. (a) As for Figure 6.14a, but with scaling factors derived from Figure 6.17b. E_2 is 1.53 ± 0.21 deg. Subject KL.

(b) The data of Figure 6.17b after shifting each of the peripheral data sets leftwards along the x-axis according to scaling factors predicted by the regression of Figure 6.20a.

Figure 6.21 compares the data from the curvature detection experiment (which had a baseline orientation range of zero degrees) with the two discrimination stimuli (baseline orientation ranges of 30 deg and 105 deg). The data points are taken from Figures 6.06-8b, 6.12-14b and 6.18-20b, and data from different eccentricities have been combined. At small values of chord length, performance is relatively independent of baseline orientation range. However, at larger values of chord length, performance for the more curved stimuli becomes relatively poorer. This could be the result of a Weber-type process since, for any given chord length, sag increases as a function of the orientation range of the curve. At large chord lengths, therefore, the sag of the curves becomes greater for the stimuli with larger orientation range.

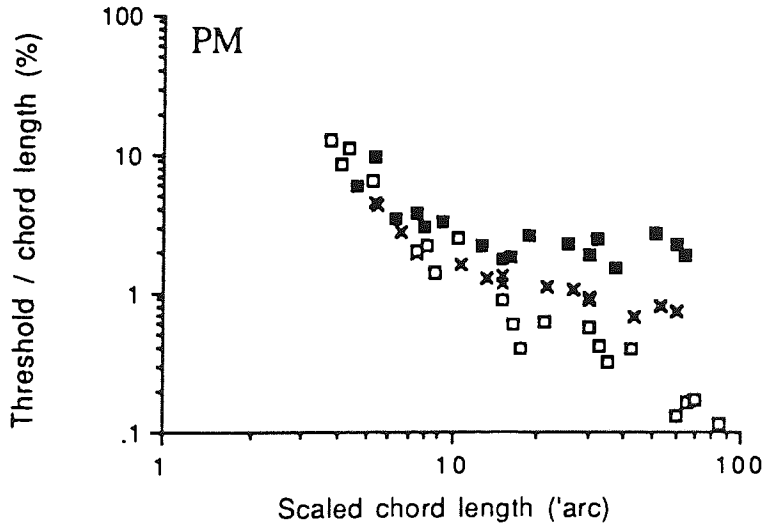

Figure 6.21. See following page for legend details.

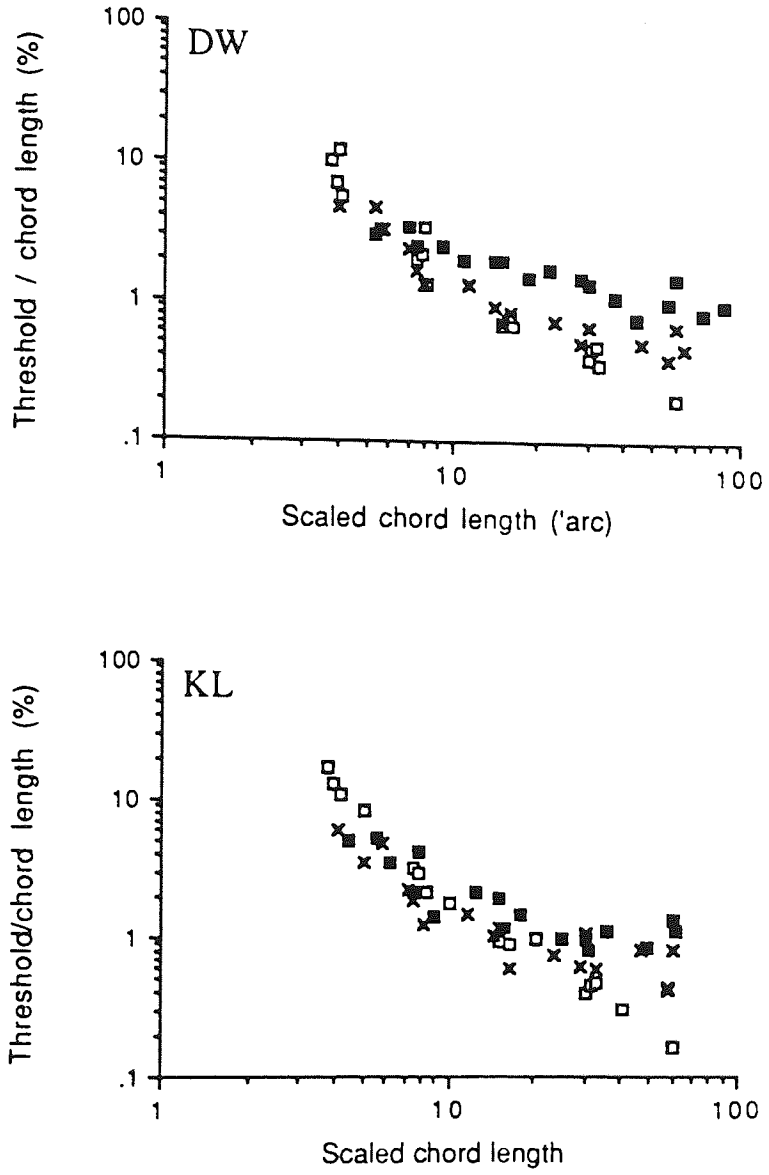

Figure 6.21. Data from previous Figures of scaled data combined. For subject PM, data is combined from Figures 6.06b, 6.12b and 6.18b; for subject DW the data is from Figures 6.07b, 6.13b and 6.19b; for subject KL data is taken from Figures 6.08b, 6.14b and 6.20b. Open squares represent the curvature detection task where baseline orientation is zero (6.06-08b), crosses represent the discrimination task for a 30 deg baseline orientation range (6.12-14b), filled squares for a 105 deg baseline orientation range (6.18-20b).

6.4 Discussion

The main finding of the experiments is that curvature detection and discrimination, like so many other visual tasks (Whitaker et al., 1992a), can be equated at the fovea and in the periphery simply by a change of scale. The rate of magnification required is defined by an E_2 of approximately 1.5-2 deg. In other words, given a certain foveal stimulus size, equivalent performance will be obtained at an eccentricity of 1.5-2 deg simply by doubling the size of the stimulus in every dimension. Differences in E_2 values between the detection task and the two discrimination tasks at different baseline orientation ranges were small considering the vast range of E_2 values which occur between tasks (Whitaker et al., 1992a,b). For the detection condition, E_2 varied between 1.68-1.85 deg; for the shallower baseline curve (30 deg orientation range) E_2 was found to be 1.40-1.51 deg; and for the steeper standard curve (105 deg orientation range) E_2 was 1.53-2.25 deg.

It is of interest to consider the relationship of curvature discrimination to other tasks which exhibit similar E_2 values. Orientation discrimination has been shown to have an E_2 of 1.95 deg (Mäkelä, Whitaker and Rovamo, 1993). Vernier acuity, both for two-dot and two-line stimuli, has an E_2 of between 1 and 2 deg (Whitaker et al., 1992b). The similarity of these values is perhaps suggestive that a similar neural substrate underlies all of them. Indeed, it has been argued that the orientation selectivity of spatial filters underlies curvature discrimination in foveal vision (Blakemore and Over, 1974; Crassini and Over, 1975a,b; Wilson, 1985; Fahle, 1986; Wilson and Richards, 1989). Further, the role of orientation has long been recognised in vernier acuity tasks (Andrews, 1967; Sullivan et al., 1972; Watt, Morgan and Ward, 1983; Watt and Campbell, 1985) and, in addition, Andrews et al. (1973) have emphasised the similarity of vernier and curvature detection.

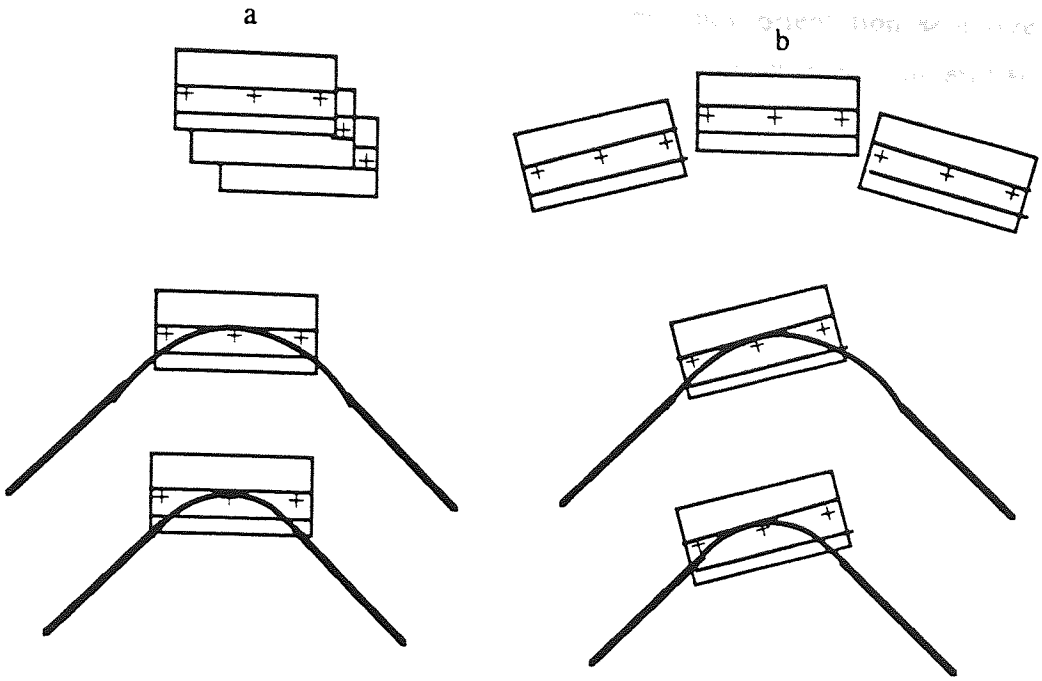

Figure 6.22. a & b. Model of curvature processing (from Wilson, 1985). See text for explanation.

Wilson and his co-workers (Wilson, 1985, 1986; Wilson and Richards, 1989) have developed a model which predicts how the behaviour of both vernier acuity and curvature discrimination is based upon the same spatial frequency and orientation selective mechanisms. The model consists foveally of six distinct classes of orientation-selective, spatial frequency tuned mechanisms. A simplified explanation of the model as applied to curvature discrimination is shown in Figure 6.22. In Figure 6.22a, three filters are shown, each consisting of an excitatory zone (+++) flanked by inhibitory zones on each side. The filters are displaced vertically to represent spatially nearest neighbours in the model, and are also shown separated horizontally for clarity. The model pools the differential responses of the unit centred on the point of maximum curvature and its two nearest spatial neighbours to give a response. In the second part of 6.22a, the broad curve stimulates most of the excitatory area of the filter, giving a large response. The sharper curve shown below this invades more of the inhibitory surround of the filter than the broader curve and so will generate a smaller response. Similarly, the model pools responses from units with other preferred orientations centred on the point of maximum curvature, as shown in Figure 6.22b. The filters shown here are rotated by ±15 deg, and are again separated horizontally for clarity. As before, the broader curve invades less of the inhibitory region of the filter than the sharper curve, and will result in a stronger response, enhancing the overall discrimination performance. Wilson and Richards (1989) showed that the model described above can explain curvature processing for relatively high curvatures. For

lower curvatures, rather than using lower frequency orientation selective units, orientations are compared at points displaced a fixed distance (8.2 min arc) along the tangent to the curve by high frequency local processing units.

However, before one assumes that all positional tasks which can be explained in this way behave similarly with eccentricity, it is worth pointing out the important exceptions of bisection acuity and spatial interval discrimination which decline at a much faster rate with increasing eccentricity (Klein and Levi, 1987; Virsu et al., 1987; Levi and Klein, 1990a; Whitaker et al., 1992a). If all these positional tasks share a common stage along the lines which Wilson suggests, it is clear that there exist additional factors which lead to some of them possessing markedly different peripheral gradients. More recently (Wilson, 1991a,b), the influence of spatial undersampling and position irregularity has been taken into consideration, which helps to explain the more rapid decline in tasks which are susceptible to these factors.

Previous attempts to determine the eccentricity-dependence of curvature detection and discrimination have been sparse and incidental. Wilson (1985) compared curvature discrimination at the fovea and out to 8 deg in the periphery. He chose peripheral stimuli which were magnified to the extent that they doubled in size at 8 deg eccentricity. This choice was based upon the change in scale of spatial mechanisms suggested by Swanson and Wilson (1985). Curvature discrimination was then found to vary with eccentricity at the same rate as that which had been chosen to magnify the peripheral stimuli. At first sight this appears to contradict the present findings since the data suggest that Wilson (1985) under-magnified his peripheral stimuli which may be predicted to give poorer peripheral performance and hence a smaller (rather than larger) E_2 value. However, the critical factor is that the curves which Wilson used at the fovea were rather large, having a chord length of at least 42 min arc. This is considerably larger than the optimum chord length for discrimination at the fovea (see Figures 6.09-11a and 6.15-17a). With increasing eccentricity, the relatively slow increase in magnification chosen by Wilson (1985) results in chord lengths which become progressively closer to optimum, hence the rather modest increase in curvature thresholds. There is therefore no contradiction between the present results and those of Wilson (1985), it is just another example of how an initial choice of stimulus size can lead to distortions in the rate at which observed performance changes.

Fahle (1986) states that curvature detection thresholds increase from 30 sec arc at the fovea to 8 min arc at an eccentricity of 30 deg. This corresponds to an E_2 value of 2 deg. However, several important points suggest that this apparent agreement with the

present findings is fortuitous. Firstly, his chord length was a constant 3.5 deg at all eccentricities. Second, curve width was arbitrarily chosen to be 5 min arc at the fovea and 12 min arc at all other eccentricities. Finally, his data show that the orientation of the curved stimulus is a factor in determining thresholds. In the fovea, an oblique effect is observed in that stimuli oriented along the major meridia have lower thresholds than those oriented on oblique axes. Watt and Andrews (1982) showed foveal curvature discrimination to be as accurate for oblique stimulus orientations, but threshold precision was maintained over a smaller orientation range than for stimuli oriented along major meridia. In the peripheral visual field, Fahle (1986) noted that the oblique effect is replaced by an orientation effect, with performance for radially oriented stimuli being superior to that for tangential ones. Such effects have also been noted for grating resolution (Rovamo, Virsu, Laurinen and Hyvarinen, 1982). Thus, the true E_2 value is likely to be heavily dependent upon stimulus orientation, and it should therefore be stressed that the results of the current study were obtained for curves oriented tangentially (the midpoint of the curve was orthogonal to the meridian).

To date, the most thorough investigation of curvature detection at different eccentricities has been by Hess and Watt (1990). Their curvature stimulus was a straight line with three bumps, the largest, central one being on the opposite side to the axis of the stimulus than the two bumps on either side. The task was to detect a deviation from linearity. However, rather than being interested in how detection itself varies as a function of eccentricity, they used their data to optimise the spatial and temporal parameters of their stimuli at each peripheral location, and incorporated these in subsequent experiments. Examination of their data indicates two important differences to the present findings. Firstly, at all eccentricities their detection thresholds demonstrate a distinct minimum at intermediate values of spatial extent (space constant) of the bump. At higher space constants, detection thresholds increased sharply. This is in contrast to curvature detection thresholds using stimuli whose curvature is monotonic along their length such as the ones used in this experiment. These latter stimuli generate detection thresholds which demonstrate a broad plateau with increasing chord length (Andrews et al., 1973; Watt and Andrews, 1982; Figure 6.03-5a, this study). Secondly, it appears that the bump detection task of Hess and Watt (1990) behaves differently with respect to eccentricity. Optimum detection thresholds for subject RFH (who was provided with a straight reference line against which to compare the stimulus with the bump) increase by a factor of approximately 18 between 0 and 16 deg eccentricity, and the optimum space constant increases by a similar factor (their Figure 4). The data therefore suggest an E_2 value slightly less than unity. Subject RJW (who was not provided with a straight reference line) demonstrates a different trend in that the

optimum space constant increases by a factor of approximately 9 times whereas optimum thresholds show a much more rapid decline by a factor of at least 100. This is contrary to the concept of spatial scaling which predicts exact correspondence between the eccentricity-related increase in these two factors. Curvature detection and bump detection must behave differently with respect to eccentricity.

In summary, the increase in curvature detection and discrimination thresholds as a function of eccentricity are demonstrated using a spatial scaling method which makes no initial assumptions regarding the relative size of visual stimuli at various eccentricities. The differences in E_2 values between curvature detection and discrimination tasks are small in relation to inter-task variations in peripheral gradients, which may differ over 100-fold. However, performance in curvature tasks does appear to demonstrate a similar eccentricity dependence to tasks such as vernier acuity and orientation discrimination. This lends support to the view that performance in each of these tasks may share a common genesis in the eccentricity dependent distribution of neural elements selective for orientation.

Chapter 7
Kinetic presentation of a differential light stimulus

7.1 Introduction

Measurement of the differential light threshold in the form of perimetry is clinically used to assess visual function. The stimulus for differential light threshold determination is usually a sharp-edged target of specified spatial and temporal parameters. In static perimetry, the threshold luminance, ΔL, is determined at specific locations within the visual field whilst in kinetic perimetry ΔL remains constant and the eccentricities are found at which the stimulus represents threshold (see Chapter 2).

Attempts to M-scale perimetric profiles using the equations of Rovamo and Virsu (1979) and Drasdo (1977) have failed to provide an isosensitive perimetric profile by removing eccentricity dependence, as was described in greater detail in Chapter 4. The explanations which have been proposed to account for this failure of scaling include the need to adjust stimulus luminance with retinal eccentricity (Rovamo et al., 1985), interactions with the way in which spatial summation varies with eccentricity (Wild et al., 1986, 1987; Wood et al., 1986) and differences between the mapping densities of M- and P-ganglion cells (Drasdo and Thompson, 1989). With one exception (Drasdo and Thompson, 1989), these studies have *a priori* utilised a particular magnification factor in an attempt to equate foveal and peripheral performance, on the assumption that all visual tasks vary with eccentricity at the same rate. This approach can only indicate whether the particular magnification factor is satisfactory in describing the differences between central and peripheral vision. If performance at different eccentricities is not made equivalent by this method, it may either be that the magnification factor used was inappropriate or that the task cannot be equated across eccentricities by simple magnification scaling. A more useful method is to find the appropriate scaling factors to equate performance across the visual field without prior assumptions regarding magnification values, as in the method of spatial scaling which is used in this study.

Experiments which examine performance in peripheral vision usually use young observers. Little is therefore known about how the rate of decline in performance in the periphery varies as a function of age. The differential light threshold represents an ideal task with which to investigate this question, since it is a simple task which is commonly used clinically to examine performance across a wide age-range of observers. Previous studies using a single target size at all eccentricities have shown that static perimetric sensitivity declines as a function of age, with a mean sensitivity loss of 0.05-0.08 log units per decade over the central 30 deg (Brenton and Phelps, 1986; Haas, Flammer

and Schneider, 1986; Jaffe, Alvarado and Juster, 1986; Heijl, 1987; Johnson et al., 1989). Some workers have found that sensitivity loss is not linear with age, but occurs at an accelerated rate beyond 50 years of age (Johnson and Choy, 1987; Collin, Han and Khor, 1988). There is also some evidence (Johnson and Choy, 1987) to suggest that the distribution of sensitivity in older subjects is bimodal, reflecting two 'normal' elderly populations: those in excellent ocular health, and those showing early preclinical pathological signs.

In addition to the 'sinking of the hill of vision' with age described above, several conventional perimetric studies show that the hill of vision becomes steeper with age (Jaffe et al., 1986; Katz and Sommer, 1986; Heijl, 1987; Johnson et al., 1989), and that the variability of peripheral thresholds increases, in addition to the decrease in sensitivity. However, Haas et al. (1986) find that the centre and far periphery of the field are more affected by age than midperipheral regions. In contrast, Brenton and Phelps (1986) find the effect of age to be homogenous at all locations, resulting in no change to the slope of the hill of vision.

Kinetic perimetric studies also show sensitivity losses with age, which are seen as constriction of central and peripheral isopters (Drance, Berry and Hughes, 1967; Wolf and Nadroski, 1971; Williams, 1983; Egge, 1984). The area of a central isopter in a 60 year old subject is 52% of that of a 20 year old (Williams, 1983).

The loss of perimetric sensitivity with age has been suggested to be due to neural rather than optical factors (Johnson et al., 1989). By using a yellow target on a high luminance yellow background, possible age variations due to pupil size and lens transmission losses were minimised. Even under these conditions however, an age related loss of visual field sensitivity was observed of approximately the same magnitude as with traditional 'white-on-white' perimetry. These results enabled Johnson et al. to conclude that visual field sensitivity losses with age are primarily due to neural losses rather than preretinal factors.

In the present study the method of spatial scaling was applied to kinetic perimetry and E_2 values are determined for various visual field meridians for both young and older normal adults. The reasoning behind this was two-fold: firstly, to investigate the differences in peripheral visual function between different age groups; and secondly, to discover why scaling with conventional cortical magnification factors fails to equate the differential light threshold across the visual field.

7.2 Methods

Subjects

The sample consisted of 10 young subjects (mean age 23.6 years, SD 2.4 years, 6 males, 4 females) and 10 elderly subjects (mean age 69.6 years, SD 6.2 years, 5 males, 5 females). All subjects underwent a full ophthalmological investigation before participating in the study. Exclusion criteria included systemic conditions with known ocular involvement, systemic medication with known effects on the central nervous system, past history of eye disease, use of topical eye treatment, positive family history of glaucoma in a first degree relative, positive family history of diabetes mellitus and neurological or psychiatric illness. Further, all subjects had normal fundi and no lenticular opacity within the undilated pupillary area. All had intraocular pressures less than 21mmHg, normal static central fields (Humphrey Field Analyser Program 30-2 and STATPAC analysis) and ametropia below ±5DS and ±2DC. Corrected visual acuity was equal to or better than 6/6 for the younger subjects and 6/7.5 for the elderly observers. All subjects were highly experienced in both static and kinetic automated perimetry, having participated in a previous study (Hudson and Wild, 1992). Measurements were made using the right eye of each subject. All subjects wore their distance prescription corrected where necessary for the viewing distance of 33cm. Natural pupils were used throughout (young subjects mean 5.4mm, SD 1.2mm; elderly subjects mean 3.9mm, SD 0.9mm). Pupil diameter was measured on the video fixation monitor, with correction made for the magnification effects of the optical system of the monitor.

Apparatus

A Humphrey 640 Visual Field Analyser incorporating automated kinetic capabilities was used for the experiment. This is an automated projection perimeter described in Chapter 5. Stimuli corresponding to Goldmann sizes I, II and III (relative diameters 1.00, 1.82 and 3.66) were used in the experiment, and additionally, constructed stimuli with relative diameters 2.81 and 5.36 were also used. Calculation of the relative diameters and construction of the additional stimuli are discussed in Chapter 5. Stimulus velocities of 1-9 deg/s are available in steps of 1 deg/s for kinetic presentation of the stimuli. In order that all stimuli moved at the same number of stimulus diameters per second, it was necessary to magnify the stimuli in both size and velocity relative to the smallest stimulus (size I) moving at the slowest velocity (1 deg/s). The design was therefore constrained by the available velocities to a largest stimulus size of size IV with a velocity of 8 deg/s.

Procedure

The differential light threshold was established kinetically at the fovea by moving the size I stimulus at a velocity of 1 deg/s across a point corresponding to the intersection of the four lower fixation lights of the perimeter (normally used to aid fixation in the determination of the static macular threshold). This method was chosen in preference to static determination of the foveal threshold due to statokinetic dissociation in the normal visual field (Hudson and Wild, 1992). Threshold was determined by a staircase procedure and taken as the highest dB value (lowest increment) stimulus which was consistently seen. Kinetic measurements using the same luminance were then taken for the larger stimuli which were magnified in both size and speed such that all moved at approximately the same number of stimulus diameters per second. The stimulus sizes used were: relative size 1.82, speed 2 deg/s; relative size 2.81, speed 3 deg/s; relative size 3.66, speed 4 deg/s; relative size 5.36, speed 6 deg/s. Size is expressed relative to the diameter of the smallest stimulus (Goldmann I) as described in Chapter 5. Larger stimuli were excluded since, at the luminance level employed, they were often visible at 75 deg eccentricity, the starting point for the kinetic presentation. In addition, it has been suggested that kinetic velocities above 6 deg/s should be avoided due to the effects of reaction time (Johnson and Keltner, 1987).

Stimuli were presented along twelve meridians throughout the visual field using the 'Autotest 1' feature of the kinetic program, which presents stimuli along meridians spaced 30 deg apart. Presentations involved moving the target towards fixation from 'unseen' to 'seen'. For the larger stimuli, presentations began at an eccentricity of 75 deg, but for the smaller stimuli which were visible only within 20 deg, presentation commenced at 30 deg eccentricity in order to save time and prevent subject fatigue. The stimuli were presented in pseudo-random order of meridian. The size of the stimulus used was also randomised, but the subject was informed of which stimulus size to expect before presentation began. Fixation was monitored using the video camera of the HFA, and a trial was discarded if a fixation loss was noted.

Following an initial trial to familiarise the subject with the procedure, data collection took place over two sessions held within a maximum of 14 days of each other. Each session lasted approximately one hour, with frequent rest periods interspersed in each session. Threshold was determined four times for each stimulus size, including the foveal measurement. The eccentricity threshold along each meridian was represented as a mean of these four determinations. Standard errors were typically 6% of threshold for both the young and elderly individuals.

7.3 Results

Group mean eccentricity thresholds as a function of relative stimulus diameter for the young observers along four of the twelve meridians tested are shown in Figure 7.01. The stimuli used to obtain the data in this figure have the same luminance and are identical apart from their relative magnification. The data points can therefore be used to give a direct value of the scaling factors required to equate threshold as a function of eccentricity. This method differs from that used in Chapter 6, where thresholds were found for a range of target sizes and the entire functions were compared at different eccentricities to determine scaling factors. Note also that unlike the scaling factor graphs in Chapter 6, here eccentricity is the dependent variable and so is shown on the y-axis. The data in Figure 7.01 were fitted by a univariate linear regression which was constrained to pass through the data point representing the smallest stimulus size, since this was used to calculate all the other relative diameters. The regression was weighted according to the inverse of the variance of each data point. Along the 75, 165 and 255 deg meridians, the eccentricity threshold increased in a linear fashion with increasing relative diameter. The linear fit for meridians in the temporal visual field (such as 345 deg) was less satisfactory compared to the other meridians. A region exists in the latter function where a small change in relative diameter (from 2.81 to 3.66) produces an unexpectedly large change in eccentricity threshold. This type of non-linearity has been found in numerous previous studies which have examined meridians close to the blind spot. In conventional perimetric studies which describe sensitivity as a function of eccentricity, the non-linearity manifests itself as a plateau of isosensitivity extending from around 10 to 30 deg eccentricity, although its extent is somewhat variable (Harvey and Pöppel, 1973; Johnson et al., 1978; Lie, 1980).

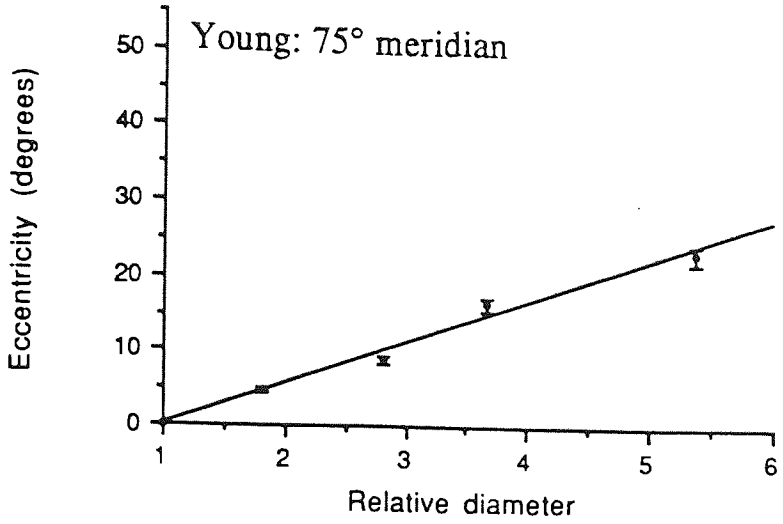

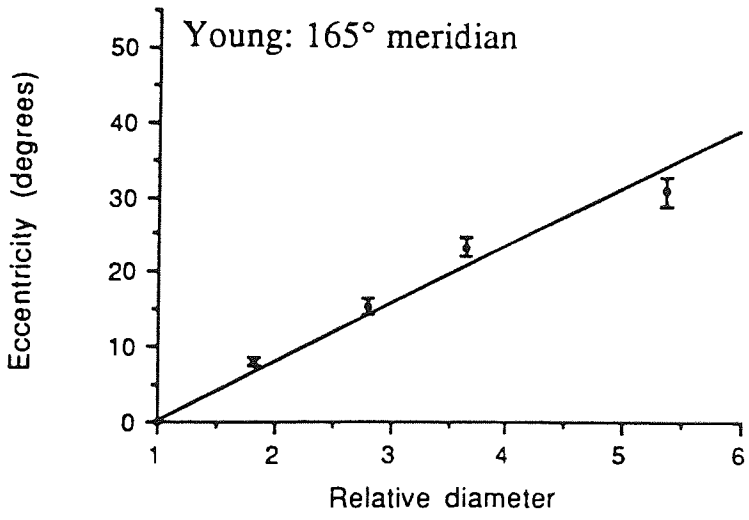

Figure 7.01. See following page for legend.

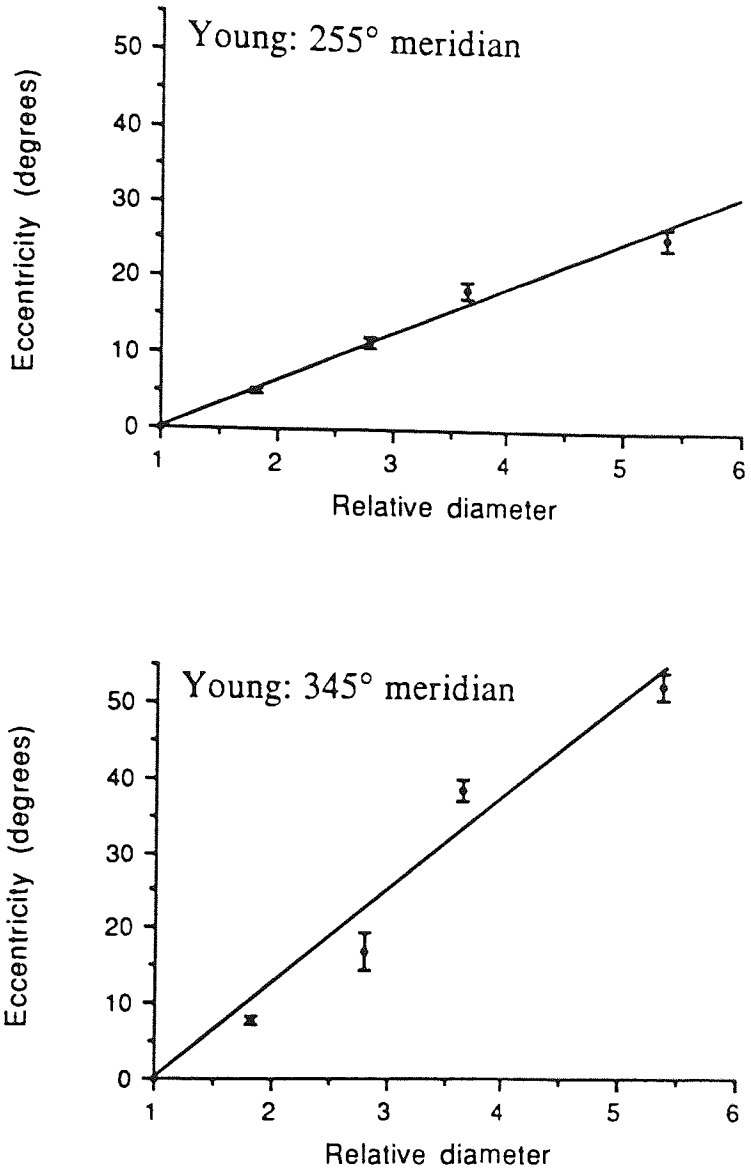

Figure 7.01. Eccentricity thresholds as a function of relative stimulus diameter for four visual field meridians. Stimulus luminance was held constant at the level corresponding to that obtained at the fovea for the smallest stimulus. Data points represent the mean and standard error of the eccentricity thresholds for the 10 young subjects. The data are fitted with a line of least squares residual deviation, which has been constrained to pass through the point (1, 0). The gradient of the least squares fit represents E_2, and the E_2 value can be conveniently visualised by locating the eccentricity threshold at a relative diameter of 2. Unlike the scaling factor vs eccentricity plots in Chapter 6, here a steeper gradient indicates a larger E_2 value.

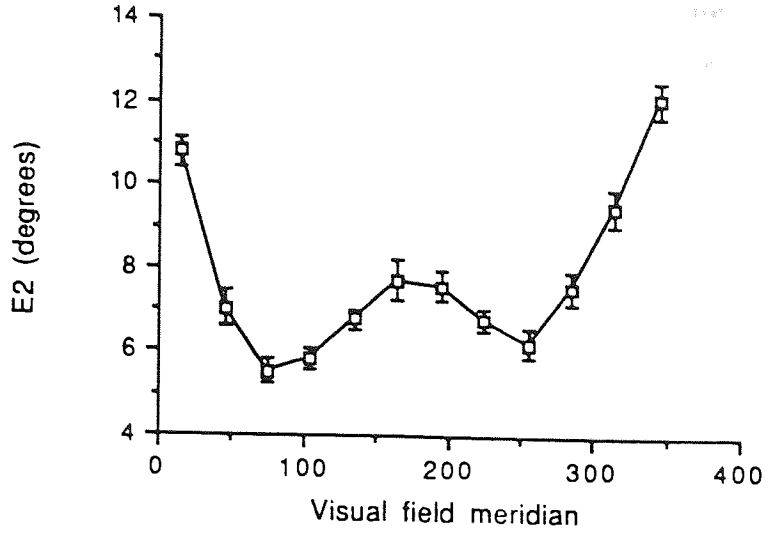

Figure 7.02. (a) Variation in E_2 with visual field meridian for the young group. E_2 values were calculated individually for each subject along each meridian. The data points represent the resulting group mean and standard error.

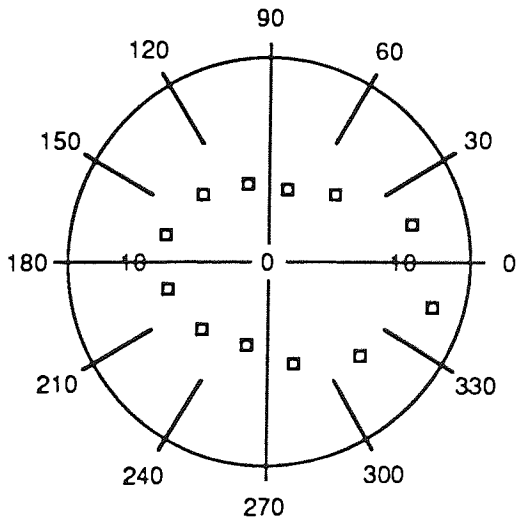

(b) The same data as in (a) but represented as a polar plot.

E_2 values for each visual field meridian were derived for individual subjects from the gradient of the linear regression relating their eccentricity threshold to relative diameter. The group mean E_2 value is shown as a function of visual field meridian in Figure 7.02a. The function shows a peak in the nasal visual field (approximately 165 deg) and a distinct peak along the temporal meridians close to the blind spot (15 and 345 deg) where the linear fit to the data breaks down. These peaks are separated by troughs at 75 and 255 deg. E_2 values vary between 5 and 12 deg depending upon meridian. The data are also presented as a polar plot in Figure 7.02b, and in tabular form in Table 7.01.

Meridian (deg)	E_2 value (mean of 10 young observers)	Standard error
15	11.04	0.40
45	7.11	0.44
75	5.59	0.30
105	5.89	0.25
135	6.88	0.25
165	7.87	0.49
195	7.78	0.38
225	6.88	0.30
255	6.29	0.35
285	7.68	0.38
315	9.71	0.47
345	12.60	0.46

Table 7.01. E_2 values for kinetic presentation of a differential light stimulus. Mean E_2 values and standard errors for 10 young observers are shown for 12 visual field meridia.

Group mean eccentricity thresholds for the older observers are shown in Figure 7.03. The striking feature of the data along these four meridians, and indeed the other meridians which are not shown, is that the increase in thresholds with size is non-linear. Linear regression provided a significantly poorer goodness-of-fit for the elderly data compared to the equivalent data for the young group ($p<0.001$). Eccentricity thresholds rise rapidly at first with increasing diameter and then more slowly as stimulus diameter increases further. For comparison purposes, the linear relationships found for the younger observers (Figure 7.01) are also shown on each graph. The data represent a clear departure from the usual eccentricity-dependent variation in visual performance which almost always approximates to linearity (Weymouth, 1958; Drasdo, 1991; Whitaker et al., 1992a, Chapter 6). E_2 values calculated from the second-order

polynomial functions fitted to the data for the elderly observers fail to describe the curvilinear nature of the data, and should be compared cautiously with E_2 values derived from linear data (such as those for the younger observers). E_2 values for the elderly subjects varied between 7.5 and 11.5 deg and exhibited the same meridional trend as the data for the younger subjects.

The results demonstrate that there is not a constant factor which relates the performance of the elderly group to that of the younger group. This difference is highlighted in Figure 7.04 which shows eccentricity thresholds at which the stimuli become visible along each meridian. These eccentricity thresholds were obtained using stimulus luminances which represented threshold at the fovea. As would be expected, the average differential light sensitivity at the fovea was considerably lower for the elderly than for the young (31.7±1.89dB and 35.3±0.79dB respectively). Having accounted for this difference in foveal sensitivity, small target diameters are detected at greater eccentricities by the elderly group than by the younger group. The majority of elderly individuals showed this trend. The difference is least marked in the temporal meridian. As target diameter increases, the difference in performance between the two age groups lessens, and eventually, at the largest diameter the age effect is reversed, particularly in the temporal field meridians.

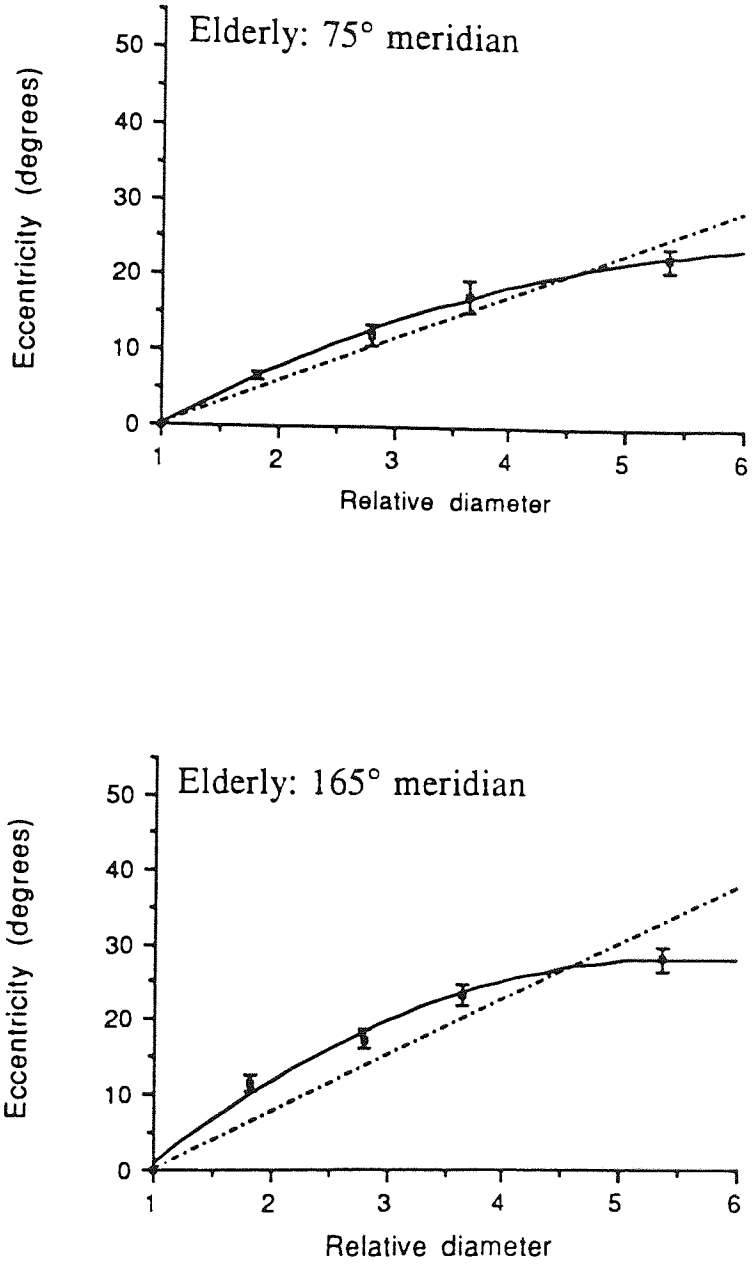

Figure 7.03. See following page for legend.

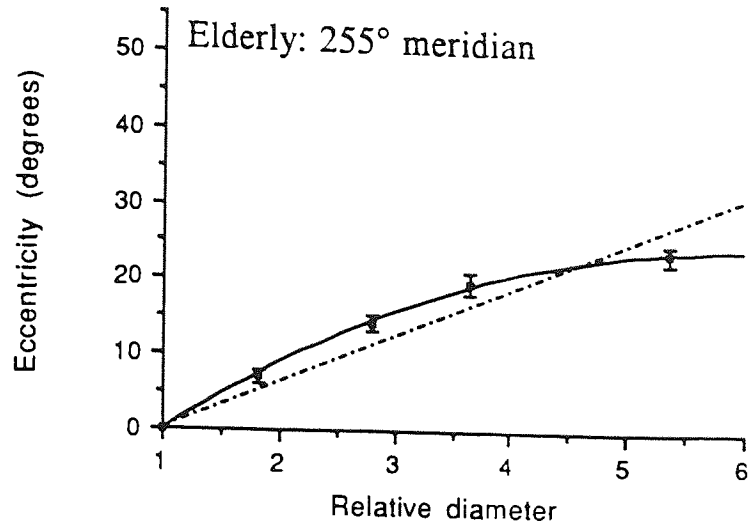

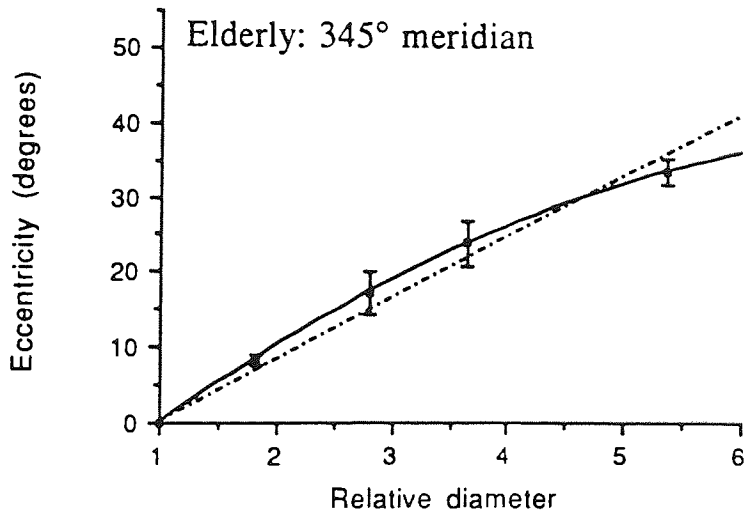

Figure 7.03. Eccentricity thresholds as a function of relative stimulus diameter in the elderly group for the same four visual field meridians as illustrated in Figure 7.01. The data are fitted with a second-order polynomial curve of least squares residual deviation, which has been constrained to pass through an eccentricity of zero when relative diameter is unity. Again, this is a measured point, and not merely an arbitrary point of origin. The regression line which was used to fit the young data for each corresponding meridian in Figure 7.01 is shown for comparison.

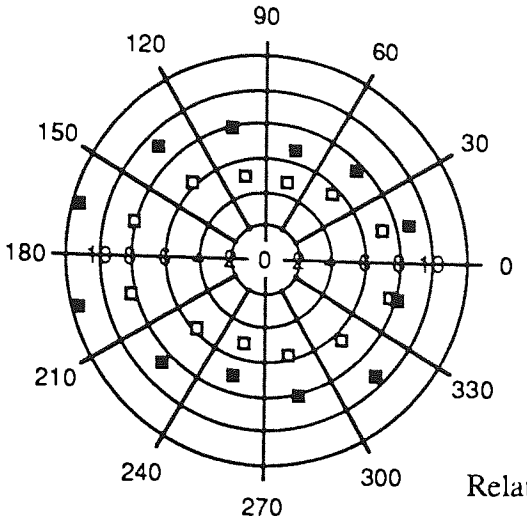

Relative diameter 1.82

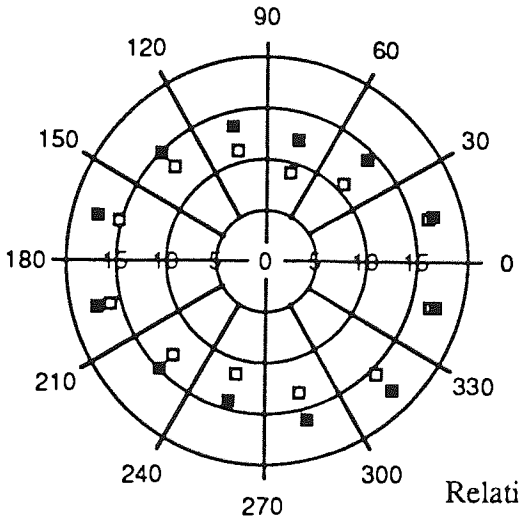

Relative diameter 2.81

Figure 7.04. See following page for legend.

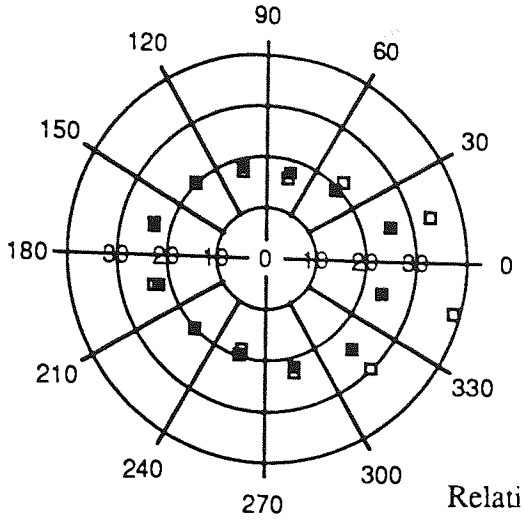

Relative diameter 3.66

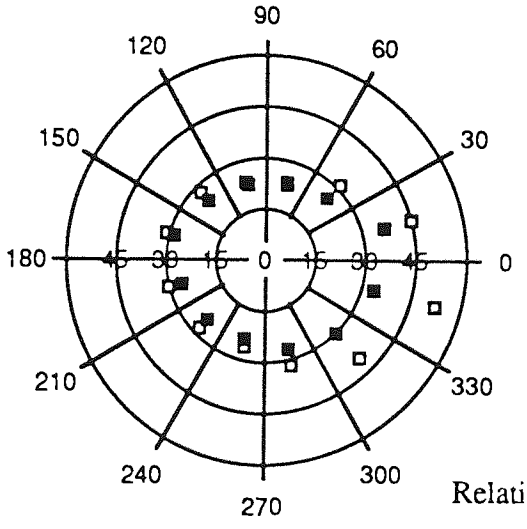

Relative diameter 5.36

Figure 7.04. Polar plots representing mean eccentricity thresholds as a function of visual field meridian for four relative stimulus diameters. Meridians are represented by different radii, while eccentricity is depicted along the radii. Note that the eccentricity scales vary between plots. Each data point represents a mean of 10 observers - young subjects (open squares), elderly subjects (filled squares). Average standard errors were 6.4% and 8.6% of the mean for young and elderly observers respectively. For each observer the stimulus luminance was that obtained at the fovea for the smallest diameter.

7.4 Discussion

For the young observers, the variation in the differential light threshold with eccentricity is qualitatively similar to the behaviour of many other visual thresholds. The increase in stimulus size necessary to produce performance equivalent to that at the fovea increases in a roughly linear fashion with eccentricity. This is true of visual acuity (Weymouth, 1958), contrast sensitivity (Rovamo and Virsu, 1979), various types of movement detection and discrimination (Levi et al., 1984; Johnston and Wright, 1986; Whitaker et al., 1992a) and many hyperacuity tasks (Levi et al., 1985; Whitaker et al., 1992a,b; Mäkelä et al., 1993; Chapter 6). Such a relationship is not directly evident in the usual type of static perimetric study which uses a single stimulus size and measures the differential light threshold at various eccentricities.

However, previous studies which have systematically varied stimulus diameter and obtained spatial summation curves at several eccentricities also point to this linear relationship. Wilson (1970) examined spatial summation under photopic conditions across the retina. He found the critical area (Ac, defined in Chapter 2) to increase with eccentricity from 5 to 55 deg, while the 'critical threshold' ($\Delta I / I_{(Ac)}$) remained constant across this range. Spatial summation was appropriately represented by a curve with a upper segment of slope -1, followed by a segment of steadily decreasing slope with increasing stimulus area. Spatial summation curves were identical at each eccentricity locus apart from a shift to larger sizes along the x-axis with increasing eccentricity. Wilson was the first to demonstrate that spatial summation curves were identical with eccentricity apart from a change of scale, by displacing peripheral curves along the size axis such that all the data could be superimposed to form a single spatial summation curve. However, the absence of an equivalent foveal function makes the calculation of an E_2 value from this data unreliable.

Johnson et al. (1978) also examined detection thresholds to perimetric stimuli, which were of 500ms duration on a background of luminance 3.18 cdm^{-2} (10asb). Their data were presented as summation curves of log threshold vs log area for each eccentricity, which are shown replotted as a function of stimulus diameter in Fig 7.05a (their Figure 4). The data curves are displaced from each other merely by a shift along the x-axis. The amount by which data at different eccentricities is displaced relative to the foveal data can be established by eye, and this is shown expressed as the scaling factor (in diameter terms) as a function of eccentricity in Figure 7.05b. The regression fitted to the data is of the form:

$$\log F = \log (1 + (E / 1.94))$$

and so, from Equation 4.01, $E_2 = 1.94 \pm 0.14$ deg for the nasal visual field. The data are shown scaled by this value in Figure 7.05c, which removes much of the eccentricity dependence from the data.

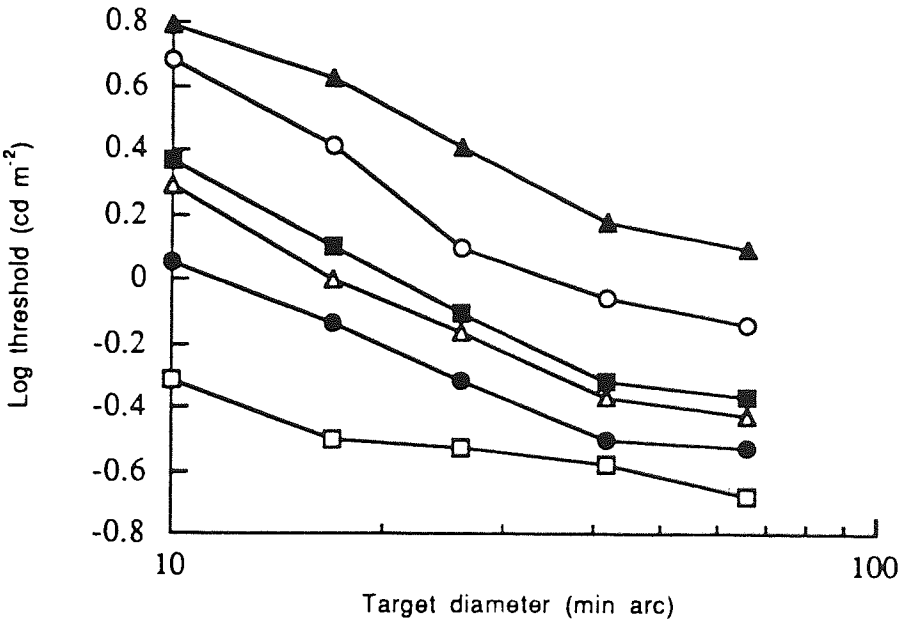

Figure 7.05. (a) From Johnson et al. (1978). Detection thresholds for a differential light stimulus as a function of stimulus diameter for various stimulus eccentricities along the horizontal meridian of the nasal visual field. Open squares: 0 deg; closed circles: 2 deg; open triangles: 5 deg; closed squares: 10 deg; open circles: 20 deg; closed triangles: 30 deg.

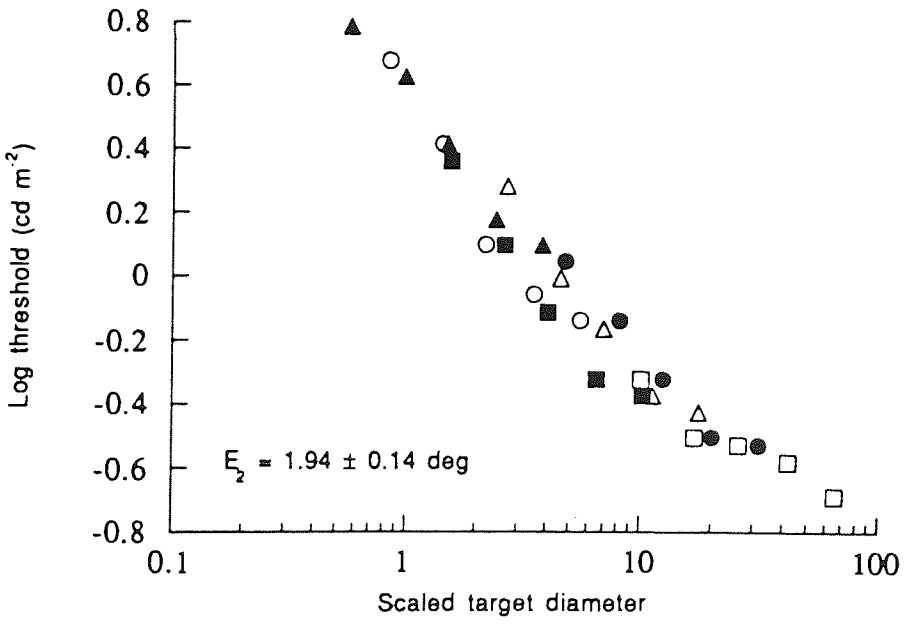

Figure 7.05. (b) Scaling factors, expressed in terms of relative diameter, describing the shift in size required to superimpose peripheral data curves from Fig 7.05a onto the foveal curve. The scaling factors are plotted against their respective eccentricities.

(c) Data of Fig 7.05a, scaled according to the E_2 value derived from Fig 7.05b (1.94 ±0.14 deg). Symbols as for Figure 7.05a.

Lie (1980) found that for detection of targets on a background luminance of 0.3 cdm^{-2}, the shape of spatial summation curves remained invariant with retinal locus, changing only in position on the log size axis. The change in position increased steadily with eccentricity, apart from in the region 12-21 deg in the nasal visual field, where a plateau of isosensitivity was noted. As with the data described above, the amount by which the peripheral data curves are displaced from the foveal data can be estimated by eye to give scaling factors. These are shown in Figure 7.06. The regression has the form:

$$\log F = \log (1 + (E / 8.79))$$

and so from Equation 4.01, E_2 is 8.79 ± 0.69 deg for the nasal visual field.

Figure 7.06. From the data of Lie (1980). Scaling factors, expressed in terms of size, against their corresponding eccentricities. The regression through the data is $\log F = \log (1 + (E / 8.79))$.

Inui et al. (1981) used a fundus controlled perimeter to investigate spatial summation to 10 deg in the periphery. They found that the critical area increased with eccentricity at a rate described by the equation:

$$\text{Critical area (Ac)} = 0.55\ E + 4.15$$

In this case, the y-intercept does not equal unity, as the data is not expressed in relative terms. The equation is thus of the form:

$$Ac = Ac_0 (1 + (E / E_2))$$

or,

$$Ac = Ac_0 + ((Ac_0 / E_2)\ E) \qquad \text{Equation 2.09}$$

The gradient of the function gives the parameter (Ac_0 / E_2), and so E_2 is given by (Ac_0 / gradient). Therefore, E_2 = (4.15 / 0.55) = 7.55 deg for nasal visual field.

Table 7.02 below summarises the E_2 values found for detection thresholds of stimuli of varying sizes. It can be seen that for the nasal visual field, E_2 for a size scaled light detection task has generally been found to vary from 7 - 10 deg. The only exception to this is the study of Johnson et al. (1978) where a smaller E_2 value is observed. In comparison, the E_2 value for 165 deg in nasal visual field found in this study is 7.87 ± 0.49 deg.

Authors	E_2 (deg)	Ecc range (deg)	Field meridian
Wilson (1970)	10.33	5-45	Nasal
Johnson et al (1978)	1.85	0-30	Nasal
Lie (1980)	8.05	0-45	Nasal
Inui et al (1981)	7.55	0-10	Nasal

Table 7.02. E_2 values for light detection thresholds found in previous studies.

In comparison with other tasks, the E_2 values found for the differential light threshold are high. Estimates of E_2 for grating acuity are about 1.5-3 deg (Chapter 2) whereas the majority of hyperacuity tasks have much lower E_2 values, reaching as low as 0.1 deg for bisection acuity (Whitaker et al., 1992a). Only unreferenced movement detection exhibits E_2 values in the same region as the differential light threshold (Levi et al., 1984; Whitaker et al., 1992a). From a physiological point of view, these large E_2 values raise important questions as to the regional distribution of the mechanisms underlying the differential light threshold. One striking aspect of the meridional trend of the young subjects' data is the presence of naso-temporal asymmetry. This phenomenon is not restricted to the differential light threshold but is found in a variety of other psychophysical tasks (Wertheim, 1891; Johnson et al., 1978; Fahle and Schmidt, 1988; Paradiso and Carney, 1988; Anderson et al., 1991), with performance in the temporal field declining at a slower rate than in the nasal field. The same meridional trend is present in ganglion cell density, in that density in the nasal *retina* falls off at a considerably slower rate than in any other meridian (Schein, 1988; Silveira et al., 1989; Wässle et al., 1989; Curcio and Allen, 1990). However, the eccentricity-dependent variation in the differential light threshold cannot be explained by a reduction in ganglion cell density alone, for this falls off at a much more rapid rate. Drasdo (1991) quotes an E_2 value of just 1.29 deg for the eccentricity-dependent variation in density of the total human ganglion cell population. The explanation must be that some

factor varies with eccentricity in such a way that it counteracts the relatively rapid decline in ganglion cell density. As suggested by previous authors (Wood et al., 1986; Wild et al., 1987), this factor would appear to be ganglion cell receptive field area which increases with eccentricity in approximate inverse proportion to ganglion cell density (Perry et al., 1984; Perry and Cowey, 1985). Hence, although the number of ganglion cells at a specific eccentricity declines fairly rapidly, an increase in mean dendritic field area improves their potential for spatial summation. As a result, the increase in stimulus size necessary to produce an equivalent differential light threshold to that found at the fovea changes considerably more slowly than ganglion cell density alone would predict.

The results for the elderly observers show a non-linear relationship between eccentricity and stimulus size (Figure 7.03). This differs from the younger observers and from the majority of studies examining other tasks. It raises the important question of whether eccentricity-dependence in other tasks, if measured in an older population, would also demonstrate non-linear behaviour of this type. One possible reason for the non-linearity in the elderly data could relate to reaction time differences. It is important to note that this cannot be a result of a uniform age-related increase in reaction time across the visual field, since all stimuli moved the same number of stimulus diameters per second. Given a linear relationship, the effect of an overall increase in reaction time would therefore be to decrease the gradient of the function without disturbing its linearity. However, if age differences in reaction time were more pronounced in the periphery than at the fovea, this could result in data such as has been found in the present study. I have found no study that discusses eccentricity related effects of age on reaction time. There is some evidence that foveal reaction time increases slightly with age (Teichner, 1954; Keele, 1986), and also some evidence that reaction time for young subjects increases slightly with eccentricity (Teichner, 1954; Rains, 1963; Ball and Sekuler, 1980), but possibly only for low rates of stimulus movement (Tynan and Sekuler, 1982). In addition, it is well established that age-related deficits in visual performance become exaggerated at high temporal frequencies (Owsley, Sekuler and Siemsen, 1983; Tyler, 1989; Elliott et al., 1990). Therefore, the non-linearity which is observed could be related to deficient processing of the larger stimuli which move at the highest velocities. A further factor which could affect the detection of the larger stimuli is reduced spatial summation in the elderly. One study has suggested that this occurs at the fovea (Owsley and Sekuler, 1982), but this is not supported in studies which have examined the periphery (Dannheim and Drance, 1971; Brown et al., 1989).

Alternatively, the variation in age-related sensitivity loss in different areas of the visual field could be a result of a differential distribution of neural degeneration. The majority of recent reports indicate that the location of age-related loss in achromatic photopic visual function lies within the neural system. This has been suggested for visual field sensitivity (Johnson et al., 1989) as well as for visual acuity (Weale, 1975) and spatial and temporal contrast sensitivity (Morrison and McGrath, 1985; Elliott et al., 1990). These reports suggest that normal age-related lenticular and pupillary changes are of minor importance. Neural cell death, degeneration and neurotransmitter changes are known to occur as a function of age within the visual pathways from retina to striate cortex (Ordy, Brizzee and Johnson, 1982; Gao and Hollyfield, 1992; Spear, 1993). If these changes were to differentially affect the foveal neural representation, a pericentral sparing in sensitivity would become evident. A relatively small age-related loss in parafoveal sensitivity compared to that of the fovea has been found with focal cone electroretinograms (Birch and Fish, 1988), as well as with visual field sensitivity (Haas et al., 1986; Heijl, 1987). However, this does not explain the finding of a relatively greater loss in sensitivity in the more peripheral regions compared to the parafovea, although normal age-related changes are commonly found in the retinal periphery (Jones and Reidy, 1985) and it has been suggested that the peripheral fundus is selectively vulnerable to age-related impairment (Foos and Trese, 1982).

Whilst all studies which have examined the effect of age upon the differential light threshold are agreed that performance declines in the elderly, there is differing opinion as to how this loss of sensitivity varies with visual field location (Jaffe et al., 1986; Haas et al., 1986; Heijl, 1987; Johnson et al., 1989; Drance et al., 1967). Most studies conclude that the decline increases with eccentricity such that the hill of vision becomes steeper in the elderly (Jaffe et al., 1986; Heijl, 1987; Johnson et al., 1989). However, Haas et al. (1986) suggest that the situation is more complex in that the age-related loss of sensitivity is concentrated at the fovea and in the periphery with a pericentric area separating these two regions in which the decline is less marked. Such a situation is also suggested in the data of Heijl (1987).

In this study, stimulus sizes are defined at various eccentricities and along different meridians which would be expected to produce identical performance to that at the fovea. Using such a sequence of stimuli and having set ΔL to threshold at one position in the visual field, then the presentation of an appropriate stimulus size at another part of the field with the same ΔL should also produce a threshold response. If this presentation did not reach threshold, it would indicate the presence of a loss of sensitivity relative to the normal visual field. Rovamo et al. (1985) have previously

termed such a series of equivalent stimulus sizes 'perimetrograms'. However, the potential simplicity of such a technique must be compromised by the effect of subject age which is shown to have a marked effect upon the eccentricity-dependent nature of the differential light threshold.

In conclusion, it is found that E_2 for light detection with kinetic presentation has a high value in comparison to other visual tasks. This value is dependent on visual field meridian, following the qualitative distribution of retinal ganglion cells, but also involving additional factors, most likely an increase in spatial summation area with eccentricity. With increasing age, the decline in the differential light sensitivity with eccentricity becomes non-linear. When compared to younger observers, the elderly show a preferential loss of sensitivity centrally and beyond 20 deg, with a relative sparing of the pericentral region.

Chapter 8
Static presentation of a differential light stimulus

8.1 Introduction

In the previous study (Chapter 7) the effects of spatial summation were implicated in the determination of kinetically presented differential light thresholds across the visual field. Spatial summation describes the relationship between the differential light threshold and stimulus size. The reduction in threshold with increasing stimulus size indicates a process of spatial integration of light energy within the visual system. The area of a test stimulus and its differential light threshold can be described by the equation:

$$\Delta I / I \propto A^{-K} \qquad \text{Equation 8.01}$$

where A is stimulus area and ΔI is the luminance increment necessary to detect a stimulus on a background of luminance I. The exponent K is known as the 'summation coefficient' and has a value between 0 and 1. The value of K indicates the extent of spatial summation with complete summation being indicated by a K of unity. In other words, the threshold luminance for detection of a small stimulus of relatively brief duration on a uniform background is inversely related to its area (Ricco's Law). As the stimulus increases in size beyond a critical area, K decreases and the summation becomes partial. Specific laws of partial summation have been suggested (Piper's law K=0.5, Pieron's Law K=0.3, Goldmann's approximation K=0.8, Weber's Law K=0), but it is generally held that K changes continuously as a function of stimulus size, rather than in a series of successive steps. When summation is partial, as the stimulus area increases so does the total light energy required for threshold to be reached, so that the luminance per unit area falling within the critical area remains constant. When K is 0, Weber's Law is obeyed, and increases in target area do not affect detection thresholds.

The results of Chapter 7 showed a non-linear relationship for the elderly subject group between eccentricity and target size. Possible factors suggested to explain this non-linear behaviour included the effects of reaction time, and changes in spatial summation in the elderly. There is little available information concerning the effects of age on spatial summation across the visual field, and amongst those studies which have been published there is little consensus of opinion. Studies by Dannheim and Drance (1971) and Brown et al. (1989) have concluded that spatial summation does not vary with age, but that elderly subjects simply show reduced sensitivity compared to their young counterparts. This has been disputed by Owsley and Sekuler (1982), who found a

reduced ability in the elderly to see larger targets, stating that this was indicative of reduced spatial summation.

Spatial summation is known to vary with the eccentricity of stimulus presentation. Summation curves have been shown to have identical shape with change in locus (Wilson, 1970; Lie, 1980), but the area over which complete summation occurs increases steadily with eccentricity (Sloan, 1961; Wilson, 1970; Dannheim and Drance, 1971; Greve, 1973; Lie, 1980; Wood et al., 1986; Wild et al., 1987). The increase in critical area with eccentricity means that for targets of constant size, the summation coefficient K increases with eccentricity (Fankhauser and Schmidt, 1960; Sloan, 1961; Johnson et al., 1978).

Wilson (1970) first demonstrated that spatial summation curves were identical with eccentricity apart from a change in scale by displacing peripheral curves along the size axis such that all the data could be superimposed to form a single spatial summation curve (see Chapter 7). Wilson's concept of an eccentricity related change in spatial scale has since been expanded such that the rate of decline in peripheral visual performance can be quantified, and the method is referred to as spatial scaling (Chapter 4).

It has been suggested that the development of isosensitive perimetric visual field profiles by scaling peripheral target size would be a significant innovation (Wood et al., 1986; Wild et al., 1986, 1987). Such isosensitive profiles, or 'perimetrograms' (Rovamo et al., 1985) would have the benefit of ease of interpretation. By using size scaled stimuli, sensitivity of the central and peripheral visual field can be made equivalent, the critical parameter being the rate at which stimulus size must increase with eccentricity. As was shown in the previous chapter, the potential for producing perimetrograms is seriously compromised by the age related differences found with kinetic presentation of the differential light stimulus. This may not necessarily be the case for static stimulus presentation, which is now investigated here.

In the present study the static differential light threshold is examined using automated perimetry for various target sizes across the central visual field for both young and elderly observers. Spatial summation curves are constructed at a series of visual field locations, and this allows quantification of eccentricity related changes in the spatial scale of the visual system in both young and older subject groups. The data is also compared with that obtained with kinetic stimulus presentation, to show the differences introduced by stimulus movement in the results of each age group.

8.2 Methods

The sample consisted of 10 young subjects (mean age 23.6 years, SD 2.9 years, 5 males, 5 females) and 10 elderly subjects (mean age 72.0 years, SD 5.2 years, 6 males, 4 females). Exclusion criteria were the same as those in Chapter 7. All subjects were highly experienced in perimetry, having participated in previous studies (Hudson and Wild, 1992; Chapter 7). Measurements were made using the right eye of each subject. All subjects wore their distance prescription corrected where necessary for the viewing distance of 33cm.

A Humphrey 640 Visual Field Analyser (HFA) was used in the experiment (see Chapter 5 for details). Goldmann target sizes I-V were used in this study, representing relative stimulus diameters of 1.00, 1.82, 3.66, 7.30 and 14.62.

Stimuli were presented statically using a custom profile program on the HFA and a sustained presentation time of 500ms. Peripheral thresholds were measured for Goldmann sizes I-V at points every 6 deg between 6 and 30 deg along the 75/255 and 165/345 deg visual field meridia. These meridia were chosen as they correspond to the meridia of lowest and highest rate of decline of visual performance with eccentricity for kinetic presentation of a differential light stimulus (Chapter 7). Subjects maintained central fixation during this portion of the experiment.

Foveal data was obtained by two different methods. Firstly, the 'foveal threshold' option of the static profile program was used. This option presents a foveal stimulus in isolation at the intersection of the four lower fixation lights of the perimeter. There is no uncertainty in this method as to where the stimulus will appear, as threshold is determined for a single point. In this respect, the method is different to peripheral data collection, where the stimulus may appear at any one of several locations at a given time. For this reason, a second method of foveal data collection was also used. Three distractor stimuli were presented in addition to the foveal stimulus, again using the custom program, in order to make the methodology of foveal and peripheral data collection more comparable to each other. The distractors were positioned at 6 deg eccentricity along the 165, 255 and 345 deg meridia. The distractors simply introduced some uncertainty as to the position of the next stimulus, and their values were not included in the data collection. Only three distractors were used in order to avoid subject fatigue. The introduction of distractors into foveal threshold measurements lowered sensitivity significantly ($p<0.05$), and this effect was independent of stimulus size ($p>0.05$). However, the effect was considerably smaller (0.53 dB) for the young subject group compared to the elderly subject group (2.50 dB). The results

subsequently discussed in this paper concern the foveal data obtained with the distractor stimuli.

Each subject completed the threshold program once for each stimulus size for all peripheral and foveal data points. The foveal and certain peripheral points underwent double threshold determination. In these cases, the mean of the two values was used as representative of that observer. Results are presented as the mean of the 10 observers in that age group. Standard errors were typically 2% of threshold for the young group, and 4% of threshold for the elderly. Five of the subjects in each group repeated the experiment a second time in order to obtain repeatability data (Bland and Altman, 1986; Elliott and Bullimore, 1993). The coefficient of repeatability (COR) is an indicator of the reliability of a test, or the consistency in test scores between sessions. COR describes the 95% confidence limits for any discrepancy between test and retest data. For normally distributed data, the COR is 1.96 times the standard deviation of the discrepancy. In this way, COR for the young subject group was calculated to be 0.40 log units, whilst for the elderly it was 0.45 log units.

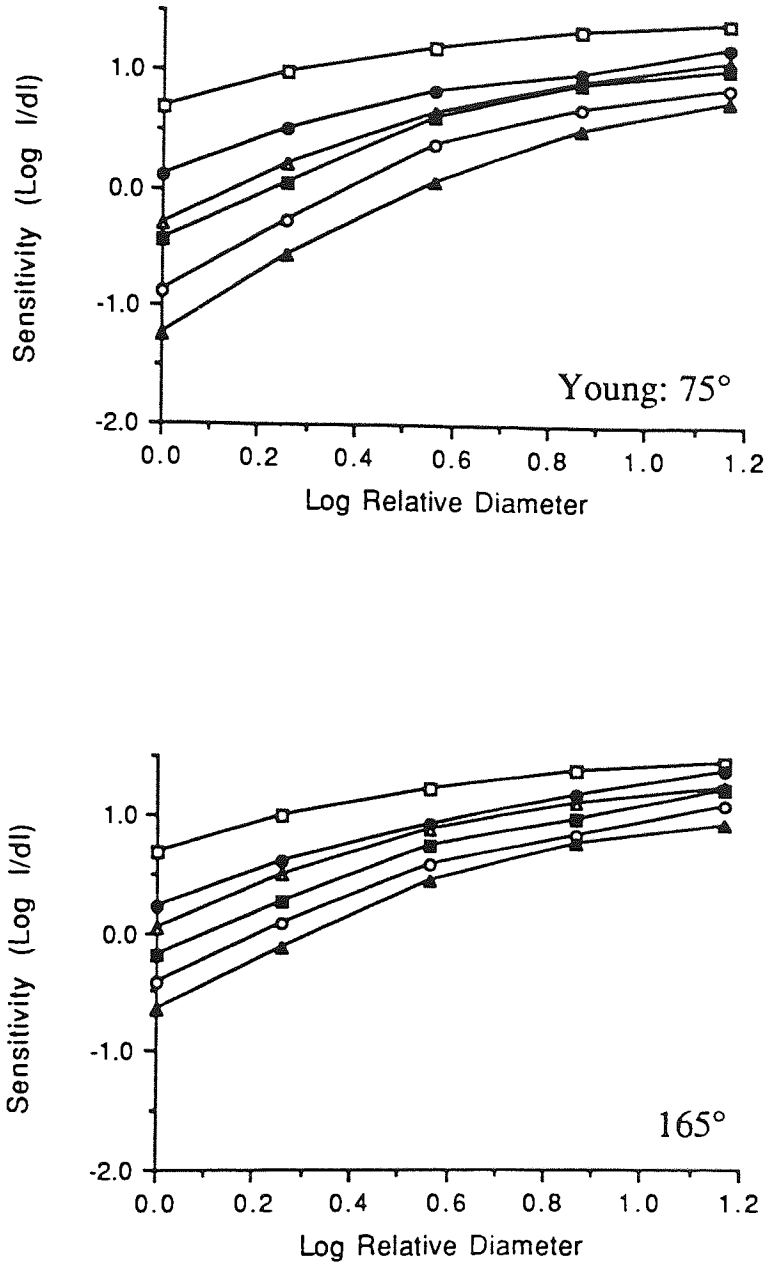

Figure 8.01. See following page for legend.

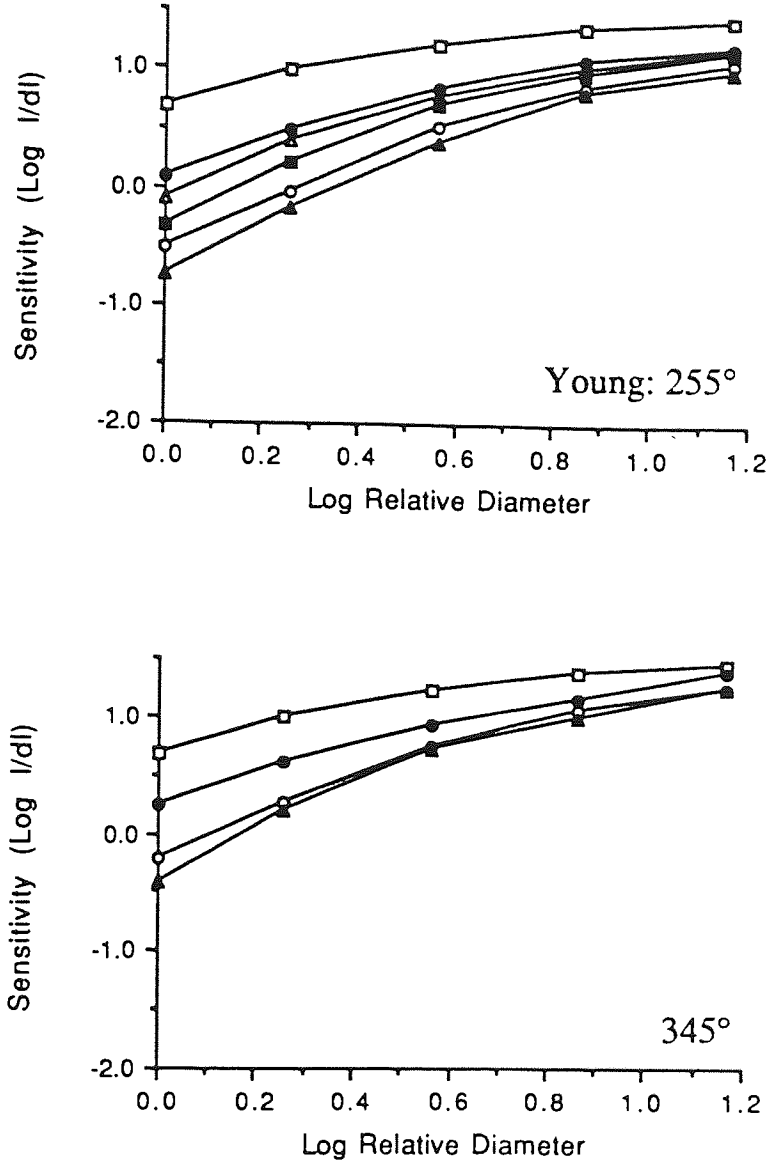

Figure 8.01. Sensitivity, log I/ΔI, plotted as a function of log diameter, expressed relative to that of the smallest target, in log units. Each data point represents the mean of ten young observers. Average standard error was 2% of threshold. The four graphs represent measurements obtained along one visual field meridian of the right eye: 75° (superior field), 165° (nasal field), 255° (inferior field) and 345° (temporal field) respectively. Symbols indicate sensitivity at various retinal eccentricities: 0° (open squares); 6° (closed circles); 12° (open triangles); 18° (closed squares); 24° (open circles); 30° (closed triangles). The 12° and 18° eccentricity data for the 345° meridian has been removed as the data points fell partially within the subjects' blind spot.

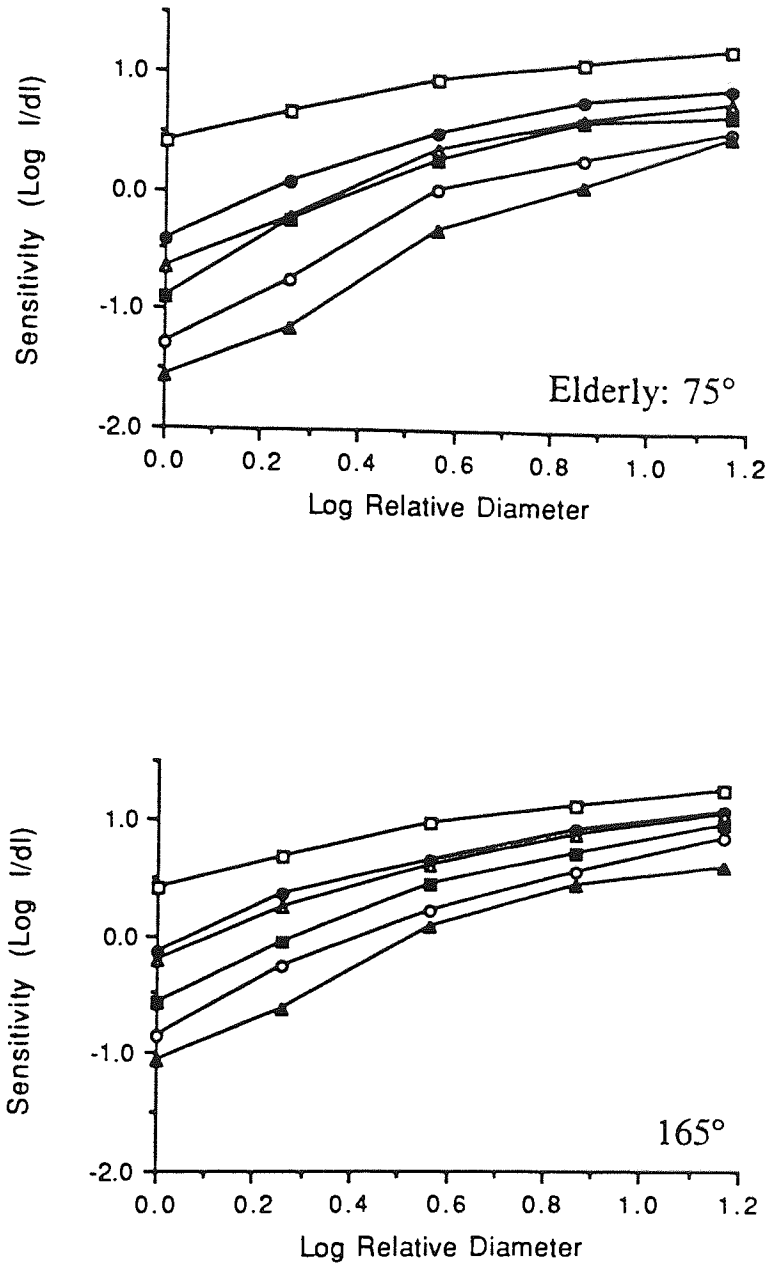

Figure 8.02. See following page for legend.

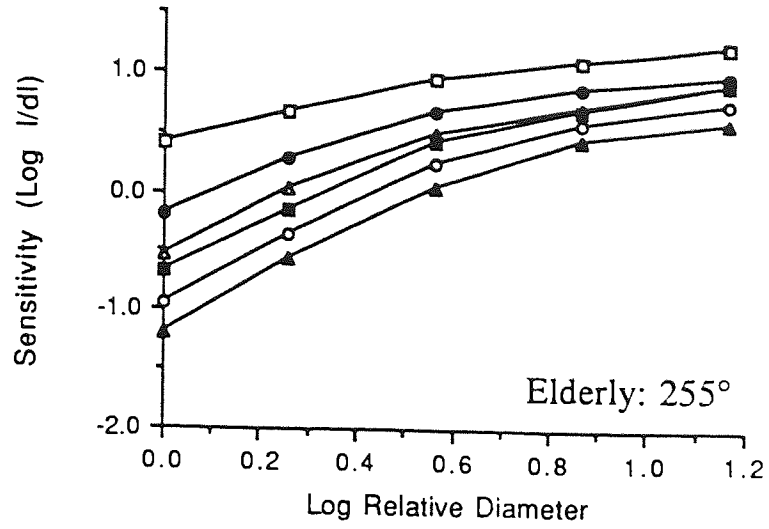

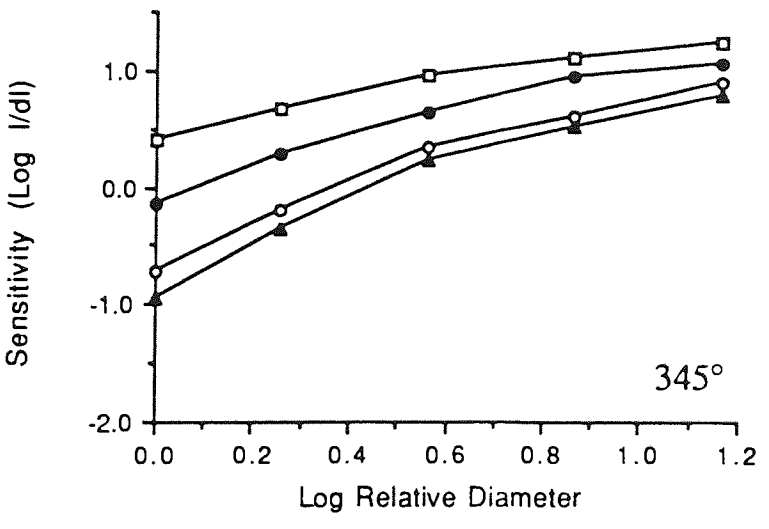

Figure 8.02. As for Figure 8.01, but for ten elderly observers. Average standard error was 4% of threshold.

8.3 Results

Mean sensitivity for the young group as a function of relative stimulus diameter along the four visual field meridia tested are shown in Figure 8.01, while the equivalent data for the elderly observers is shown in Figure 8.02. The figures demonstrate an increase in sensitivity as target size increases. The rate of sensitivity change, indicating the extent of summation, increases both with increase in eccentricity and with decrease in stimulus size. These are both well documented observations (Fankhauser and Schmidt, 1960; Sloan, 1961; Wilson, 1970; Johnson et al., 1978; Lie, 1980; Inui et al., 1981; Wild et al., 1987). The peripheral curves are offset from the foveal data by a shift along the size axis, as would be expected if peripheral visual performance differed from that at the fovea simply by a change of scale. This shift reflects the rate at which stimulus size must increase in order to result in performance equivalent to that at the fovea, and was quantified by moving the peripheral curves along the size axis such that by eye they were superimposed on the foveal data to give an optimum fit (as in Chapter 6). The amount of shift required is classified as a scaling factor, and these scaling factors are then plotted against their respective eccentricities. A regression of the form of Equation 4.01 is then fitted to the data, constrained to pass through a scaling factor of 1 at 0 deg eccentricity, since the foveal data scaled relative to itself results in a scaling factor of unity. From the regression, the E_2 value can be calculated according to Equation 4.01. The functions for successively greater eccentricities are then scaled by applying the equation:

$$\text{Scaled relative diameter} = \text{relative diameter} / (1+E / E_2) \qquad \text{Equation 6.03}$$

to the data for each eccentricity. The effect of this transformation is shown in Figures 8.03 and 8.04 for the young and elderly observers respectively. The data curves for different eccentricities collapse together to form a single function, thus removing eccentricity dependence from the data. E_2 values derived in this way are shown in Table 8.01, and are similar for the two age groups except along the 345 deg meridian, although this difference fails to reach significance ($t=2.33$, $df=4$, $p>0.05$).

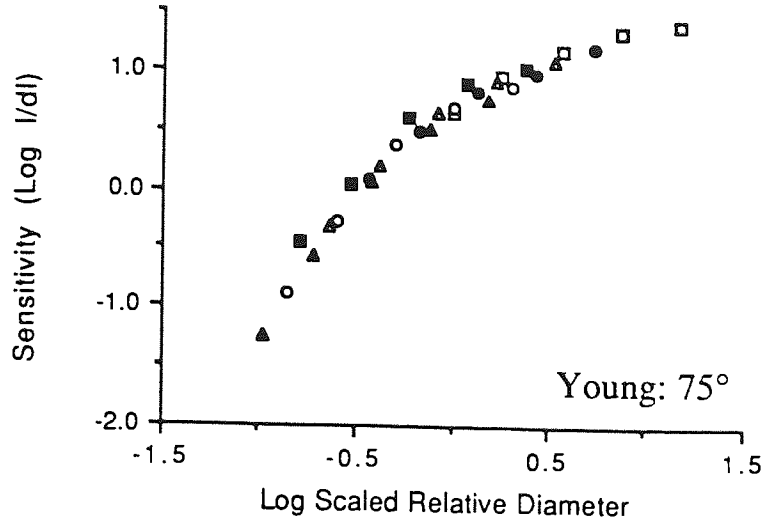

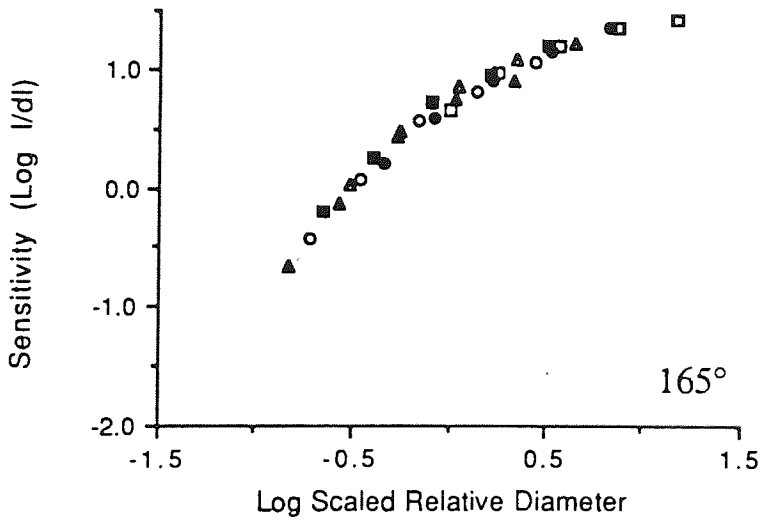

Figure 8.03. See following page for legend.

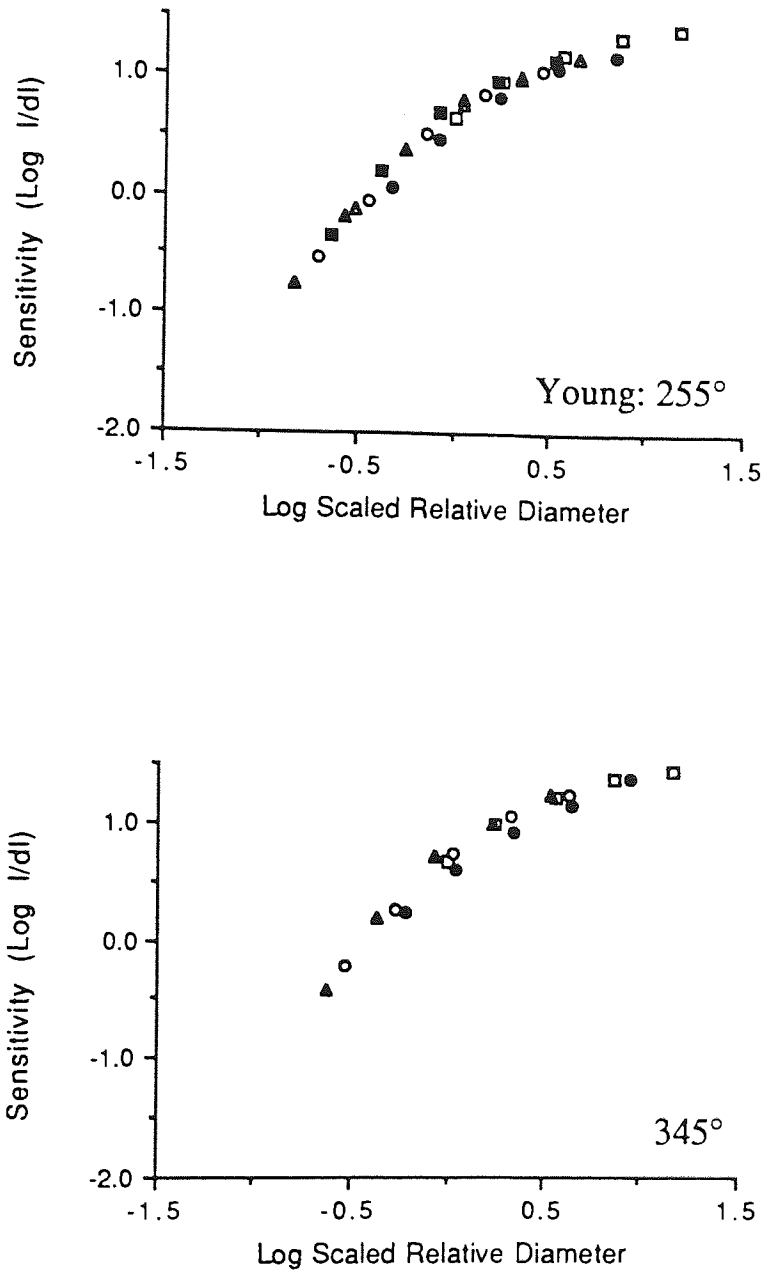

Figure 8.03. Sensitivity, log I/ΔI, plotted as a function of relative stimulus diameter scaled at each eccentricity according to E_2 values as defined in Table 8.01, for the young observers. Symbols are as for Figure 8.01. Note how scaling in this manner removes the eccentricity dependence from the data.

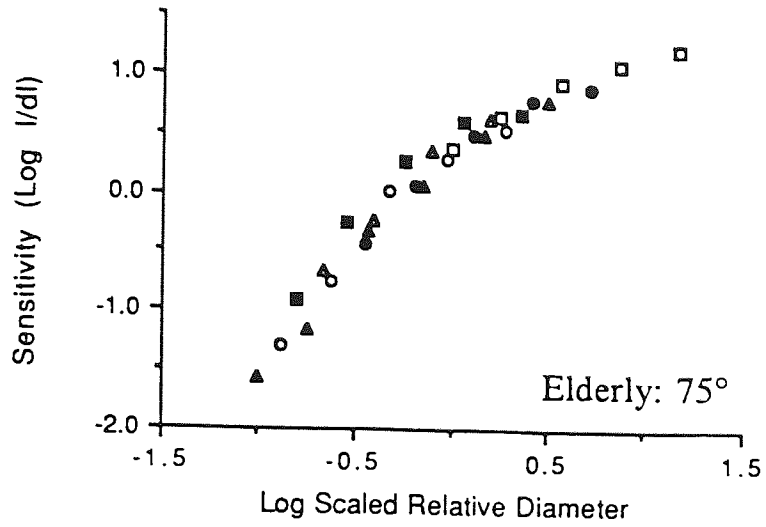

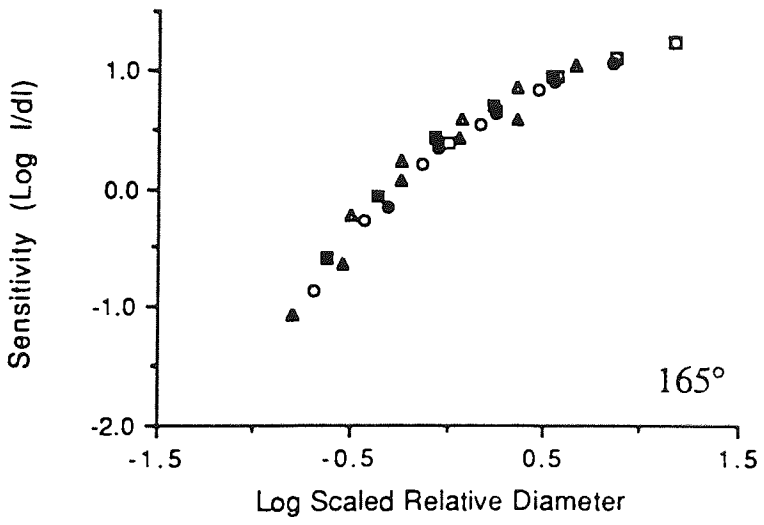

Figure 8.04. See following page for legend.

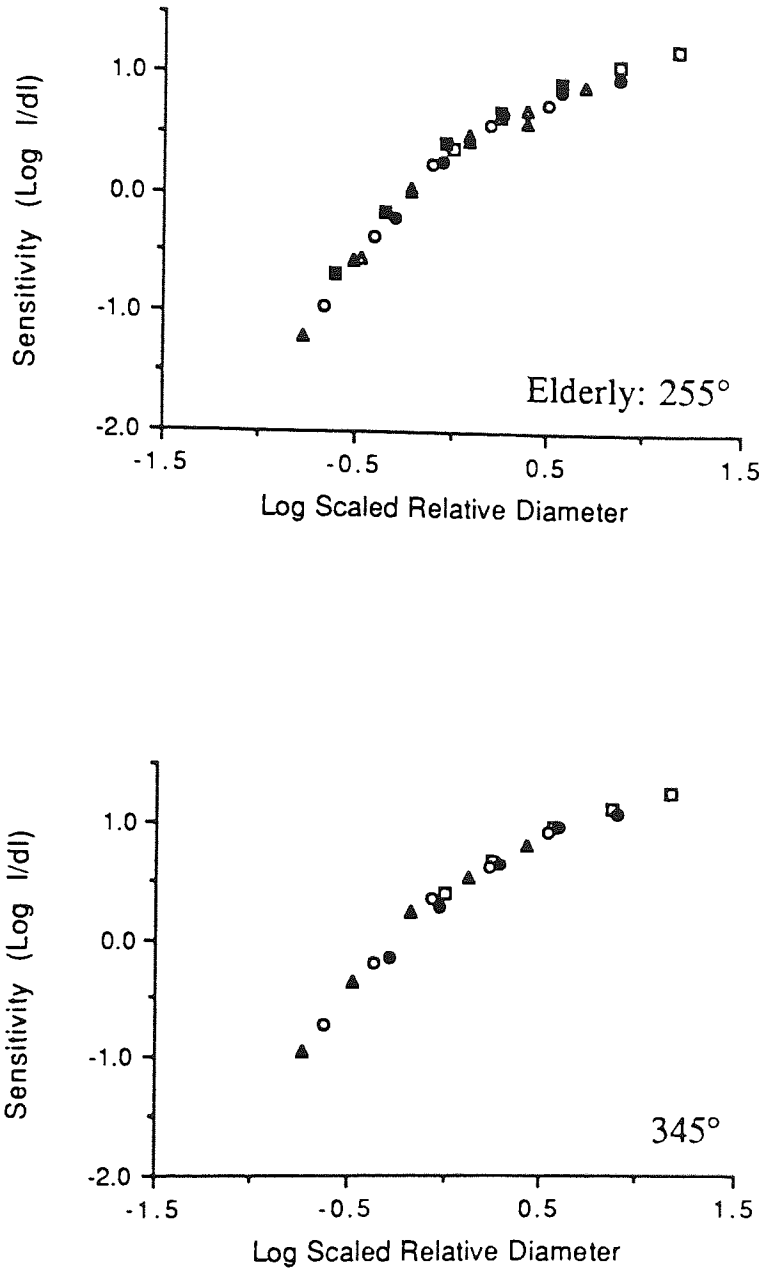

Figure 8.04. As for Figure 8.03, but for the elderly observers.

Meridian	E_2 Young	R^2	E_2 Elderly	R^2
75°	3.55±0.20°	0.964	3.33±0.33°	0.902
165°	5.24±0.25°	0.976	5.65±0.48°	0.933
255°	5.32±0.31°	0.952	5.99±0.36°	0.956
345°	9.35±1.05°	0.931	6.85±0.23°	0.994

Table 8.01. E_2 values (±standard error) as a function of meridian and age group for static differential light thresholds, with the corresponding R^2 values indicating how well the regression describes the data.

In Figure 8.05 the scaled data of the young and elderly groups are replotted as spatial summation curves, with stimulus area substituted for relative diameter. The data have been fitted with second order polynomial functions, which are described in Table 8.02. The gradients of these second order polynomials change linearly with log stimulus area, reflecting the gradual and continuous decrease in summation coefficient (K) from unity (Ricco's Law) to zero (Weber's Law). The data of the young and elderly observers appear to be of the same shape, but are on the graphs in different positions. Shifting the data along either the x- or the y-axis reduces the differences between the two sets of data. This observation was quantified by shifting the data of the elderly observers by amounts approximated by eye along the axis in question in order to superimpose it on the data of the young observers as best as possible. Following this shift, the resulting data was fitted with a single second order polynomial, and the value of the residual sum of squares calculated. The amount of shift minimising the residual sum of squares was determined, and the percentage variance removed by this shift calculated by comparison with the residual sum of squares of the original unshifted data.

Meridian	Young	R^2	Elderly	R^2
75°	$y = 0.788 + 0.582x - 0.154x^2$	0.980	$y = 0.457 + 0.627x - 0.144x^2$	0.974
165°	$y = 0.793 + 0.555x - 0.127x^2$	0.989	$y = 0.477 + 0.627x - 0.139x^2$	0.981
255°	$y = 0.759 + 0.588x - 0.145x^2$	0.986	$y = 0.420 + 0.675x - 0.158x^2$	0.989
345°	$y = 0.733 + 0.615x - 0.141x^2$	0.977	$y = 0.429 + 0.648x - 0.131x^2$	0.993

Table 8.02. Equations of the polynomial regressions used to fit the young and elderly group data in Figure 8.05.

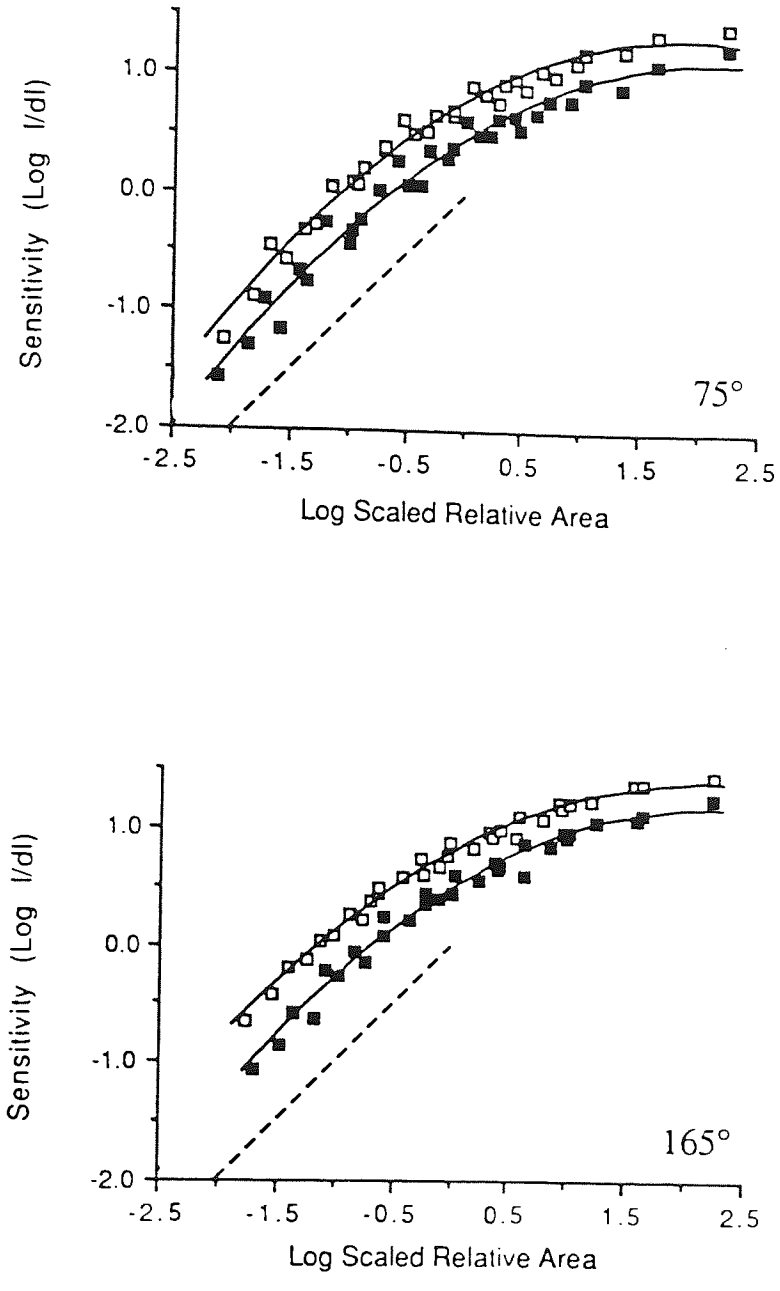

Figure 8.05. See following page for legend.

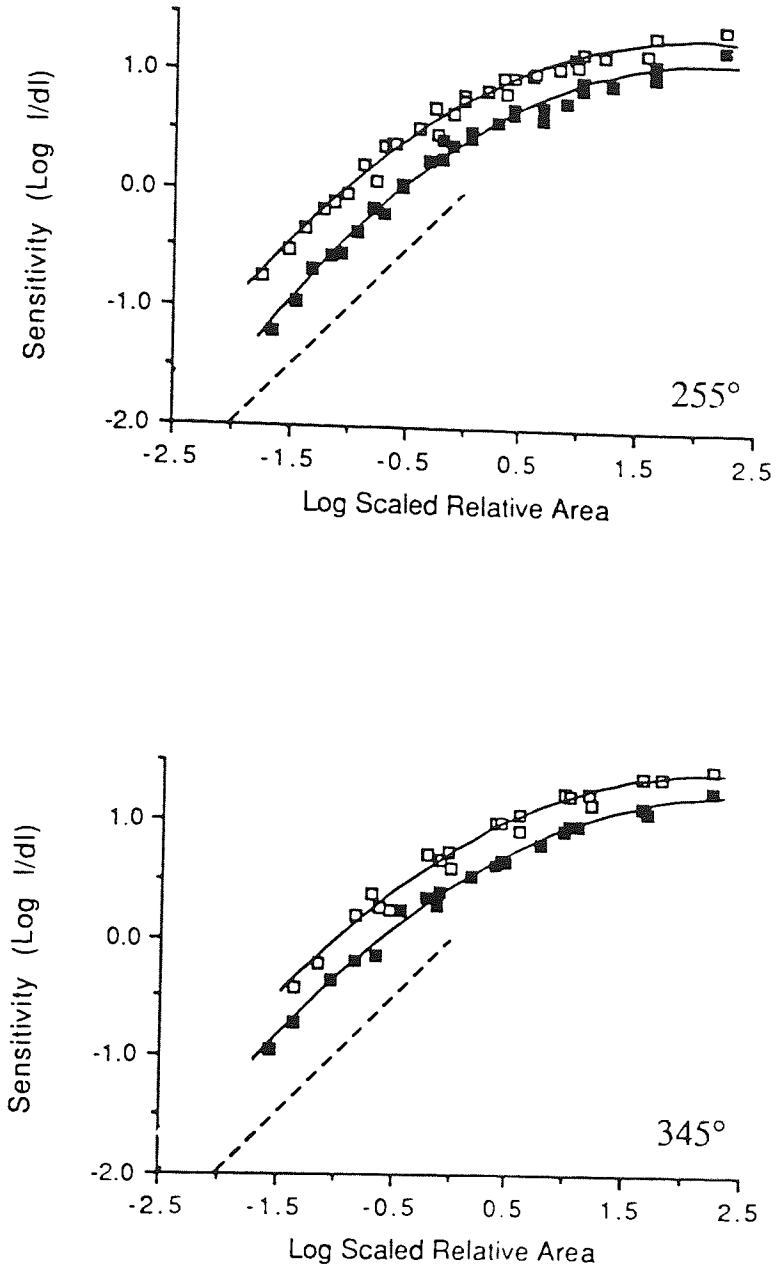

Figure 8.05. Composite graphs showing the data from Figures 8.03 and 8.04. Young - open squares; elderly - closed squares. The curves fitted to the data are best fitting second order polynomials, with equations listed in Table 8.02. The dotted line indicates a slope, or summation coefficient, of one (Ricco's Law).

If the data of the elderly observers is shifted up the y-, or sensitivity, axis by 0.3 log units, an average of 78% of the variance between the two data sets is removed. An average of 74% of the variance is removed from the data by a 0.4 log unit shift of the elderly data leftwards along the x-, or size axis. A combination of x- (0.2 log units leftwards) and y- (0.2 log units upwards) shifts removes an average of 81% of the variance, although some improvement in the variance removed would, of course, be expected by the use of two factors. The physiological consequence of a shift along the y-axis is that of a simple reduction in sensitivity with age, whilst the consequence of an x-axis shift is a change in the scale of the elderly visual system towards larger target sizes.

8.4 Discussion

The individual summation curves are of the same shape with eccentricity, but are simply displaced along the size axis. The curves can be superimposed to form a single curve, which is well fitted by a second order polynomial, and removes eccentricity dependence from the data. This agrees with previous work (Wilson, 1970; Lie, 1980) and supports the premise that the mechanisms underlying the foveal and peripheral differential light threshold are the same apart from a change in scale. Further, the displacement of the curves along the size axis appears to change approximately linearly with eccentricity. For the young, this agrees with several previous studies involving many different tasks, as was noted in Chapter 7. The decline in visual performance with eccentricity for elderly observers is less well documented, but for kinetic differential light stimuli, the relationship becomes non-linear (Chapter 7). However, it should be noted that in Figures 8.01 and 8.02 the sensitivity does not appear to change markedly between 12 and 18 deg in either the young or elderly groups, indicating a slight plateau in the increase of size scale with eccentricity. This is in agreement with Lie (1980), who also found such a plateau.

It is important to understand the differences between the present method and conventional perimetric techniques. The latter involve measuring differential light thresholds to a stimulus of the same size over the visual field. Herse (1992) found an E_2 of 3.71 deg for the differential light threshold averaged across meridians and noted that this lay within the range of E_2 values quoted for contrast sensitivity and resolution. However, the study used a constant sized stimulus (Goldmann III) at all eccentricities. This is an inappropriate method by which the eccentricity-dependent nature of any task should be quantified since a stimulus of a certain size might be optimum for one visual field location but not for another. For instance, larger stimuli are much more likely to be optimum for the periphery, resulting in a gradual decline in performance away from the

fovea, whilst smaller stimuli would result in a much more rapid deterioration. Hence, depending upon the stimulus size chosen, a wide variety of apparent E_2 values can be obtained for the same task. This highlights the importance of using a method of spatial scaling with which to define E_2 values rather than relying upon an arbitrary choice of stimulus size.

Rather than using a constant sized stimulus, measuring thresholds at each eccentricity for a series of stimulus sizes, as in the present study, allows performance to be compared for equivalent sized stimuli at different eccentricities. The current results show similar E_2 values for the two age groups, indicating that peripheral performance relative to that at the fovea in this task does not vary greatly with age. Since this is the case, the viability of clinically useful 'perimetrograms' becomes more realistic. Regardless of age, if luminance threshold is set at some value which represents threshold at some visual field location, such as the fovea, equivalent performance can be attained across the visual field by scaling peripheral stimulus diameters in accordance with the E_2 values determined in this study.

Conventional perimetric studies tend to show that the hill of vision becomes steeper with age (Jaffe et al., 1986; Heijl, 1987; Johnson et al., 1989). A relevant point is the use of distractor stimuli with which to establish foveal thresholds. Without such distractors, the methodology of presentation is not similar at all locations. Such a proviso is of great importance since the method of spatial scaling compares all peripheral data with that obtained at the fovea. In the absence of these distractors, the foveal sensitivity of the elderly group is raised, which in turn leads to an apparent increase in the rate at which performance declines with eccentricity and a smaller E_2 value.

Another procedure which can show a differential influence of distractors on elderly visual performance is the 'Useful Field of View' (UFOV) test (Ball, Owsley, Sloane, Roenker and Bruni, 1993). This is a test of visual attention consisting of a central identification task coupled with a peripheral localisation task, which may be embedded in distractor stimuli. The useful field of view so measured represents the spatial area within which a person can be alerted to visual stimuli. UFOV is claimed to have high sensitivity and specificity in predicting which older drivers have a history of car crashes (Ball et al., 1993). The foveal thresholding procedure used in the current study is simpler than that of the UFOV, and utilises an existing clinical instrument. As such, it might provide an alternative method for identifying older drivers with selective attention difficulties that affect driving performance.

For the young observers, the static E_2 values (Table 8.01) are slightly smaller than those obtained using a kinetic method of presentation (Table 7.01). This suggests that the peripheral retina is relatively more sensitive to a moving target than to a static spot of light. Although this difference is small compared to differences in E_2 values between unrelated tasks, it does suggest that the method which is used to determine thresholds (in this case the differential light threshold) can influence peripheral gradients.

For the elderly observers, E_2 values have been derived from the static data since the scaling factors for this task increased approximately linearly with eccentricity. Further, these E_2 values are comparable to those obtained for young observers, as discussed above. This was not the case for the kinetic data (Chapter 7). For kinetic presentation of the differential light stimulus, the decline in thresholds with eccentricity was non-linear, with a preferential loss of sensitivity centrally and beyond 20 deg, and a relative sparing of the pericentral region. The major difference between the two methods of data collection was the movement of the stimulus in the kinetic presentation. This suggests that the non-linearity observed in the elderly data might be due either to eccentricity related differences in the processing of a moving stimulus, or to variations in reaction time with eccentricity in the elderly.

The variation of E_2 with meridian of presentation is such that the superior field shows the most rapid decline in performance with eccentricity ($p<0.01$). Nasal and inferior fields show no difference ($p>0.1$). For the young group the E_2 for the temporal meridian is significantly larger than for the nasal meridian ($t=3.81$, $df=6$, $p<0.01$), thus demonstrating a naso-temporal asymmetry in performance, which has been found for many other tasks (Wertheim, 1891; Johnson et al., 1978; Fahle and Schmidt, 1988; Paradiso and Carney, 1988; Anderson et al., 1991; Scobey and van Kan, 1991).

Previous studies on the change in spatial summation with age have come to differing conclusions. Dannheim and Drance (1971) examined spatial summation with age group foveally and along the 45 deg visual field meridian in photopic conditions. They found that the differential threshold was higher in older observers for all target sizes than for younger subjects. They attributed this to a "decrease in retinal sensitivity with age". It was also found that as target size increased, thresholds declined at the same rate for all age groups, suggesting that spatial summation remains unchanged in later life. Brown et al. (1989) examined detection thresholds as a function of target size in both young and elderly observers at an eccentricity of 10 deg, and in agreement with Dannheim and Drance, found a decrease in elderly retinal sensitivity and no significant difference in

photopic critical summation areas with age. Assuming a simple reduction in sensitivity with age, the present data suggest a loss of approximately 0.3 log units for a mean age group difference of 48.4 years. This compares well with previous estimates of loss of perimetric sensitivity of 0.05-0.08 log units per decade over the central 30 deg field (Brenton and Phelps, 1986; Haas et al, 1986; Heijl, 1987; Johnson et al., 1989).

Owsley and Sekuler (1982) initially found similar results at the fovea to those described above (decreased sensitivity but no change in summation). However, once they applied an appropriate correction for the viewing distance, and undefined compensations were made for blur and reduced retinal illumination in the elderly, thresholds improved for small targets, but little change occured in the thresholds for the larger targets. This indicated that less summation was taking place in the elderly than in the younger subjects, and the authors concluded that the elderly may have a neural loss resulting in a relative difficulty in seeing larger targets. However, it is now unequivocally established that contrast sensitivity loss with age occurs preferentially for small stimuli (Derefeldt, Lennerstrand and Lundh, 1979; Owsley et al., 1983; Elliott et al., 1990). Indeed, this is suggested by the present data since a combination of lower differential light sensitivity and a shift in sensitivity towards larger target sizes with increasing age best accounts for the differences observed.

Several factors could contribute to the lower differential light sensitivity found in the older subject group. Firstly, perimetric routines such as the one used here are criterion dependent in that more cautious observers appear to have lower sensitivity. Quantifying this effect in the data is not possible, but the use of highly trained subjects is likely to have minimised its impact. True sensitivity loss may arise due to neural or optical factors. Senile miosis and increased absorption of the ocular media will serve to reduce retinal illumination for the elderly observers. In addition, increased forward light scatter in the elderly eye will degrade retinal image quality. Both of these factors, reduced retinal illumination and increased scatter, would be expected to have a preferential effect on the smaller target sizes (Wood, Wild and Crews, 1987; Wood, Wild, Smerdon and Crews, 1989). The result of this would be to affect the manner in which data from different eccentricities can be scaled, since small target sizes at the fovea are compared to larger stimuli in the periphery by the horizontal scaling technique. There is no evidence for a breakdown of scaling in the elderly data (Figure 8.04), suggesting that these optical factors are of minor importance. This is consistent with recent work suggesting that the reduction in visual field sensitivity with age is mainly due to neural rather than optical factors (Johnson et al., 1989).

In conclusion, changes in static differential light thresholds across the visual field are found to be simply due to a change of scale. Whilst the rate of scale change is approximately the same for both young and elderly observers, differences in performance can be explained by a combination of lower sensitivity and a shift in sensitivity towards larger stimulus sizes with increasing age.

Chapter 9
Resolution in the presence of flanking elements

9.1 Introduction

The previous chapters have demonstrated that for the majority of tasks examined, foveal and peripheral vision can be equated by a change of size scale. The eccentricity related rate of magnification change appears to be dependent upon the visual task in question, with tasks such as certain hyperacuities requiring much more eccentricity-related magnification than visual acuity, which in turn requires more magnification than light detection tasks or movement detection tasks (Weymouth, 1958; Westheimer, 1982; Levi et al., 1985; Johnston & Wright, 1986; Drasdo, 1991; Whitaker et al., 1992b; Chapters 6, 7 and 8). The common feature of all these tasks, however, is that all need to be magnified at a rate which is approximately linear as a function of eccentricity.

One interesting consideration, which may shed some light on the mechanisms behind the existence of diverse peripheral gradients, is what happens in a situation where visual performance is known to be determined by a combination of two factors which have dramatically different rates of eccentricity dependence when operating in isolation. A good example of this is the case of visual acuity in the presence of flanking elements, which is now examined in this study. The literature regarding visual acuity as a function of eccentricity has been reviewed in Chapter 2.

The probability of correctly identifying a target such as a letter is generally reduced when that target is surrounded by other items. This effect has variously been named 'lateral masking', 'crowding phenomenon', 'spatial interference' and 'contour interaction'. The term 'spatial interference' is used throughout this thesis. Spatial interference effects occur throughout spatial vision, having been shown for letter recognition (Bouma, 1970; Loomis, 1978; Toet and Levi, 1992), Llandolt ring recognition (Flom, Weymouth and Kahneman, 1963b; Jacobs, 1979; Nazir, 1992), digit recognition (Strasburger et al., 1991), tilt judgements (Andriessen and Bouma, 1976), stereoacuity (Westheimer and Troung, 1988), and vernier acuity (Westheimer and Hauske, 1975; Levi et al., 1985, Chapter 2).

The types of flanking element used to introduce spatial interference have varied across studies, and have included bars (Flom et al., 1963b; Jacobs, 1979), squares (Loomis, 1978, Nazir, 1992), different coloured targets (Bouma, 1969), digits (Strasburger et al., 1991) and letters (Bouma, 1970; Loomis, 1978; Nazir, 1992). The degree and

extent of spatial interference increases as the similarity between target and flanks increases (Nazir, 1992; Kooi, Toet, Tripathy and Levi, 1994). Flanks have a more deleterious effect on thresholds if they are similarly oriented to the target, rather than having a different orientation (Andriessen and Bouma, 1976). A single flank is more effective at reducing recognition of a target if it is placed at a more eccentric location than the target, rather than closer to fixation than the target (Bouma, 1970; Wolford and Chambers, 1983; Banks, Larson and Prinzmetal, 1979).

Spatial interference can be described in terms of its extent (the distance over which interactions occur), or in terms of its magnitude (the effect on thresholds). A detailed study of spatial interference in central vision was made by Flom et al. (1963b), who examined the percentage of near threshold Llandolt rings correctly identified in the presence of flanking bars for foveal vision of normal and amblyopic observers. They concluded that the extent of spatial interference in angular terms was proportional to the observer's minimum angle of resolution, being approximately 5 times the MAR, or one Snellen letter width.

The magnitude and extent of spatial interference has generally been considered to be greater in peripheral vision than at the fovea (Bouma, 1970; Andriessen and Bouma, 1976; Jacobs, 1979; Levi et al., 1985; Flom, 1991). For complete visual isolation of peripheral targets, Bouma (1970) suggested that no letters should be placed within 0.5E of a letter target, where E is the eccentricity of the target. Andriessen and Bouma (1976) found a similar extent of spatial interference for tilt judgments of 0.4E. For vernier acuity, the extent of spatial interference is reported to extend to 0.15E (Levi et al., 1985). These values imply that the extent of spatial interference increases linearly with eccentricity, and also that there is no spatial interference in the fovea. There has been less evidence to demonstrate that spatial interference is not peculiar to peripheral vision, but also exists at the fovea (although on a much minified scale) and thereby represents a quantitative rather than qualitative difference between foveal and peripheral vision (Loomis, 1978; Levi et al., 1985; Toet & Levi, 1992).

Jacobs (1979) used similar Llandolt ring stimuli with flanking bars to those used by Flom et al. (1963b) to examine acuity in the presence of bars from 0-10 deg eccentricity. Jacobs found that while the bars had little noticeable effect on foveal thresholds, at peripheral locations, interference was observed as far as 5 bar widths separation (the maximum examined). Since thresholds were affected more by the presence of the bars in the periphery than at the fovea, the effect of the bars was to increase the rate of threshold decline with eccentricity, which is shown in Figure 9.01.

E_2 values are 1.15 ± 0.11 deg for the isolated Llandolt ring, and 0.62 ± 0.07 deg for Llandolt ring acuity with additional bars placed 0.5 gap widths from the target.

Figure 9.01. Data from Jacobs (1979). Minimum angle of resolution as a function of eccentricity. Open squares, and solid line: isolated Llandolt rings; Crosses, and dashed line: Llandolt rings flanked by bars at 0.5 gap widths separation. The regressions on the graph were fitted to the data in logarithmic format (see Chap 2) on the y-axis, and are: solid line: logMAR = -0.39 + log (1 + (E / 1.15)); dashed line: -0.35 + log (1+ (E / 0.62)).

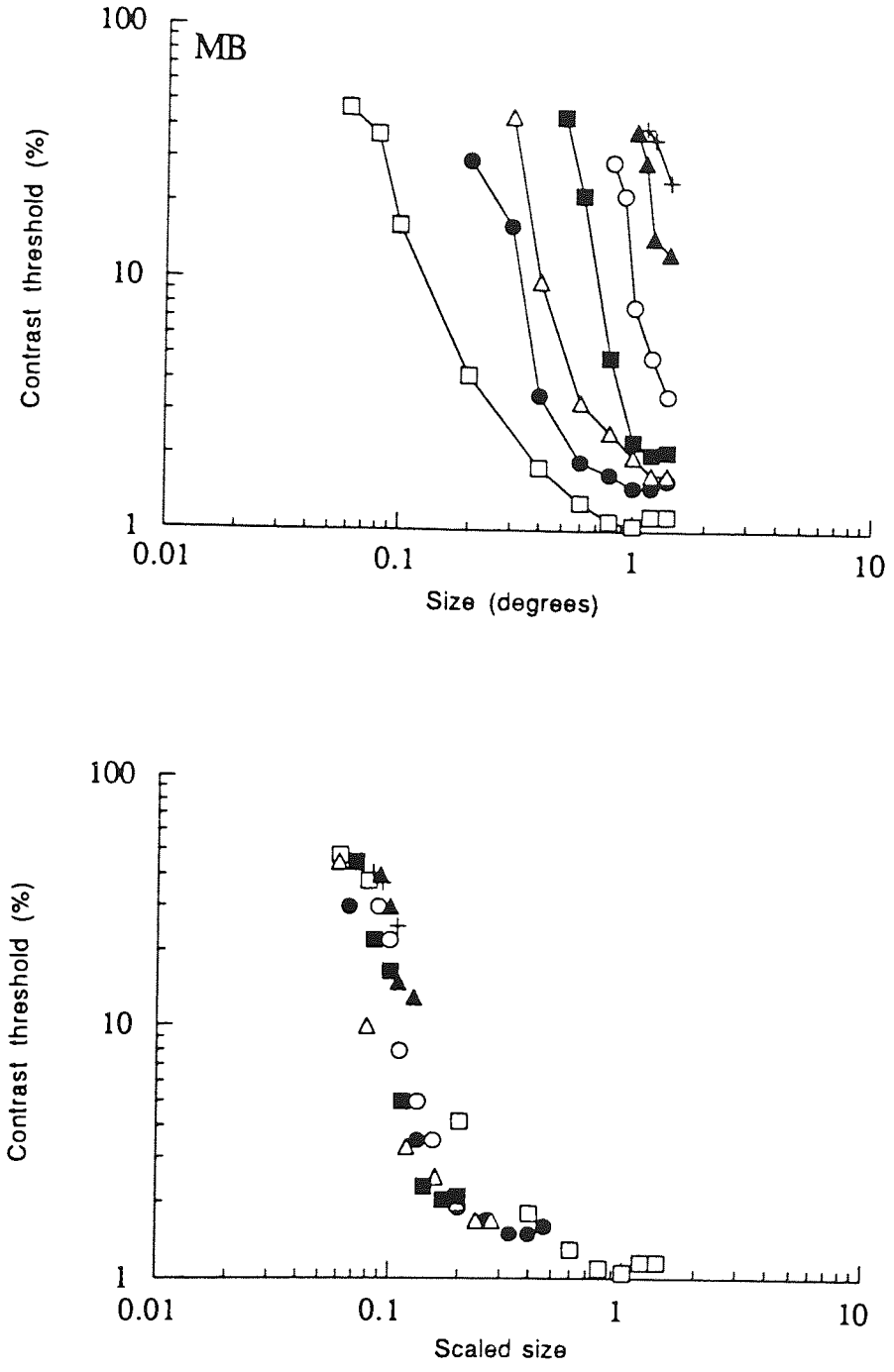

Figure 9.02. Data from Strasburger et al. (1991), observer MB, left visual field. (a) Contrast thresholds for digit recognition when flanked by two digits at an edge to edge separation of one character width, plotted against digit size. Open squares: 0 deg; closed circles: 2 deg: open triangles: 4 deg; closed squares: 6 deg; open circles: 8 deg; closed triangles: 10 deg; crosses: 12 deg. (b) Data of a, scaled on the x-axis according to the equation: SF = 1 + (E / 1.00).

Strasburger et al. (1991), as already mentioned in Chapter 2, examined contrast thresholds for digit recognition as a function of eccentricity. In addition to single digit recognition data, contrast thresholds were found for digits surrounded by another digit on each side, with an edge to edge separation of one character width. The authors suggested that fovea and periphery were qualitatively different, since on log-linear plots they found strong crowding effects in peripheral vision, but not at the fovea. However, the data for their subject MB is reevaluated on logarithmic axes in Figure 9.02a. In Figure 9.02b the data has been scaled according to an E_2 value of 1.00 deg, which can be seen to remove most of the eccentricity dependence from the data. Analysed in this way, it would appear that foveal and peripheral data differs merely by means of a change in size scale. For subject KZ (not shown) E_2 is 0.92 deg. These E_2 values compare with those found for an isolated digit of 1.57 deg (MB) and 1.31 deg (KZ).

Toet and Levi (1992) firstly measured thresholds for 75% correct discrimination of the orientation of letter T's from 0-10 deg in inferior field. They found that E_2 was 2.04 ± 0.19 deg, as an average of 6 observers. The size of the targets was then increased to 1.5 times threshold, and were surrounded on either side by a flanking T. The separation of the flanking T's was then found which reduced discrimination to 75%. This separation was taken as indicative of the extent of the zone of spatial interaction. E_2 values for the extent of spatial interference were very much smaller than those for resolution, averaging 0.34 ± 0.04 deg for horizontal orientation of the stimulus arrangement in the inferior visual field, and 0.18 ± 0.03 deg for vertical stimulus arrangement. Spatial interference zones were thus found to grow much more rapidly with eccentricity than acuity thresholds. Additionally, the zone of spatial interference was found to be elliptical in the peripheral visual field, with the long axis along the meridian passing through central vision, and the minor axis perpendicular to this.

In summary, whilst the size of a just resolvable test target presented in isolation needs to be increased at a certain rate with increasing eccentricity, the size of the zone of spatial interaction increases at a much faster rate (Jacobs, 1979; Toet and Levi, 1992). Therefore, visual acuity decreases more rapidly with eccentricity for test targets which are surrounded by flanking stimuli.

The study of Toet and Levi (1992) investigated the extent of spatial interference effects for a single specific magnitude of resolution threshold elevation. In the present study, the work of Toet and Levi (1992) is extended: using a method of spatial scaling, the individual and combined effects of resolution and spatial interference are examined as a function of eccentricity for a range of target-flank separations, threshold levels and

visual field meridia. The initial reason for performing these experiments was to discover whether the linear nature of eccentricity-related magnification remained when a variable combination of two factors (in this case resolution and spatial interference) determined visual performance. The manner in which the two factors behave with eccentricity may be able to shed some light on how limiting factors at various levels of the visual system combine to produce the observed variations in performance across the visual field for any given task. Additionally, the results enable the effect of flanking elements on resolution thresholds to be predicted using a simple formula which depends only upon eccentricity and the distance between the target and its surrounding elements.

9.2 Methods

Subjects

Two observers (DW and KL) participated in the experiment. Both were pre-presbyopic moderate myopes (<4.50DS) and wore their full foveal distance correction. Corrected acuities for both DW and KL, measured on a LogMAR chart at a luminance of approximately 100 cd m^{-2}, were -0.14 (6/4.3 Snellen equivalent). Both subjects were experienced in making foveal and peripheral judgements of this type, and underwent extensive practice sessions before data collection began.

Stimuli

Stimuli were presented on the face of an Eizo 8060 colour monitor and were controlled by a Research Machines Nimbus AX microcomputer (see Chapter 5 for details). Targets consisted of three dark bars (1.9 cd m^{-2}) presented on a homogenous light background (35 cd m^{-2}) and the monitor was surrounded by an approximately equiluminant surround. The width and separation of the bars was equal whilst their length was 5 times this value in order to make the the horizontal and vertical dimensions of the target identical (Figure 9.03). The target was presented either on its own (unflanked condition) or was surrounded by four flanking elements which were identical to the target but the orientation of each was randomly either horizontal or vertical and varied orientation from trial to trial (Figure 9.03). The flanking elements were separated from the target by a distance s, measured from edge to edge. The separations investigated were always a fixed multiple (0.5, 1, 2, 4 or 7) of the target size, T, in addition to an unflanked condition in which the flanking elements were absent. For the foveal condition only, a separation of 0.25 times the target size was also used. Target size was varied by changing viewing distance so that for any given separation (defined in multiples of target size), all stimuli were magnified or minified versions of one another.

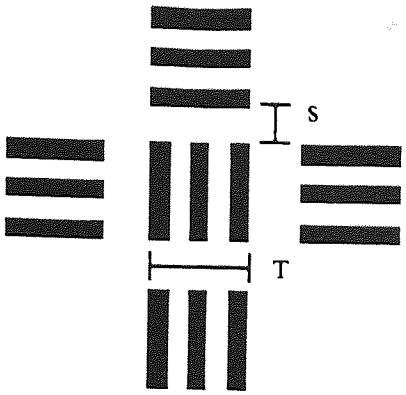

Figure 9.03. The stimulus configuration used in the experiment. See text for details. The separation, s, between the target and flanks is a multiple of target width, T.

Procedure

Following a 500msec exposure time, the subjects' task was to identify whether the bars of the central target were oriented vertically or horizontally. Visual feedback was provided following a correct response. Immediately following feedback, the next stimulus appeared. Each block of trials consisted of 40 presentations of a random combination of at least three flanking conditions at a single viewing distance. At least 5 different viewing distances were used for each flanking condition, and these were selected to give a range of correct responses between 50% and 100% correct. Blocks of trials were repeated following which a psychometric function was fitted to the data for each flanking condition. Psychometric functions were based on at least 400 responses and the viewing distance which produced a 75% correct response level was calculated by probit analysis of the data. The visual angle subtended by the gap between the bars of the target at this viewing distance was then accepted as the resolution threshold. Eccentricities of 0, 2.5, 5 and 10 degrees were investigated in the nasal, superior, temporal and inferior visual field meridia. For peripheral viewing a small fixation spot was continuously present either on the monitor or on the surround.

9.3 Results

Figure 9.04 shows how resolution thresholds increase with eccentricity for each flanking condition and also for the no-flank situation for four visual field meridia. At the fovea, unflanked resolution thresholds are 0.55 and 0.64 min arc for KL and DW respectively. These values are slightly less than the resolution thresholds measured with the LogMAR chart (0.72 min arc for both observers), but highlight the fact that foveal resolution thresholds well below 1 min arc should be expected for normal, young observers under high contrast conditions. The slight difference in acuity level is

probably due to the fact that the letters on the acuity chart are likely to be affected by spatial interference from their nearest neighbours (separated by one letter width), and a difference in threshold criterion for the two tasks. With increasing eccentricity, both flanked and unflanked resolution thresholds increase in an approximately linear manner. The introduction of flanking elements has only a small effect on foveal resolution thresholds but has a marked effect in the periphery, and this effect becomes greater with increasing flank proximity. The rate at which thresholds increase as a function of eccentricity was calculated on logarithmic axes by fitting the data for each flanking condition by a regression according to the equation

$$\log Te = \log To + \log (1 + (E / E_2)) \qquad \text{Equation 2.10}$$

where Te represents resolution threshold at an eccentricity E, To is the foveal threshold and E_2 is the parameter governing the rate of increase in threshold with eccentricity. E_2 represents the eccentricity at which the foveal threshold (To) doubles. Logarithmic axes were used for the regression since on this scale the standard error of acuity values is a constant proportion of the mean (Westheimer, 1979a; Chapter 2). The data are shown on linear axes to highlight the linear rise of thresholds with eccentricity.

Figure 9.05 shows E_2 values derived in this way for all flanking conditions along each of the four principal meridia, and for both observers. E_2s are always largest for the unflanked condition and decrease as the flanking elements are moved closer to the target. Unflanked E_2s lie between 1 and 2.1 degrees (see Table 9.01), corresponding well with analysis of previous findings for resolution tasks (Table 2.02). Higher E_2 values in the horizontal meridia as compared to the vertical are also well documented (Wertheim, 1891; Nazir, 1992; Chapter 7). An increase in the rate of threshold change with eccentricity in the presence of flanking elements has also been noted (Jacobs, 1979; Toet and Levi, 1992; Strasburger et al., 1991), and this is reflected in the decrease in E_2 values as flanking elements are placed more proximal to the target.

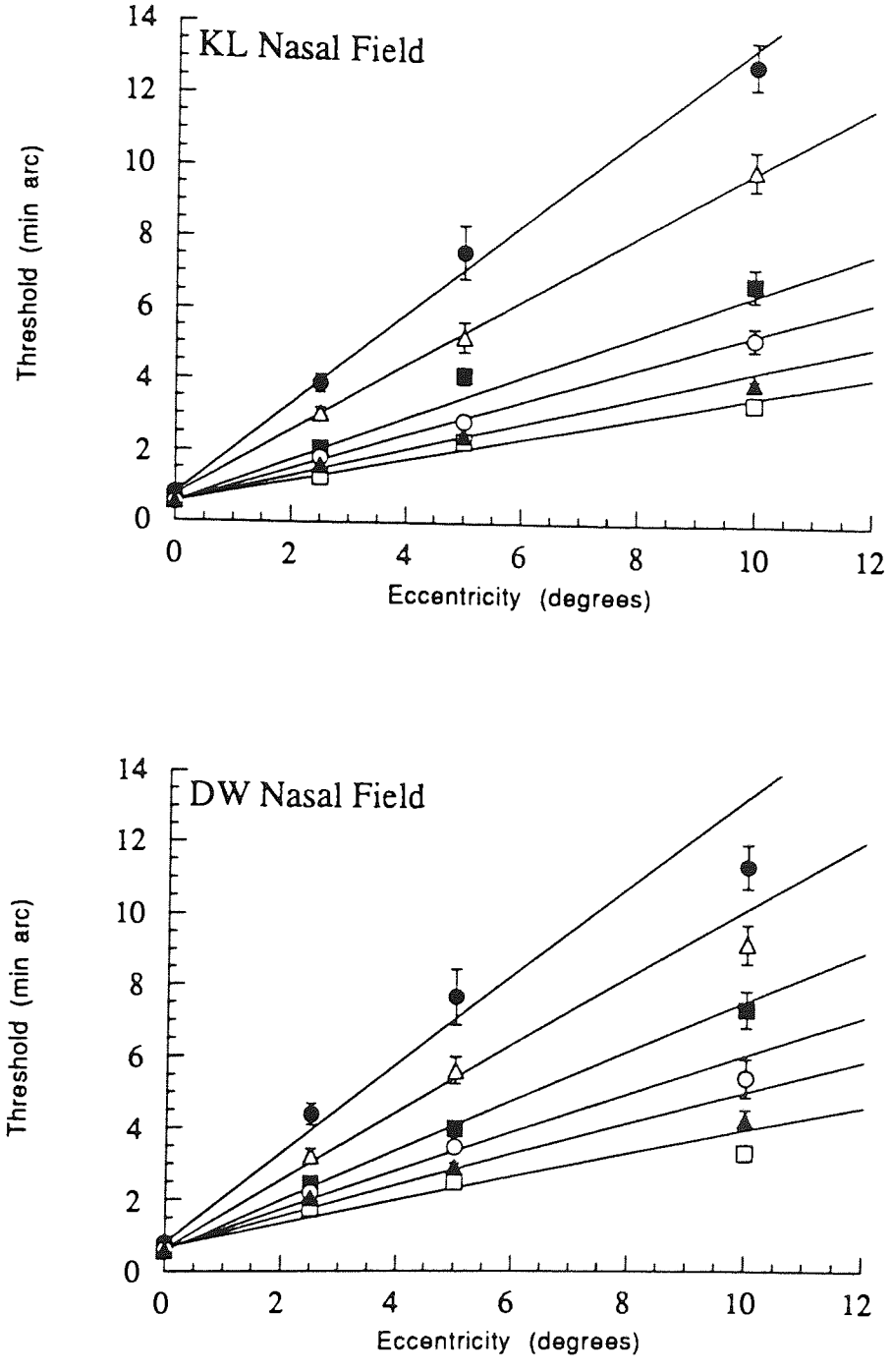

Figure 9.04. See subsequent page for legend.

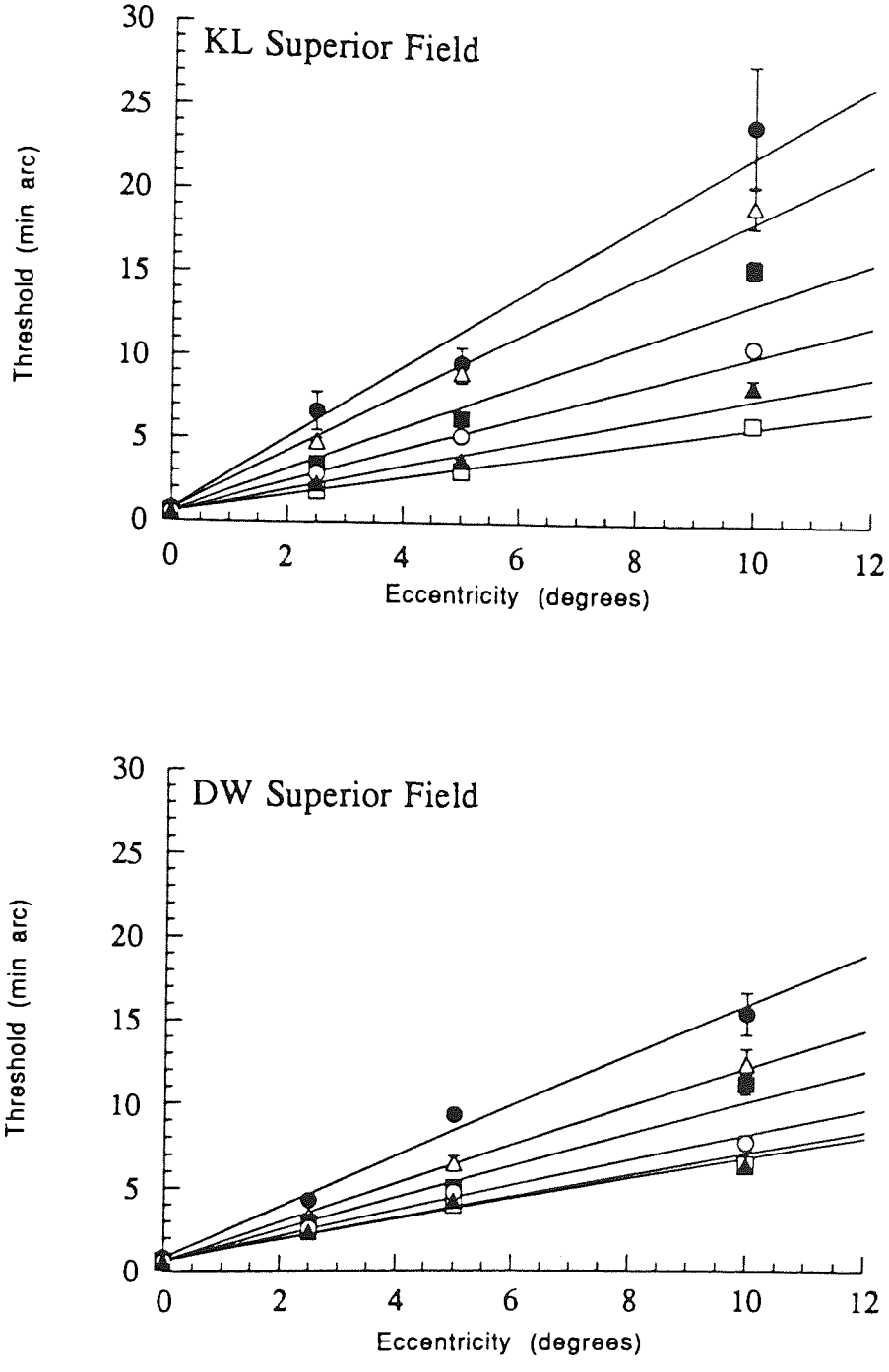

Figure 9.04. See subsequent page for legend.

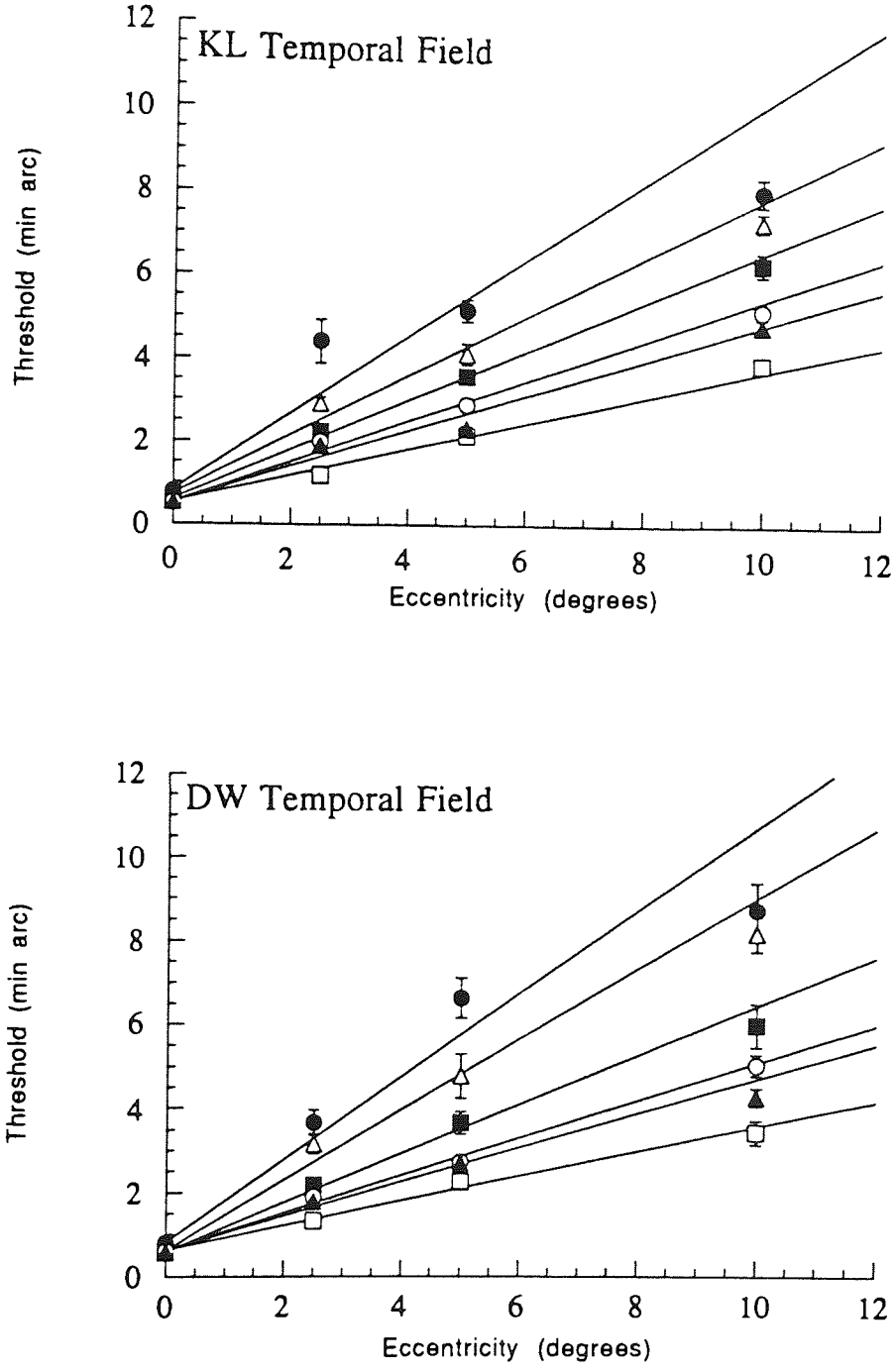

Figure 9.04. See following page for legend.

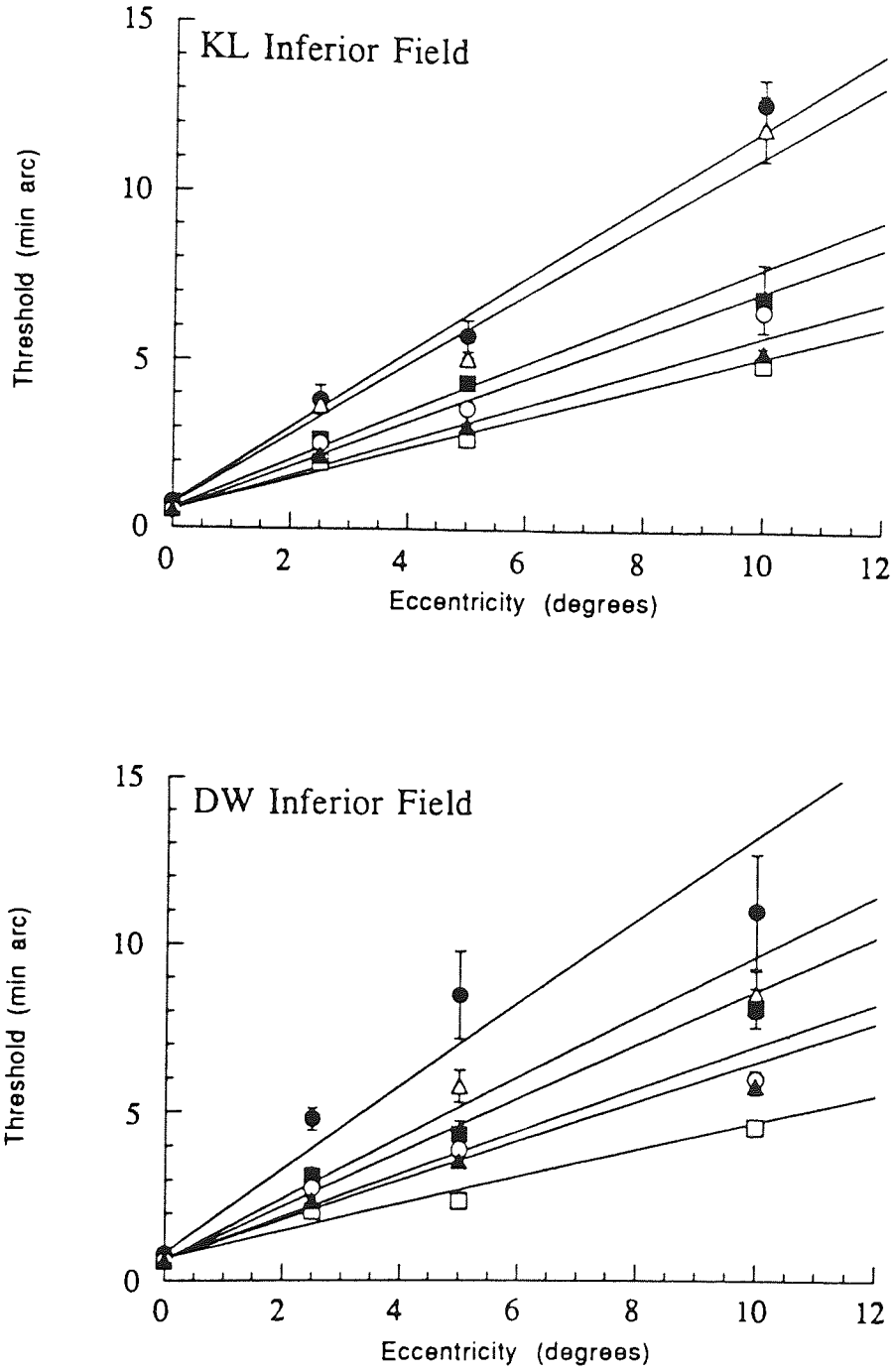

Figure 9.04. Resolution thresholds for discrimination of target orientation at various eccentricities, under several flanking conditions and visual field meridia. Subjects KL and DW. Open squares: unflanked conditions; filled circles: relative separation 0.5; open triangles: relative separation 1; filled squares: relative separation 2; open circles: relative separation 4; filled triangles: relative separation 7. Error bars show standard error.

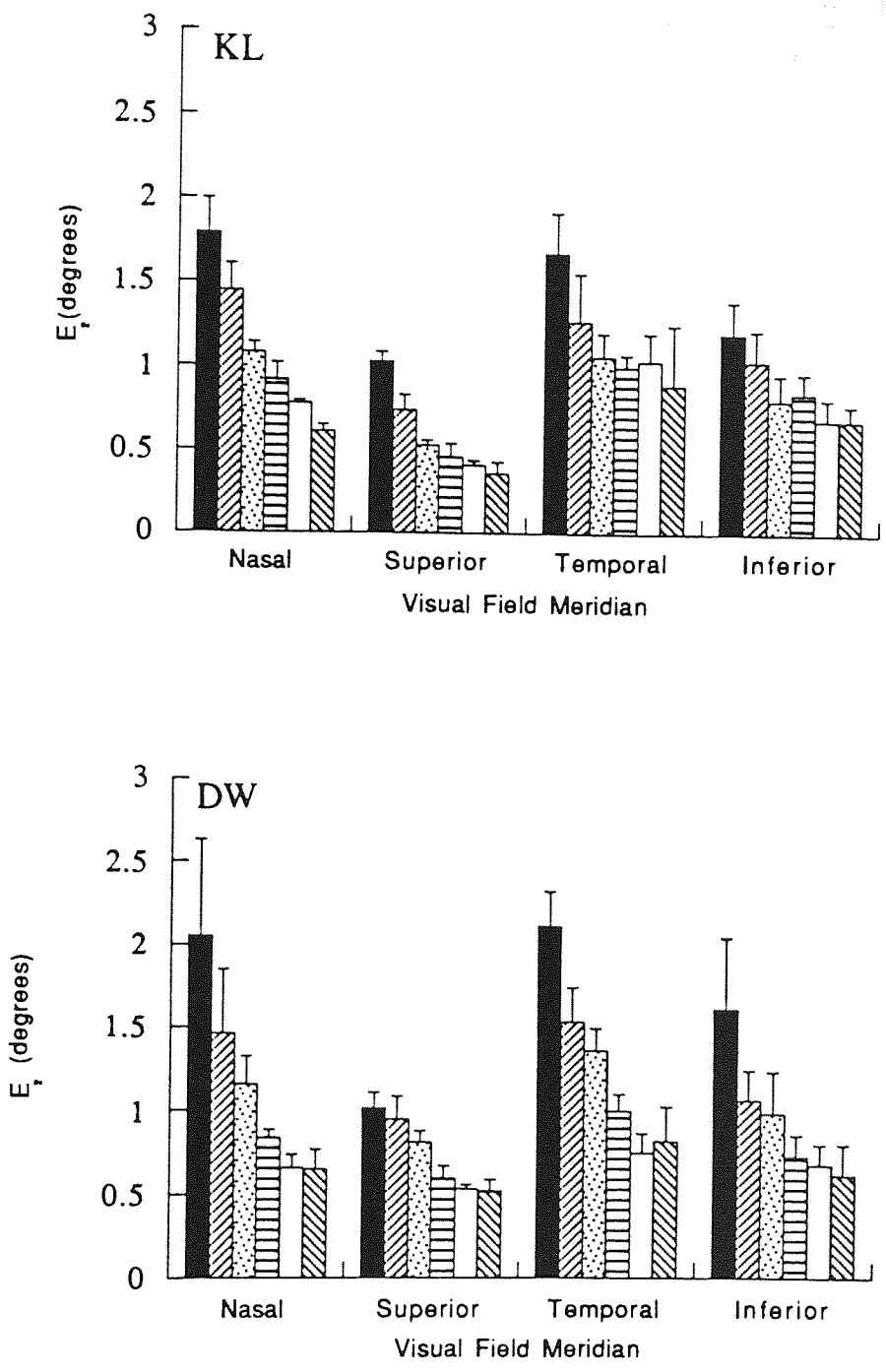

Figure 9.05. E_2 values derived from data in Fig 9.04 for each flanking condition and four visual field meridians. As flanks are placed closer to the target, E_2 becomes smaller, i.e. performance deteriorates more rapidly with increasing eccentricity. Black columns: unflanked condition; right to left diagonal striped columns: relative separation 7; spotted columns: relative separation 4; horizontal striped columns: relative separation 2; white columns: relative separation 1; left to right diagonal striped columns: relative separation 0.5. Standard error bars are shown.

Subject	Field meridian	E_2 (resolution)	E_2 (interference)
KL	Nasal	1.79±0.21°	0.17±0.01°
	Superior	1.03±0.06°	0.06±0.01°
	Temporal	1.69±0.24°	0.20±0.01°
	Inferior	1.21±0.19°	0.20±0.01°
DW	Nasal	2.05±0.58°	0.11±0.01°
	Superior	1.02±0.09°	0.12±0.01°
	Temporal	2.12±0.21°	0.15±0.01°
	Inferior	1.62±0.43°	0.09±0.01°

Table 9.01. E_2 values and standard errors, in degrees, for uncrowded resolution and for the extent of spatial interaction zones under all experimental conditions.

In Figure 9.06 thresholds for each flanking condition are expressed relative to the no-flank situation. The relative threshold indicates the magnitude of spatial interference, with a relative threshold of 1 showing the absence of any spatial interference. These relative thresholds are plotted against the absolute separation, s, between the target and flanking elements at threshold. Absolute separation was calculated as the product of the relative separation and the target width at threshold, with the latter value represented by 5 times the threshold bar width. Plotting the data in this way shows how the extent of the interaction zone changes with eccentricity. At the fovea, the flanking elements can encroach within 10 min arc of the target without having much effect on thresholds. However, at 10 degrees eccentricity, the equivalent distance is well over 100 min arc. The rate at which the interaction zones increased in size with eccentricity was estimated by the amount by which the peripheral data curves need to be shifted leftwards in order to fit the foveal curve. Values of F, the eccentricity-dependent scaling factor, were estimated by eye as in Chapters 6 and 8, and were plotted against their respective eccentricities. A regression of the form of Equation 4.01 fitted to the data allowed E_2 values to be derived, where the value of E_2 this time gives an indication of the rate at which the interaction zones increase in size with eccentricity. E_2 values for interaction zones for each meridian are shown in the second column of Table 9.01. They are very much smaller than E_2s for resolution (Figure 9.05, and Table 9.01), indicating that interaction zones increase in size much faster with eccentricity than the minimum resolvable gap size (Toet and Levi, 1992). As with resolution however, the smallest E_2 values for interaction zones tend to occur along vertical meridia, whilst the largest values are found along the horizontal meridia.

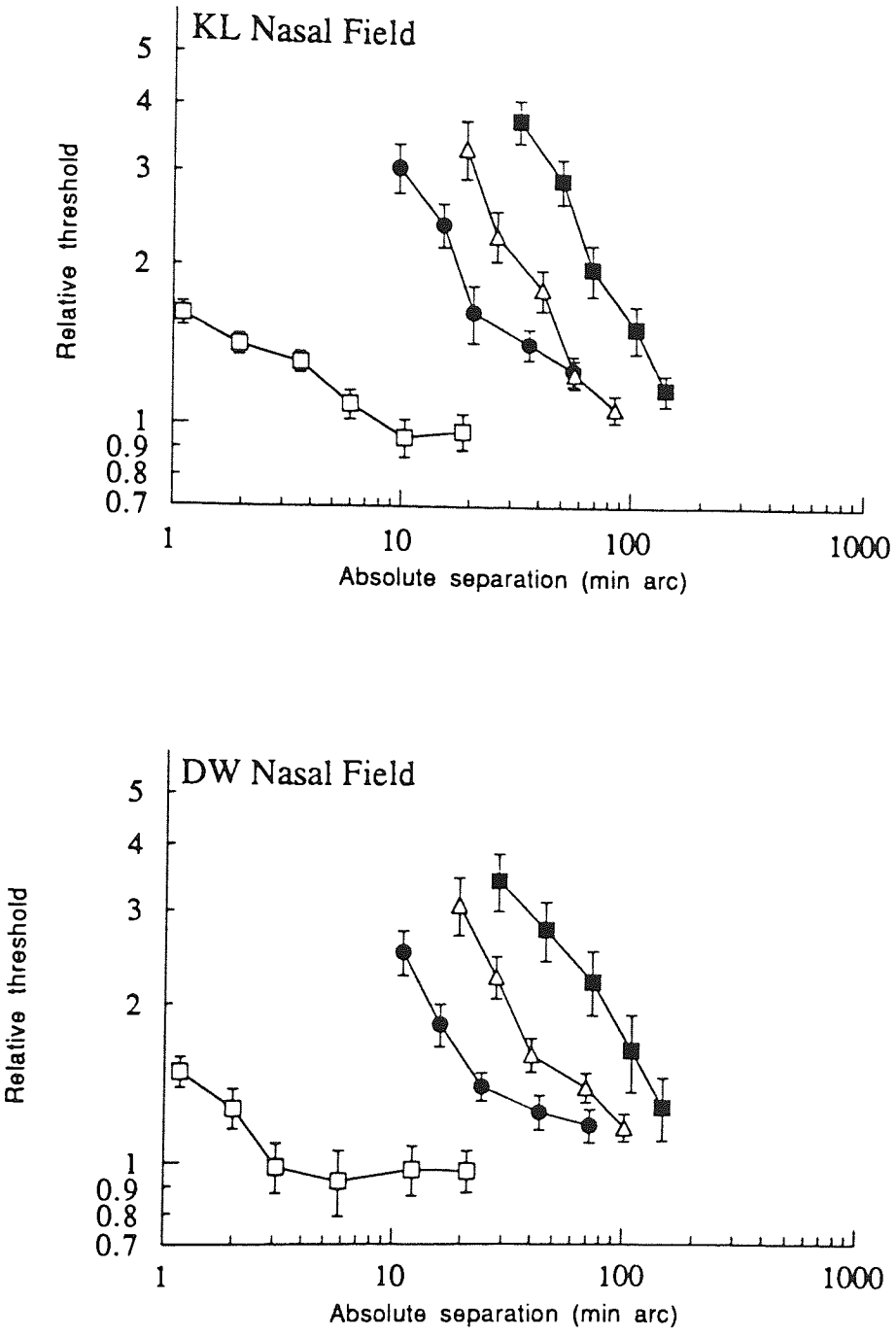

Figure 9.06. See subsequent page for legend.

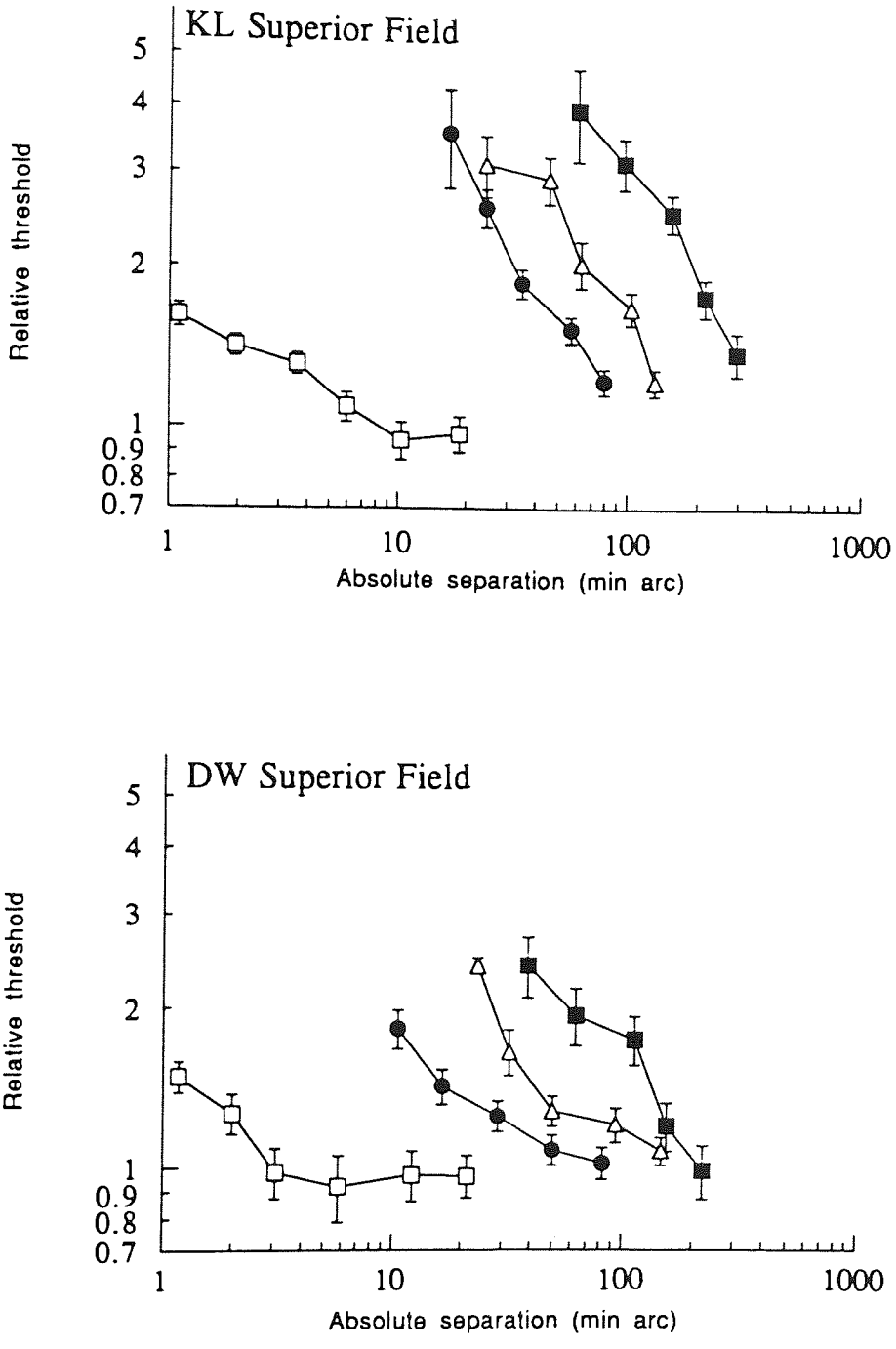

Figure 9.06. See subsequent page for legend.

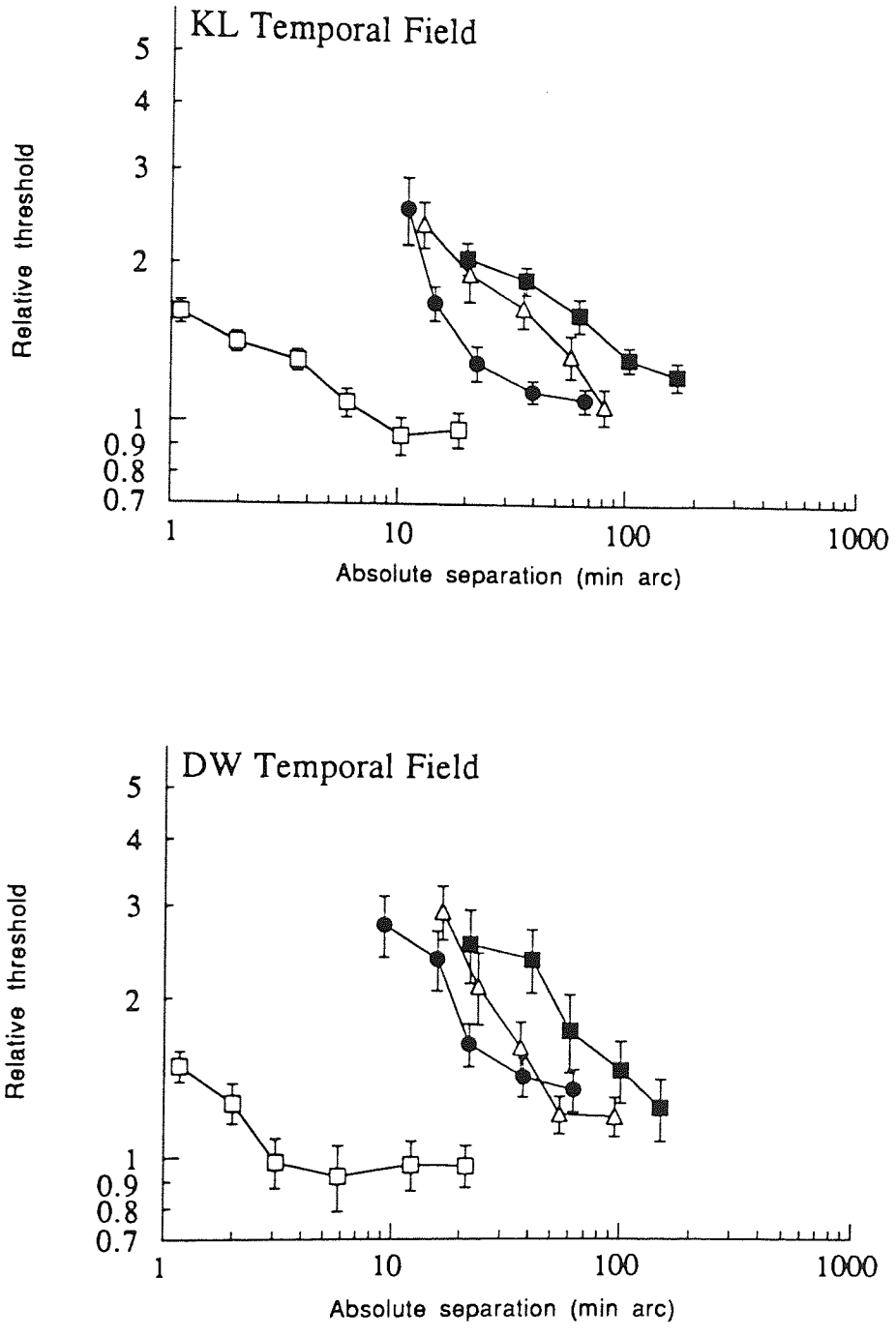

Figure 9.06. See following page for legend.

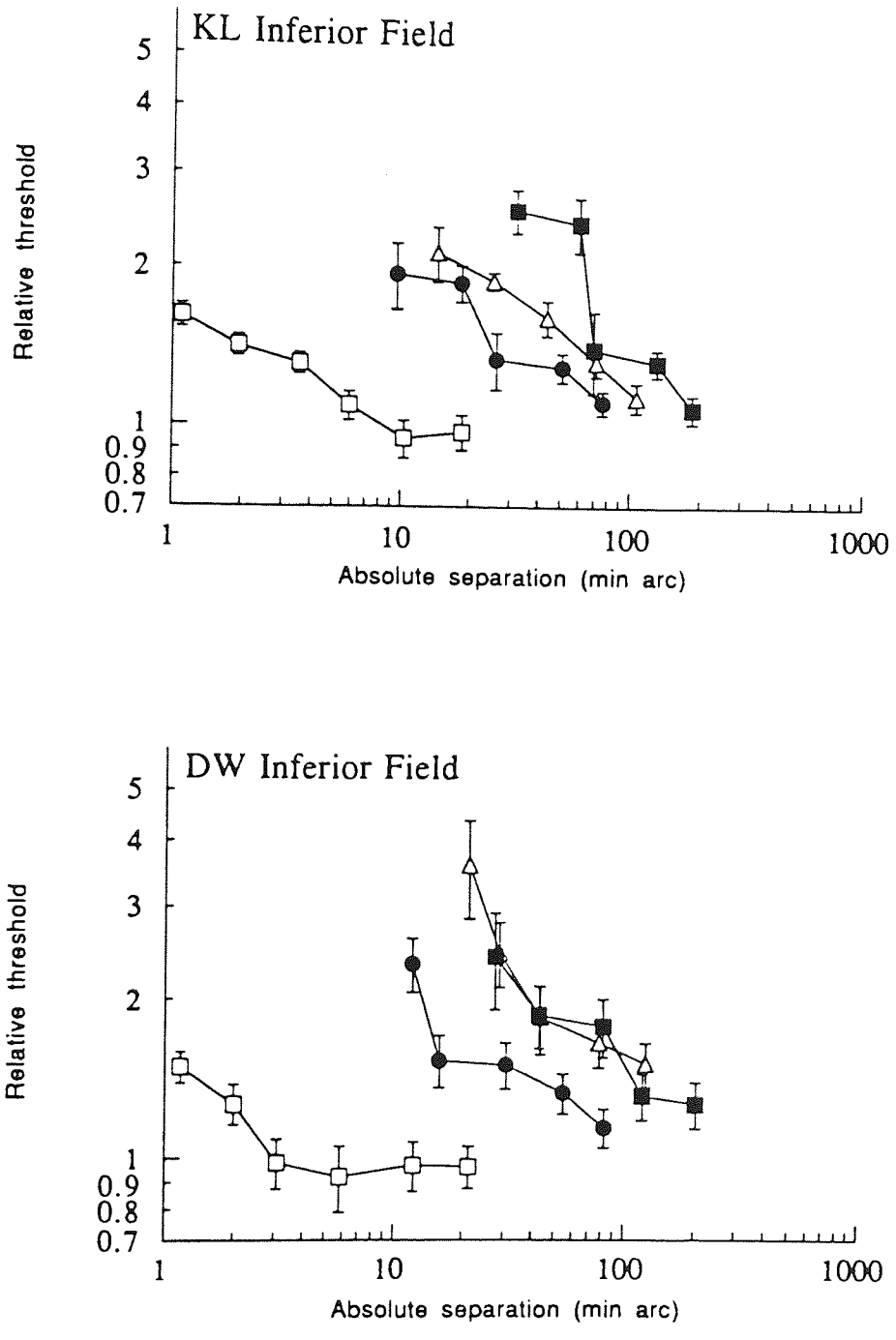

Figure 9.06. Thresholds for flanked conditions, expressed relative to unflanked thresholds, are shown plotted against the absolute separation (in minutes of arc) between targets and flanks at threshold. Open squares: 0°, filled circles: 2.5°, open triangles: 5°, filled squares: 10°.

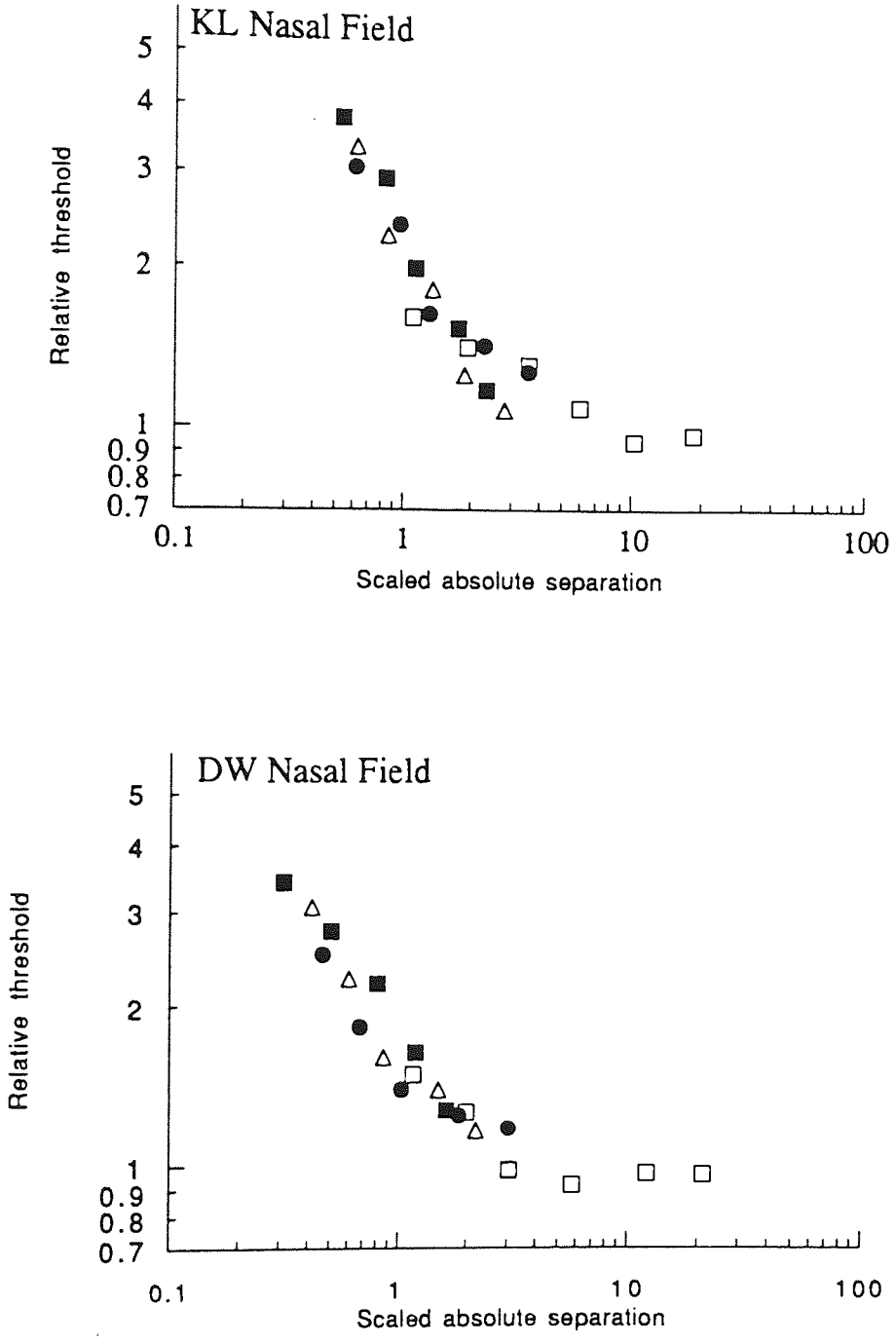

Figure 9.07. See subsequent page for legend.

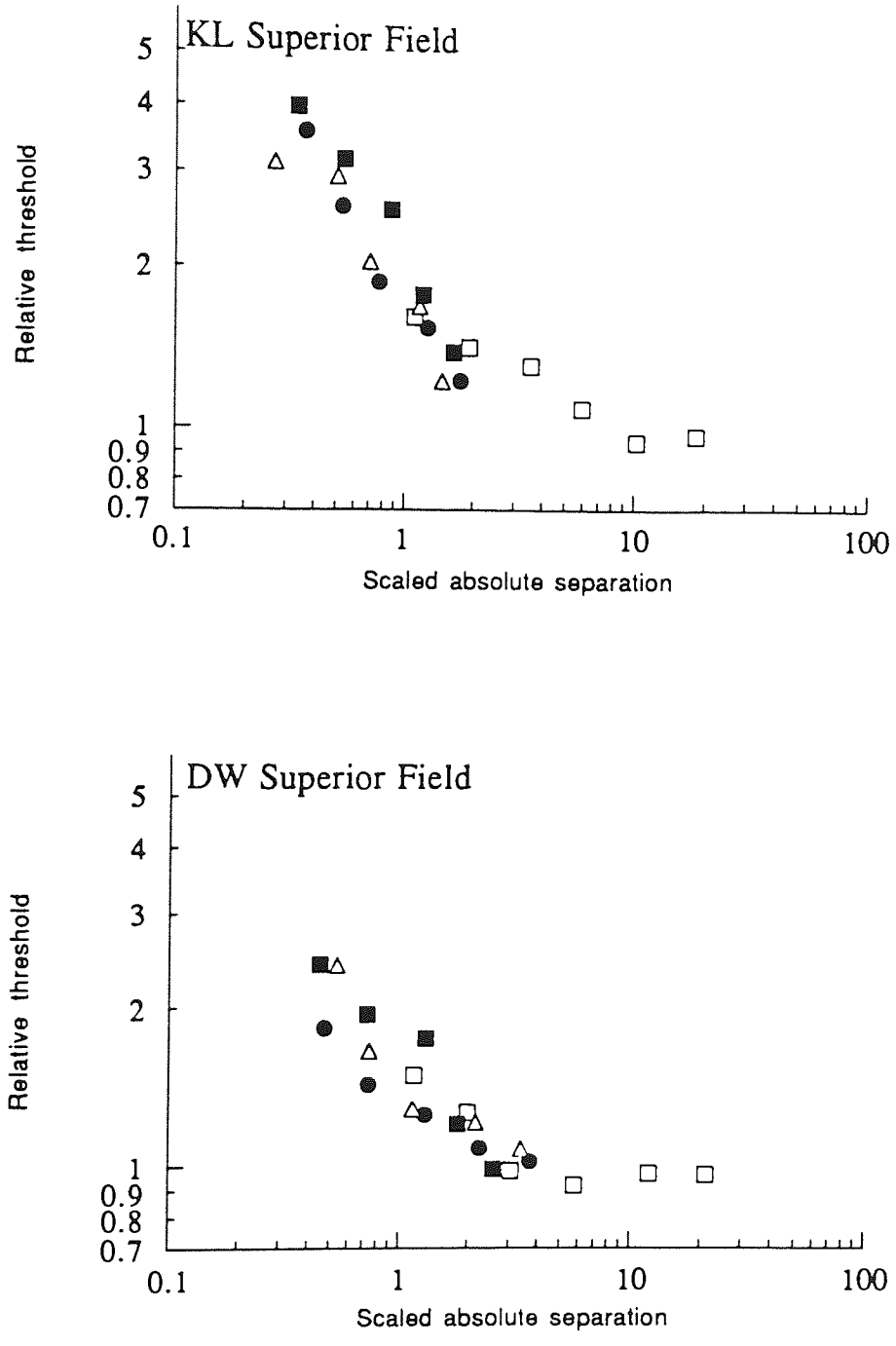

Figure 9.07. See subsequent page for legend.

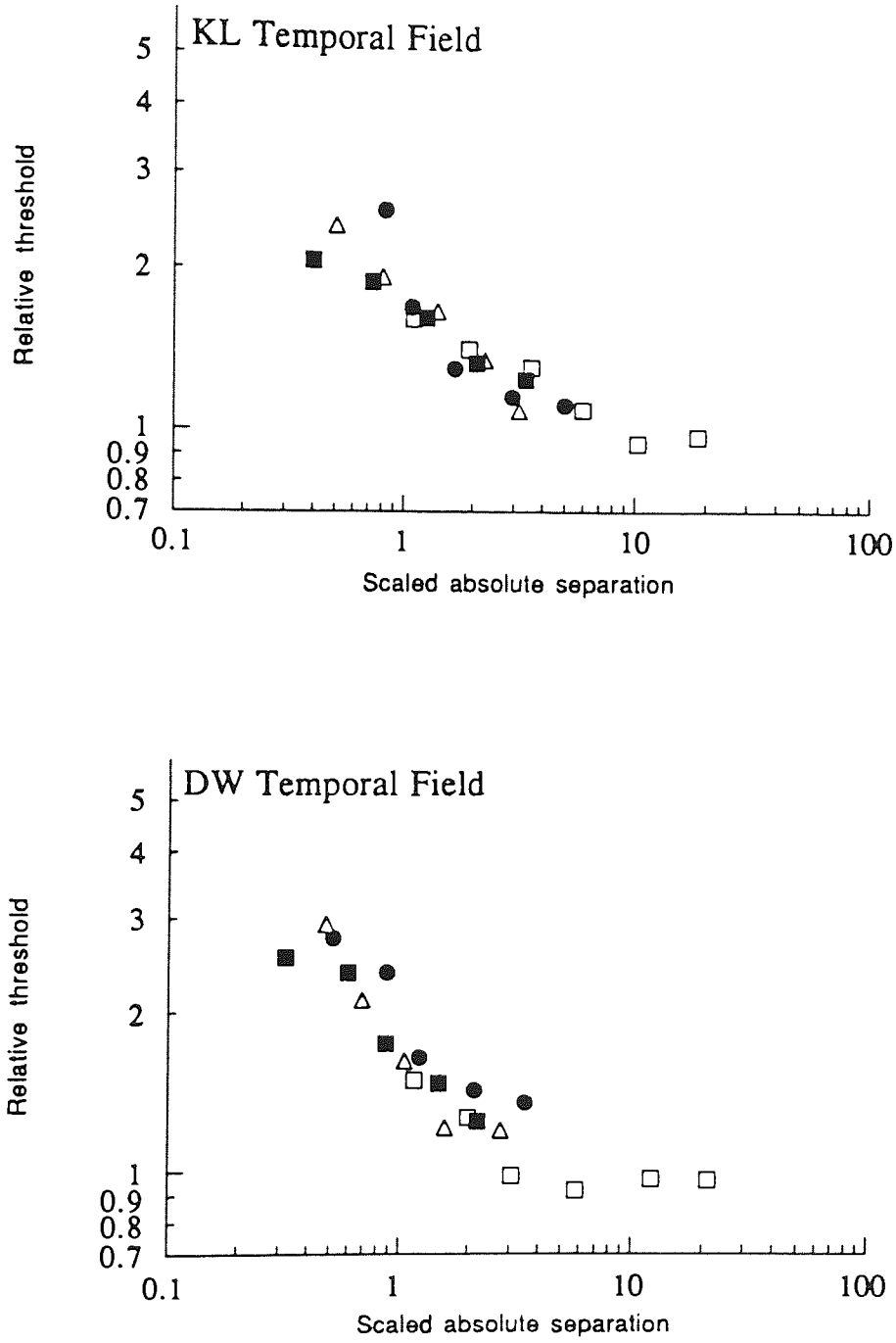

Figure 9.07. See following page for legend.

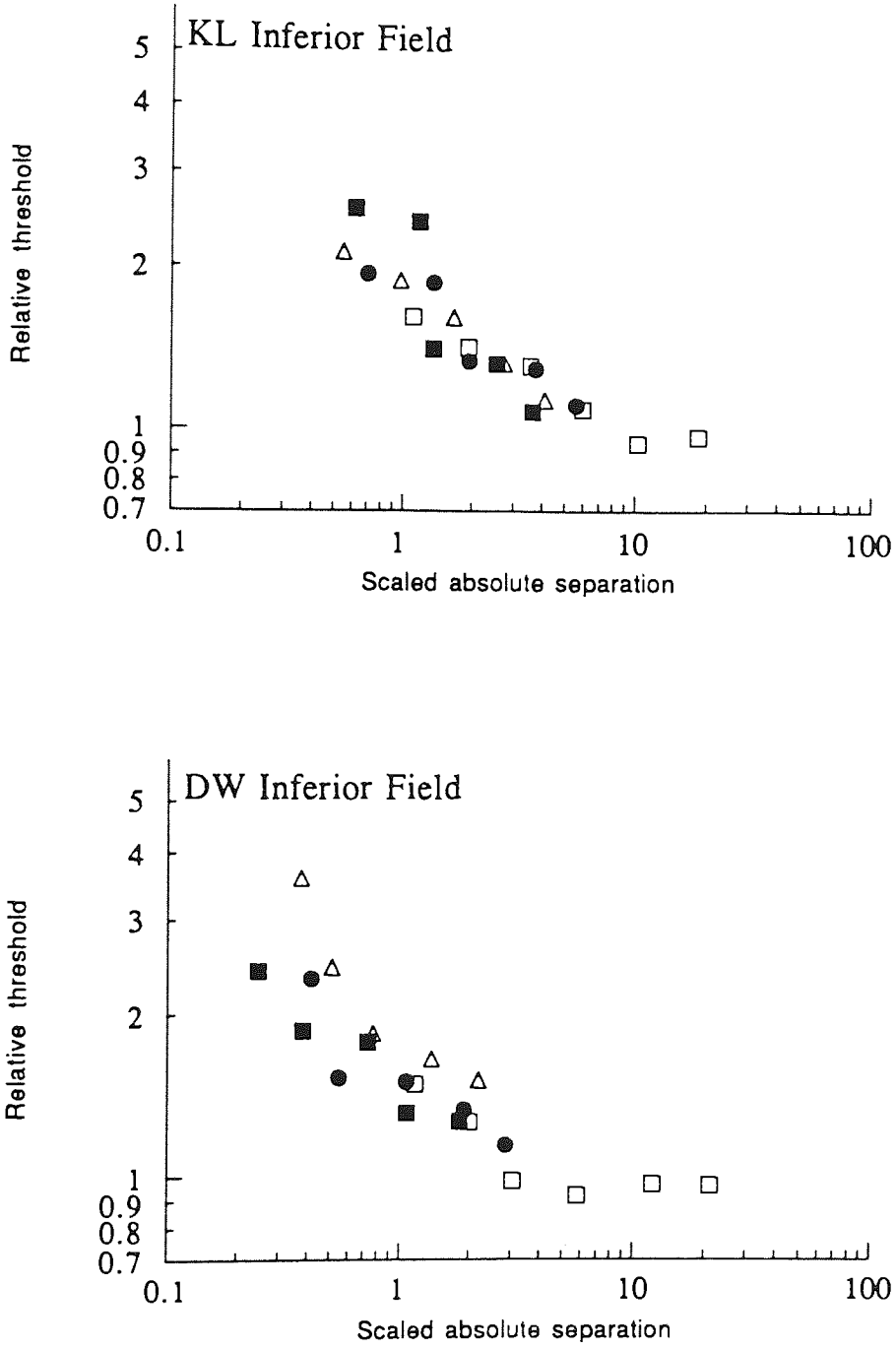

Figure 9.07. The data of Fig 9.06 after shifting each of the peripheral datasets leftwards along the x-axis according to scaling factors defined by the equation: $s_{scaled} = s / (1 + E / E_2)$, where s is absolute separation. The effect of this is to collapse the data from Fig 9.06 onto an approximately single function. Symbols as for Fig 9.06.

Figure 9.07 shows the data of Figure 9.06 plotted as scaled separation, s_{scaled}, obtained by dividing the actual separation, s, by the scaling factor F, ie:

$$s_{scaled} = s / (1 + (E / E_2)) \qquad \text{Equation 6.03}$$

This removes the eccentricity dependence from the data and indicates that spatial interference is qualitatively the same at all eccentricities, differing only in terms of extent. Figure 9.08 shows the complete data for the fovea and for each meridian, scaled according to the relevant E_2 value. The data are well described by a function of the form

$$T_{rel} = 1 + (k1 / s_{scaled}) \qquad \text{Equation 9.01}$$

where T_{rel} is the relative threshold, s_{scaled} is the scaled absolute separation and k1 is a constant. Thus, when s_{scaled} is very large T_{rel} equals 1, and so the flanked thresholds approximate to the unflanked thresholds, as would be expected when the crowding elements are far removed from the target. The actual foveal data points at large values of separation tend to fall slightly below the predicted values. This discrepancy is explained by the observation of both subjects that judging the orientation of the central target actually became easier when flanking targets were present (provided they were sufficiently far away to minimise spatial interference) since they provided multiple comparison examples to which the orientation of the central target could be compared. It might be suggested that the plateau should be allowed to float freely at large separations rather than constrain it to 1. When this is done, the fit obviously improves, as would be expected from the addition of an extra free parameter, but the effect is small (R^2 values increase from 0.910 to 0.917 for subject KL and from 0.876 to 0.887 for DW). However, constraining the plateau to a value of 1 seems to be preferable since it takes into account the more representative situation where the flanking stimuli are not spatially identical to the target, and thereby cannot provide any cue to the target's orientation.

If s_2 is now taken to be the scaled separation at which the unflanked threshold doubles (ie $T_{rel}=2$) then, from Equation 9.01:

$$2 = 1 + (k1 / s_2)$$

therefore $s_2 = k1$

so that, from Equation 9.01 $T_{rel} = 1 + (s_2 / s_{scaled})$ Equation 9.02

Least-squares regression analysis of the data in Figure 9.08, with each data point weighted according to its inverse variance, revealed values for s_2 of 0.73±0.02 for KL and 0.55±0.02 for DW. Further, substituting Eqn 6.03 into Eqn 9.02, the effect of flanking elements on resolution thresholds can be predicted by just two variables, their eccentricity (E) and their angular separation from the target (s), since

$$T_{rel} = 1 + [(s_2 / s) (1 + (E / E_2))] \qquad \text{Equation 9.03}$$

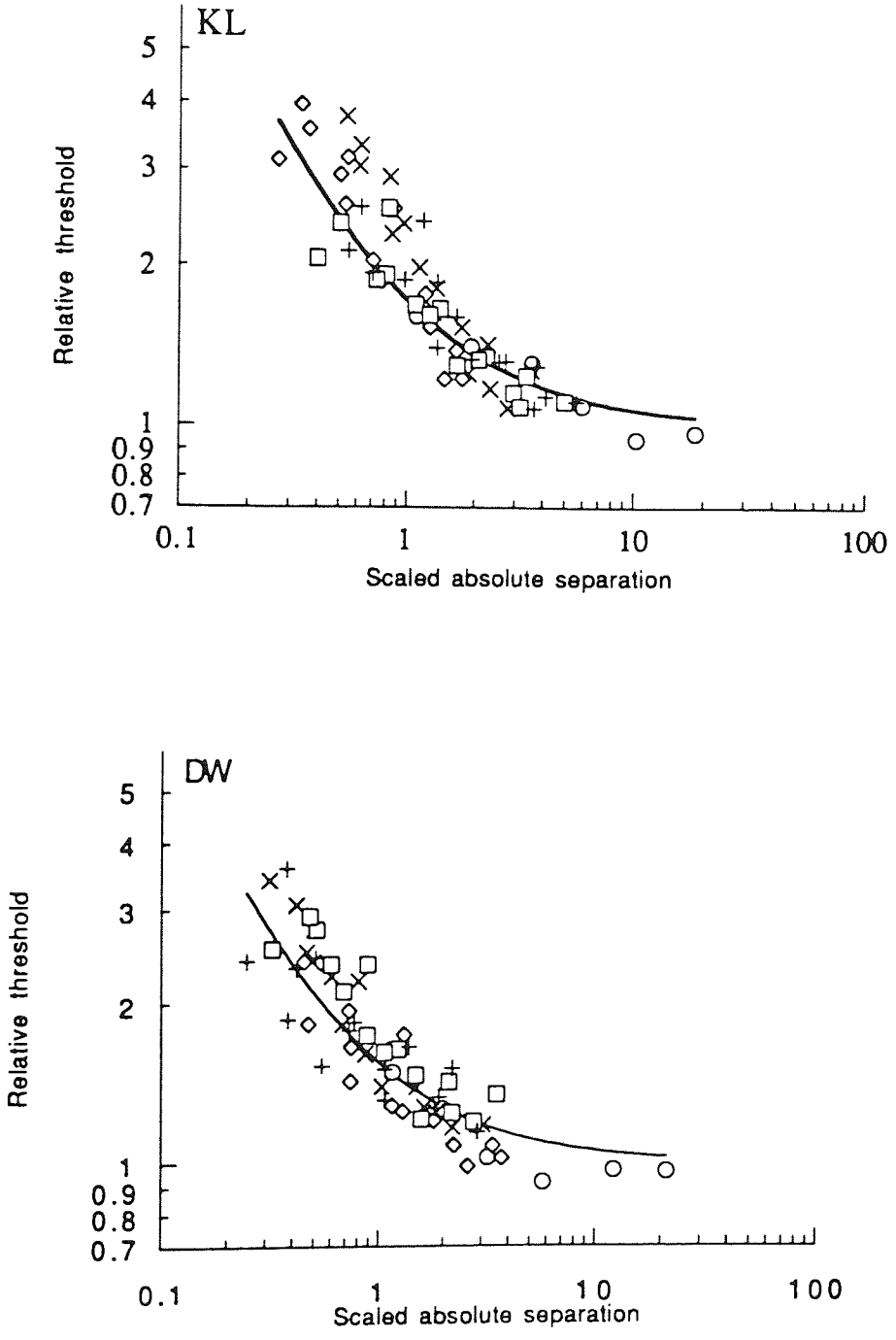

Figure 9.08. The scaled data of Fig 9.07 combined across visual field meridia. The data is fitted with a curve of the form of Equation 9.02: $T_{rel} = 1 + (s_2 / s_{scaled})$. For KL, $s_2 = 0.73 \pm 0.02$ minutes of arc whilst for DW, $s_2 = 0.55 \pm 0.02$ minutes of arc. Symbols: open circles: fovea; oblique crosses: nasal field; open diamonds: superior field; open squares: temporal field; ordinal crosses: inferior field.

9.4 Discussion

Previous interest in the effects of spatial interference have focussed on two factors - the magnitude of the effect and its spatial extent. Equation 9.03 specifies the magnitude of the interference for any given spatial separation. Quantifying the spatial extent of the interaction zone is rather problematic, since it depends critically upon the arbitrary decision as to when an interaction effect becomes significant. In other words, when is T_{rel} greater than unity? Bouma (1970) reports significant interaction effects at separations up to half the eccentricity (0.5E), and a zone of similar size has been found for interference with orientation discrimination (Andriessen and Bouma, 1976). It is clear, however, that these statements must be over-simplifications since they imply an infinitely small interaction zone at the fovea, which is plainly not the case (Flom et al., 1963b; Loomis, 1978; Levi et al., 1985; Toet and Levi, 1992). A more realistic viewpoint is given by Levi and Klein (1985) and Levi et al. (1985) where the extent of the zone of interference in a vernier acuity task is modelled in terms of a constant multiple of (E+k) where k is a constant. This view is similar to the present analysis, since Equation 9.03, averaged across subjects and meridia, becomes

$$T_{rel} = 1 + [(0.011 / s) (1+ (E / 0.14))]$$

where s is in units of degrees.

Rearranging,

$$s = (0.079 / (T_{rel}-1)) \times (E + 0.14) \qquad \text{Equation 9.04}$$

which gives, for any chosen value of T_{rel}, the extent of the interaction zone. For example, taking $T_{rel} = 1.5$ (as in the study of Toet & Levi, 1992), the extent of the interaction zone becomes 0.16(E + 0.14) degrees. At anything other than very small eccentricities, of course, the constant of 0.14 becomes insignificant. Hence, an approximation to Bouma's interference zone of 0.5E can be obtained by choosing $T_{rel} = 1.16$. However, the arbitrary nature of such attempts at quantifying the spatial extent of zones of interference is rather unsatisfactory, since the zones should be viewed as continuous in nature, as is shown in Figure 9.09 which depicts Equation 9.04 graphically. In Figure 9.09 the vertical solid lines represent the resolution thresholds for eccentricities 0, 2.5, 5 and 10 deg. The dotted lines show the threshold level which would be observed if flanks were placed at that location relative to a target at the location indicated by the resolution threshold. The magnitude of spatial interference is seen to be a rapidly declining function with distance from the target with no defined 'cut-off' point, showing that the decision as to the point at which interference has become significant is somewhat arbitrary. The extent of spatial interference (denoted by the width of the dashed line functions) can be seen to increase far more rapidly with eccentricity than resolution thresholds (denoted by the height of the solid lines), and depends on the magnitude of threshold rise taken to indicate significant interference.

Further, at no eccentricity does the extent of spatial interference fall to zero. Even at the fovea, interference extends over a small, but finite range. It is clear that spatial interference constitutes a factor of relatively greater importance in peripheral vision, since the extent of interaction zones increases in the periphery at such a faster rate than resolution. No doubt this has implications for people who habitually use their peripheral retina, for example, eccentrically fixating amblyopes and low vision patients with central field loss.

Two limitations of the model derived in Equation 9.03 which restrict its general applicability should be noted. First, four flanks were used which were spatially identical to the target. It is well established (Nazir, 1992; Kooi et al., 1994) that the effect of flanks is dependent on their similarity to the target, with flanks of greater similarity causing greater interactions. If the experiments were repeated with different types of flanking elements, then the magnitude of the spatial interference function (Equation 9.03) would be expected to change. Such variations might be in terms of colour, shape, contrast polarity, luminance, eye of origin, or stereoscopic depth (Kooi et al., 1994). Further, this experiment, unlike that of Toet and Levi (1992), was not designed to dissociate the tangential and radial dimensions of the interaction zone. Toet and Levi found that interaction zone dimensions increased faster with eccentricity for flanks which were positioned tangentially to the target (E_2 = 0.18 deg) rather than radially (E_2 = 0.34 deg). The present E_2 values for spatial interference of 0.1-0.2 deg presumably reflects a combination of crowding effects in these two directions.

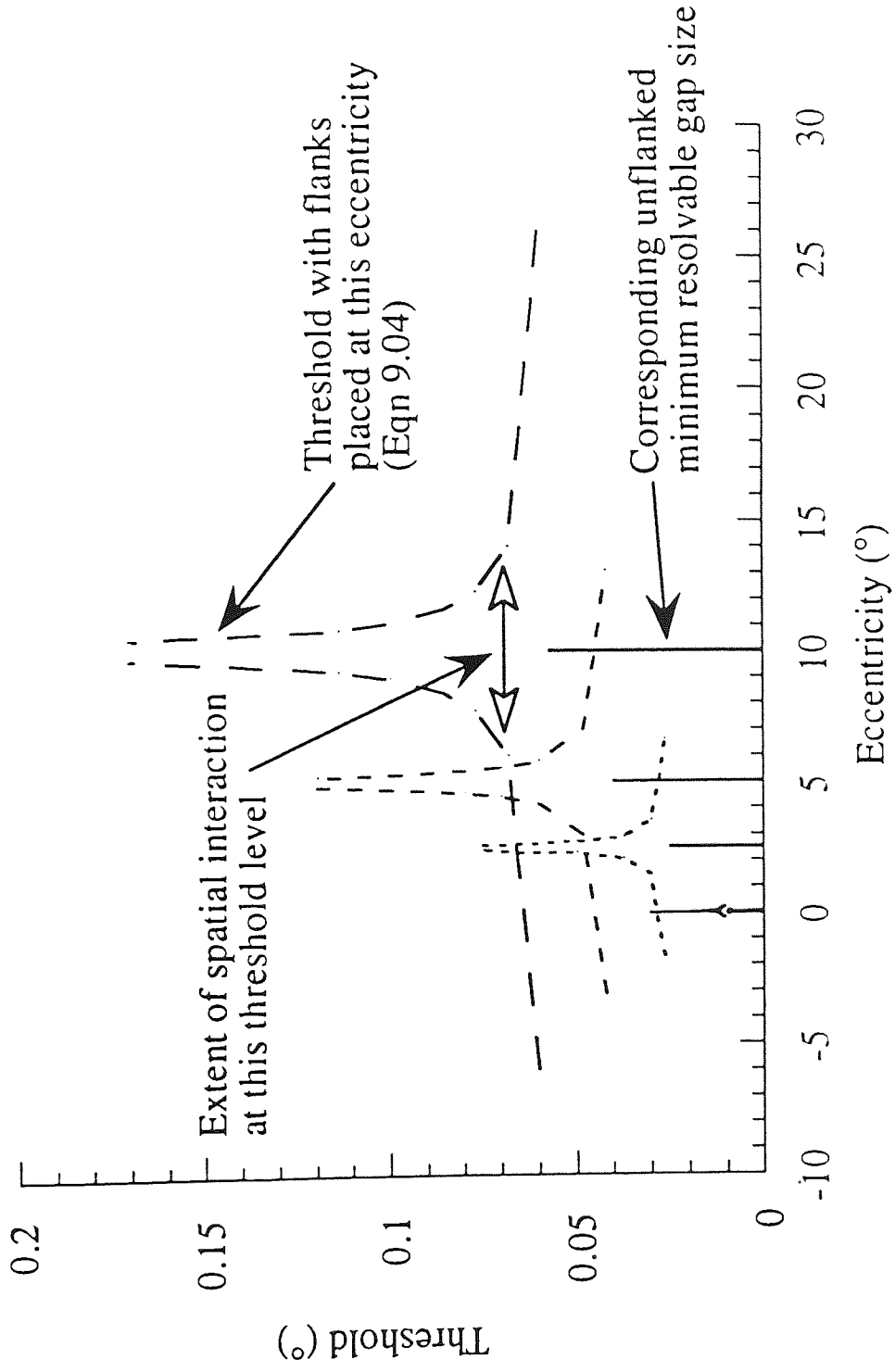

Figure 9.09. Graphic depiction of Equation 9.04. See text for explanation.

The results demonstrate that a range of E_2 values can be obtained from a combination of two factors, which individually have markedly different eccentricity dependencies. These two factors are resolution, with an E_2 value of 1.0-2.0 deg, and spatial interference, with an E_2 of 0.1-0.2 deg. As flanking elements are placed closer to the target, the weighting of the interference factor in the task becomes greater, and the E_2 value is progressively reduced from that for resolution alone. In this way one can envisage that the E_2 for any specific task depends on which factors influence thresholds, and their relative weighting in the task. The large range of E_2 values which occur for different tasks may therefore be explained by the combined effects of a relatively small number of fundamental factors which determine visual performance. The eccentricity dependence of these factors might vary markedly, depending on where in the visual pathway performance is limited. Limitations may, for example, occur at an optical, retinal or at some cortical level. However, despite recent advances in understanding the limits imposed by front-end mechanisms (Banks et al., 1991; Drasdo, 1991; Anderson et al., 1991), the eccentricity dependencies introduced at successive physiological levels of the visual pathways are not yet well established. These considerations are crucial to the present findings since it is clear that resolution and spatial interference arise at different physiological levels within the visual pathway. Whereas resolution thresholds can be predicted in terms of optical and retinal factors alone (Anderson et al., 1991), spatial interference must arise at a postchiasmal level, beyond the level of monocular convergence (Andriessen and Bouma, 1976; Levi et al., 1985; Flom, 1991; Toet and Levi, 1992; Kooi et al., 1994), since dichoptic experiments which have presented targets to one eye, and flanks to the other find approximately as much spatial interference as is found monocularly (Flom, Heath and Takahashi, 1963a; Westheimer and Hauske, 1975; Levi et al., 1985; Kooi et al., 1994).

In conclusion, the results show that resolution and spatial interference are qualitatively similar across the visual field, differing only in quantitative size scale. The quantitative change of scale is markedly different for the two factors, with E_2 for resolution being 1.0-2.0 deg and that for spatial interference being 0.1-0.2 deg. The results therefore reflect one example of the situation where two factors which arise at different levels of the visual system and have quite distinct retinotopic distributions combine to produce intermediate rates of performance change as a function of eccentricity. The weighting of each factor in determining the overall level of performance is clearly dependent upon the spatial (and presumably also temporal) characteristics of the stimulus, and it is these which define the task itself.

Chapter 10
Word recognition and reading

10.1 Introduction

While resolution (Chapter 9) and letter recognition tests are of great value in research and clinical settings, in the real world people use such abilities in order to be able to read. Considerable evidence exists to support the view that low vision patients with central visual loss cannot read as fast as those with intact central fields, even after training (Legge, Rubin, Pelli and Schleske, 1985b; Whittaker and Lovie-Kitchen, 1993; Cummings, Whittaker, Watson and Budd, 1985). In addition, despite enlargement of letter size to compensate for eccentric viewing, peripheral reading speed in normal observers does not approach that achieved using the fovea (Turano and Rubin, 1988). It would therefore appear that the peripheral visual field is qualitatively inferior to the fovea for the task of reading, a suggestion which has also been made for the task of phase discrimination (Rentschler and Treutwein, 1985; Bennett and Banks, 1987; Stephenson et al., 1991; also Chapter 4). Such observations of an inferiority of peripheral vision are contrary to most other aspects of visual performance, which can be made equivalent at different eccentricities simply by a change of size (Rovamo and Virsu, 1979; Koenderink et al., 1978; Virsu et al., 1987; Whitaker et al., 1992a; Chapters 6-9).

It is well established that resolution performance deteriorates more rapidly with eccentricity for test targets surrounded by flanking stimuli (Jacobs, 1979; Toet and Levi, 1992; Chapter 9). This is due to a rapid increase in the size of spatial interference zones on moving away from the fovea (Toet and Levi, 1992; Chapter 9). Peripheral targets are relatively more 'crowded' and less easily recognised than central targets when letter separation is kept constant and eccentricity is varied. As a possible means of counteracting this effect, Toet and Levi (1992) have suggested that text viewed peripherally might benefit from further increase in letter spacing in addition to magnification.

Reading is a complex task involving visual sensory input, accurate eye movements, and higher cognitive aspects of comprehension. Despite the obvious importance of reading skills in extrafoveal regions for low vision patients, there is doubt as to the origin of their deficit in performance. The aforementioned task complexity has no doubt contributed to this situation. In this study it is investigated whether there are any circumstances under which peripheral word recognition can be made equal to that at the fovea, and consider the possible advantage to be gained by increasing letter separation

at a faster rate than the increase in letter size (Toet & Levi, 1992). Further, it is asked whether the documented deficits in peripheral reading performance can be explained by psychophysical aspects of word recognition, or whether they lie in other areas such as cognitive processing abilities or the accuracy of saccades.

The study investigates the performance of three tasks at various locations in the visual field. These tasks are size thresholds for word recognition, word recognition rates for random strings of unrelated words, and reading rates using meaningful sentences.

10.2 General Methods

Stimuli were presented on the face of a Macintosh M1212 Colour Display (see Chapter 5 for details). Stimulus presentation was controlled by software written and compiled in Microsoft Basic and run on a Macintosh Centris 650 PC. Black letters of luminance 5 cd/m^2 were presented on a white background of 115 cd/m^2, giving a Michelson contrast of 92%, and the monitor was masked by a wide (60 cm square) equiluminant surround.

In Experiments 1 and 2, each trial presentation consisted of one of ten words presented in uppercase sans serif Helvetica font. The proportional spacing of the font was replaced with a fixed spacing so that each letter was separated from the next by a constant edge-to-edge separation. Each word presented consisted of five letters, the first and last being random letters used to standardise the crowding effect. These letters were to be ignored during word identification, and varied from trial to trial. The central three letters made up one of the following words: APE, AXE, PEN, PEA, PAN, PAD, BED, BAD, DAD and VAN. These words were constructed from the limited number of letters which possessed the same boxed dimensions within the font. The vertical boxed dimension was always 30% larger than the horizontal. The stimulus arrangement is shown in Figure 10.01. The task of the observer was to correctly identify the word, i.e. it was a 10 alternative forced choice procedure. A selection of unrelated words were used in order to reduce as far as possible the confounding effects of text comprehension. The effects of spatial interference, or 'crowding', were also standardised by the use of single words whose letters (including the outer ones) were all surrounded by other letters at the same separation.

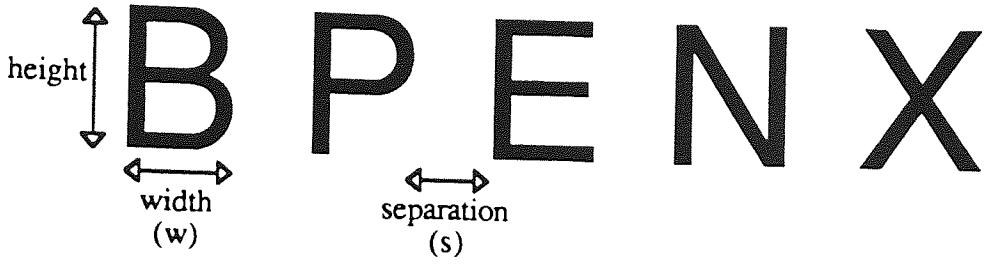

Figure 10.01. The stimulus configuration for Experiments 1 and 2 consists of five letters. The central three letters make up a word, which the observer has to correctly identify; the outer two letters are random, and are present to standardise the spatial interference for each of the letters in the target word. Each letter is drawn within an imaginary box, whose vertical dimensions are 30% larger than the horizontal. The width of the letter (w) in minutes of arc defines the letter size. Letter spacing is measured as the edge-to-edge separation of adjacent letters (s), and is expressed in multiples of letter width.

Stimulus size was defined as the width of the capital letters, depicted by w in Figure 10.01, and was varied by a combination of changing letter size on the screen and varying viewing distance. All stimuli were simply magnified or minified versions of one another. Letter separation in the first two experiments was defined by the edge to edge separation of the characters, and is depicted by the distance s in Fig 10.01. Separations were defined in terms of multiples of letter width, and these were 0.25, 0.50, 0.75, 1.0, 1.5, 2 and 3 times the width. Eccentricities of 0, 2.5, 5 and 10 deg in the inferior visual field were examined, and eccentricity was defined as the angle between fixation and the centre of the letter string. A fixation target was provided by a small dark spot placed on the screen or surround.

Three observers participated in the experiments: KL and DW, who were experienced observers, and MR, who was naïve as to the purpose of the experiment. All observers underwent training in the task before data collection began. The observers were aged 25, 31 and 21 years respectively, were all moderately myopic (<4.50DS) and wore their distance refractive correction for the experiments. Data collection was monocular using the dominant eye. Dominance was determined subjectively using a pointing test.

10.3 Experiment 1: Word recognition

10.3.1 Methods

The purpose of this experiment was to determine threshold letter sizes at different visual field locations for words having various letter separations. For each separation, a viewing distance was chosen based on data from pilot experiments. Threshold was then determined using a staircase technique. After each 500 ms presentation, a correct word identification made the following word size smaller in every dimension, whilst an incorrect response made the following word size larger. Step size was limited by the available font sizes, and varied between 0.067 and 0.08 log units, with an average of 0.075 log units. The procedure stopped after 8 reversals, with threshold being accepted as the mean letter size from the last 6 of these. Final threshold was taken as the mean of at least four staircase runs.

10.3.2 Results

Figure 10.02 depicts threshold letter sizes for word recognition as a function of eccentricity, for all the separations examined. A regression of the form:

$$\log(Te) = \log(To) + \log(1 + (E / E_2)) \qquad \text{Equation 2.10}$$

was applied to the data for each letter separation (see Chapter 2). The data are shown on linear axes in Figure 10.02 however, in order to highlight the linear rise in thresholds with increasing eccentricity. In Equation 2.10, Te represents the peripheral word recognition threshold, To is the foveal threshold, E is eccentricity and E_2 describes the rate of change of letter size with eccentricity. E_2 values are given in Table 10.01. As the letter separation increases, the more stretched words require less magnification to be seen in the periphery, and the gradient of the functions shown in Figure 10.02 flatten, raising the E_2 value.

Separation (letter widths)	E_2 (degrees)		
	KL	DW	MR
0.25	0.67±0.05	0.68±0.04	0.75±0.13
0.50	0.66±0.05	0.68±0.06	0.79±0.14
0.75	0.70±0.09	0.65±0.07	0.71±0.06
1.00	0.81±0.09	0.80±0.03	0.83±0.07
1.50	0.73±0.05	0.82±0.10	0.81±0.15
2.00	0.76±0.04	0.90±0.12	0.80±0.12
3.00	0.89±0.05	0.90±0.06	0.89±0.07

Table 10.01. E_2 values and standard errors, in degrees, for word recognition thresholds under all experimental conditions.

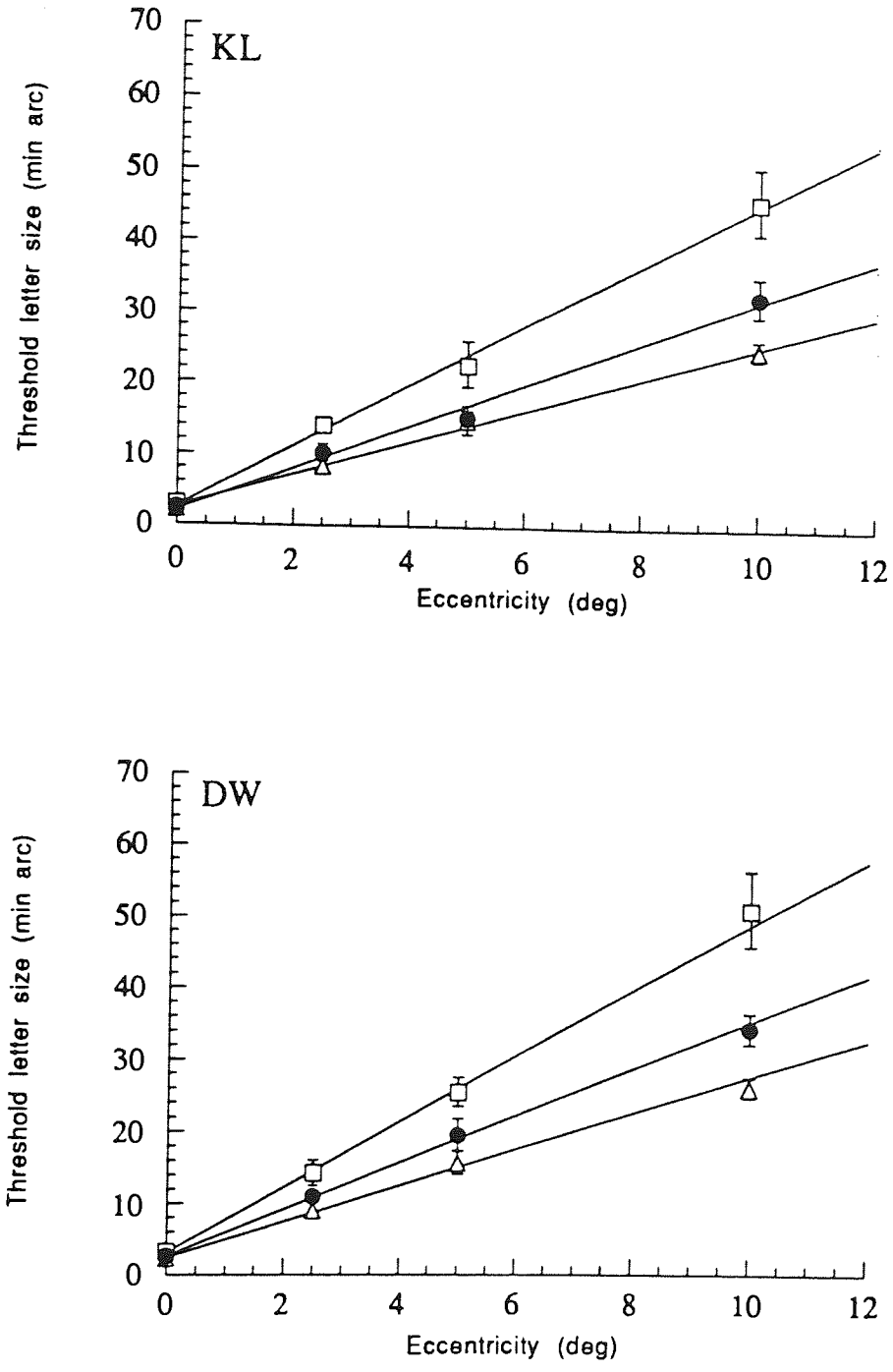

Figure 10.02. See following page for legend.

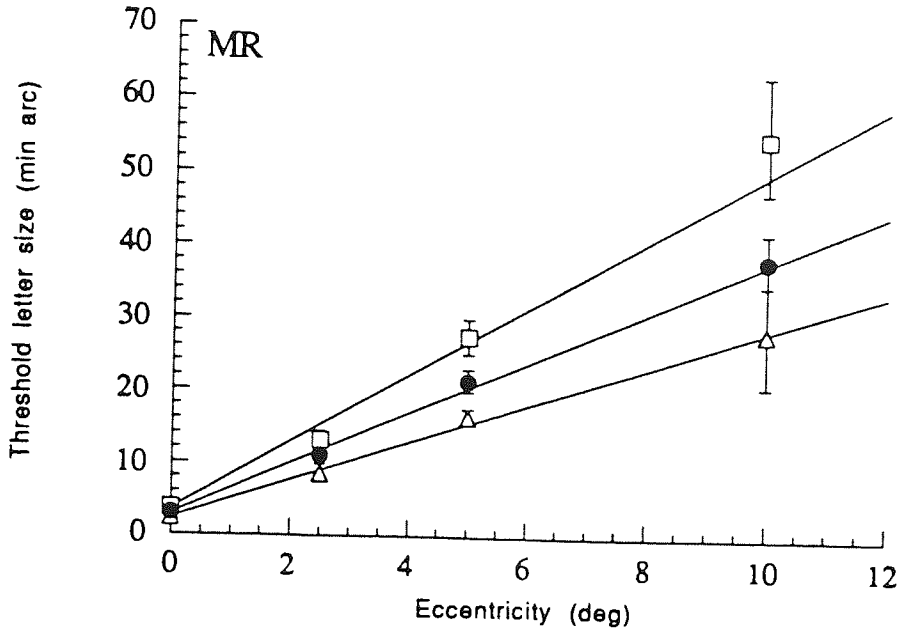

Figure 10.02. Threshold letter width (min arc) for identification of a three letter word embedded in a five letter string is shown for various eccentricities, under several letter spacing conditions. Thresholds rise approximately linearly with eccentricity under all conditions. E_2 values are derived from the best fit regression through the data points on log axes (Table 10.01). Subjects KL, DW and MR. Open squares: 0.25 letter widths edge-to-edge separation; filled circles: 1 separation; open triangles: 3 separation. Error bars show standard error of the mean. The other separations examined are omitted for clarity.

From Figure 10.02, it can be seen that at a specific eccentric location, threshold letter size is smaller for words of greater letter spacing. However, it cannot be concluded from this observation that with greater letter spacing, overall word lengths are shorter. A representation of overall word length can be achieved by calculating the threshold size of the three letters plus two spaces comprising the three letter word. Figure 10.03 shows how threshold word lengths vary with separation at all eccentricities examined. As separation increases beyond one letter width, word lengths increase in size. Therefore, although with larger letter separations threshold letter size is smaller, the reduction in size is outweighed by the greater gap size, and threshold word lengths actually increase slightly at larger separations.

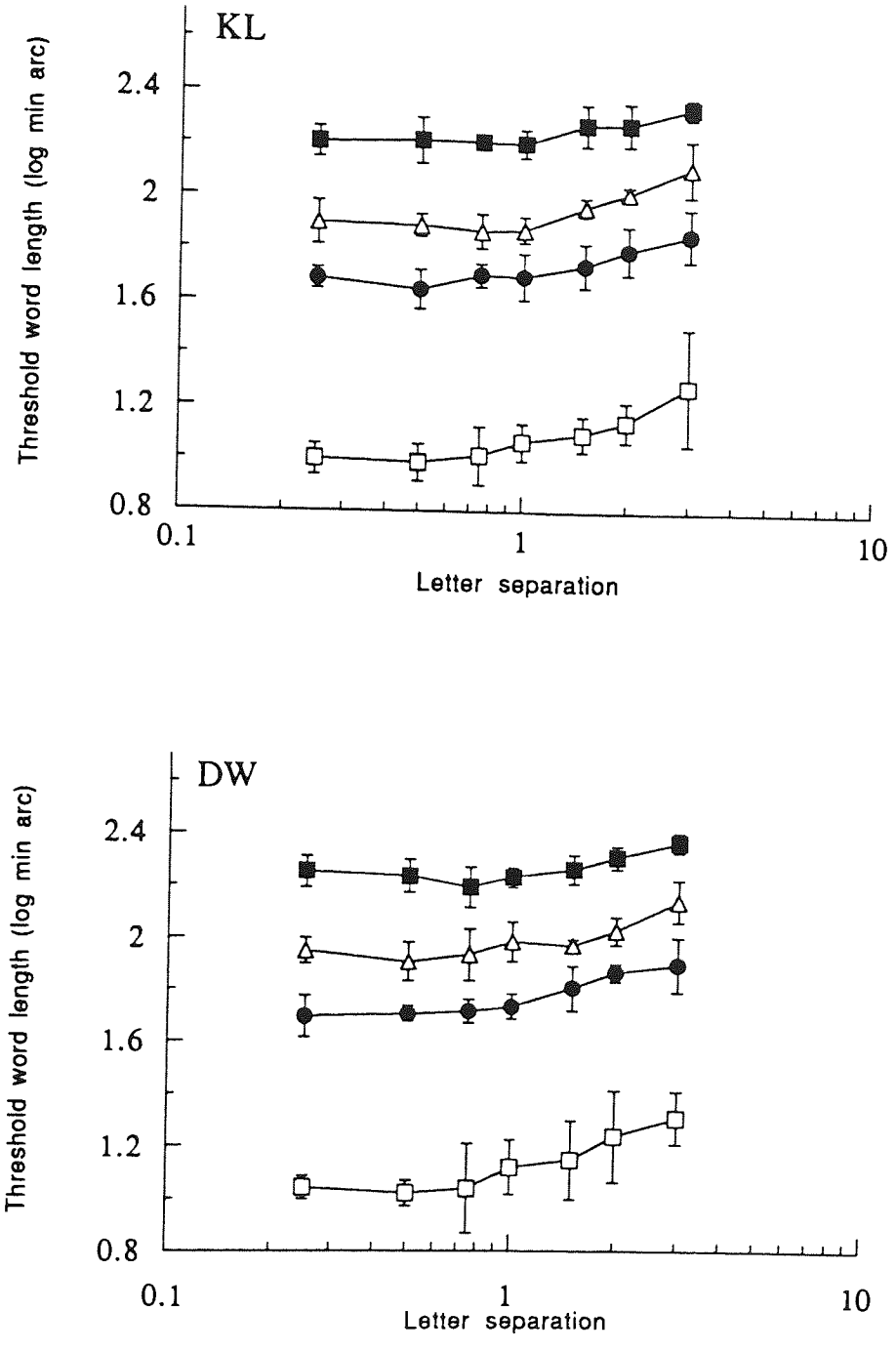

Figure 10.03. See following page for legend.

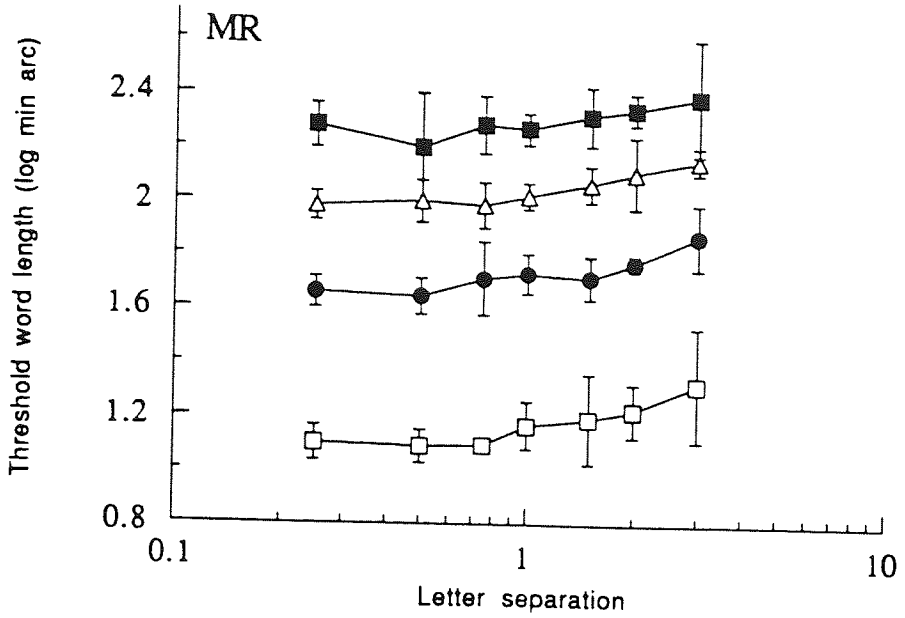

Figure 10.03. Word lengths as a function of edge to edge separation expressed in multiples of target width. Note that with increasing separation above a separation of 1 letter width, word lengths at a specific location increase in size, despite threshold letter sizes being smaller (Fig 10.02). Subjects KL, DW and MR. Open squares: fovea; filled circles: 2.5° inferior field; open triangles: 5° inferior field; filled squares: 10° inferior field. Error bars show standard error of the mean.

10.4 Experiment 2: Word recognition rate

10.4.1 Methods

The purpose of this experiment was to determine word recognition rates across the visual field as a function of stimulus size. In order to avoid the possibly contaminating effects of eye movements, peripheral words were presented using the rapid serial visual presentation method, or RSVP (Potter, 1984). Using this technique, words are presented in rapid succession at the same location, obviating the need for fixation saccades. Saccadic eye movements are thought to impose an upper limit on conventional reading speed (Rubin and Turano, 1992).

Threshold exposure duration for letter separations of 0.25 and 2 times letter size were determined using a staircase technique at a number of target sizes, this time using word duration as the staircase variable. Five random words from the ten available were presented sequentially, each for a given duration, at the same location. Words were presented in immediate succession, with no blank space between presentations. The

subject gave verbal responses as to which words had been presented. If all five words were identified correctly, and in the correct order, then the word exposure duration decreased by 0.1 log units for the next presentation. If errors were made, the duration increased by 0.1 log units. The procedure stopped after 8 reversals, and threshold exposure duration was taken as the mean of the last 6 of these. A mean of at least four duration thresholds was taken to represent the final threshold. Exposure duration was converted into a reading rate in words per minute by:

$$\text{Rate (wpm)} = (1000 / \text{exposure duration (ms)}) \times 60 \qquad \text{Equation 10.01}$$

10.4.2 Results

Figures 10.04 and 10.05 show how rates of word recognition vary with letter size at separations of 0.25 and 2 times letter width respectively. At all eccentricities, recognition rates improve as letter size increases and reach a plateau at larger sizes, where little further improvement is achieved by further enlargement of the letters. This plateau occurs at approximately the same rate for all eccentricities, showing that peripheral recognition rates can be as good as at the fovea if large enough target sizes are used.

The data at all eccentricities are fitted with curves of the form

$$\text{Reading rate (wpm)} = k1 \times (1 + ((k2 - k3) / (\text{scaled size} - k3)))^{-1} \qquad \text{Equation 10.02}$$

The reasoning for using this equation is as follows. When the scaled size is very large, reading rate approximates to k1. Hence, k1 estimates the maximum reading rate plateau. In addition, when scaled size is equal to k2, reading rate is half its maximum value. This value will be termed the 'critical size' after Rubin and Legge (1989), who used the term 'critical contrast' to describe the contrast level at which reading rate is half its maximum. Further, the value of k3 gives the size at which reading rate tends to zero.

The peripheral data curves appear to be of the same shape as the foveal data curve, but are offset along the x- or size axis. The rate at which target sizes must increase with eccentricity to maintain the same reading rate can be estimated by the amount by which the peripheral data curves need to be shifted leftwards in order to fit the foveal curve. This is equivalent to dividing the letter sizes at peripheral locations by an eccentricity-dependent scaling factor, F. Values of F were derived firstly by making an estimate of such a scaling factor which was likely to superimpose one of the peripheral functions onto the foveal data if the letter size of each peripheral data point was divided by the scaling factor. The suitability of this estimate was then assessed by calculating the sum of squares of the residual deviations around a best fitting template to the data of the two eccentricities when superimposed. The template used was that of Equation 10.02.

Another estimate of the scaling factor was then made and the procedure repeated. This process was continued until a scaling factor was found which produced the minimum sum of squares of the residual deviations. Having derived these scaling factors, a regression of the form of Equation 4.01 was applied to the data to derive E_2 values. These values represent the eccentricity at which foveal stimulus size must double in order to maintain reading rate and are shown in Table 10.02.

The E_2 values obtained for the reading rate data are somewhat smaller than those for word recognition (Experiment 1) which involved a constant 500ms (120wpm) presentation time. The temporal aspect of the reading rate stimulus appears to reduce peripheral visual performance such that slightly more peripheral magnification is needed.

Subject	E_2 value (degrees)	
	0.25 sep	2 sep
KL	0.36±0.02	0.45±0.04
DW	0.39±0.01	0.60±0.03
MR	0.54±0.02	0.69±0.03

Table 10.02. E_2 values and standard errors, in degrees, for reading rates under all experimental conditions.

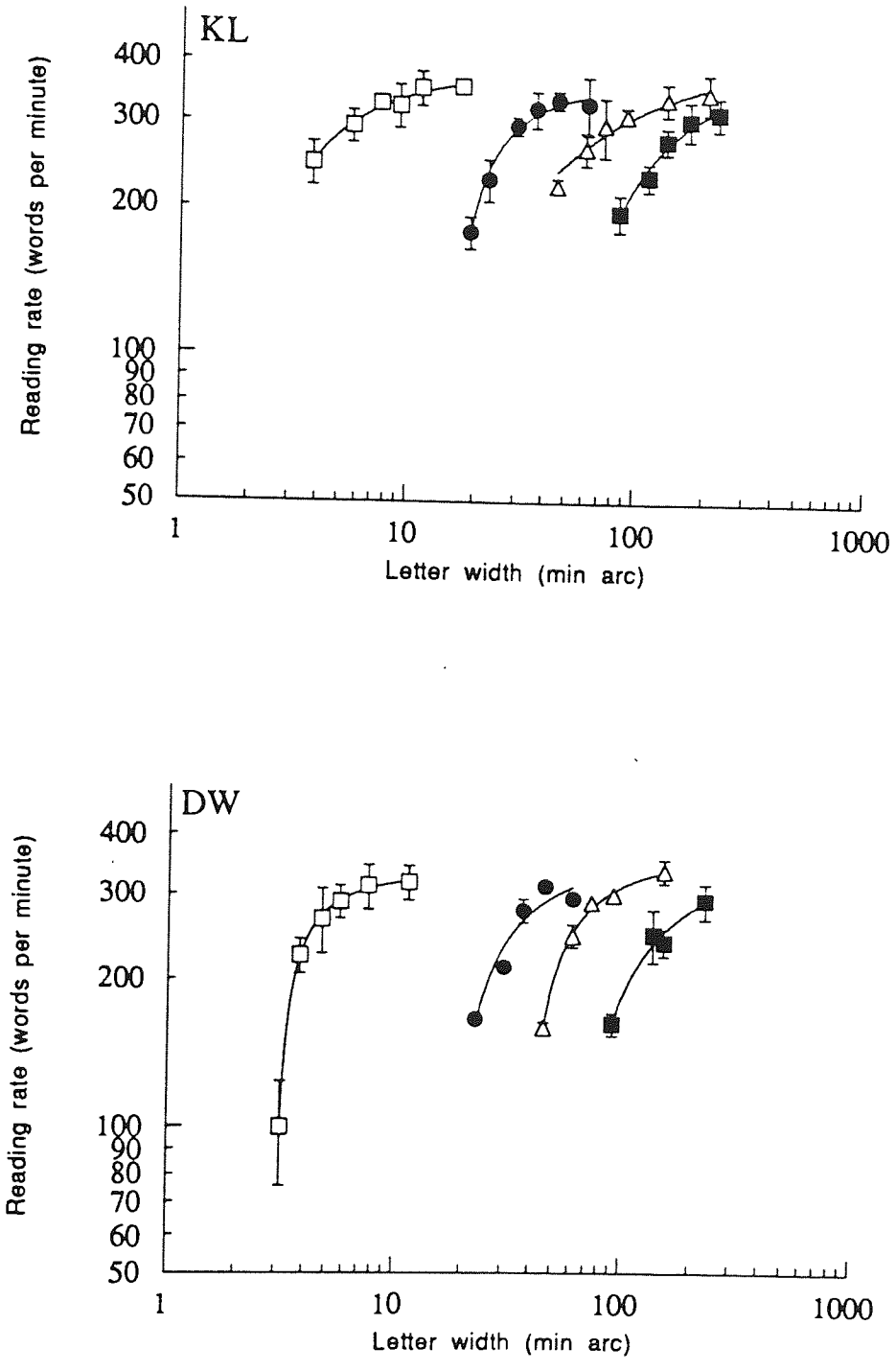

Figure 10.04. See following page for legend.

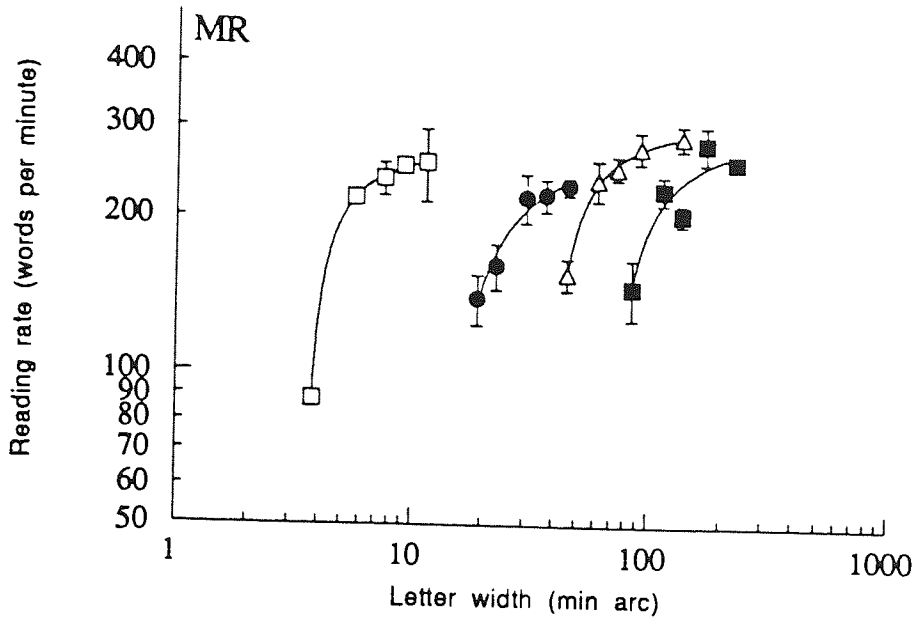

Figure 10.04. RSVP reading rate, in words per minute, for words of various letter sizes at several eccentricities. Letter spacing is constant at an edge to edge separation of 0.25 x letter width. Data for each eccentricity is fitted with a regression of the form of Equation 10.02 (see text). Subjects KL, DW and MR. Open squares: fovea; filled circles: 2.5° inferior field; open triangles: 5° inferior field; filled squares: 10° inferior field. Error bars show standard error of the mean.

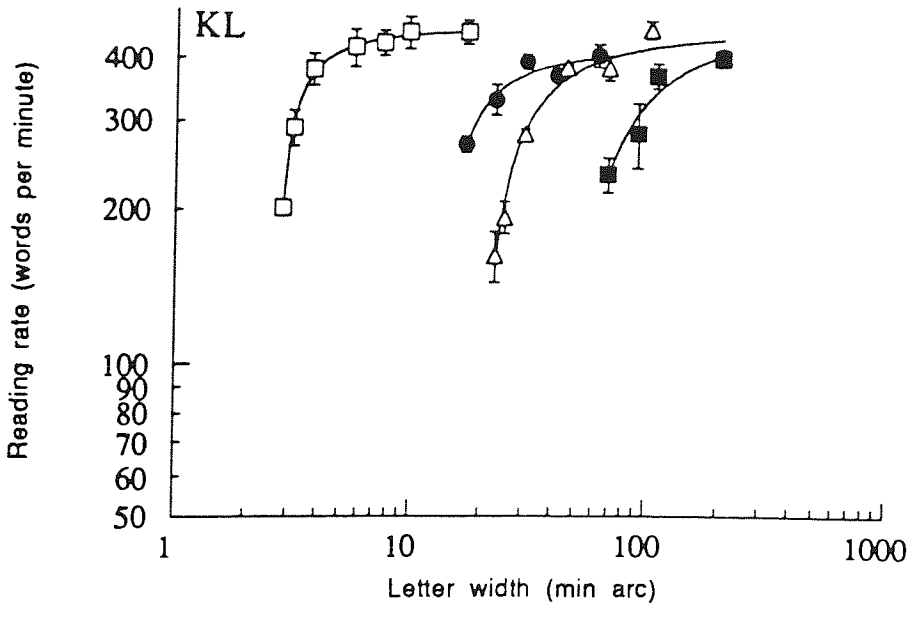

Figure 10.05. See following page for legend.

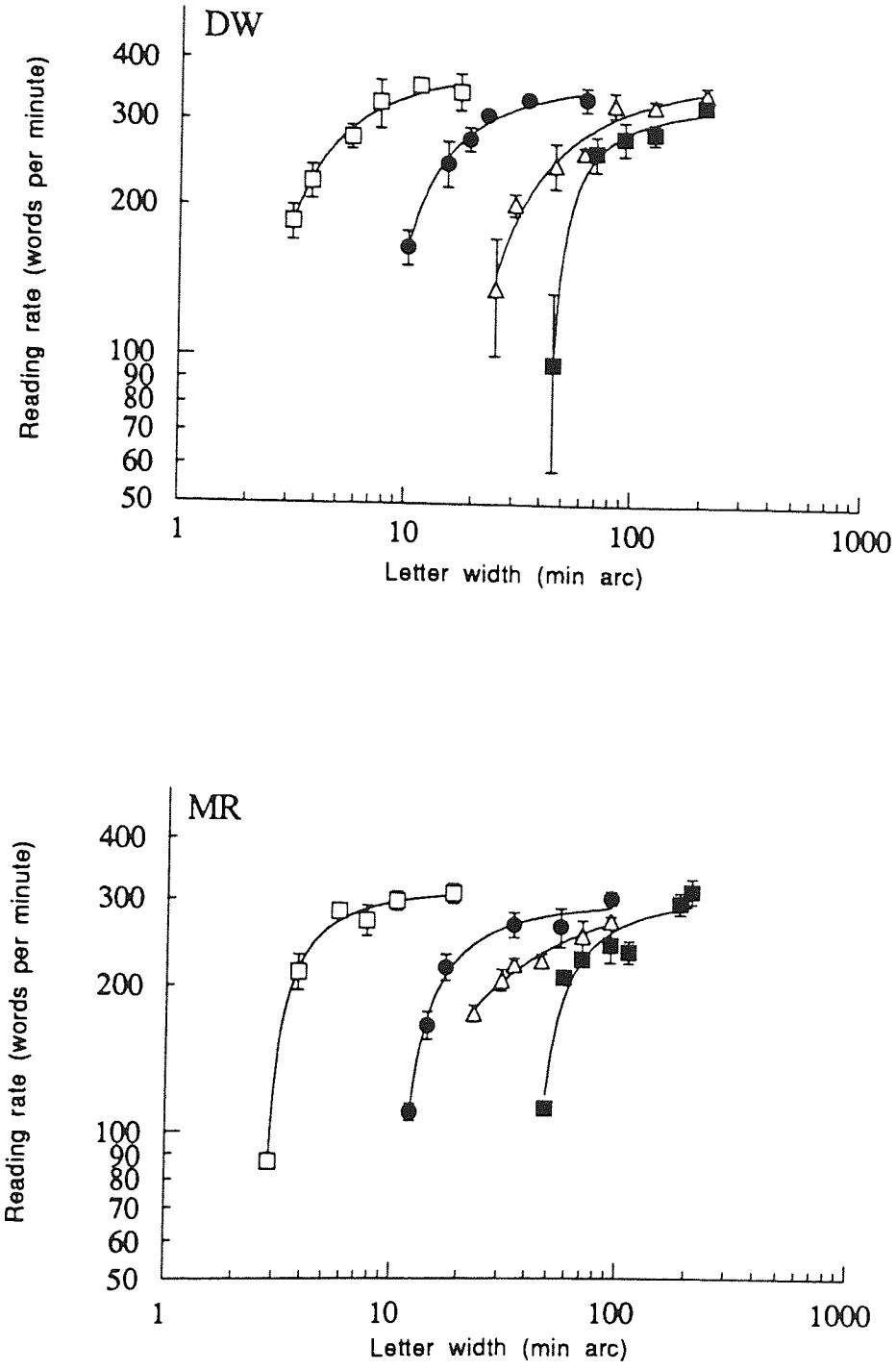

Figure 10.05. As for Fig 10.04, but letter spacing is 2 x letter width.

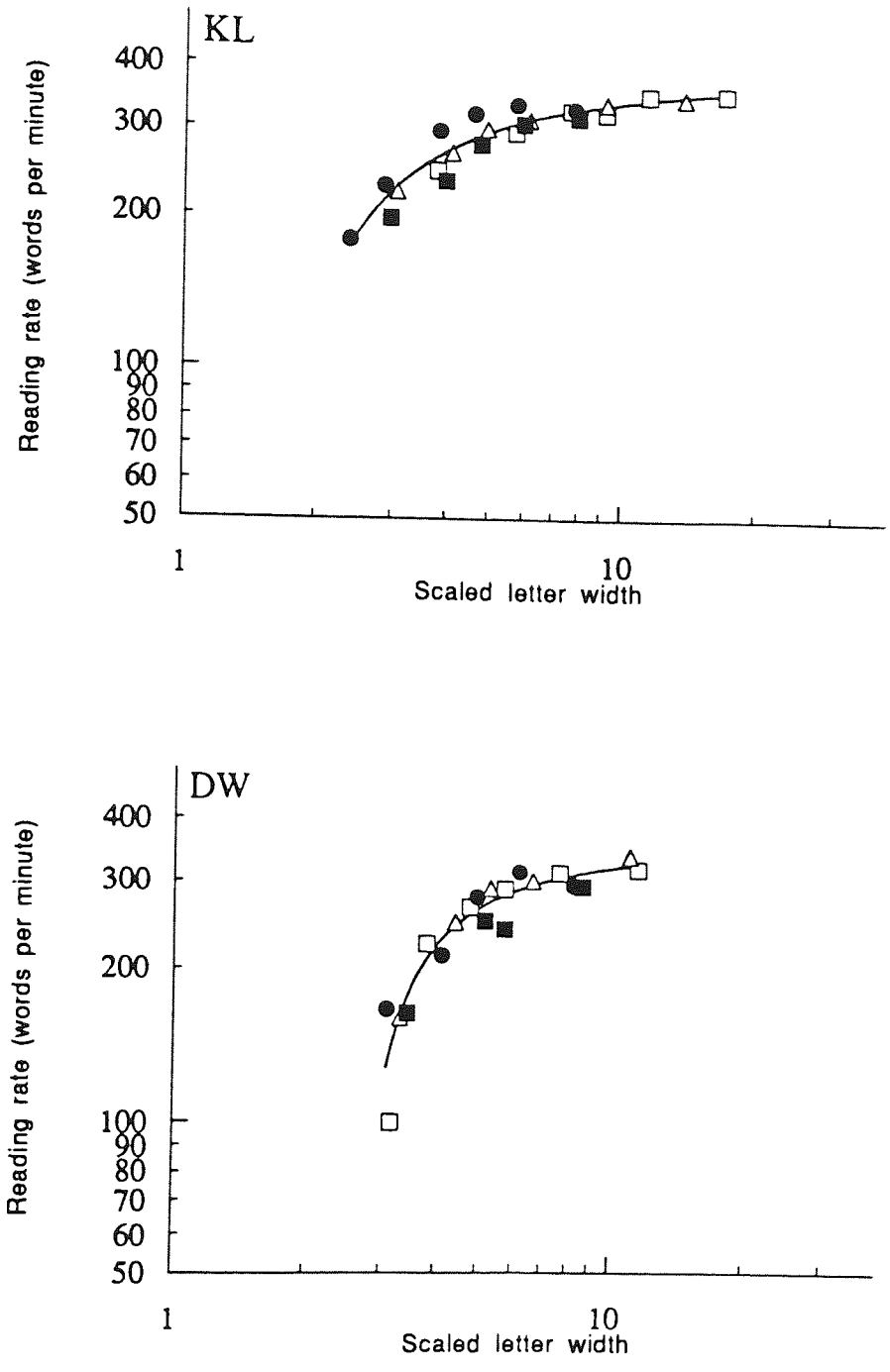

Figure 10.06. See following page for legend.

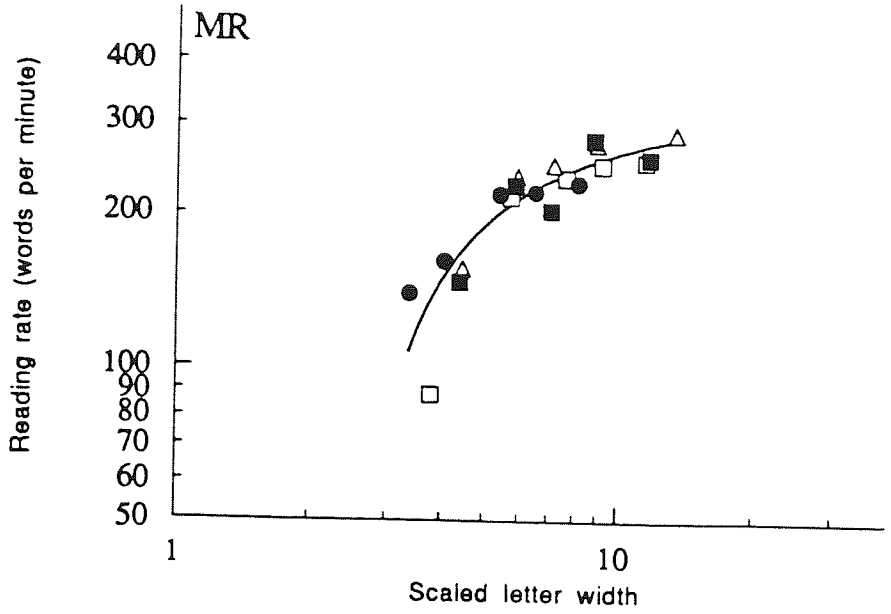

Figure 10.06. The data of Fig 10.04 after shifting each of the peripheral datasets leftwards along the size axis according to scaling factors defined by Equation 6.03. The resulting single function is fitted with a regression curve whose form is described in the text (Equation 10.02). Symbols and subjects as for Figure 10.04.

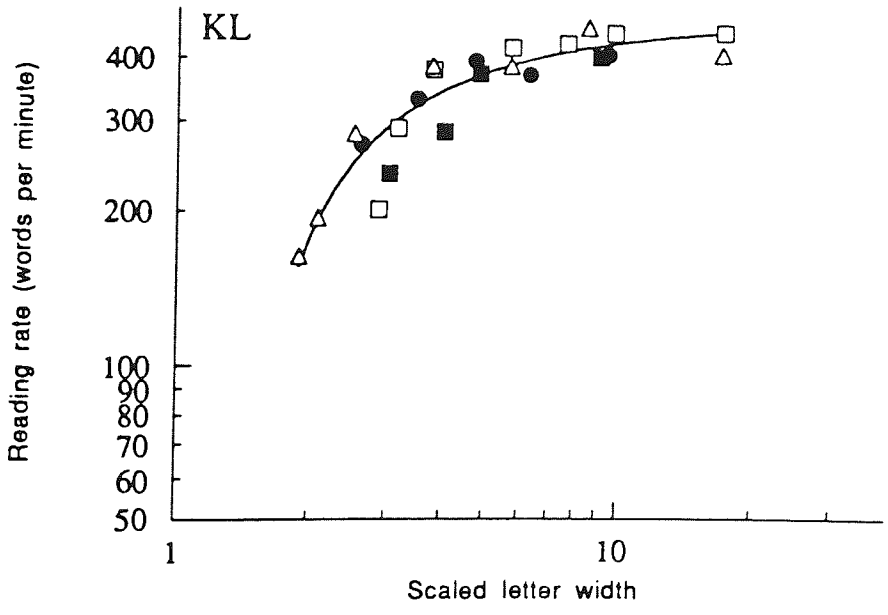

Figure 10.07. See following page for legend.

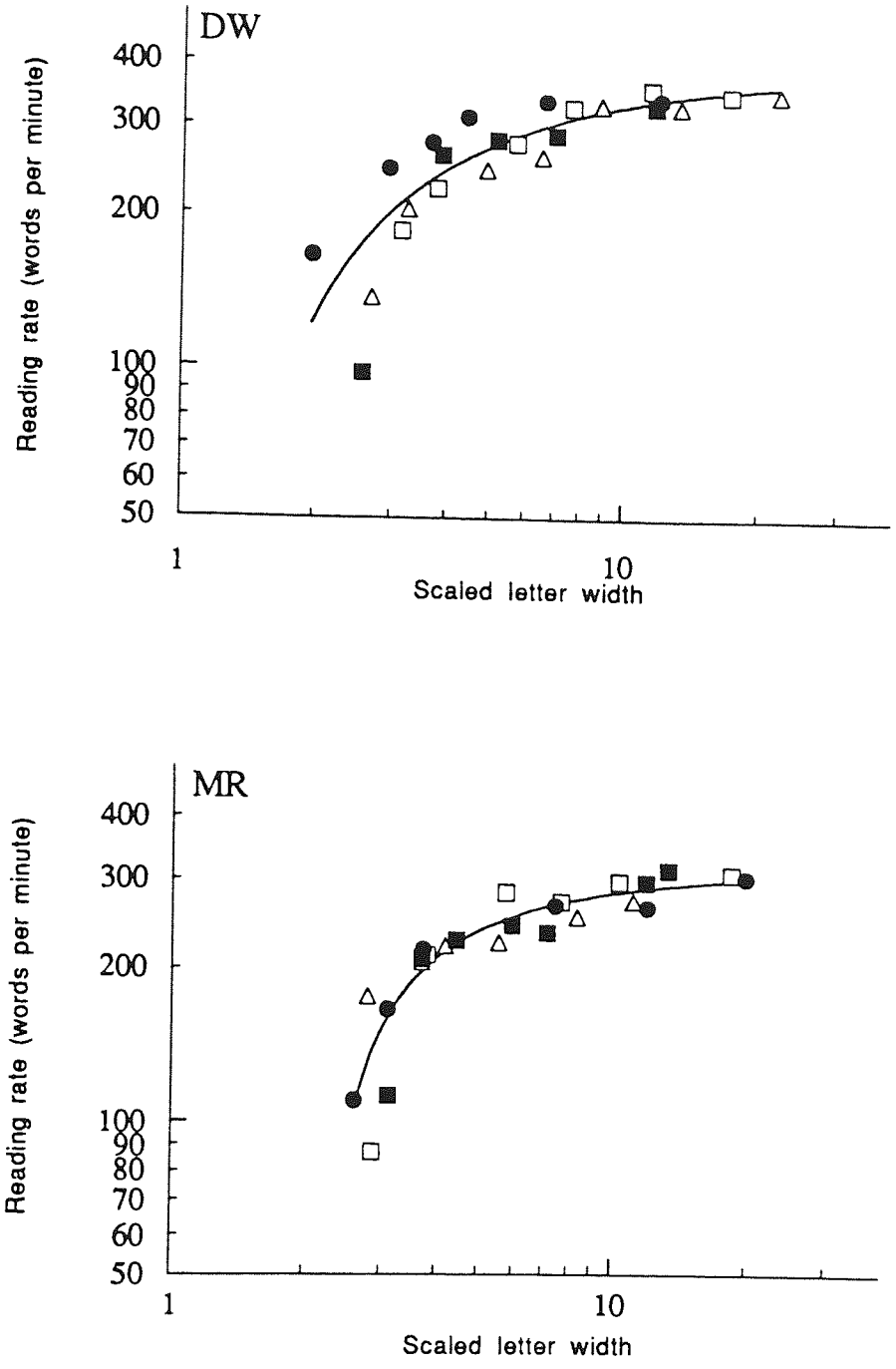

Figure 10.07. As for Fig 10.06, but using the 2 x separation data of Fig 10.05.

Figures 10.06 and 10.07 show the data from Figures 10.04 and 10.05, but with letter size scaled according to eccentricity using the relationship

$$\text{scaled letter size} = \text{letter size} / (1 + (E / E_2)) \qquad \text{Equation 6.03}$$

Note how this removes the eccentricity dependence from the data, highlighting that the difference between foveal and peripheral word recognition performance is a difference of scale (quantitative) rather than a qualitative difference.

The scaled data are fitted with regression of the form of Equation 10.02, and parameters from the curve fitting procedure are shown in Table 10.03. There is a tendency for critical size (k2) to be smaller for all observers in the wider letter spacing condition. Additionally, one observer (KL) shows a markedly increased maximum reading rate (k1) for the wider letter separation.

Subject	Edge sep	k1(wpm)	k2 (min arc)	k3 (min arc)	R
KL	0.25	384.95±14.93	2.58±0.12	1.55±0.28	0.946
DW	0.25	356.21±20.38	3.44±0.14	2.62±0.18	0.948
MR	0.25	335.56±33.61	4.37±0.49	2.49±0.47	0.918
KL	2	484.67±26.14	2.45±0.18	1.39±0.24	0.920
DW	2	393.38±26.82	2.88±0.32	1.25±0.42	0.895
MR	2	317.92±14.46	3.09±0.15	2.12±0.21	0.931

Table 10.03. Parameters from curve fitting of Figures 10.06 and 10.07, with standard errors, for all experimental conditions.

10.5 Experiment 3: Reading rate

10.5.1 Methods

The results of Experiment 2 show that word recognition rates can be equated across the visual field by appropriate magnification of the stimulus. The task employed in the previous experiments differs in several important respects from that of reading. The major differences are the lack of meaning in the random word strings, and the use of random letters at each end of the letter string to standardise crowding. Additionally, the task consisted of only a small number of words, and only uppercase letters, which is not the case in most reading tasks. The purpose of the next experiment was therefore to examine whether the results of the previous experiment also apply to a more realistic reading task.

In this experiment, the stimulus words were again constructed in Helvetica font but this time with both upper and lower case letters used, as in a normal sentence. Letters were

presented with variable pitch (proportional spacing) as is found in fonts in general use. The spatial interference was therefore not standardised as in Experiments 1 and 2.

Again, an RSVP method of presentation was used in order to minimise the effect of eye movements on the results. Threshold reading rate in words per minute was found by the method of limits for 0 and 5 degrees eccentricity in the inferior field for two types of stimuli. The first type of stimulus was a sentence of 6-8 words length taken from standard reading texts (Ames, 1980; Neale, 1989). The sentences were relatively simple and aimed at children with a reading age of approximately 9 years. The sentence was presented initially at a rate too fast to be read (2000 wpm). The sentence was then presented again, but with the reading rate in words per minute reduced by 0.05 log units. The procedure continued until the sentence was read correctly. The second type of stimulus consisted of a random selection of 5 words from a bank of 400 words taken from the sentences of the standard reading texts (Ames, 1980; Neale, 1989). The words changed randomly from presentation to presentation. All five words had to be reported correctly, and in the correct order, for a positive response. The purpose of this second experiment was to be able to directly compare the effects of sentence meaning as opposed to random word strings.

10.5.2 Results

Figure 10.08 shows the results for observers KL and DW respectively. Filled symbols represent data obtained with meaningful sentences, while open symbols show the results for the random words condition. Each set of data is fitted with a regression according to Equation 10.02. Maximum reading rates are shown in Table 10.04, having been calculated from Equation 10.02. The data show that reading rate with meaningful sentences cannot be equated across the visual field by simple magnification. The maximum foveal reading rate with meaningful sentences is higher than that achieved at 5 deg eccentricity, even when peripheral stimuli are magnified appropriately.

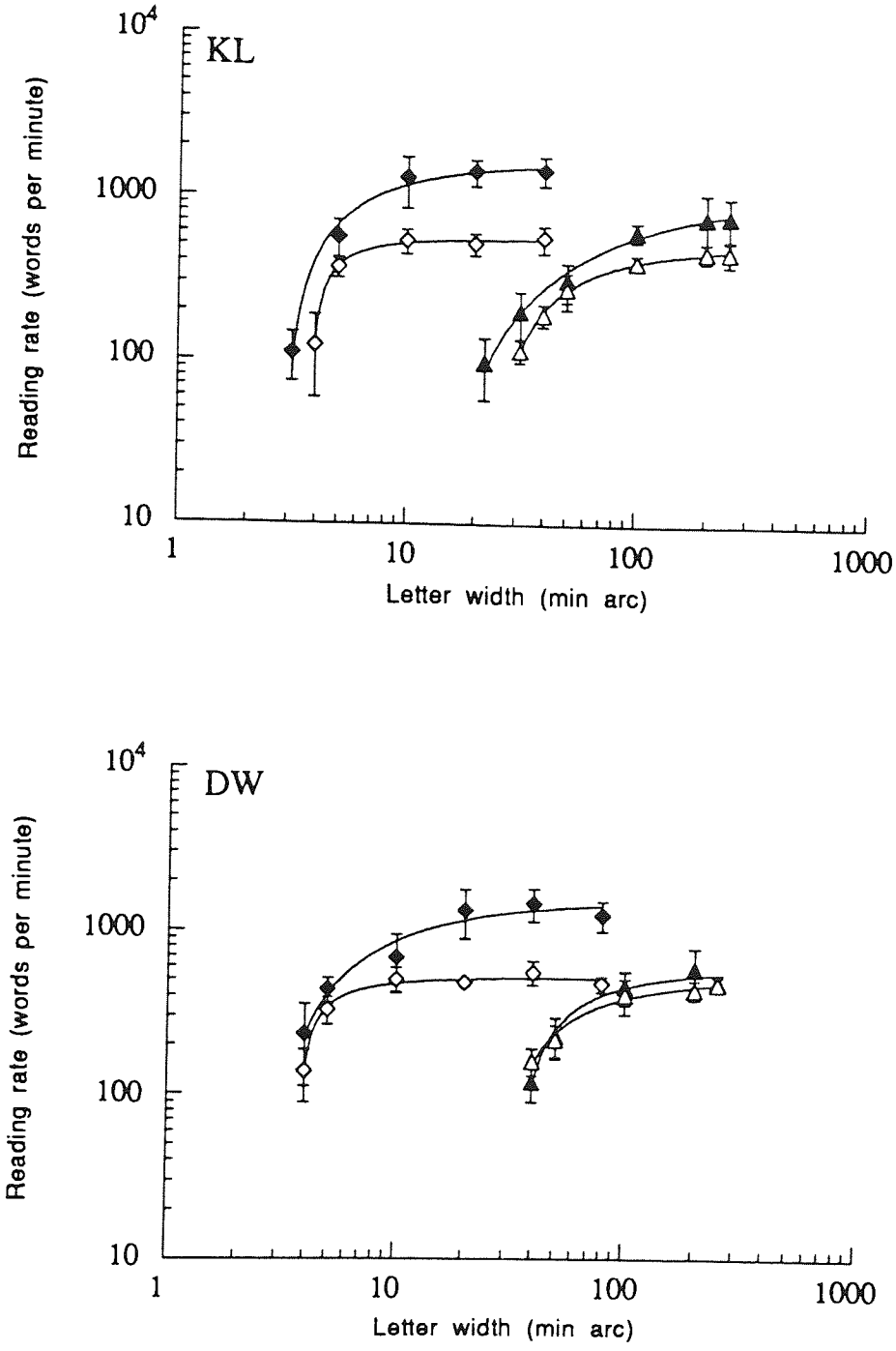

Figure 10.08. RSVP reading rate, in words per minute, for words of various letter sizes at several eccentricities. Data for each eccentricity is fitted with a regression of the form of Equation 10.02 (see text). Subjects KL and DW. Filled symbols: meaningful sentences; open symbols: random words. Diamonds: 0°; triangles: 5°. Error bars show standard error of the mean.

For random word presentation, the results are similar to those obtained for Experiment 2, although maximum rates are somewhat faster. This suggests that the lack of meaning, the use of letters to standardise crowding, and/or the use of exclusively upper case letters in Experiment 2 has had a slight detrimental effect on maximum reading rate (compare Tables 10.03 and 10.04). The data is however, markedly different from the data obtained with meaningful sentences comprised of the same words. For the unrelated words condition, reading rate rises to approximately the same rate at 0 and 5 deg eccentricity, as was found in Experiment 2.

Subject	Condition	Eccentricity (deg)	Max rate (wpm)
KL	Sentences	0	1721±152
KL	Sentences	5	1050±90
DW	Sentences	0	1558±218
DW	Sentences	5	619±81
KL	Random words	0	583±20
KL	Random words	5	548±11
DW	Random words	0	532±26
DW	Random words	5	538±41

Table 10.04. Maximum reading rates and standard errors derived from curve fitting of Figure 10.08.

10.6 Discussion

Word recognition in the periphery can be made as good as that at the fovea, provided that the letters are large enough. The magnification needed for words presented at a specific location can be predicted from the E_2 value, which defines the eccentricity at which targets must double in size in order to remain comparable with the fovea (Levi et al., 1985). For word recognition thresholds, E_2 values decrease with decrease in letter separation, and vary between 0.6 and 1 deg, for a 500ms presentation time. The change in E_2 with letter separation reflects the effects of spatial interference across the visual field. The extent of spatial interference increases far more rapidly with eccentricity than does resolution (Toet and Levi, 1992; Chapter 9) which results in tasks with more proximal contours having thresholds raised more by spatial interference in the periphery, which in turn lowers E_2 values.

For each separation, word recognition rate using the RSVP method rises to approximately the same maximum rate at each eccentricity (Figures 10.04 and 10.05). Unrelated words can therefore be recognised as fast in the periphery as at the fovea, so long as the letters are large enough. The finding that recognition rate can be made

equally good across the visual field is in agreement with Whittaker, Rohrkaste and Higgins (1989). Whittaker et al. (1989) examined recognition of four letter words, and found little crowding effect evident in their word recognition task, although it should be noted that with a four letter word, only two of the four letters are crowded by surrounding letters on both sides. Using words of twice the threshold recognition size, Whittaker et al. (1989) found that the exposure duration needed for word recognition speed was almost the same at the fovea and at 10 deg in the superior field, although a slightly wider letter spacing was required at the eccentric location in order to achieve this. However, there is no reason to expect that a word which is twice recognition threshold in the periphery will be as visible and read as fast as a word which is twice recognition threshold in the fovea. From the data in the current study, it can be seen that the E_2 values for word recognition (Experiment 1) and word recognition rate (Experiment 2) are not quite the same. More magnification is required to maintain recognition rate across the visual field than to maintain recognition thresholds.

In contrast, reading rate using meaningful sentences rather than random word strings cannot be equated across the visual field by magnification (Figure 10.08). There is a qualitative superiority of the fovea over the periphery in terms of the maximum reading rate achieved. This finding confirms the report of Rubin (1993) who used an RSVP methodology similar to ours and examined reading performance at different eccentricities using a wide range of letter sizes (ie. no pre-chosen magnification factors were used). Asymptotic reading rate in the periphery did not match that at the fovea. A different result was found by Arditi, Knoblauch and Grunwald (1990) who found that RSVP values for meaningful sentences were approximately equal at 0 and 2 deg for both fixed and variable pitched text. However, the finding that reading rate cannot be made equivalent across the visual field also appears to agree with the conclusions of Turano and Rubin (1988) and Rubin and Turano (1994). For text which was magnified peripherally according to the cortical magnification equations of Rovamo and Virsu (1979), these studies found that peripheral reading speeds with RSVP presentation did not approach those achieved foveally. At the fovea, a stimulus size of 24 min arc was used which resulted in a reading rate of 1270 wpm, while at 5 deg eccentricity a stimulus size of 60 min arc gave a reading rate of 270 wpm. Both reading rate values are comparable with the present findings (see Figure 10.08). However, the M-scaling equations used have an equivalent E_2 value of 3.4 deg. As the E_2s in the current study are much smaller, it is clear that their peripheral text was not large enough to adequately reflect the potential of the eccentric location. This emphasises the point that a single factor, such as the cortical magnification factor or 'M-scaling' procedure cannot equate performance across the visual field in all tasks. Instead, magnification factors are highly

dependent upon the task itself, so that scaling factors or E_2 values found for one task can rarely be applied successfully to other tasks (Whitaker et al., 1992a). With a spatial scaling procedure such as is used here, the decline in reading rate with eccentricity is shown not to be as precipitous as M-scaling procedures suggest, but a qualitative difference still remains between fovea and periphery.

Impressive foveal reading rates of up to 1800 ± 250 wpm have previously been reported using the RSVP method (Turano and Rubin, 1988; Rubin and Turano, 1992). The present results concur with these values for sentences having meaning, with the highest reading rate plateau for this condition found to be 1721 ± 152 wpm. In comparison, the highest foveal plateau reading speed in the unrelated words condition is 583 ± 20 wpm. Previous authors have noted that recall of scrambled RSVP sentences at the fovea is poorer than that of ordered sentences (Forster, 1970; Potter, 1984). No previous study has compared performance with scrambled and ordered sentences for eccentric viewing, where the present results show that the superiority of reading rate for meaningful sentences over random words is reduced (KL) or absent (DW).

During the experiments, the subjective impression of the observers was that at the fovea only 2-3 key words from the 6-8 word sentence needed to be seen to 'solve' the sentence correctly. Identification of a few words allowed a correct interpretation of the entire sentence without the observer being conscious of having seen every word in the sentence. This observation has been previously noted (Forster, 1970; Potter, 1984). Conversely, in the periphery the observers had to be aware of virtually every word in the sentence before it could be interpreted, a situation more analogous to the unrelated words condition, where knowledge of some of the words did not provide clues as to the identity of the other words. The data shows this observation in that, for DW, peripheral performance is very similar for both related and unrelated word conditions. For subject KL, meaningful sentences still produce some advantage in maximum peripheral reading rate at the eccentric location, but this is less than that observed at the fovea.

The only difference between the presentations in the two parts of the third experiment was in the semantic structure of the words to be recognised. It seems that with meaningful sentences an observer is able to make use of redundancy in the sentence structure, or can use contextual information gained from the words observed in order to reconstruct the remainder of the sentence and improve reading rate performance above that for unrelated words. The results show that this cognitive ability to correctly identify

meaningful sentence structure from a perceptually limited input appears to be selectively available at the fovea, but not eccentrically.

It has been suggested that a reduced ability to perform pattern analysis in the periphery may underlie the reduction in RSVP reading rate with eccentricity (Turano and Rubin, 1988; Rubin and Turano, 1994). This is also suggested by previous work (Rentschler and Treutwein, 1985; Bennett and Banks, 1987; Stephenson et al., 1991) which has found phase discrimination to be inferior in peripheral vision. However, the present results show that word recognition can be equated across the visual field by appropriate magnification, as has been shown in previous studies of letter and word recognition (Whittaker et al., 1989; Farrell & Desmarais, 1990; Higgins et al., 1992). Only when meaning is introduced to the sentence stimuli does the fovea gain a superiority over peripheral vision. In other words, the fovea is better than the periphery at extracting meaning from sentences for which the psychophysical visual input can be equally well observed. It is known that processing of cognitive tasks such as reading take place in a number of localised cortical areas (Posner and Carr, 1992). Separate cortical areas have been identified which deal with development of visual word forms, semantic operations, and phonological coding (Posner, Petersen, Fox and Raichle, 1988; Petersen, Fox, Snyder and Raichle 1990). Possible retinotopic distributions in these areas are not known, and it is not inconceivable that projections to these cortical areas are foveally dominated

Several methods are available by which to measure reading rate apart from the RSVP technique used in this study. In unconstrained reading procedures, the subject reads a passage of static text as fast as possible either orally or silently. The time taken to read the passage, and the accuracy achieved are measured. In the PAGE technique employed by Rubin and Turano (1992), the number of words correctly read in a fixed time period was used to calculate reading rate. These unconstrained techniques utilise eye movements to scan the text in order to position the next word or group of words onto the fovea. Ultimately in these procedures, subjects are able to choose their reading speed, and maximum reading rates are generally lower than when using other methods (Whittaker and Lovie-Kitchen, 1993). Legge et al. (eg. 1985a,b) introduced the technique of forced scrolling to the psychophysical investigation of reading. Text is scrolled in a continuous motion from right to left in front of the subject. The scrolling speed is gradually increased, forcing the subject to read aloud at an increasingly faster rate, until the subject suddenly starts missing words. The transition from accurate to highly inaccurate reading is abrupt and well defined. The transition point defines the

maximum reading rate, which can be in the order of 250 words per minute in normal observers (Legge, Pelli, Rubin and Schleske, 1985a).

Deficits have been reported for peripheral reading speeds of scrolled text and free reading tasks (Legge et al., 1985b; Whittaker and Lovie-Kitchen, 1993; Cummings et al., 1985). Indeed, Whittaker and Lovie-Kitchen (1993) considered eccentricity of fixation *per se* to be an impediment to reading, as unconstrained reading rate was found to decrease when subjects used the eccentric retina for fixation, even when field of view and visual acuity losses were accounted for. It has been suggested that saccadic eye movements are the limiting factor in conventional foveal reading speeds (Rubin and Turano, 1992), and this appears to be a major factor in the deficits found in peripheral scrolled and free reading performance. It is known that foveating saccades are the fastest and most accurate type of saccades (Whittaker and Cummings, 1990), and so when reading peripherally, eye movements will be slower and less accurate than with central fixation. Previous work has implicated inadequate peripheral eye movement control in the poor standard of reading eccentrically (Turano and Rubin, 1988; Arditi et al., 1990). The RSVP method used in this study eliminates such oculomotor considerations, and still finds a peripheral deficit in reading performance. Such a deficit was also found for low vision observers with central field loss, using RSVP stimuli (Rubin and Turano, 1994). It was concluded that saccadic eye movements contribute to, but do not totally account for, the reduced reading rate of eccentrically viewing subjects. The present results suggest that differences in reading rate across the visual field, which remain after eye movement effects have been accounted for by use of an RSVP technique, are due to differences in cognitive interpretation of sentences rather than qualitative variations in early visual processing.

Since poor peripheral eye movement control appears to contribute to reduced peripheral reading rates in freely read text, then one might expect more compressed text to result in improved reading rates at the fovea, since proportionately fewer fixational eye movements are required (Moriarty and Scheiner 1984; Arditi et al., 1990). In this situation, threshold letter sizes are larger than for more widely spaced text, but word lengths are shorter, resulting in the need for fewer eye movements. However, for a reading rate task such as RSVP, which requires no fixational eye movements, it appears that a slight advantage may be gained by using more widely spaced letters. The letter size required to read at half the maximum rate (k2) is consistently smaller for the wider spaced condition, as is the size at which reading becomes impossible (k3). In addition, maximum reading rates (k1) tend to be faster under the wider spaced condition, although this difference is only pronounced for one subject (KL). In the

RSVP task, the word length is an unimportant parameter, as eye movements are not required.

Previous studies have found that patients with central visual field loss possess markedly lower reading rates than normals (Legge et al., 1985b; Legge, Ross, Isenberg and LaMay, 1992; Cummings et al., 1985; Whittaker and Lovie-Kitchen 1993). As the present results demonstrate, the reason for this performance deficit in patients is not due to a qualitative difference in word identification between normal central and peripheral vision, but may be partly due to cognitive differences in addition to deficits in peripheral eye movement control. Foveal and peripheral reading performance cannot be made equal with a change of size scale, even with appropriate print magnification. However, using the RSVP technique, sentences viewed at 5 deg eccentricity could be read at a rate of up to 583 wpm if appropriately magnified. The advantage of eliminating the confounding effects of eye movements supports the conclusion of Rubin and Turano (1992) that RSVP may prove useful as a reading aid for the partially sighted.

In conclusion, the results of this study show that with the effects of eye movements eliminated, the visual word recognition abilities of peripheral retina are not qualitatively different from those at the fovea, but differ simply by a change in size scale. However, the fovea shows a superiority over the periphery in making sense of and understanding meaningful sentences, which is reflected in higher reading rates for foveally fixated rather than eccentrically viewed text. The ability of the eccentric retina to read is limited by more than its inability to process letters of small size.

Chapter 11
'Weber's Law' in spatial interval discriminations

11.1 Introduction

In the preceding chapters, the eccentricity related decline in visual performance has been examined for various tasks. A different approach to the investigation of peripheral vision is taken in this chapter, and the role of eccentricity in determining 'Weber's law' for position is examined.

One of the primary goals of early vision is the localisation of objects and parts of objects relative to their surroundings. This provides for a logical spatial order of the visual world and a cohesive back-drop against which occurrences of particular significance, such as object movement, may be reliably identified. In line with most other sensory modalities, where the just noticeable stimulus difference is determined by the magnitude of the stimulus, so the accuracy with which objects in visual space may be localised relative to one another is directly proportional to their separation. This is often known as 'Weber's law' for position. For spatial interval discrimination tasks (discussed in Chapter 2), above an optimum value spatial interval thresholds increase in proportion to separation (Westheimer and McKee, 1977b; Westheimer, 1979b), ie:

$$\Delta s / s = \text{constant} \qquad \text{Equation 2.01}$$

where s is the separation of the objects, and Δs is the just noticeable change in separation, or the position threshold.

A full explanation for 'Weber's law' for position has not yet been arrived at, although the topic has received widespread recent investigation. By their nature, the stimuli used to determine interval thresholds are spatially extensive, as they consist of two features separated by a gap, so that not all parts of the stimulus lie at the same eccentricity. For 'foveal' presentation of an interval discrimination task, fixation is midway between the two features defining the interval. Neither feature is at 0 deg eccentricity, but at some eccentric location defined by the separation of the stimuli. As separation increases, so does the eccentricity of the stimulus components. Yap, Levi and Klein (1989) and Levi and Klein (1990b) both examined spatial interval discrimination as a function of eccentricity, allowing eccentricity and separation to covary, and size scaling peripheral stimuli by a prechosen E_2 value of 2.5 deg. Eccentricities from '0' to 10 deg in inferior visual field were investigated in both cases. E_2 values for optimum thresholds were found to be in the range 0.6-0.8 deg, while values for optimum separation were 1.9-2.4 deg. It was concluded that optimum separation was governed by retinal factors such as cone spacing, while optimum thresholds were determined by the cortical

sampling grain. The reason for the two scaling factors required by these studies probably lay in their use of 'foveal' data (Whitaker et al., 1992a). The eccentricity of 'foveal' spatial interval stimuli is dependent on feature separation, and will not actually represent performance at 0 deg. Since E_2 represents the eccentricity at which foveal thresholds double, accurate quantification of foveal performance is critical.

In order to investigate the effect of eccentricity and the effect of separation independently, it is necessary to position stimuli on an iso-eccentric arc (Levi et al., 1988; Levi and Klein, 1989, 1990a; Whitaker et al., 1992a) whereby separation is changed by moving the stimuli around the arc and eccentricity is changed by varying its radius. Levi et al. (1988) used an iso-eccentric arc paradigm in the construction of their three element bisection task, in order to separate the roles of eccentricity and separation in determining position thresholds. Figure 11.01 shows an example of their stimuli which were presented at a constant eccentricity of 10 deg, and with separation varied. The outer test stimuli in Figure 11.01 are placed on the iso-eccentric arc, but the middle reference is placed midway between the outer lines, and not on the arc. The eccentricity of this middle reference is therefore not a constant 10 deg: its eccentricity increases as separation decreases.

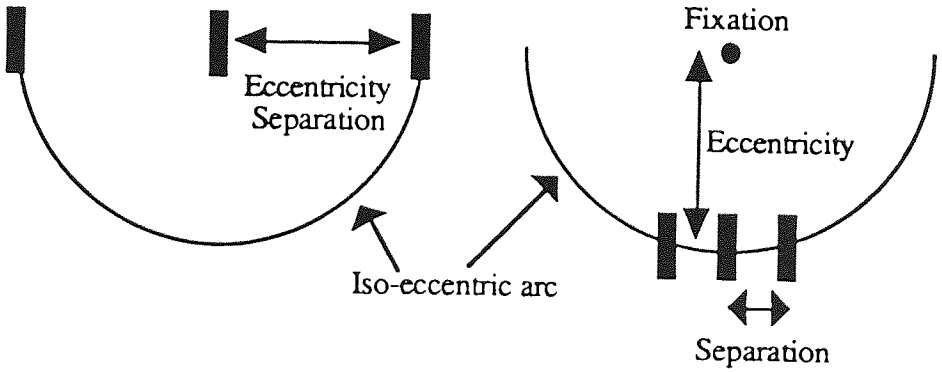

Figure 11.01. Bisection stimuli of Levi et al (1988) arranged on an iso-eccentric arc. The arc is not visible to the observer. Note that only the outer 'test' stimuli fall on the iso-eccentric arc; the eccentricity of the central 'reference' stimulus depends on the separation of the outer stimuli.

The results of the study are shown schematically in Figure 11.02. Rather than thresholds increasing as a function of separation with eccentricity held constant, as predicted by Weber's law (dashed line) thresholds were found to be roughly constant with increasing separation at approximately 2% of eccentricity, and even decreased slightly at large separations. The results were rather surprising, even to the authors, since 'Weber's law' is so pervasive throughout sensory physiology.

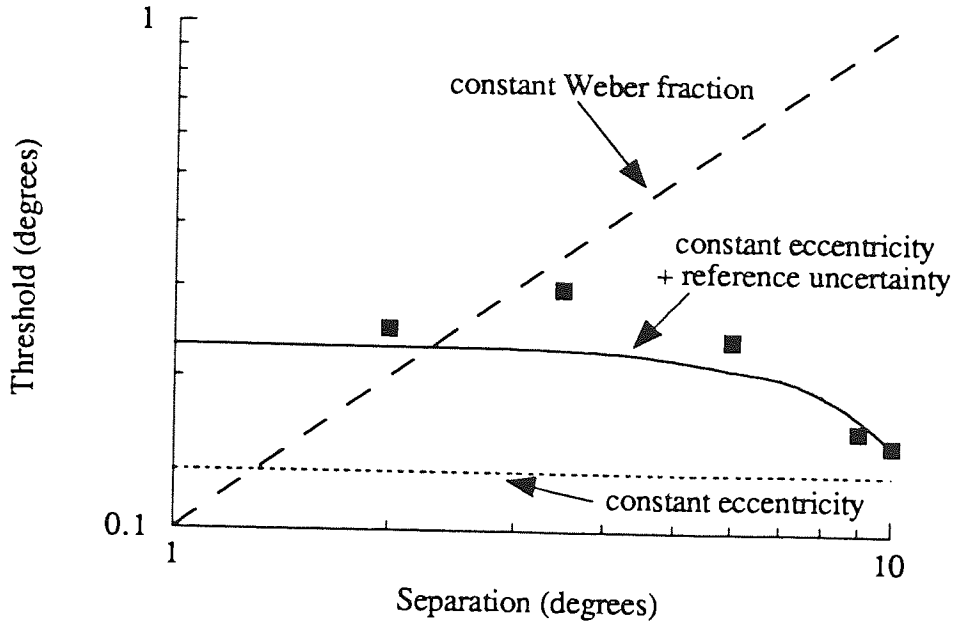

Figure 11.02. Schematic representation of the results of Levi et al (1988), their Figure 6. The mean results found for three observers (filled squares) were fitted with the curve described as 'constant eccentricity + reference uncertainty'.

It was concluded that the results for 10 deg eccentricity were consistent with a 'spatial grain' hypothesis, whereby position thresholds for large separations are determined by estimating the cortical distance separating targets of interest. Such an estimation is independent of separation, much like our ability to use a ruler to measure to 1mm accuracy, whatever the distance measured. The slightly higher thresholds at the smaller separations examined were explained as being due to the influence of increased positional uncertainty of the middle reference line as the separation decreased, and its eccentricity increased. The 'spatial grain' hypothesis for larger eccentricities or separations is also in agreement with the original model of Klein and Levi (1987), where it was suggested that thresholds for fovea-centred bisection tasks at small separations (<15 min arc) are in good agreement with the predictions of localised spatial filter models (Klein and Levi, 1985; Wilson, 1986), while thresholds at larger separations are constant in terms of cortical units.

Morgan and Watt (1989) disagreed with Levi et al.'s (1988) assertion that Weber's law at large separations is an artefact of eccentricity. They pointed out that only a single eccentricity was examined in the previous study, and to conclude that eccentricity

determines thresholds would require data from several eccentricities. It was also noted that the central reference line did not fall on the iso-eccentric arc, as described above. In support of these objections, Morgan and Watt presented thresholds obtained for discrimination of the lengths of arcs as a function of arc length, which were presented on iso-eccentric arcs of radii varying from 0.5 to 4 deg. Thresholds increased with arc length, as would be expected from a Weber relationship, and depended little on eccentricity, contrary to Levi et al.'s (1988) results.

In response to Morgan and Watt (1989), Levi and Klein (1989) reiterated their hypothesis in this paper and a subsequent one (Levi and Klein, 1990a). Thresholds were determined for a wider range of conditions than previously (Levi et al., 1988): both two element spatial interval discriminations and three element bisection discriminations were examined for high visibility stimuli at eccentricities between 0.625 and 10 deg on iso-eccentric arcs. Thresholds obtained on arcs of different radii scaled simply with an E_2 of approximately 0.45 deg (Levi and Klein, 1990a). The results were consistent with the hypothesis that both separation and eccentricity can determine positional thresholds under certain conditions. At small separations relative to eccentricity (where the angle subtended by the fixation point and the outer pair of iso-eccentric lines is less than 30 deg) thresholds are proportional to separation and demonstrate a Weber fraction of 0.03-0.05. At separations more comparable to eccentricity (angle greater than 30 deg, or separation greater than half the eccentricity), thresholds are proportional to eccentricity and depend little on separation. For any combination of separation and eccentricity the more sensitive of the two mechanisms determines threshold. With respect to Morgan and Watt's (1989) study, it was suggested that judgements in their arc length discrimination task were made on the basis of chord length, and that the task was inherently more difficult at longer lengths, accounting for the rise in thresholds which they found.

Burbeck and Yap (1990b) provided further support for a two mechanism explanation of Weber's law for position. Using a spatial interval discrimination task, the effects of separation, eccentricity, target length and exposure duration on thresholds were investigated. For a fixed separation, eccentricity had little effect on thresholds to 15 deg, beyond which thresholds rose. For fixed eccentricities, using an iso-eccentric arc, thresholds were proportional to separation. At separations greater than 6 deg however, thresholds lost their separation dependence and became more dependent on eccentricity. Their interpretation of the results was that for small separations relative to the eccentricity, thresholds are determined by a separation dependent mechanism, while for

large separations relative to eccentricity, thresholds depend solely on eccentricity and are determined by a separation independent mechanism.

McKee et al. (1990) used a separation discrimination task in which two line pairs were presented either side of fixation, and the subject's task was to determine which pair had the wider separation. When the separation of the pairs was changed without altering the eccentricity (36 min arc), thresholds remained unchanged, demonstrating that eccentricity and not separation determined threshold for this task.

In addition to use of an iso-eccentric arc, Whitaker et al. (1992a) scaled stimulus size as a constant fraction (11%) of separation in order to directly examine the effects of eccentricity on spatial interval discriminations. Eccentricities from 0.267-10 deg in inferior visual field were examined. Spatial interval discrimination thresholds, when expressed as a Weber fraction (threshold as a percentage of separation), scaled simply with eccentricity with a single scaling factor. E_2 values were calculated to be 0.17±0.03 deg for observer PM, and 0.19±0.05 deg for observer DW with an interstimulus interval of 50 ms, and 0.22±0.01 for PM and 0.07±0.01 for DW with an interstimulus interval of 500 ms. That the data scales simply with eccentricity agrees with previous studies (Levi and Klein 1989, 1990a) but the methodology does not disentangle the separate roles of all the factors involved in determining threshold. Since at any eccentricity size was scaled according to separation, any trend at a constant eccentricity may be due to a combination of varying size and separation. However, the results do support the view of the previous studies described that eccentricity is a major factor in producing 'Weber's law' for position.

Levi and Klein (1992) examined bisection thresholds using fovea-centred narrowband Gabor line stimuli. With high contrast stimuli, thresholds at all spatial scales were proportional to separation, so long as very small separations were avoided. At small separations, but not large ones, thresholds were contrast dependent. Thresholds were also independent of spatial frequency and bandwidth.

Waugh and Levi (1993) provide additional evidence for the two mechanism hypothesis. In this study, contrast dependency was studied for vernier acuity over a range of feature separations. At small (less than 4 min arc) separations, thresholds fall as contrast rises, at least to 30 times the contrast detection threshold. This finding is consistent with the contrast response properties of localised spatial filters (Levi and Klein, 1985; Wilson, 1986). At separations greater than 4 min arc, thresholds are only weakly dependent on contrast above 2-3 times contrast detection threshold. This latter finding is more

consistent with a 'local sign' model, where the absolute position labels for each vernier line are compared, and positional uncertainty increases with eccentricity.

In summary, most studies to date conclude that 'Weber's law' for position is achieved by a separation dependent mechanism at small separations, and by an eccentricity dependent mechanism at large separations. At small values of stimulus separation a direct prediction of the Weber relationship holds by assuming that separation is based on the output of receptive fields whose extent envelopes both stimuli (Klein and Levi, 1985; Wilson, 1986). For larger separations, sufficiently large filters are unlikely to exist in early vision. It seems, therefore, that each of the two stimuli whose separation is to be judged are located individually under these conditions and a secondary mechanism exists whereby their separation is encoded. It is at this stage that the Weber relationship occurs. One suggestion (Levi et al., 1988; Levi and Klein, 1989; 1990a) is that at larger eccentricities, Weber behaviour is produced by an absolute positional uncertainty that is proportional to eccentricity. In other words, a feature can be localised to an absolute position with a constant uncertainty in cortical terms.

A radically different view of 'Weber's law' for position to that proposed above has recently been forwarded by Hess and Hayes (1993). They propose that 'Weber's law' is only found for stimuli which are broad-band in the spatial domain, i.e. the dot and line stimuli used in previous investigations. For narrow-band stimuli, 'Weber's law' does not hold, but successively lower frequency mechanisms (which are presumed to mediate performance at higher separations) result in higher positional thresholds. In other words, 'Weber's law' only occurs because of a shift in spatial scale with increasing eccentricity. Levi and Klein (1992) have argued against an earlier report of these findings and have suggested that the inability to demonstrate a Weber relationship is due to the use of stimuli of low contrast and small separation. For high contrast narrow-band stimuli they show that 'Weber's law' can be easily demonstrated. They predict that low-contrast narrow-band stimuli should also demonstrate a Weber relationship provided their separation is not too small. The present study is designed, in part, to test this prediction. More than this, however, the present study takes into consideration the potentially confounding effects of spatial scale, separation and eccentricity as contributors to 'Weber's law' for position. This is achieved by using spatial interval stimuli which are narrow-band in the spatial domain, and which are positioned around an iso-eccentric arc.

11.2 Methods

Stimuli

The stimuli were two patches of sinusoidal contrast grating (the carrier grating) whose profile was modulated by a two-dimensional Gaussian envelope (Gabor patches). Examples of such Gaussian envelopes are depicted in Figure 11.03. The Gabor patches are described by

$$A \sin(2\pi Nx/\sigma) \exp(-(x^2/2\sigma^2)) \exp(-(y^2/2\sigma^2)) \qquad \text{Equation 11.01}$$

where A is the amplitude, σ is the standard deviation of the Gaussian envelope, N is the number of cycles of carrier grating per standard deviation, and x and y are the respective horizontal and vertical distance from the geometric centre of the Gabor. Examples of resultant Gabor patches are shown in Figure 11.04. The carrier grating was positioned in sine phase so as to avoid introducing any mean luminance component to the Gabor. The number of cycles per envelope standard deviation was always maintained at a constant value of 0.8, so that the individual stimuli were all magnified versions of one another. To achieve this, smaller gaussian envelopes therefore modulated higher spatial frequencies. In the Fourier domain, stimulus bandwidth at half maximum therefore has a constant value of approximately 0.55 / 0.8 (Levi and Klein, 1992) = 0.69 octaves.

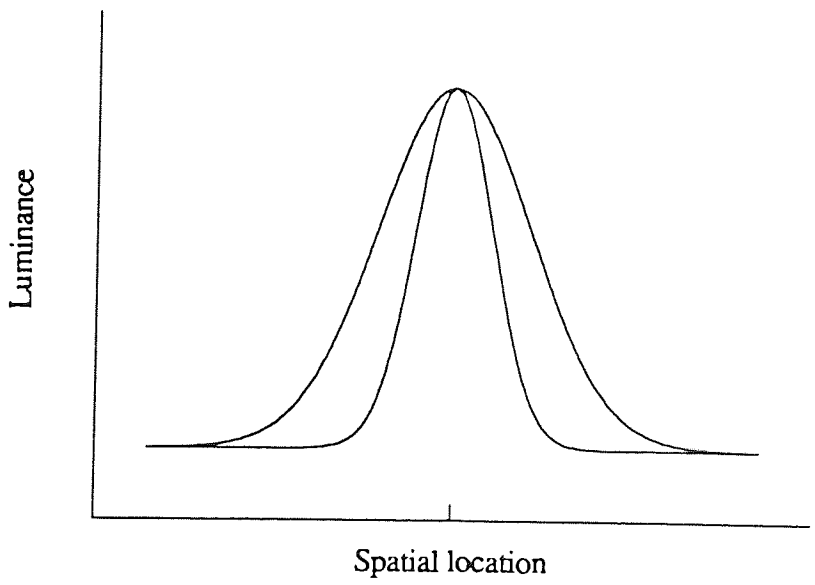

Figure 11.03. Gaussian envelopes illustrated in one dimension, having the form exp $(-(x^2)/(2\sigma^2))$. The wider envelope has a blur parameter (σ) twice that of the narrower envelope.

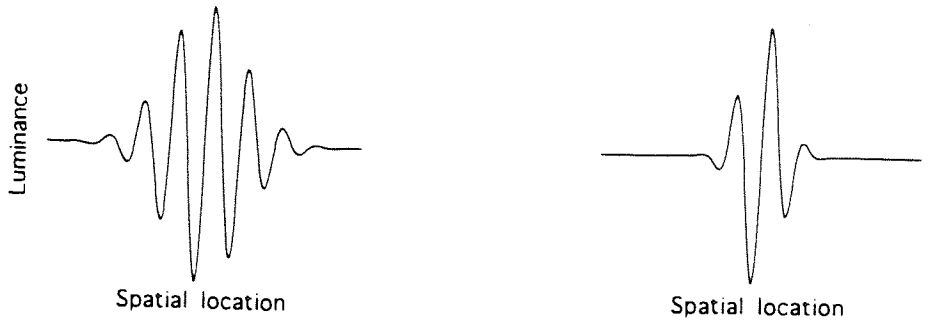

Figure 11.04. The Gaussian envelopes of Fig 11.03 modulating sinusoidal gratings to give Gabor patches. Each envelope is modulated by the same spatial frequency grating. Since the lefthand graph has the larger blur parameter (σ), it also has the larger value of N (cycles per σ). However the stimuli used in the experiment (Figure 11.05) covary σ and spatial frequency (f) to maintain a constant value for N.

The stimuli were generated with 8-bit resolution using the macro capabilities of NIH Image™1.52. Stimuli were presented on a Macintosh M1212 colour monitor whose contrast response was linearised. Mean luminance was 70cd m^{-2}. The host computer was a Macintosh Centris 650 PC. Unless indicated otherwise, all stimuli were set to twice their contrast threshold in order to allow comparison between stimulus conditions. Contrast thresholds for the simultaneous detection of both Gabor patches were established using a yes/no staircase technique. Thresholds were always considerably higher (by at least a factor of 7) than the minimum contrast afforded by the resolution of the equipment. The rather unimpressive contrast thresholds obtained were a direct result of the localised nature of the Gabor patches and the eccentric viewing of the stimuli.

The two Gabor patches were placed side by side around an imaginary circular arc in the upper visual field. Separation was varied by moving both patches around this arc, and was defined as the centre to centre distance between the patches. At the largest separation the patches were located either side of fixation (ie. the maximum separation is twice the eccentricity). For all other separations the patches were located in the upper visual field and a horizontal fixation line, which passed through the centre of the imaginary arc, was provided. To exclude the influence of the edges of the monitor, the two patches were jittered randomly in their horizontal position. Stimulus eccentricity was varied by changing the viewing distance, and hence the angular radius, of the imaginary arc. The size of the patches on the screen were varied to compensate for the changes in viewing distance. Carrier spatial frequencies of 1, 2, 4 and 8 cycles per deg were investigated. For each carrier frequency, spatial interval discrimination thresholds

were established for a range of eccentricities and separations. It is worth emphasising that for any given carrier frequency, the size of the patch (which may be denoted by the standard deviation of the Gaussian window) remained constant. The standard deviation of the Gabor patches (in degrees of visual angle) is given by

$$\sigma=0.8/f \qquad \text{Equation 11.02}$$

where f is the spatial frequency of the carrier.

Methods

Spatial interval discrimination thresholds were measured using a forced-choice method of constant stimuli. The stimuli were presented with sudden onset and offset for a duration of 500msec. Following this, the observer had to respond using the computer's mouse as to whether their separation had been larger or smaller than an internally-learnt average separation (eg. Westheimer and McKee, 1977b; Westheimer, 1979b). This average separation was constructed on the basis of previous presentations by the use of feedback, in the form of an audible 'beep', which was provided after an incorrect response ('incorrect' being judged relative to the mean of the stimulus ensemble). This obviously leads to numerous early errors in the routine, since the average separation has not yet been learnt. The first 20 trials were therefore used as a learning period and the responses to these trials were ignored in the final analysis. Following these initial trials the number of correct responses and the total number of trials at each of seven separation levels were counted. The seven separations were equally spaced and spanned a range which was known, from previous pilot experiments, to vary from approximately 0 to 100% 'larger' subject responses. Each of the seven separations were equally likely to be presented on a given trial and the routine continued for a total of 100 trials following the initial learning period. The computer then displayed the results which were analysed using probit analysis to reveal a mean separation and a threshold change in separation from the mean corresponding to the 84% correct level. Final thresholds were accepted as the mean of 2-4 of these threshold estimates, and final error estimates reflect the larger of the within- and between-run variance (Levi and Klein, 1992).

Observers

Two observers (KL and DW) participated in the experiments. Both underwent several weeks of training using different stimulus conditions before data collection began. Observations were carried out in a dimly-lit room in order to avoid reflections from the monitor. Viewing was monocular using the dominant eye and normal pupils. Both observers were pre-presbyopic and wore their distance refractive correction for all viewing conditions.

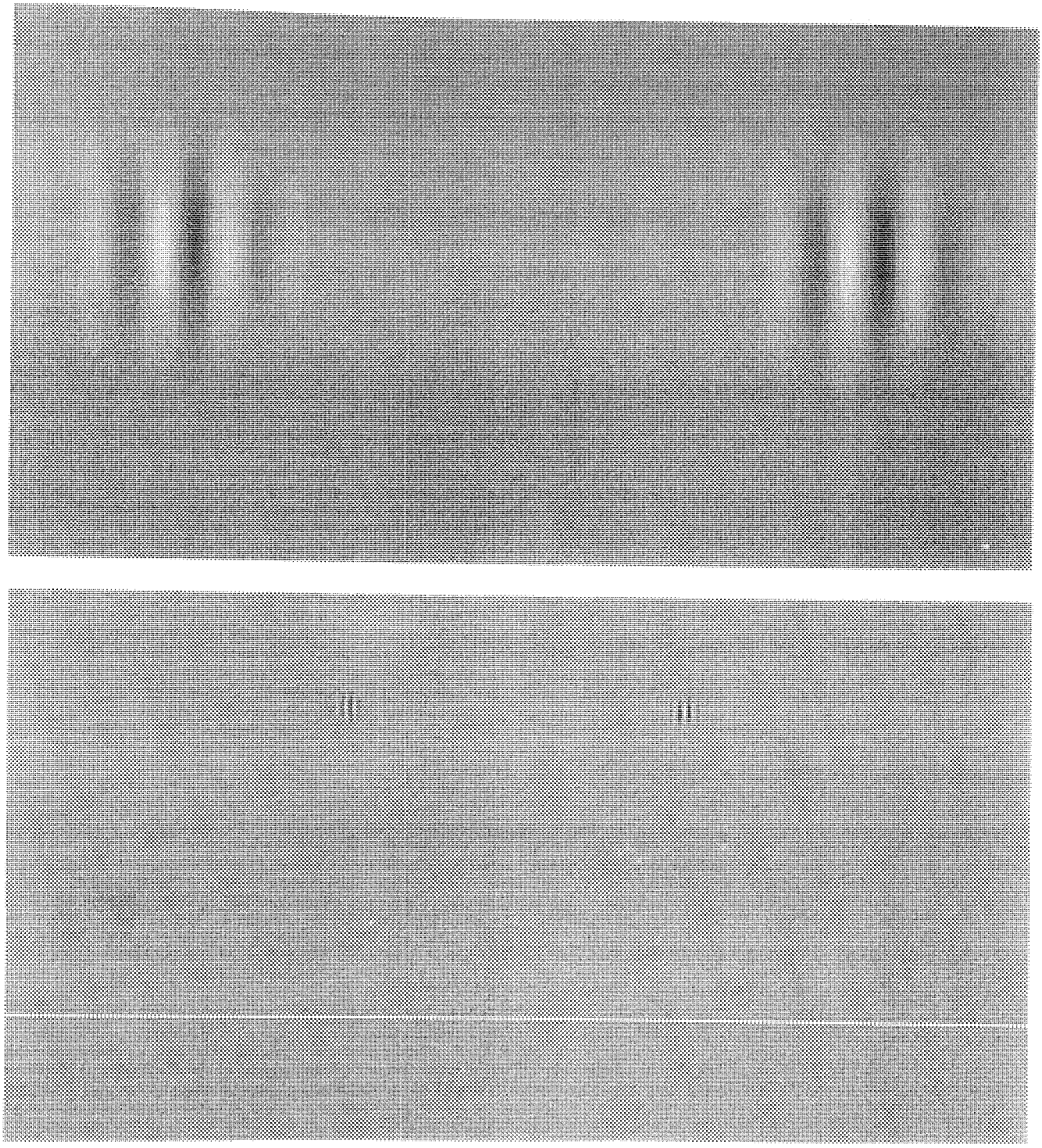

Figure 11.05. Examples of two of the stimuli used in the spatial interval discrimination task, presented on an iso-eccentric arc. Each stimulus is presented at the same eccentricity (5deg), and was viewed at the same distance (2/3m). The stimuli are shown at 95% contrast for clarity, but the actual contrast detection thresholds were very different (3% for Figure a, and 48% for Figure b).

a. σ is 0.8. Separation is 10 deg, and so the separation/eccentricity ratio is 2.

b. σ is 0.1. Separation is 5 deg, and so the separation/eccentricity ratio is 1. The horizontal fixation line was visible to the observer.

11.3 Results

Figure 11.06 shows spatial interval discrimination thresholds plotted against separation for each of four standard deviations and for both observers. Data are shown for a range of stimulus eccentricities. The small number of data points presented for the large standard deviation stimuli is a direct result of a lower limit on viewing distance (33cm). Smaller viewing distances caused problems with accommodation. Another limitation occurs for the small stimuli, where contrast thresholds at large eccentricities become too high to present stimuli at twice their contrast threshold. These are the two major constraints which limit the range of the conditions for which data is presented. The data for each stimulus size show similar trends. As eccentricity increases, so do spatial interval discrimination thresholds. Note that the extreme right hand data points of each function represent the condition in which stimuli are presented either side of fixation. In line with what might be expected of such stimuli, Weber's law appears to hold in that thresholds increase steadily as a function of separation (the dotted line represents a Weber fraction of 0.05 for KL and 0.035 for DW). However, the Weber behaviour goes further than applying only to these extreme data points, as can be seen from Figure 11.07. This shows the same data as in Figure 11.06, but with the y-axis expressed as a Weber fraction, ie spatial interval threshold as a percentage of separation. In addition, the x-axis has been normalised by expressing separation as a fraction of the eccentricity. This has the effect of collapsing the data from different eccentricities on to a single function. What this means is that Weber's law (the direct proportionality between threshold and the separation giving rise to the threshold) holds for *geometrically identical stimuli* across each eccentricity. By the term geometrically identical, I mean stimuli whose separation/eccentricity ratio is the same. Stimuli which lie either side of fixation, for example, are geometrically identical because their separation is always equal to twice their eccentricity. To use another analogy (Levi and Klein, 1989), the angle between the two stimuli stays the same as eccentricity varies.

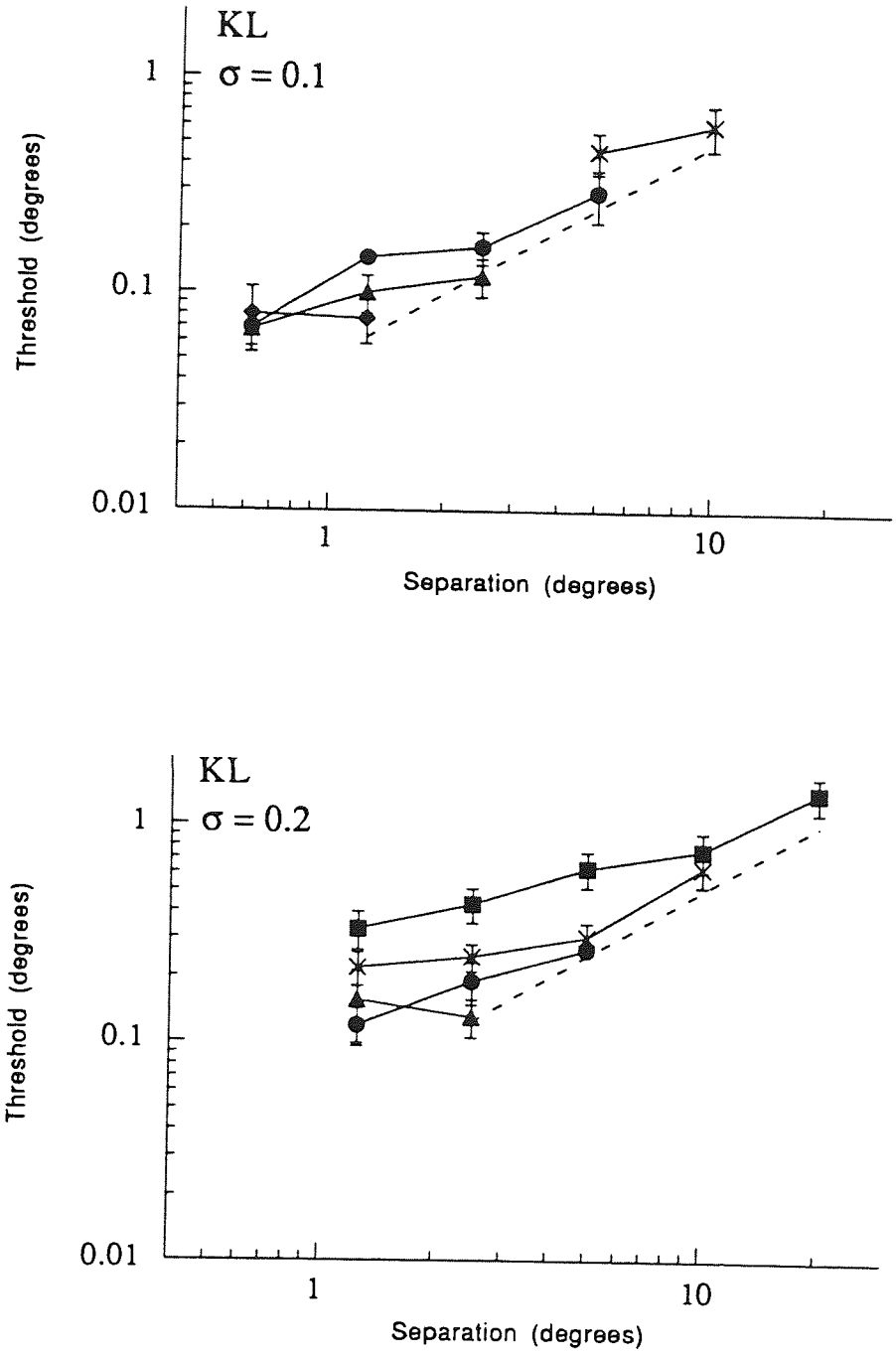

Figure 11.06. See subsequent page for legend.

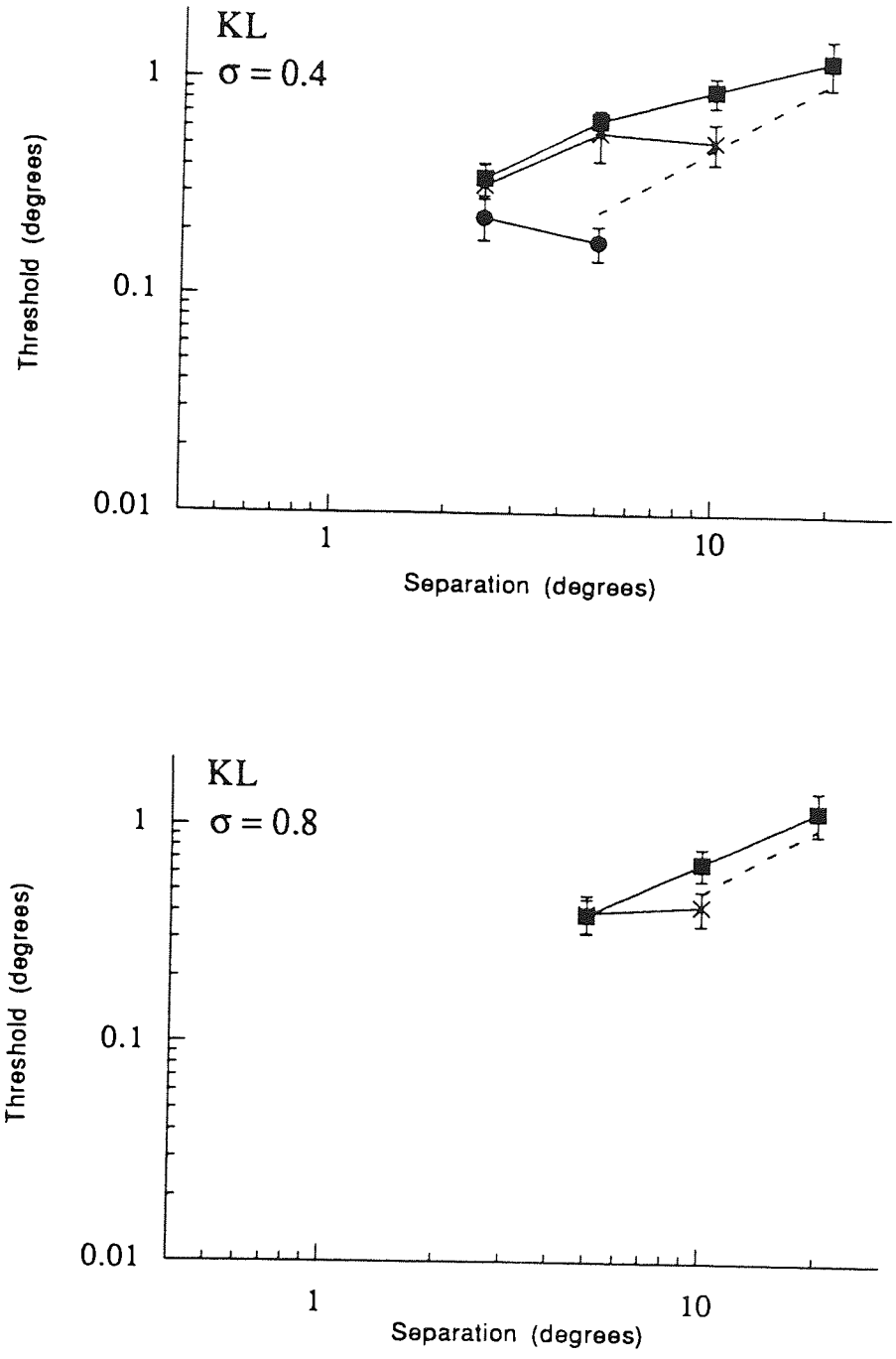

Figure 11.06. See subsequent page for legend.

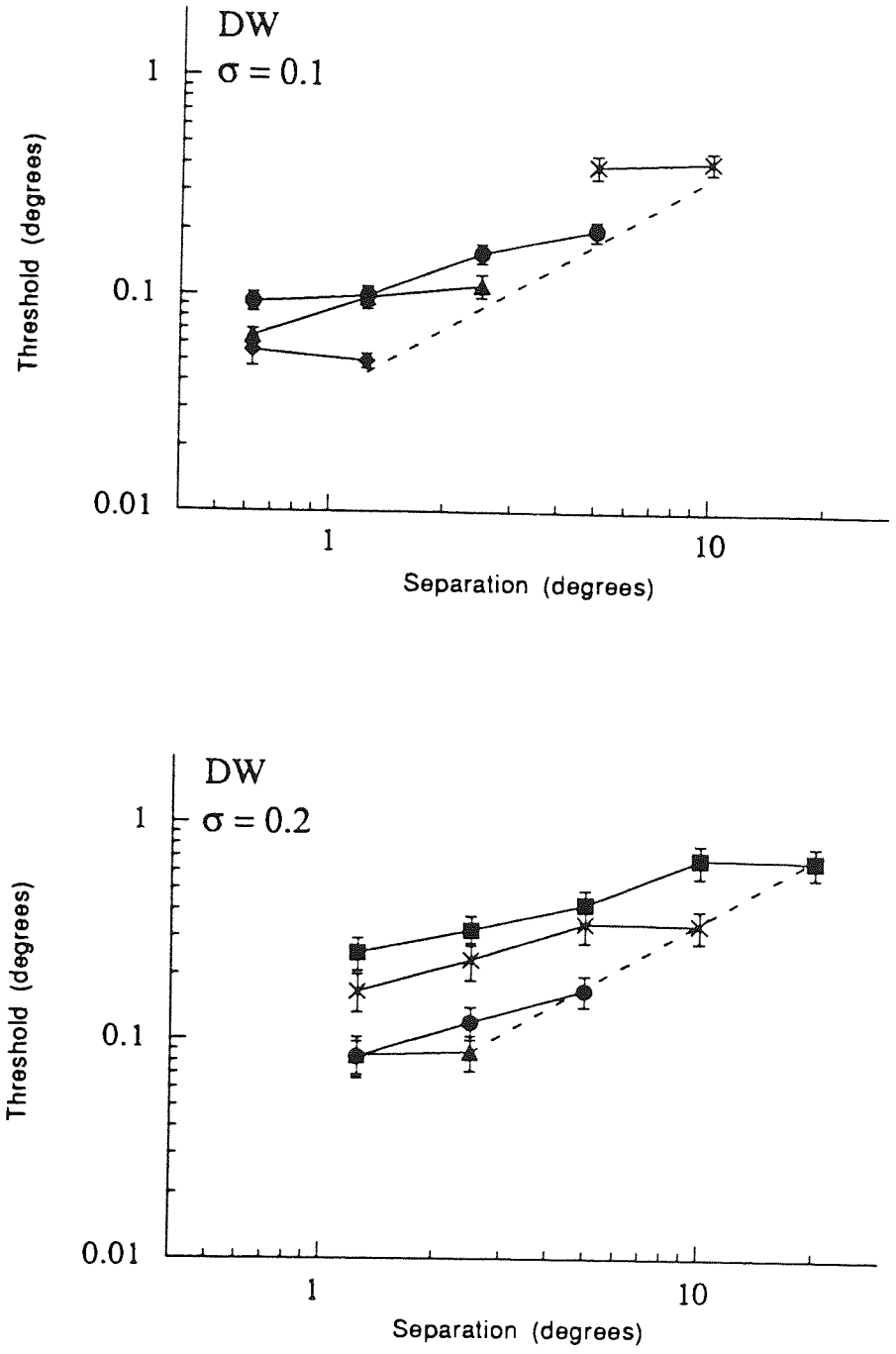

Figure 11.06. See following page for legend.

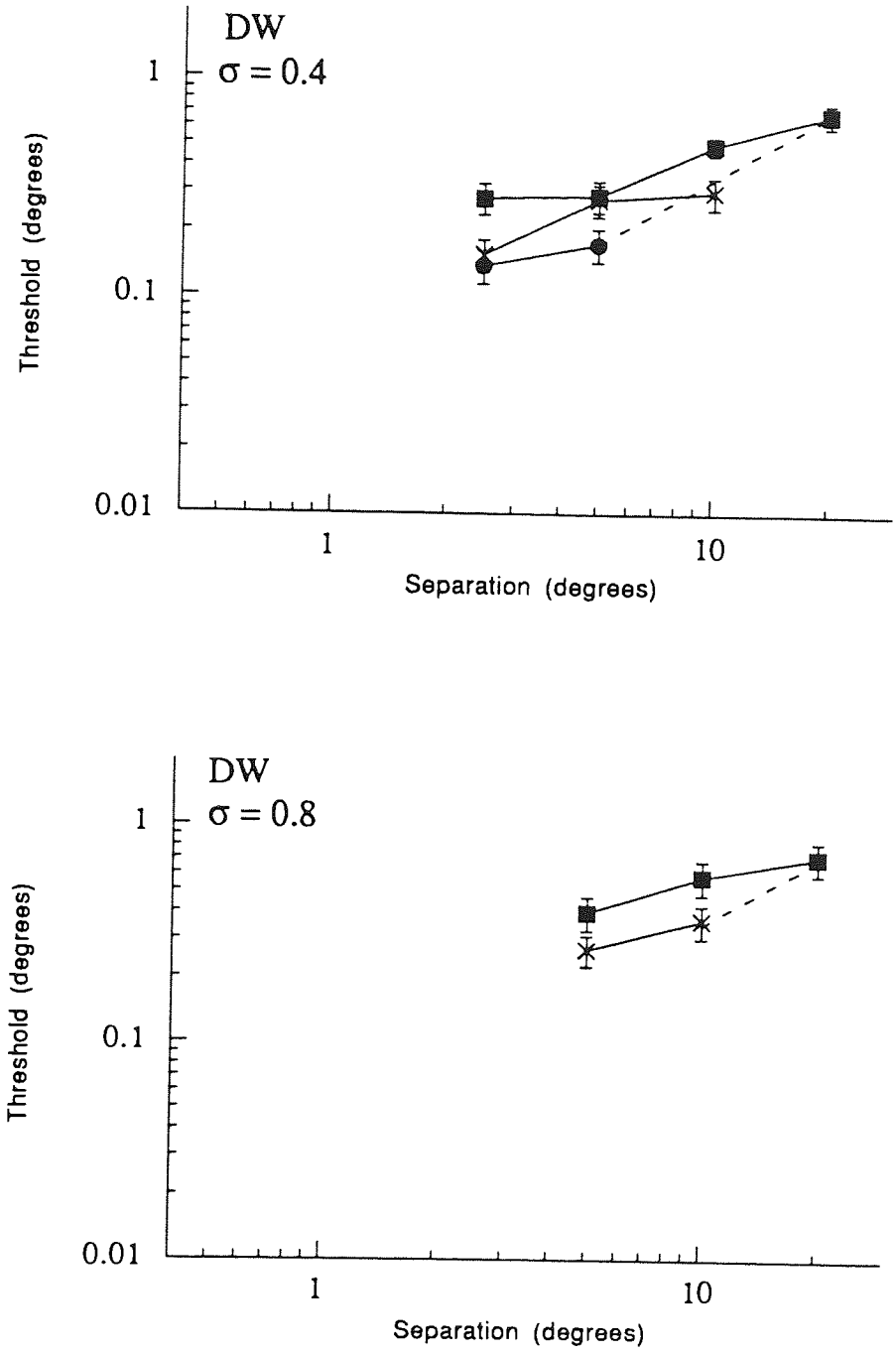

Figure 11.06. Spatial interval discrimination thresholds as a function of separation for stimuli of different blur parameters (σ of 0.1, 0.2, 0.4 and 0.8), eccentricities (0.625-10 deg) and observers (KL and DW). Symbols: diamonds: eccentricity 0.625 deg; triangles: 1.25 deg; circles: 2.5 deg; crosses: 5 deg; squares: 10 deg.

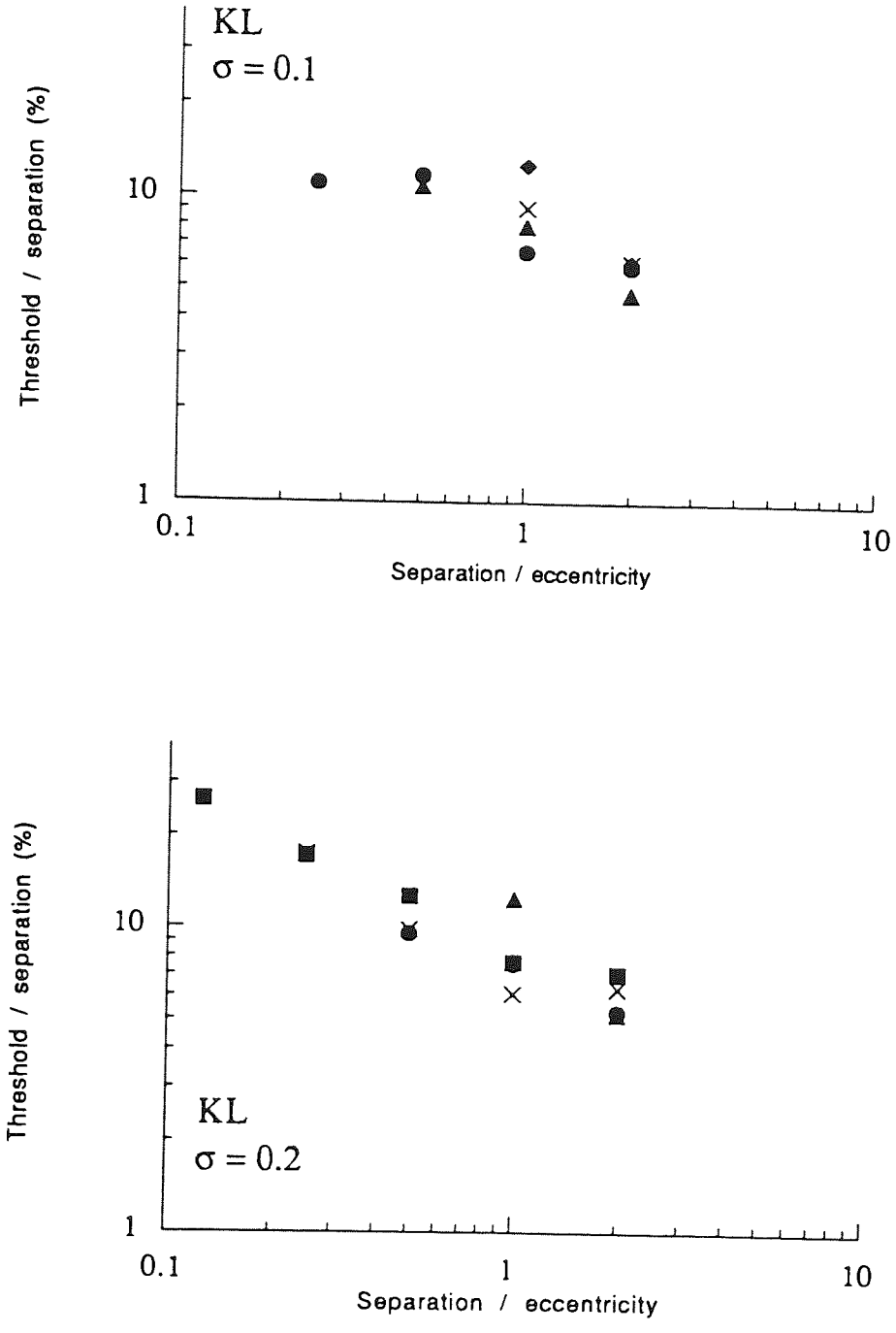

Figure 11.07. See subsequent page for legend.

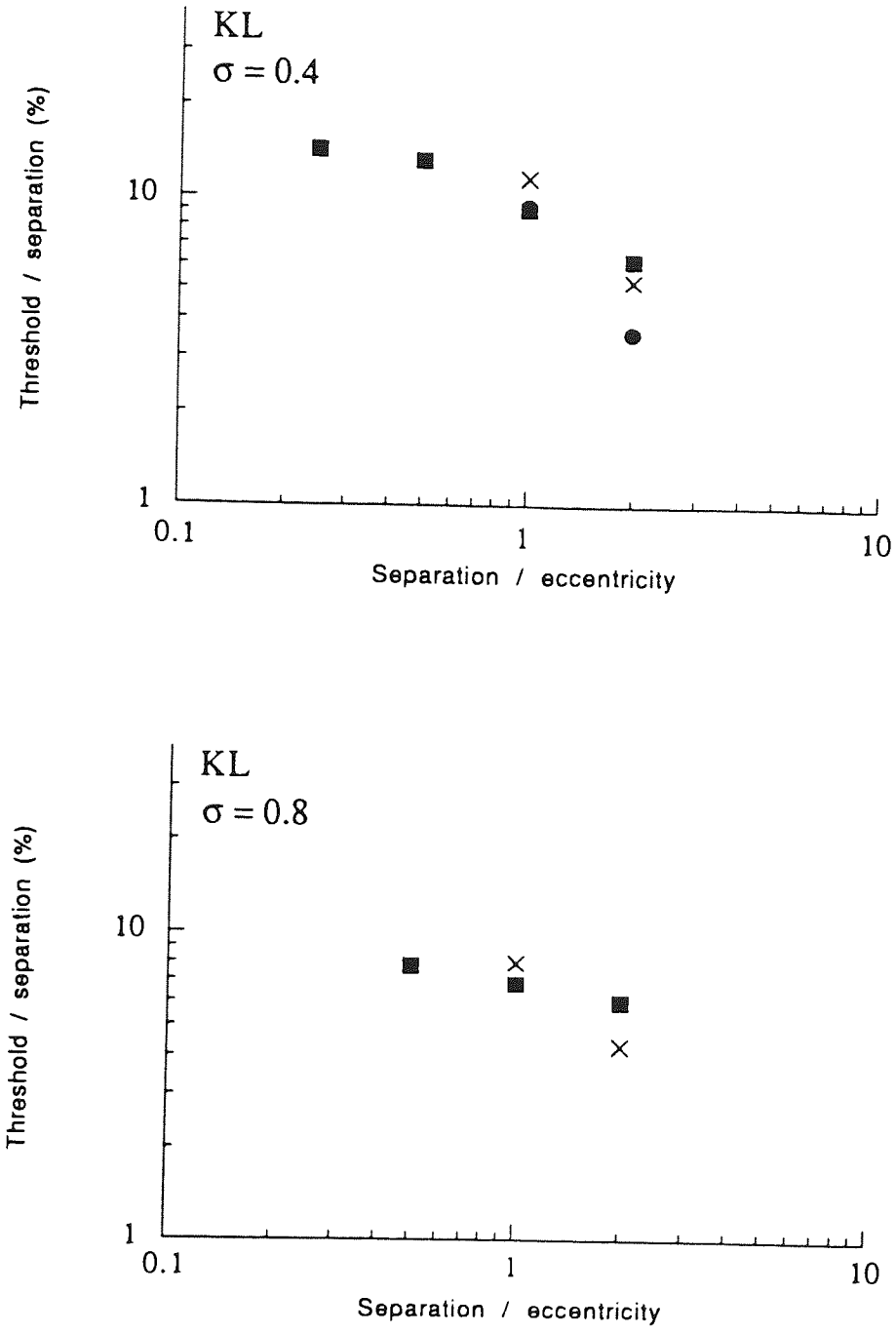

Figure 11.07. See subsequent page for legend.

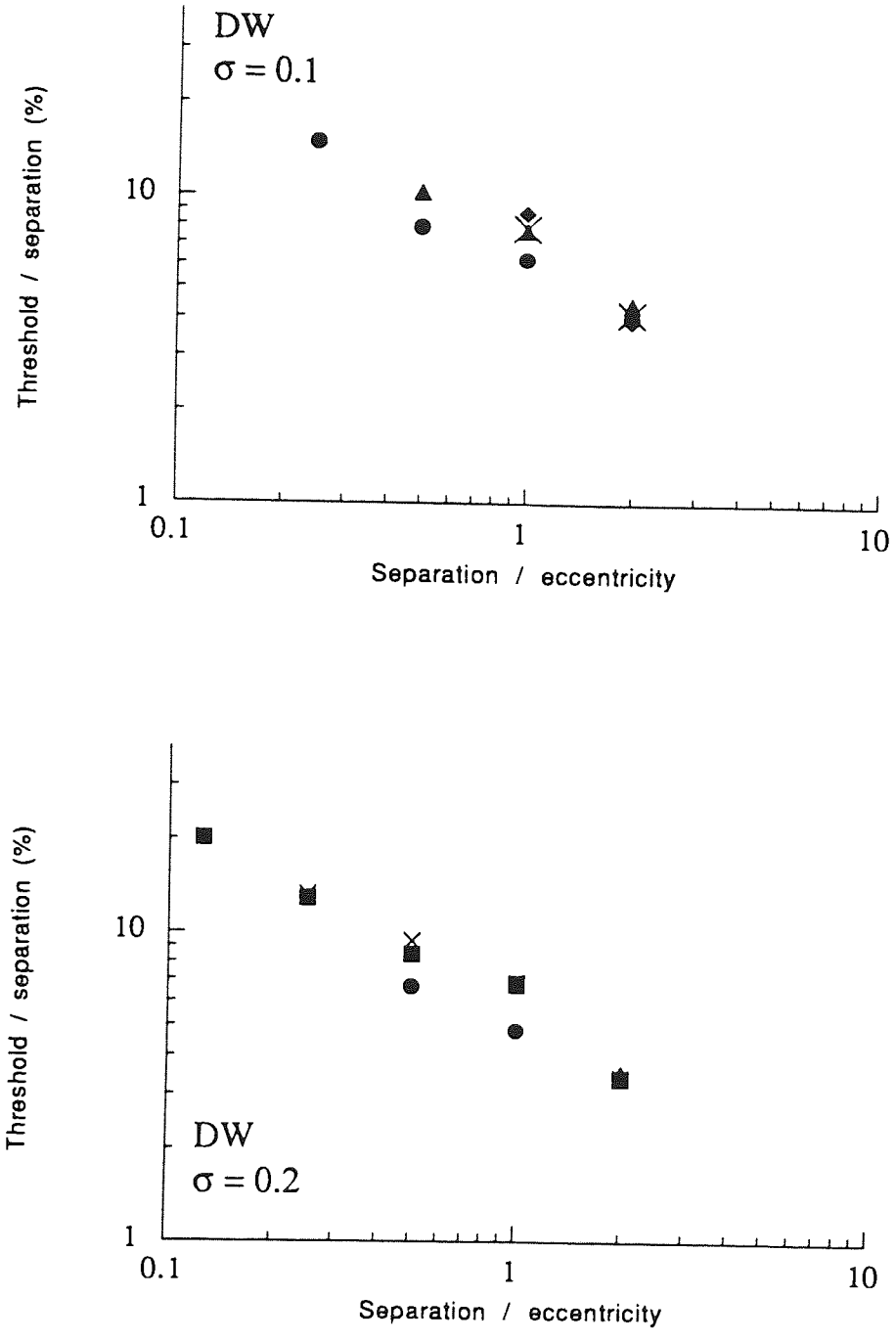

Figure 11.07. See following page for legend.

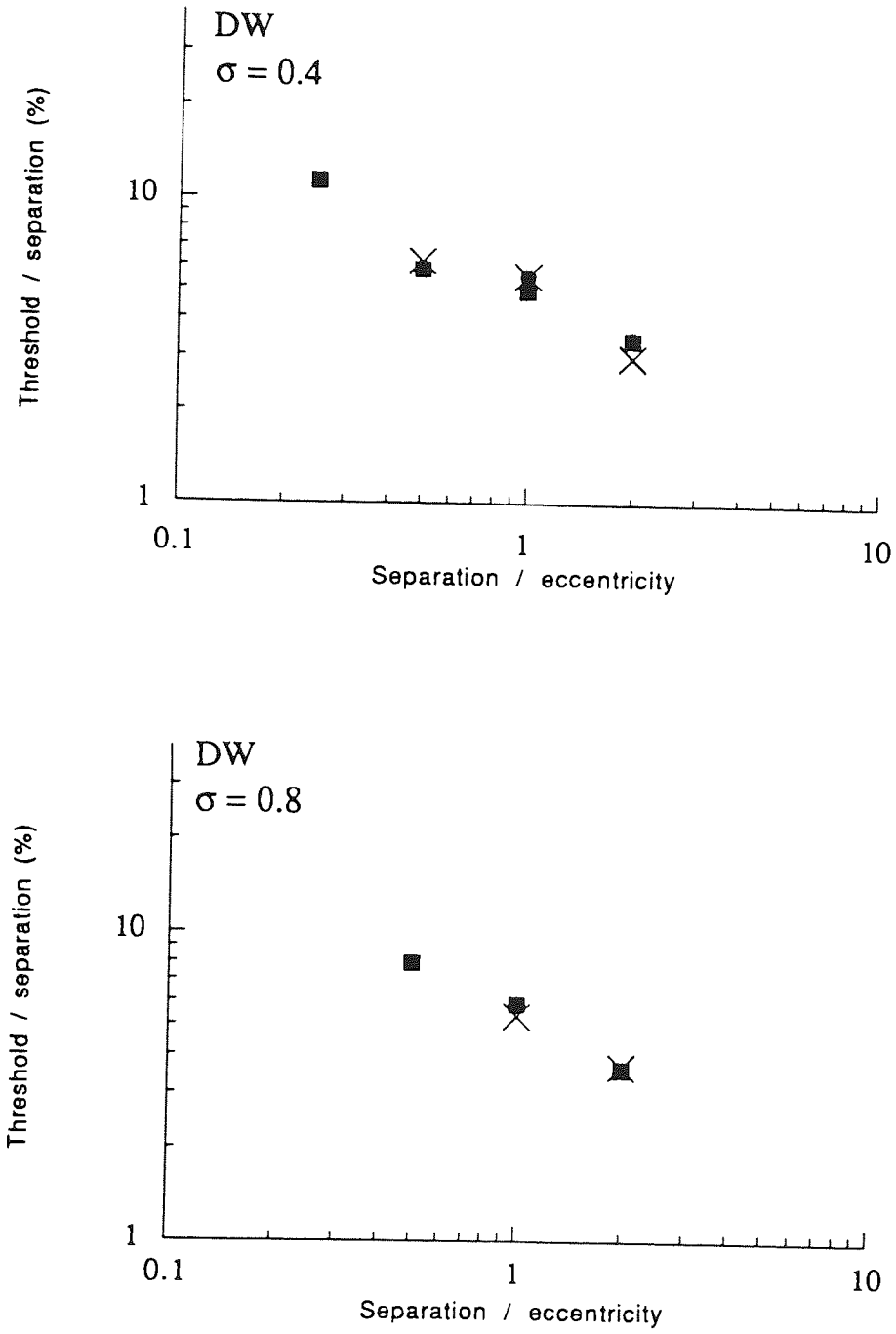

Figure 11.07. The data of Figure 11.06 normalised for each value of σ by expressing the y-axis as a Weber fraction (threshold / separation), and the x-axis as a geometric stimulus arrangement (separation / eccentricity). Symbols and observers as for Figure 11.06.

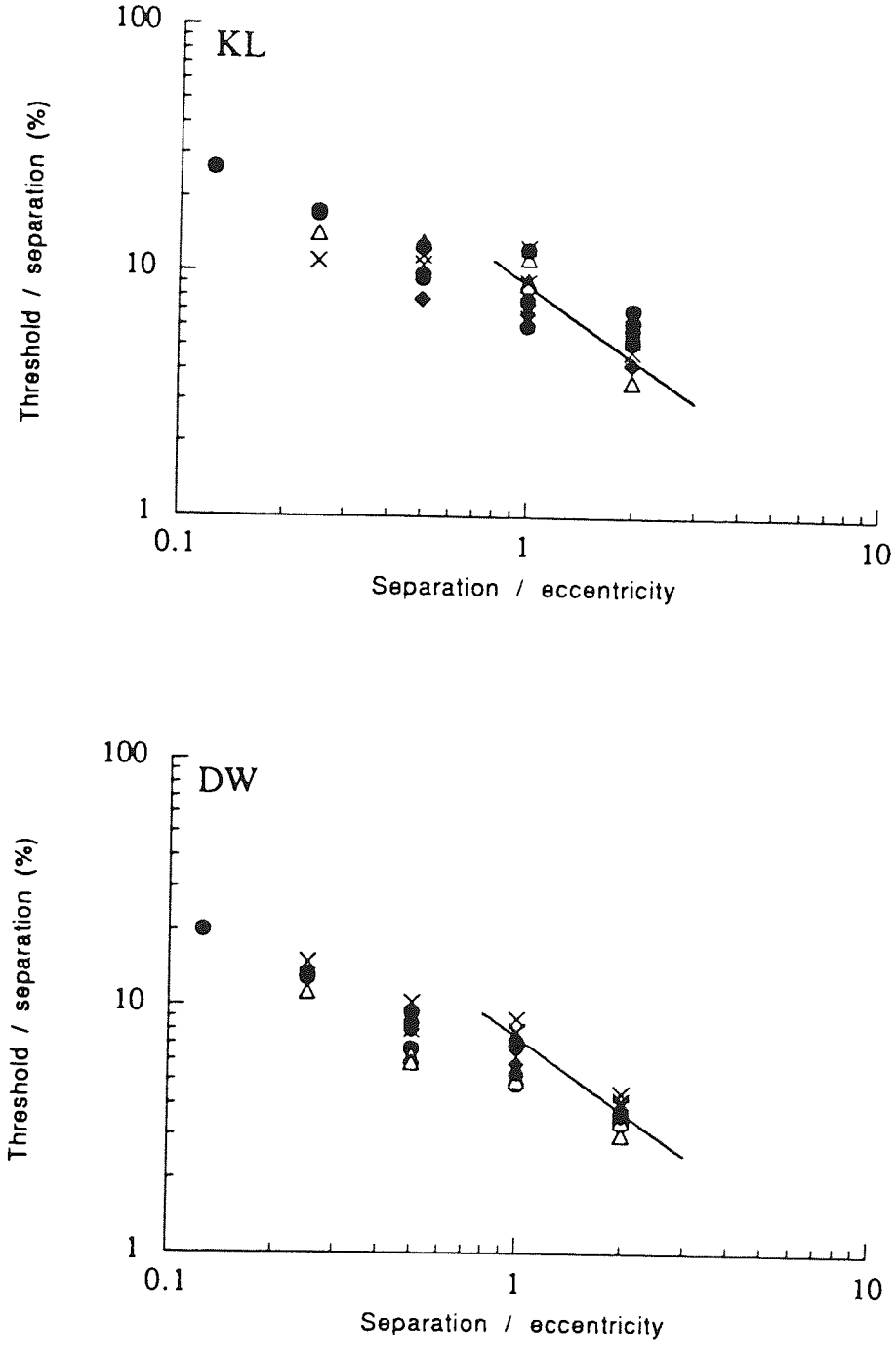

Figure 11.08. The data of Figure 11.07 is shown for all standard deviations on the same graph for each observer. Symbols: closed diamonds: σ 0.8; open triangles: σ 0.4; closed circles: σ 0.2; crosses: σ 0.1.

Moreover, the data from different sizes (different standard deviations) of stimuli can be combined, as shown in Figure 11.08, with the effect that the data again collapse to the same function. Thus, the Weber fraction appears to be independent of both stimulus eccentricity *and* the blur parameter (standard deviation) of the stimuli. The only factor which has an influence on the Weber fraction is the geometric arrangement of the stimulus, ie. the ratio of separation to eccentricity. The solid line in Figure 11.08 represents a gradient of -1. This is a special case in which data points which follow this gradient (ie the data at the two largest separation/eccentricity ratios) obey the concept that thresholds are a constant fraction (in this case 9% for KL and 7% for DW) of the eccentricity. As will be shown in the next section, the level of the Weber fraction at smaller separation/eccentricity ratios is critically dependent upon the suprathreshold contrast level at which spatial interval performance is measured.

Effect of suprathreshold contrast

Levi and Klein (1992) have noted that contrast has a differential effect on narrow-band spatial interval discrimination thresholds at small and large separations, although they did not examine the extent of this contrast dependence closely. Hess and Holliday (1992) provide a more extensive examination of suprathreshold contrast for the vernier alignment of Gabor patches. Waugh and Levi (1993) have also noted a differential contrast effect on broad band vernier targets at different separations. In this section the effect of suprathreshold contrast on the present iso-eccentric spatial interval discrimination task is investigated.

Figure 11.09(a) shows spatial interval discrimination thresholds for Gabor patches of σ=0.2 situated either side of fixation. Data are shown for four different eccentricities as a function of suprathreshold contrast level (remember that data of all the previous figures were obtained at 2x contrast threshold). As would be predicted from Figure 11.06, thresholds increase as a function of eccentricity. Once above 2x threshold, thresholds are virtually independent of suprathreshold contrast level. This is shown even more clearly in Figure 11.09(b) where the data have been expressed as a Weber fraction. This collapses the data from each eccentricity together. The straight line represents a best fitting regression line to the data for contrast levels of 2x threshold and above. Its exponent is only -0.002 for KL and -0.04 for DW, highlighting the independence of spatial interval thresholds for stimuli situated either side of fixation to suprathreshold contrast.

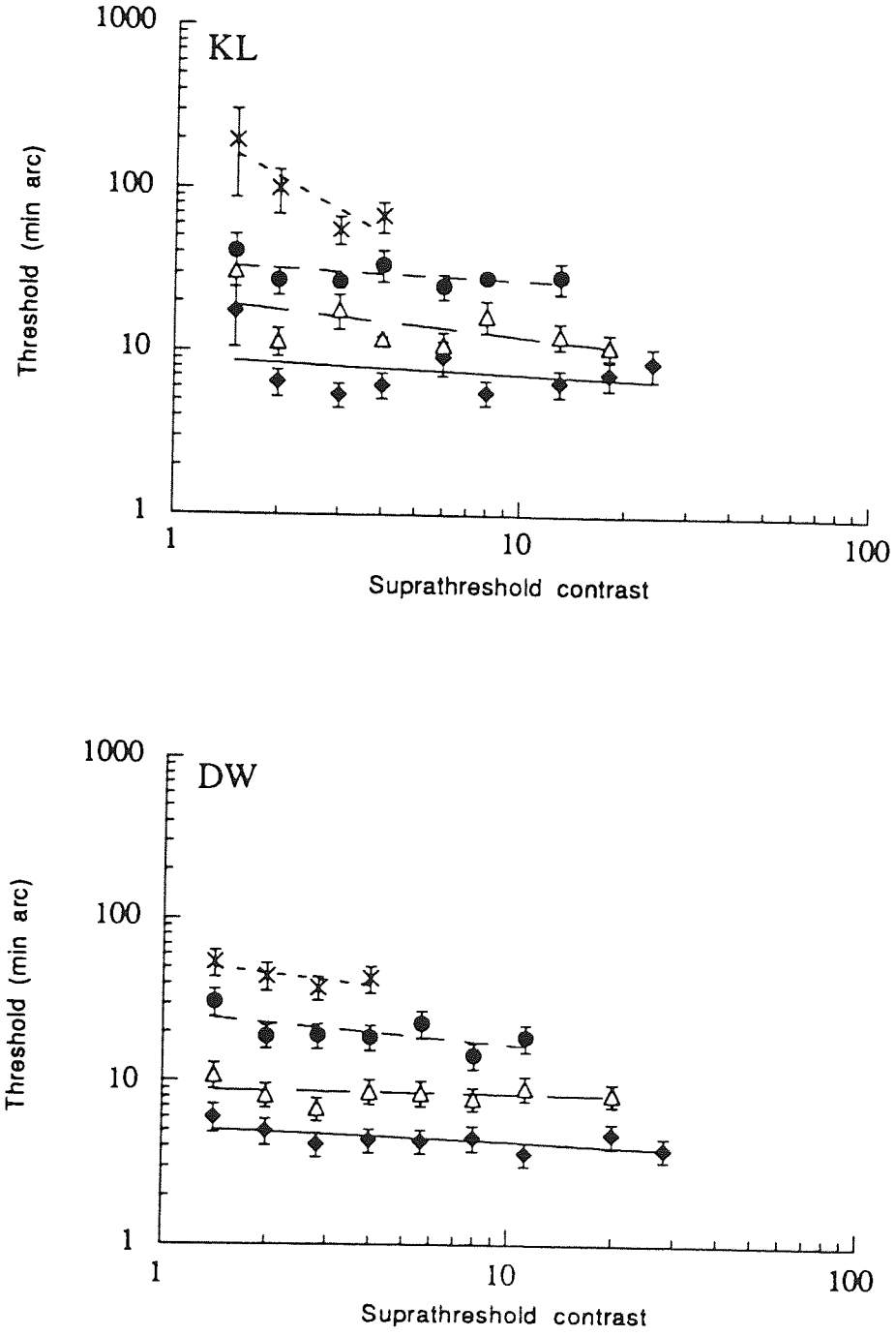

Figure 11.09. a. Spatial interval discrimination thresholds for several eccentricities as a function of suprathreshold contrast. Contrast is expressed in multiples of the contrast detection threshold. σ is 0.2 for all stimuli, and the separation/eccentricity ratio is 2. Observers KL and DW. Symbols: closed diamonds: 1.25 deg eccentricity; open triangles: 2.5 deg; closed circles: 5 deg; crosses: 10 deg.

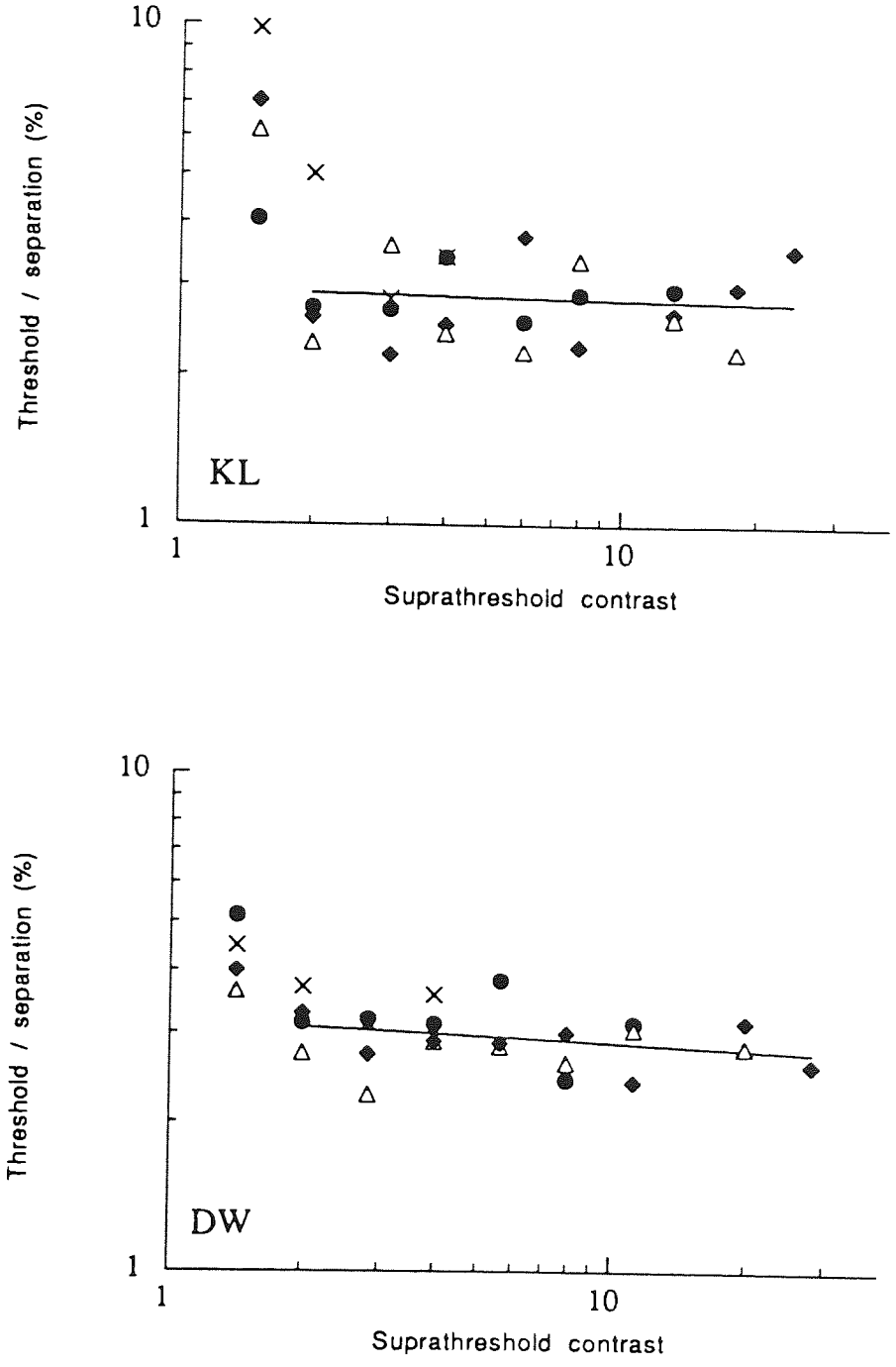

Figure 11.09. b. Data of Figure 11.09a, with the y-axis expressed as a Weber fraction (threshold/separation). Symbols as for Figure 11.09a.

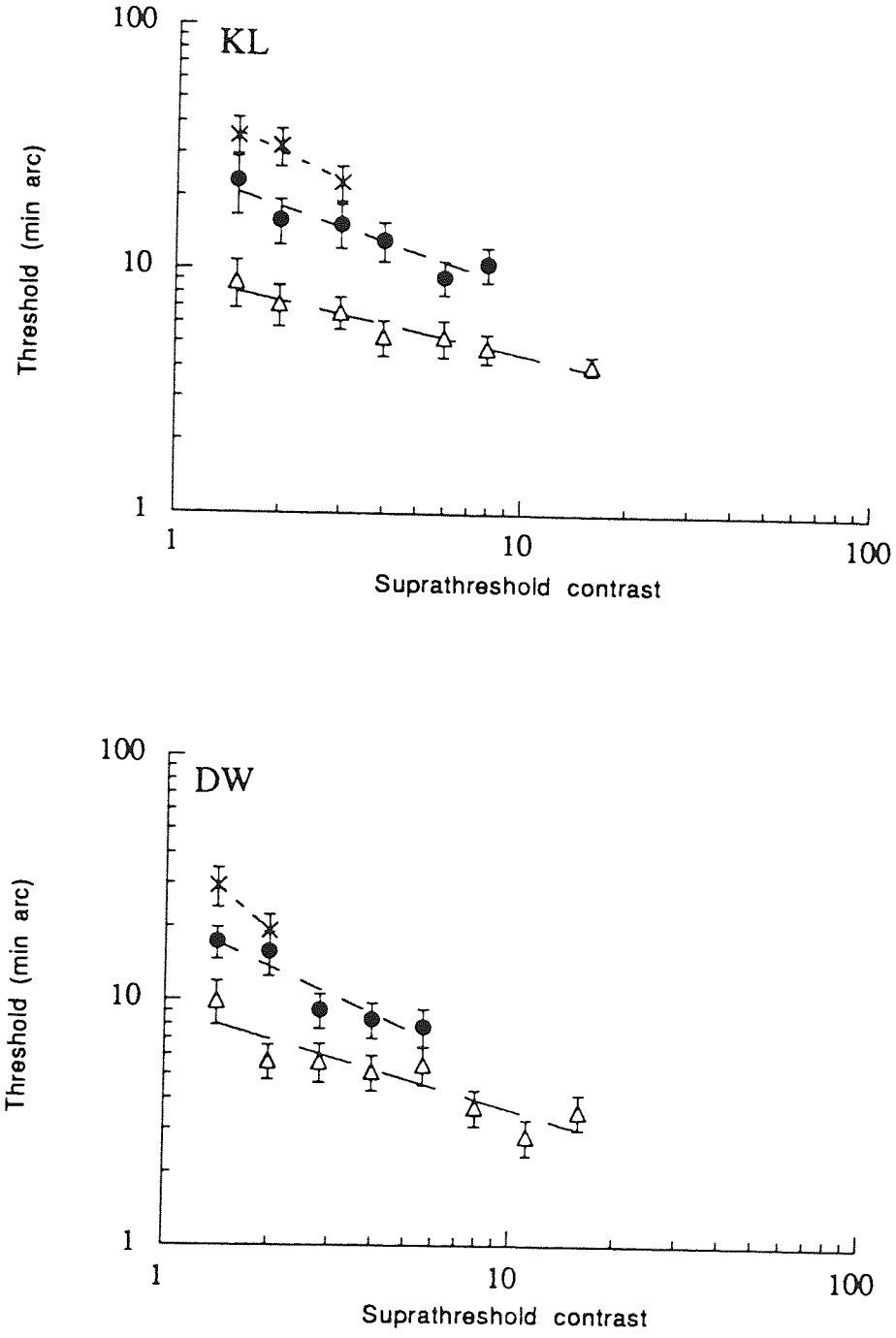

Figure 11.10. a. Spatial interval discrimination thresholds for several eccentricities as a function of suprathreshold contrast. Contrast is expressed in multiples of the contrast detection threshold. σ is 0.2 for all stimuli, and the separation/eccentricity ratio is 0.25. Observers KL and DW. Symbols: closed diamonds: 1.25 deg eccentricity; open triangles: 2.5 deg; closed circles: 5 deg; crosses: 10 deg.

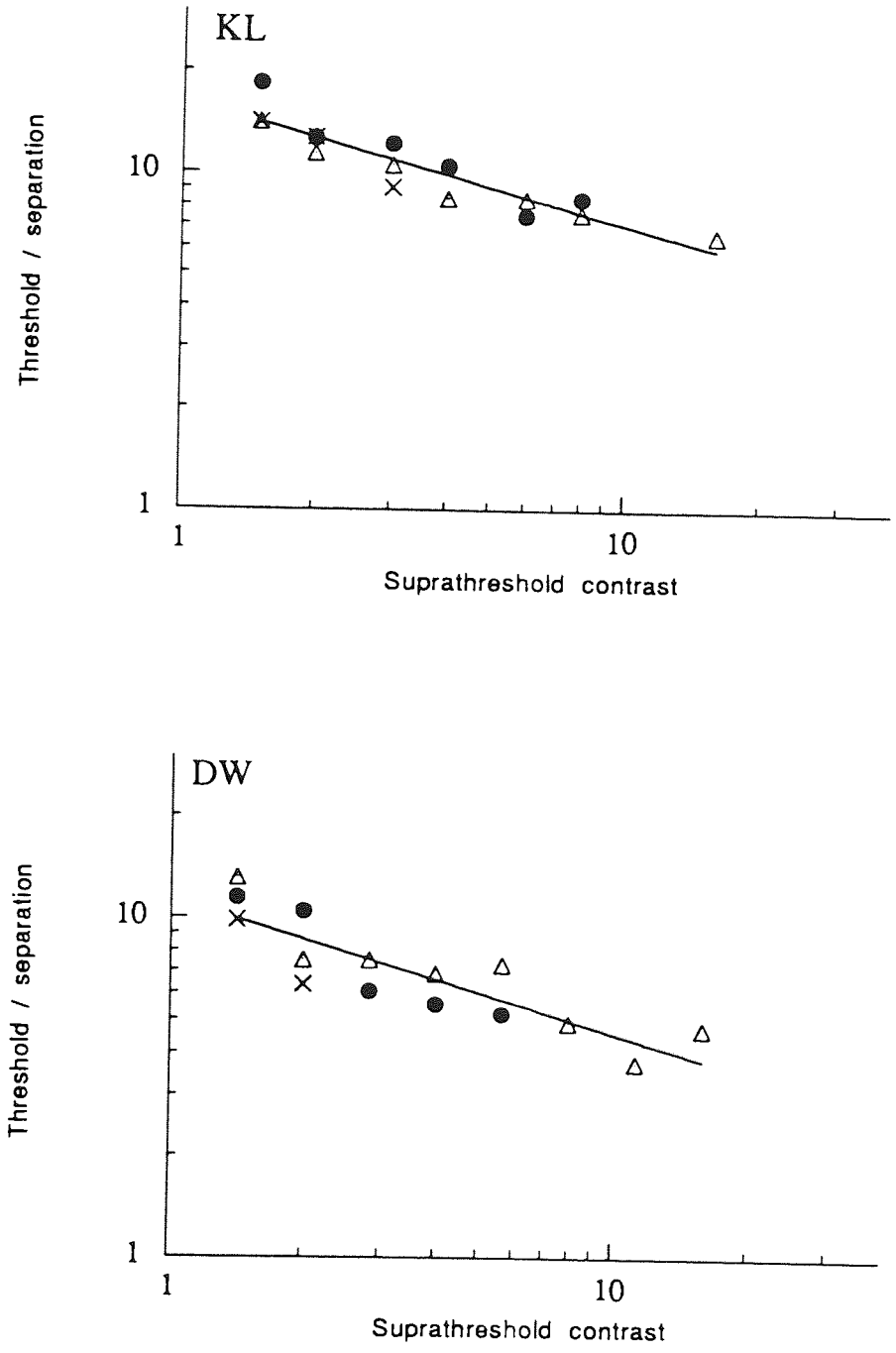

Figure 11.10. b. Data of Figure 11.10a, with the y-axis expressed as a Weber fraction (threshold/separation). Symbols as for Figure 11.10a.

A different situation occurs for geometric arrangements of the patches where the separation/eccentricity ratio is smaller. The data of Figure 11.10(a) show data for a separation/eccentricity ratio of 0.25. It is clear that thresholds for this geometric arrangement show a marked dependence on suprathreshold contrast level. Again the data from different eccentricities can be equated by expressing performance as a Weber fraction (Figure 11.10(b)) and the regression line through the resulting data set has an exponent slightly less than an inverse square root relationship, being -0.36 for KL and -0.39 for DW.

What these results show is that the precise shape of the function shown in Figure 11.08 will be dependent upon the suprathreshold contrast level chosen. Data for the larger separation/eccentricity ratios will show little improvement with increases in contrast above 2x threshold. The smaller separation/eccentricity ratios, on the other hand, are likely to improve consistently with increasing contrast, which will have the effect of flattening the function shown in Figure 11.08 at smaller separation/eccentricity ratios.

11.4 Discussion

The results provide no support for the view that 'Weber's law' arises due to changes of the spatial scale of underlying mechanisms as separation varies (Hess and Hayes, 1993). Rather, 'Weber's law' holds at each of a number of spatial scales over a wide range of separations (Levi and Klein, 1992; Figure 11.08). This difference of opinion is not a trivial one, given the undisputed importance of 'Weber's law' for separation in human vision. Levi and Klein (1992) explained an earlier report of the findings of Hess and Hayes (1993) on the basis of the small values of separation used by the latter authors, particularly given the low contrast nature of their stimuli. As Levi and Klein (1992) predict, the present results show that 'Weber's law' holds for narrowband, low visibility stimuli (2x threshold) provided very small separations are avoided. Figure 11.11 compares the present results with those of Hess and Hayes (1993) under the same conditions. Despite the small separations used by Hess and Hayes, which may be limited by crowding effects, the data hints that if extended to larger values of separation, their thresholds would be comparable to the present results, which rise as a proportion of separation.

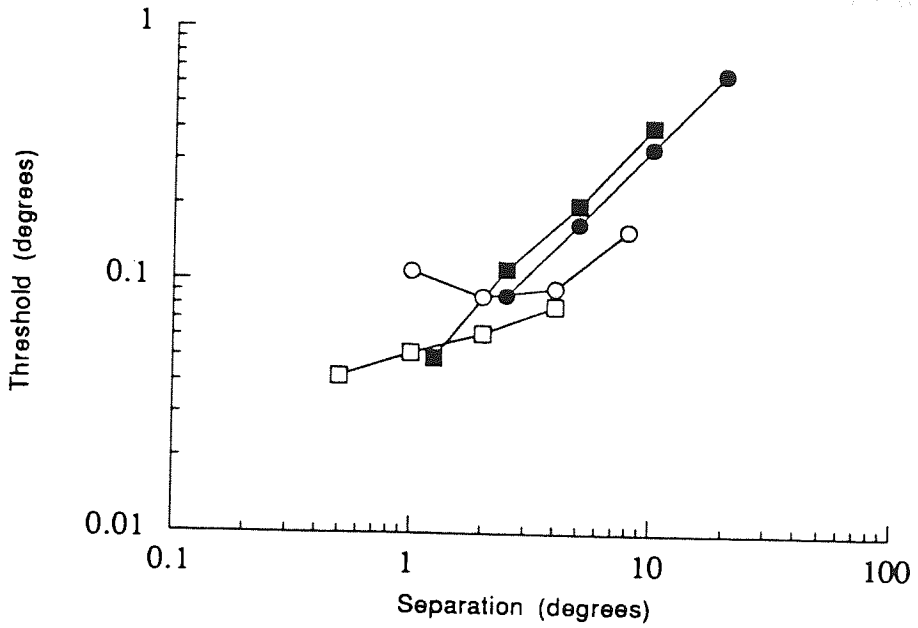

Figure 11.11. Spatial interval thresholds at a separation/eccentricity ratio of 2 for observer DW in the current study (filled symbols) are compared with results for the fovea-centred bisection task of observer RFH (Hess and Hayes (1993); their Figure 4b) (open symbols). Squares represent σ = 0.1; circles represent σ = 0.2.

Hess and Hayes (1993) proposed that the shape of the threshold vs separation function depends on the spatial scale and suprathreshold contrast of the stimuli. Contrast does have a pronounced effect on thresholds, but only at small separations relative to eccentricity (Figure 11.10), but spatial scale does not affect the Weber fraction (Figure 11.08). The highest frequency spatial scale available declines with increasing eccentricity (eg. Toet et al., 1988b), and so if spatial scale were a major factor underlying spatial interval discrimination, then for stimuli on any given iso-eccentric arc, the same spatial scale should determine thresholds for all separations. Thresholds at any eccentricity should therefore be constant for all separations. Again, the present results do not confirm this (Figure 11.06) since thresholds increase with separation.

The present data were obtained with stimuli having a constant bandwidth of 0.69 octaves. Figure 11.12 shows data obtained for stimuli with different bandwidths, ie. a constant envelope size and a varying number of cycles per envelope. Thresholds show no significant variation with respect to bandwidth. This suggests that it is the Gaussian envelope properties which determine thresholds rather than the bandwidth of the spatial frequency component, which is well established in the literature (Burbeck, 1987, 1988;

Toet and Koenderink, 1988). Toet and Koenderink (1988) showed that three blob alignment thresholds for Gabor patches at contrast detection threshold are independent of the spatial frequency of the carrier grating, but are a constant fraction of the standard deviation of the Gaussian envelope. These results suggested that the visual system assigns a single location tag to a Gabor stimulus, whose accuracy of localisation is then determined as a constant fraction of its spatial extent. In addition to showing that the spatial frequency content of widely separated objects is not important to their relative localisation (Burbeck, 1987), Burbeck (1988) has also shown that localisation accuracy is not affected if the two objects to be localised have different spatial frequency contents.

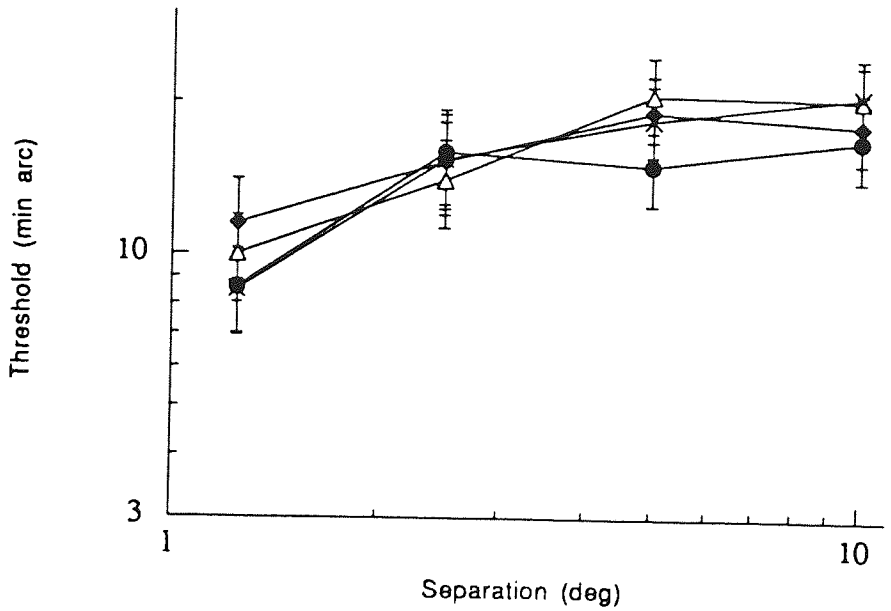

Figure 11.12. Spatial interval thresholds for fovea centred stimuli (separation/eccentricity ratio = 2) as a function of separation for stimuli of several bandwidths. Envelope size is constant (σ = 0.4). Symbols: closed diamonds: N = 1.6, bandwidth = 0.34 octaves; open triangles: N = 0.8, bandwidth = 0.69 octaves; closed circles: N = 0.4, bandwidth = 1.38 octaves; and crosses: N = 0.2, bandwidth = 2.75 octaves.

The present results show that 'Weber's law' for position is not a phenomenon peculiar to fovea-centred stimuli. Instead, series of iso-eccentric stimuli which exhibit the same ratio of separation to eccentricity (stimuli which have been termed 'geometrically similar') are likely to obey a Weber relationship. Weber performance is, however, optimum for fovea-centred stimuli (approximately 4% of separation at twice contrast threshold), and declines as the separation of stimuli decreases relative to their

eccentricity (Figure 11.08). Although this inferiority of non-fovea-centred stimuli becomes progressively less marked as contrast increases, it is quite independent of spatial scale.

The Weber relationships described so far are a direct effect of the greater eccentricity of the iso-eccentric arcs as their radii increase. Figure 11.13 accounts for this effect since both x- and y-axes are normalised relative to eccentricity. Once this has been done it can be seen that performance at the level of any given eccentricity (ie. on varying separation around the circumference of the same iso-eccentric arc) does not exhibit any convincing Weber's law behaviour. Instead, at large separation/eccentricity ratios, thresholds are separation independent, being a constant fraction of the eccentricity. At smaller ratios, performance lies between that predicted on the basis of eccentricity and that predicted by a constant fraction of separation ('Weber's law'). The transition between the two mechanisms appears to occur when the separation is equal to the eccentricity. The precise shape of the function will, however, be dependent on the suprathreshold contrast level chosen. Figure 11.09b and 11.10b show that thresholds for large separation/eccentricity ratios are contrast independent, whereas those for small ratios are likely to improve with increasing contrast. The effect of increasing contrast will be a steepening of the function shown in Figure 11.13 at smaller separation/eccentricity ratios, and a level of performance more akin to 'Weber's law' for constant eccentricity stimuli. These observations are consistent with iso-eccentric spatial interval discrimination data of previous authors (Burbeck and Yap, 1990b; Levi and Klein, 1990a; Whitaker et al., 1992a) who used high-contrast broad-band stimuli.

Additionally, Figure 11.14 shows the data with both axes normalised with respect to separation. The plot therefore represents how thresholds vary as eccentricity is changed for stimuli of a constant physical separation. Similarly to Figure 11.13, at eccentricities which are small relative to the separation, thresholds are proportional to eccentricity. At larger eccentricities relative to separation, thresholds appear to be determined on the basis of both separation and eccentricity.

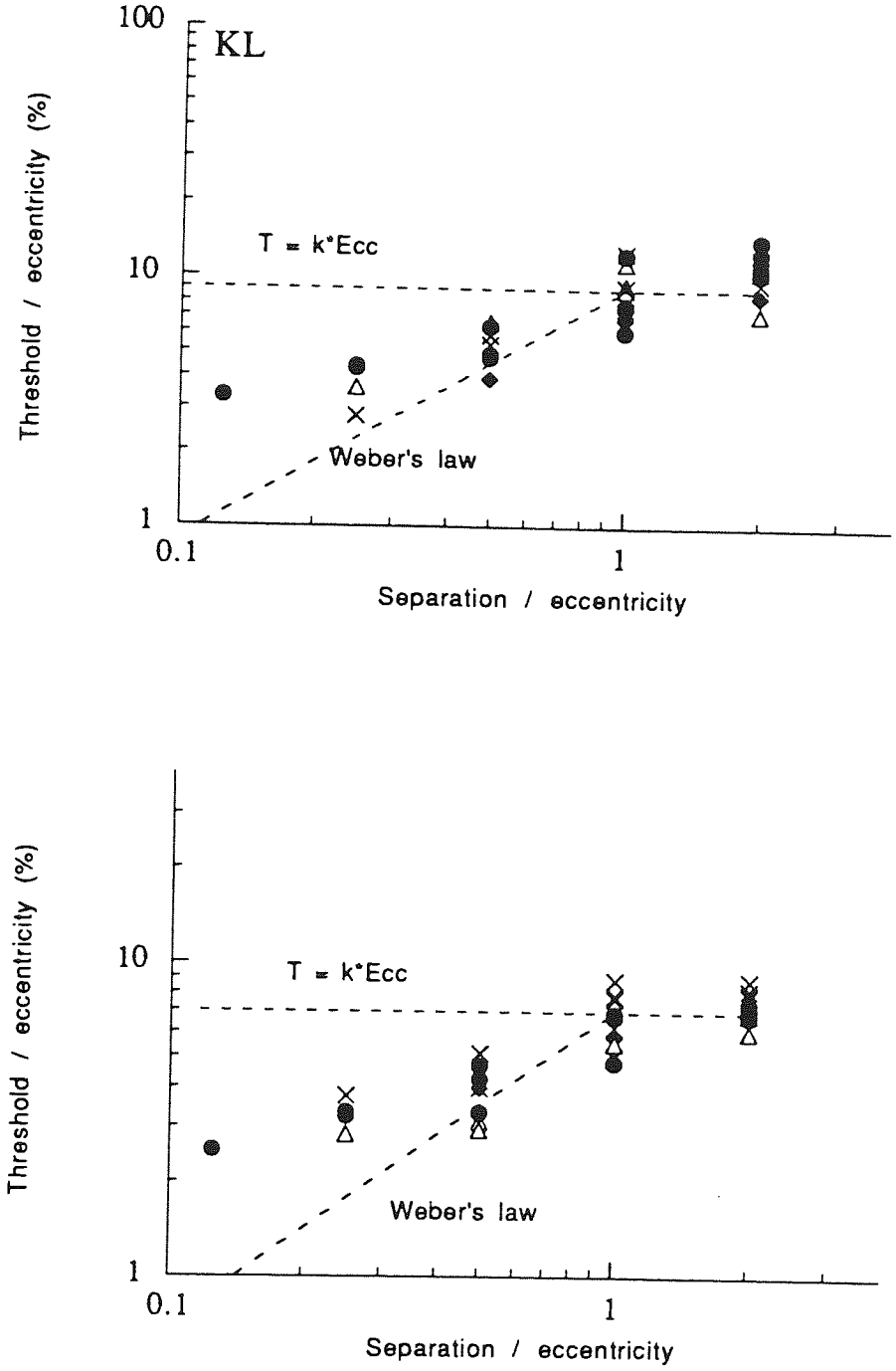

Figure 11.13. Spatial interval thresholds as a function of separation, with both axes normalised relative to eccentricity. The data shows how thresholds change on varying separation around a given iso-eccentric arc. Observers KL and DW. Symbols: closed diamonds: $\sigma = 0.8$; open triangles: $\sigma = 0.4$; closed circles: $\sigma = 0.2$; crosses: $\sigma = 0.1$.

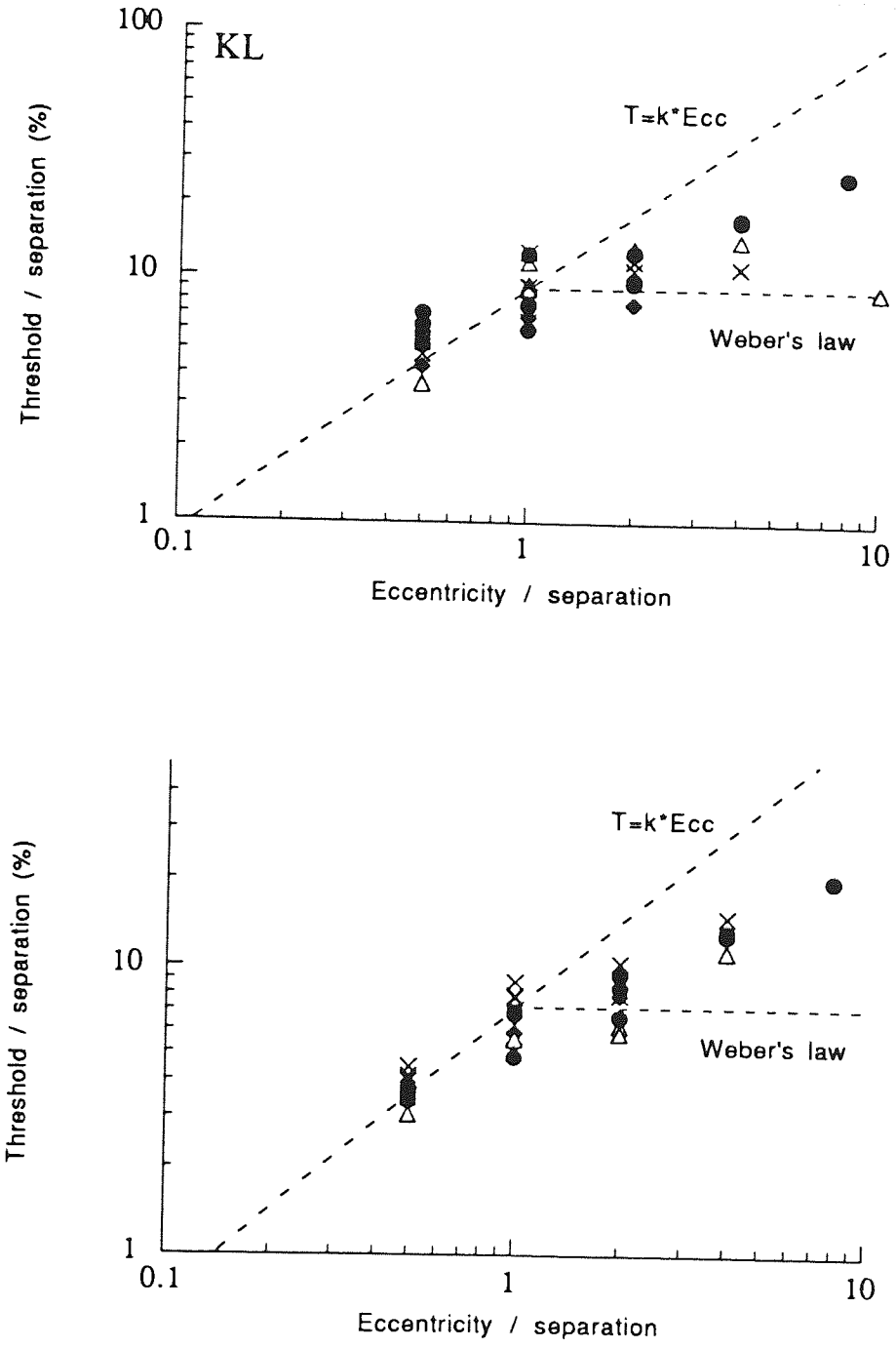

Figure 11.14. Spatial interval thresholds as a function of eccentricity, with both axes normalised relative to separation. The data shows how thresholds change for a standard separation as eccentricity changes. Observers KL and DW. Symbols as for Figure 11.13.

For any given eccentricity, the data, in line with previous studies (Levi and Klein, 1989, 1990a; Burbeck and Yap, 1990b), suggest that different encoding strategies are used at large and small separations. On an iso-eccentric arc of a given radius, performance at large separations is determined only by eccentricity and demonstrates a marked independence to suprathreshold contrast. Smaller separations are, however, contrast dependent and show a successively greater dependence upon separation (Weber behaviour) as contrast is increased. A model for encoding of separation consistent with this behaviour is shown in Figure 11.15.

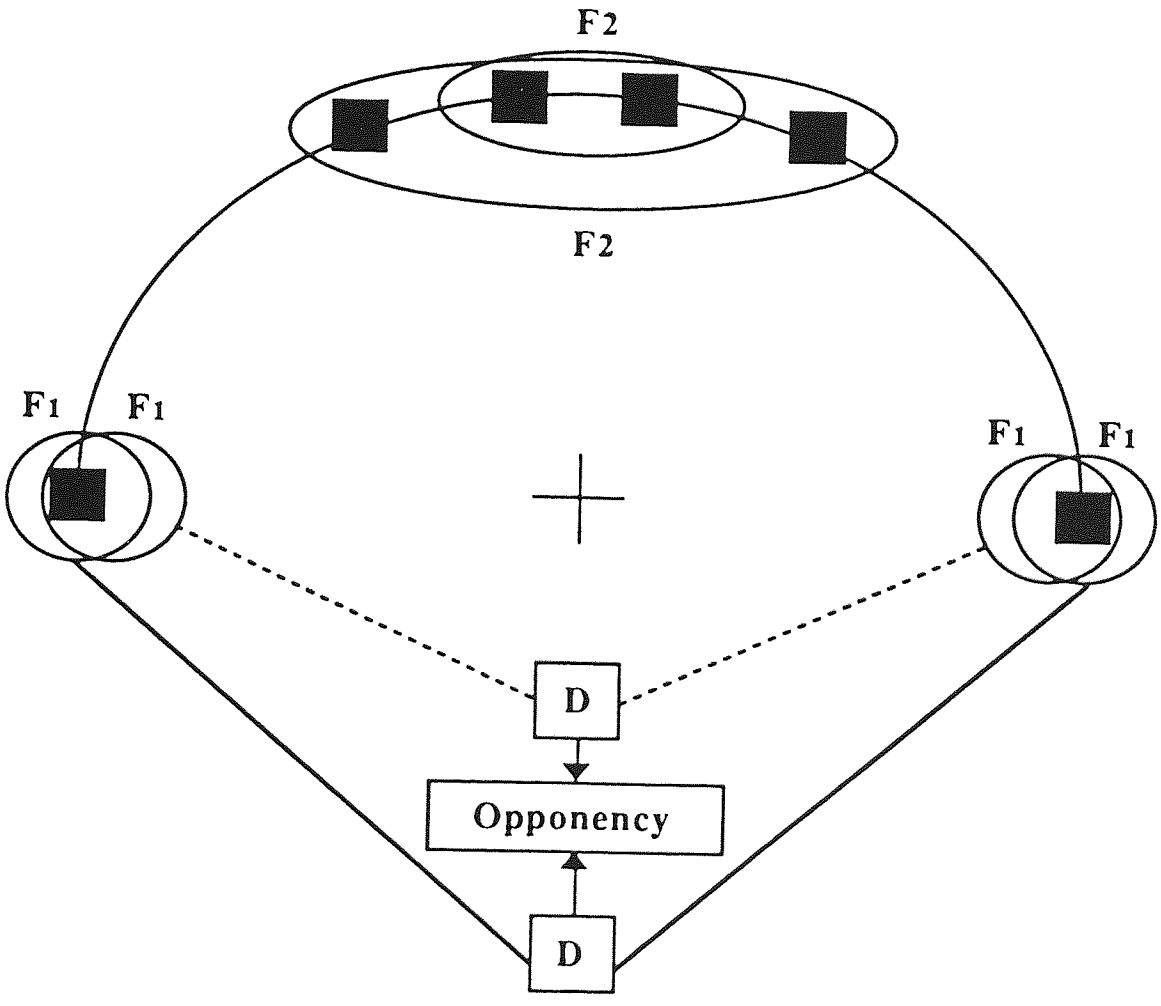

Figure 11.15. Model describing possible mechanisms of threshold determination in 'Weber's law' for position. See text for explanation.

The stimuli whose separations are to be judged are shown as black squares and are positioned around the circumference of an iso-eccentric arc whose geometric centre (marked with a cross) is meant to coincide with fixation. At large values of separation,

such as when the stimuli are either side of fixation, it is well accepted that separation cannot be encoded by filters which envelope both stimuli. Not only is there little evidence for very large fovea-centred receptive fields in early vision (Klein and Levi, 1985; Wilson, 1986), but fovea-centred separation judgements show considerable resistance to the presence of additional features placed between the stimuli whose separation is to be judged (Levi and Westheimer, 1987; Burbeck and Yap, 1990a; Burbeck and Hadden, 1993). A suitable arrangement which overcomes these two problems was proposed by Morgan and Regan (1987) and is known as a coincidence detector, denoted in Figure 11.15 by the boxes marked 'D'. Such detectors receive input from two independent filters, tuned to a specific separation. It is proposed that these two filters are non-linear and themselves receive some form of rectified input from first-stage, linear receptive fields (depicted by F1). This model conforms with the observation that the precision of large-scale separation judgements are largely independent of the spatial frequency content and polarity of the stimuli, and in addition, it allows for the encoding of separation for both first-order (luminance-modulated) and second-order (contrast- or texture-modulated) stimuli (Burbeck 1987, 1988; Toet and Koenderink, 1988). In order to explain the increase in thresholds with increasing separation of such fovea-centred stimuli, it must be supposed that uncertainty in the separation to which the coincidence detectors are tuned increases with eccentricity. This seems reasonable given that the non-linear second-stage filters themselves receive positional information from linear filters whose sampling density becomes progressively more sparse as eccentricity increases. The input to individual coincidence detectors will depend upon both stimulus contrast and separation. These two factors are unconfounded by an opponent stage which compares the output of two detectors which have slightly different separation tuning. Any variation in contrast will change the input to the two detectors equally, whereas (in this case) a reduction in separation will have a differential effect by increasing the input to one detector at the expense of the other. In line with the experimental data (Figure 11.09) the result is a contrast independent estimate of separation (Morgan and Regan, 1987).

The second encoding strategy comes into play as separation is reduced by moving stimuli around the iso-eccentric arc. At these smaller separations, sufficiently large non-linear filters exist to encompass both stimuli simultaneously. As with the filters which feed the coincidence detectors, these large filters have a high absolute positional uncertainty, but are able to provide estimates of stimulus separation due to their size-tuning properties. Weber behaviour is observed in this region since smaller filters require a proportionally smaller change in stimulus separation to elicit a suprathreshold change in response (Wilson, 1986). This type of arrangement predicts that thresholds

should improve as a power function of contrast (Wilson, 1986) which is consistent with the observed data (Figure 11.10). This second encoding strategy is more sensitive than the coincidence detector stage since it is not dependent upon the absolute positional uncertainty of the mechanisms involved. Once both stimuli are in sufficiently close proximity to fall within the largest filter at the respective eccentricity involved, then this process will begin to dominate performance, especially at high contrasts.

In conclusion, the present study takes into consideration the confounding features of spatial scale, separation and eccentricity in determining 'Weber's law' for position. This is the first study to use both iso-eccentric arcs (Levi et al., 1988; Levi and Klein, 1989, 1990a; Burbeck and Yap, 1990b; Whitaker et al., 1992a) and narrowband stimuli (Levi and Klein, 1992; Hess and Hayes, 1993). The use of a two element spatial interval task rather than the bisection task often used in previous studies (Levi et al., 1988; Levi and Klein, 1989, 1990a) ensures that the stimuli do not violate the iso-eccentric arc principle in any way. It has been found, in support of Levi and Klein (1992) but in disagreement with Hess and Hayes (1993), that spatial scale does not determine 'Weber's law' for position. Instead 'Weber's law' can be shown for geometrically similar stimuli, and the encoding strategy used to determine threshold depends on this geometric relationship between separation and eccentricity, independent of spatial scale. At large separation/eccentricity ratios, thresholds are proportional to eccentricity and show contrast independence. At small separation/eccentricity ratios, thresholds are contrast dependent and are determined by both separation dependent and separation independent mechanisms. The present results thus confirm and extend the observations of previous studies using broadband stimuli.

Chapter 12
Conclusions

12.1 Summary and conclusions

Most of the tasks in this thesis have been examined as a function of eccentricity using a method of spatial scaling. The majority of these tasks have obeyed a general magnification theory (Virsu et al., 1987) in that a foveal stimulus can be shown to have an equally detectable peripheral counterpart, provided that the peripheral stimulus is appropriately magnified. Further, the rate of change of magnification required to equate stimuli at different locations has been shown to be linear with eccentricity across the ranges examined (0-30 deg for perimetric tasks, 0-15 deg for curvature detection, and 0-10 deg for resolution in the presence of flanks, curvature discrimination and word recognition). Although it appears that only a small range of eccentricities have been exmained for many of the tasks, it should be remembered that the central 5 deg of the visual field accounts for 42% of striate cortex processing (Connolly and Van Essen, 1984). The rate of change of stimulus magnification has been denoted by the E_2 value (Levi et al., 1985), which defines the eccentricity at which foveal stimulus size must double in order to maintain performance at the foveal level. The E_2 values found in this thesis are given in Table 12.01.

The E_2 values evaluated cover a range of over 200 fold, from 0.06 deg for spatial interference zones to 12.6 deg for kinetically presented differential light stimuli. Some factors underlying such a variation in eccentricity related gradients have been suggested throughout the experimental chapters of the thesis.

For the curvature stimuli (Chapter 6), little variation in eccentricity dependency was seen for different standard curvatures, with E_2 values falling between 1.5 and 2 deg. This suggests that the mechanism underlying processing of curvature acts over all baseline curvatures, both within and without the orientation range thought to be most efficient at processing curvature (Watt and Andrews, 1982). Also of interest is that the E_2 values found for the curvature task are very similar to those of 1.95 deg found for orientation discrimination (Mäkelä et al., 1993) and 1-2 deg found for two dot or two line vernier acuity (Whitaker et al., 1992b). It is suggested in Chapter 6 that these tasks may share a common neural substrate in the orientation selectivity of spatial filters.

Task	Visual field meridian	E_2 value (deg)
Curvature detection	Nasal	1.68-1.85
Curvature discrimination (30 deg orientation range)	Nasal	1.40-1.51
Curvature discrimination (105 deg orientation range)	Nasal	1.53-2.25
Differential light stimulus - kinetic (10 young observers)	Nasal Superior Temporal Inferior	7.87±0.49 5.59±0.30 12.60±0.46 6.29±0.35
Differential light stimulus - static (10 young observers)	Nasal Superior Temporal Inferior	5.24±0.25 3.55±0.20 9.35±1.05 5.32±0.31
Differential light stimulus - static (10 elderly observers)	Nasal Superior Temporal Inferior	5.65±0.48 3.33±0.33 6.85±0.23 5.99±0.36
Resolution task (3 bar orientation discrimination)	Nasal Superior Temporal Inferior	1.79-2.05 1.02-1.03 1.69-2.12 1.21-1.62
Spatial interference zones	Nasal Superior Temporal Inferior	0.11-0.17 0.06-0.12 0.15-0.20 0.09-0.20
Word recognition (0.25 separation)	Inferior	0.67-0.75
Word recognition (2 separation)	Inferior	0.76-0.90
Word recognition rate (0.25 sep)	Inferior	0.36-0.54
Word recognition rate (2 sep)	Inferior	0.45-0.69

Table 12.01. Summary of E_2 values determined from experiments in this thesis.

The perimetric studies of Chapters 7 and 8 examined the behaviour of differential light thresholds at various locations in the central 30 deg of visual field. E_2 values for the temporal field are higher than those for nasal field, indicating that the rate of change of

performance with eccentricity is slower in temporal than in nasal field. Additionally, E_2 values for horizontal field meridia are higher than those for vertical field meridia. This meridional variation in E_2 values is also seen for the resolution task of Chapter 9. Such a meridional variation was noted to qualitatively reflect ganglion cell densities across the visual field. Quantitatively however, E_2 values for differential light stimuli are higher than the 1.29 deg suggested for all types of ganglion cell (Drasdo, 1991). It was suggested that the improved potential for spatial summation in the periphery acts as a mitigating factor against the decline in ganglion cell density in this task.

Comparing E_2 values for static and kinetic presentation of differential light stimuli for young observers indicates that kinetic E_2 values are slightly larger than those found for static presentation. The introduction of movement to this task appears to preferentially benefit peripheral thresholds, raising the E_2 value.

As mentioned above, meridional variation in E_2 values was also found for the resolution task of Chapter 9. In this case however, the E_2 values obtained for the resolution task (1.02-2.12 deg) compare reasonably well with estimates of E_2 for ganglion cells. Drasdo (1991) has suggested values of 1.29 deg for all types of gnaglion cell and 1.21 deg for P-ganglion cells alone. Performance in resolution tasks can be explained by limitations at a retinal, but post-receptoral level (Anderson et al., 1991), possibly by the spacing of P-ganglion cells (Thibos et al., 1987). The present results are consistent with these observations.

Spatial interference zones were found to have a much steeper eccentricity dependency than any of the other tasks examined, with the extent of the zones doubling in size approximately every 0.1 deg. Such a small E_2 value logically suggests a higher level limitation to processing than that observed for resolution. Indeed spatial interference can be shown under dichoptic conditions (Flom et al., 1963a; Westheimer and Hauske, 1975; Levi et al., 1985; Kooi et al., 1994), and must therefore be postchiasmal in origin. However, the E_2 value can provide no further evidence as to the underlying physiological substrate until retinotopic maps of various cortical levels are established.

The word recognition task examined in the first experiments of Chapter 10 is essentially a resolution task, in that the primary goal in successfully identifying the stimulus is to be able to resolve the letters. However, the task involves more than simple resolution in that the letters have to be recognised and strung together to form a word. Both subsequent tasks might be expected to place additional limitations on performance. However, E_2 values for word recognition (0.67-0.90 deg) are very similar to those for

three bar orientation discrimination under the same interference conditions (0.62-0.85 deg). The additional cognitive factors do not appear to affect relative performance with eccentricity.

Several factors have been identified in the experiments of this thesis which appear to contribute to the determination of relative performance changes across the visual field. The means by which these and other factors combine to produce the range of peripheral gradients observed is now considered.

A hierarchical approach to the variations in eccentricity gradients was first proposed by Levi et al. (1985). It was suggested that resolution was limited at the retinal level with an E_2 of 2.5 deg, while hyperacuities are limited cortically with an E_2 of 0.8 deg. More recent anatomical evidence suggests that any difference between E_2 values for ganglion cells (1.29 deg) and V1 (1.14 deg) is small (Drasdo, 1991). Psychophysically, the results of this thesis support the latter view. Comparing E_2 values in the nasal visual field for a resolution task (1.79-2.05 deg) and the hyperacuity task of curvature detection or discrimination (1.75-2.27 deg) shows little difference in values. Even if there is little difference in the mapping topographies of the retina and striate cortex, it does not rule out the usefulness of a hierarchical model with which to explain some of the observed eccentricity-dependent variations. One possible approach is to consider the ganglion cell level as a 'baseline level', through which all information must pass in order to be processed. The resulting gradient of various tasks can then be adapted from this baseline level by additional factors. Processes such as spatial summation (Chapters 7 and 8) and optical degradation (Deeley and Drasdo, 1987) act as mitigating factors, making the E_2 value for tasks such as spot detection larger than that for ganglion cells alone. In the opposite direction, further limitations can be placed on the peripheral performance of tasks, reducing the E_2 value. These limitations can occur at the retinal level, such as increased positional uncertainty in the periphery (Hess and McCarthy, 1994). Additionally, further limitations might occur at a post-ganglionic level if subsequent levels become more fovea-specialised. Even if the mapping of V1 has a very similar topography to that of ganglion cells, mappings of higher cortical areas (Drasdo, 1991), or different types of cells in V1 such as complex cells (Livingstone and Hubel, 1985) may well be distributed so as to reduce E_2 values for tasks limited at these levels.

In addition to hierarchical processing limitations, the visual image is processed in parallel by magno- and parvo-cellular processing streams (Chapter 3). The distinction between two processing streams provides a further opportunity for the provision of

variation in eccentricity-related gradients, since the 'baseline' ganglion cell gradient discussed above can be divided into M and P channels. E_2 values for M-ganglion cells have been proposed to be 4.76 deg, while for P-ganglion cells E_2 is 1.21 deg (Drasdo, 1991). Such a difference cannot on its own account for the wide range of E_2 values observed, but combined with the hierarchical model, provides even more possible combinations and variations on which eccentricity-related gradients might be based.

In Chapter 9 it was hypothesised that a number of fundamental factors might combine to determine threshold gradients. Any or all of the factors discussed above might be considered in such a scheme, with the weighting of each factor in the task determining the eventual threshold gradient. The weighting of various factors would be determined by the stimulus configuration itself. For example, the proximity of the position of the flanks in the resolution experiment of Chapter 9 determines the relative weighting of spatial interference and resolution factors in that task. For the task of detection of differential light stimuli, it has been suggested that threshold gradients are determined by the factors of ganglion cell density and spatial summation. It might be said that kinetic presentation of the stimulus (Chapter 7) introduces successive lateral spatial summation, thereby increasing the weighting of spatial summation in the task. E_2 values for this task are larger than those for static presentation of the same stimuli (Chapter 8), where the stimulus configuration could be considered to be less weighted to spatial summation, and therefore more weighted to the factor of ganglion cell density.

A note of caution should now be raised with respect to the identification of factors which determine relative performance across the visual field. By variation of the stimulus configuration, tasks can be weighted towards showing the eccentricity dependency of certain factors, but it is difficult to isolate these factors completely, or to tell if these factors are fundamental to threshold determination or merely combinations of other factors. Further, comparison of psychophysical E_2s with supposed underlying physiological substrates is somewhat speculative, and apparent agreements may be fortuitous.

Having discussed those tasks for which spatial scaling was successful, what about those tasks for which spatial scaling did not equate performance across the visual field? The first task which did not show a linear increase in size scale with eccentricity was for the kinetic presentation of differential light stimuli in a group of elderly observers. Thresholds rose non-linearly with eccentricity showing a preferential loss of sensitivity at the fovea and beyond 20 deg eccentricity with a relative sparing of the parafoveal

region. In comparison, thresholds for static presentation of the same stimuli rose linearly with eccentricity. The reason for the non-linearity of the elderly data would therefore seem to be related to the movement of the stimulus. Possible explanations include an increased reaction time with as a function of eccentricity with age, or deficient processing of stimuli moving at higher velocities with age.

The only other task examined for which magnification was unable to equate performance at different locations was that of reading meaningful sentences. For this task, reading rate at an eccentric location could not be made equal to that achieved at the fovea, which showed a higher maximum reading rate. This result was explained in terms of a foveal specialisation in comprehension of sentence structure.

The final chapter of this thesis has not dealt specifically with the eccentricity dependency of a task, but has instead used sets of stimuli at various peripheral locations to unravel the various contributions of eccentricity, separation and spatial scale to Weber's law for position. Using narrowband, low visibility stimuli positioned on iso-eccentric arcs, Weber's law behaviour (thresholds proportional to separation) can be shown for geometrically similar stimuli (stimuli with a constant separation / eccentricity ratio) for each of a number of spatial scales, and over a wide range of separations. Weber's law behaviour is produced at large values of separation relative to eccentricity because thresholds are proportional to eccentricity. At smaller separations relative to eccentricity, thresholds show a greater dependence on separation which increases with increasing contrast. Weber's law therefore arises from both increasing separation and increasing eccentricity. Demonstration of Weber's law for position might therefore be considered to be incidental rather than fundamental.

In conclusion, most tasks behave in peripheral vision in a qualitatively similar manner to their behaviour at the fovea, differing simply in a matter of size scale, or a quantitative difference. In other words, the periphery acts as a 'scaled up' version of the fovea for individual tasks, with the proviso that there are many different scales to which different tasks may adhere. The overall effect is that any peripheral location does in fact behave quite differently from the fovea, since many scales are in operation at the same location. Additionally, there are tasks for which a quantitative change in scale will not describe the eccentricity related variation in performance. One of those identified in this thesis is an age related change, and the other appears to relate to higher aspects of comprehension and perception. No doubt further research will be able to identify further 'unscaleable' tasks such as these.

Supporting publications

Refereed papers

D Whitaker, P Mäkelä, J Rovamo, & **K Latham** (1992). The influence of eccentricity on position and movement acuities as revealed by spatial scaling. Vision Research, 32/10: 1913-1930.

K Latham, D Whitaker, JM Wild, & DB Elliott (1993). Magnification perimetry. Investigative Ophthalmology and Visual Science, 34/5: 1691-1701.

D Whitaker, **K Latham**, P Mäkelä, & J Rovamo (1993). Detection and discrimination of curvature in foveal and peripheral vision. Vision Research, 33/16: 2215-2224.

K Latham, D Whitaker, & JM Wild (1994). Spatial summation of the differential light threshold as a function of visual field location and age. Ophthalmic and Physiological Optics, 14/1: 71-78.

Papers in submission

K Latham, & D Whitaker. A comparison of word recognition and reading rate performance in foveal and peripheral vision.
Submitted to Vision Research, April 1994.

Papers in preparation

K Latham, & D Whitaker. Mapping of spatial interference zones for visual resolution.

K Latham, & D Whitaker. Disentangling the role of spatial scale, separation and eccentricity in Weber's law for position.

Refereed conference abstracts

K Latham, D Whitaker, JM Wild, & DB Elliott (1993). Equating the differential light threshold across the visual field by magnification. Investigative Ophthalmology and Visual Science, Suppl., 34/4: 779.

K Latham, D Whitaker, & JM Wild (1993). Magnification perimetry. Ophthalmic and Physiological Optics, 13/1:107-108.

K Latham, & D Whitaker (1994). Resolution, spatial interference and visual field location. Investigative Ophthalmology and Visual Science, Suppl., 35/4: 1954.

K Latham, & D Whitaker (1995). Comparing word recognition and reading rate performance across the visual field. Investigative Ophthalmology and Visual Science, Suppl., in submission.

Presentations

Oral presentations

K Latham (1992). Magnification Perimetry.
Internal seminar, Aston University, 6/92.

K Latham (1992). Magnification Perimetry.
University of Waterloo, School of Optometry, 1/9/92.

Poster presentations

K Latham, D Whitaker, & JM Wild (1992). Magnification perimetry. Society of Experimental Optometry (SEO), Birmingham, UK, 27/7/92.

K Latham, D Whitaker, JM Wild, & DB Elliott (1993). Equating the differential light threshold across the visual field by magnification. Association for Research in Vision and Ophthalmology (ARVO), Sarasota, Florida, 2/5/93.

K Latham, & D Whitaker (1994). Resolution, spatial interference and visual field location. Association for Research in Vision and Ophthalmology (ARVO), Sarasota, Florida, 5/5/94.

References

Abramov I, & Gordon J (1977). Color vision in the peripheral retina. I. Spectral sensitivity. Journal of the Optical Society of America, 67, 195-201.

Abramov I, Gordon J, & Chan H (1991). Color appearance in the peripheral retina: effects of stimulus size. Journal of the Optical Society of America A, 8, 404-414.

Ames T (1980). Macmillan Diagnostic Reading Pack. Macmillan: Basingstoke.

Anderson DR (1992). Automated static perimetry. Mosby: St Louis.

Anderson SJ, & Hess RF (1990). Post-receptoral undersampling in normal human peripheral vision. Vision Research, 30, 1507-1515.

Anderson SJ, Mullen KT, & Hess RF (1991). Human peripheral spatial resolution for achromatic and chromatic stimuli: limits imposed by optical and retinal factors. Journal of Physiology, 442, 47-64.

Andrews DP (1967). Perception of contour orientation in the central fovea. Part II: Spatial integration. Vision Research, 7, 998-1013.

Andrews DP, Butcher AK, & Buckley BR (1973). Acuities for spatial arrangement in line figures: human and ideal observers compared. Vision Research, 13, 599-620.

Andriessen JJ, & Bouma H (1976). Eccentric vision: adverse interactions between line segments. Vision Research, 16, 71-78.

Anstis SM (1974). A chart demonstrating variations in acuity with retinal position. Vision Research, 14, 589-592.

Arditi A, Knoblauch K, & Grunwald I (1990). Reading with fixed and variable pitch. Journal of the Optical Society of America A, 7, 2011-2015.

Atchison DA (1987). Effect of defocus on visual field measurement. Ophthalmic and Physiological Optics, 7, 259-265.

Aubert H, & Förster R (1857). Beiträge zur Kenntniss des indirekte Sehens (I) Untersuchungen über den Raumsinn der Retina. Archive für Ophthalmologie, 3, 1-37.

Aulhorn E, & Harms H (1972). Visual perimetry. In: Handbook of sensory physiology, Vol VII/4, Visual psychophysics. Eds: Jameson D, & Hurvich LM. Chap 5, pp 102-145. Springer-Verlag: Berlin.

Aulhorn E, Harms H, & Raabe N (1966). Die Lichtunterschiedsempfindlichkeit als Funktion der Umfeldleuchtdeichte. Documenta Ophthalmologica, 20, 527-556.

Azzopardi P (1994). Foveal representation in the visual cortex. Departmental seminar, 11th May, Aston University.

Azzopardi P, & Cowey A (1993). Preferential representation of the fovea in the primary visual cortex. Nature, 361, 719-721.

Baker CL, & Braddick OJ (1985). Eccentricity-dependent scaling of the limits for short-range apparent motion perception. Vision Research, 25, 803-812.

Ball K, Owsley C, Sloane ME, Roenker DL, & Bruni JR (1993). Visual attention problems as a predictor of vehicle crashes in older drivers. Investigative Ophthalmology and Visual Science, 34, 3110-3123.

Ball K, & Sekuler R (1980). Models of stimulus uncertainty in motion perception. Psychological Review, 87, 435-469.

Banks MS, Sekuler AB, & Anderson SJ (1991). Peripheral spatial vision: limits imposed by optics, photoreceptors and receptor pooling. Journal of the Optical Society of America A, 8, 1775-1787.

Banks WP, Larson DW, & Prinzmetal W (1979). Asymmetry of visual interference. Perception and Psychophysics, 25, 447-456.

Barlow HB (1958). Temporal and spatial summation in human vision at different background intensities. Journal of Physiology, 141, 337-350.

Baron WS, & Westheimer G (1973). Visual acuity as a function of exposure duration. Journal of the Optical Society of America, 63, 212-219.

Bassi CJ, & Lehmkuhle S (1990). Clinical implications of parallel visual pathways. Journal of the American Optometric Association, 61, 98-110.

Bennett PJ, & Banks MS (1987). Sensitivity loss in odd-symmetric mechanisms and phase anomalies in peripheral vision. Nature, 326, 873-876.

Bijl P, Koenderink JJ, & Kappers AML (1992). Deviations from strict M-scaling. Journal of the Optical Society of America A, 9, 1233-1239.

Birch DG, & Fish GE (1988). Focal cone electroretinograms: aging and macular disease. Documenta Ophthalmologica, 69, 211-220.

Blakemore C, & Over R (1974). Curvature detectors in human vision? Perception, 3, 3-7.

Bland JM, & Altman DG (1986). Statistical methods for assessing agreement between two methods of clinical measurement. The Lancet, 1, 307-310.

Bouma H (1969). Visual isolation in eccentric form vision: the role of colour. IPO Annual Progress Report, 4, 95-99.

Bouma H (1970). Interaction effects in parafoveal letter recognition. Nature, 226, 177-178.

Bowmaker JK (1991). The evolution of vertebrate visual pigments and photoreceptors. In: Vision and visual dysfunction, Vol 2, Evolution of the eye and visual system. Eds: Cronly-Dillon JR, & Gregory RL. Chapter 4,pp 63-81. Macmillan: Basingstoke.

Brenton RS, & Phelps CD (1986). The normal visual field on the Humphrey Visual Analyser. Ophthalmologica, 193, 56-74.

Brindley GS, & Lewin WS (1968). The sensations produced by electrical stimulation of the visual cortex. Journal of Physiology, 196, 479-493.

Brown B, Peterken C, Bowman K, & Crassini B (1989). Spatial summation in young and elderly observers. Ophthalmic and Physiological Optics, 9, 310-313.

Burbeck CA (1986). Exposure-duration effects in localization judgements. Journal of the Optical Society of America A, 3, 1983-1988.

Burbeck CA (1987). Position and spatial frequency in large scale localisation judgements. Vision Research, 27, 417-427.

Burbeck CA (1988). Large scale relative localisation across spatial frequency channels. Vision Research, 28, 857-859.

Burbeck CA, & Hadden S (1993). Scaled position integration areas: accounting for Weber's law for separation. Journal of the Optical Society of America A, 10, 5-15.

Burbeck CA, & Yap YL (1990a). Spatial-filter selection in large-scale spatial-interval discrimination. Vision Research, 30, 263-272.

Burbeck CA, & Yap YL (1990b). Two mechanisms for localisation? Evidence for separation-dependent and separation-independent processing of position information. Vision Research, 30, 739-750.

Burbeck CA & Yap YL (1990c). Spatiotemporal limitations in bisection and separation discrimination. Vision Research, 30, 1573-1586.

Calvert JE, & Harris JP (1985). Cortical magnification and tilt after-effect. Journal of Physiology, 364, 36P.

Campbell FW, & Green DG (1965). Optical and retinal factors affecting visual resolution. Journal of Physiology, 181, 576-593.

Campbell FW, & Gubisch RW (1966). Optical quality of the human eye. Journal of Physiology, 186, 558-578.

Charman WN (1991). Limits on visual performance set by the eye's optics and the retinal cone mosaic. In: Vision and Visual Dysfunction, Vol 5, Limits of Vision. Eds: Kulikowski JJ, Walsh V, & Murray IJ. Chapter 7, pp 81-96. Macmillan: Basingstoke.

Collin HB, Han C, & Khor PC (1988). Age changes in the visual field using the Humphrey visual field analyser. Clinical and Experimental Optometry, 71, 174-178.

Connolly M, & Van Essen D (1984). The representation of the visual field in parvicellular and magnocellular layers of the lateral geniculate nucleus in the macaque monkey. Journal of Comparative Neurology, 226, 544-564.

Cornsweet TN (1962). The staircase method in psychophysics. American Journal of Psychology, 75, 485-491.

Cowey A (1964). Projection of the retina onto striate and prestriate cortex in the squirrel monkey, *Saimiri sciureus*. Journal of Neurophysiology, 27, 366-393.

Cowey A, & Rolls ET (1974). Human cortical magnification factor and its relation to visual acuity. Experimental Brain Research, 21, 447-454.

Crassini B, Brown B, & Bowman K (1988). Age-related changes in contrast sensitivity in central and peripheral retina. Perception, 17, 315-332.

Crassini B, & Over R (1975a). Visibility of arcs as a function of radius and chord orientation. Australian Journal of Psychology, 27, 143-149.

Crassini B, & Over R (1975b). Masking, aftereffect, and illusion in visual perception of curvature. Perception and Psychophysics, 17, 411-416.

Cummings RW, Whittaker SG, Watson GR, & Budd JM (1985). Scanning characters and reading with a central scotoma. American Journal of Optometry and Physiological Optics, 62, 833-843.

Curcio CA, & Allen KA (1990). Topography of ganglion cells in human retina. Journal of Comparative Neurology, 300, 5-25.

Curcio CA, Sloan KR, Kalina RE, & Hendrickson AE (1990). Human photoreceptor topography. Journal of Comparative Neurology, 292, 497-523.

Dacey DM, & Petersen MR (1992). Dendritic field size and morphology of midget and parasol cells of the human retina. Proceedings of the National Academy of Sciences, 89, 9666-9670.

Daniel PM, Kerr DLB, Seneviratne KN, & Whitteridge D (1961). The topographic representation of the visual field on the lateral geniculate nucleus in the cat and monkey. Journal of Physiology, 159, 87-88P.

Daniel PM, & Whitteridge D (1961). The representation of the visual field on the cerebral cortex in monkeys. Journal of Physiology, 159, 203-221.

Dannheim F, & Drance SM (1971). Studies of spatial summation of central retinal areas in normal people of all ages. Canadian Journal of Ophthalmology, 6, 311-319.

Dartnall HJA, Bowmaker JK, Mollon JD (1983). Human visual pigments: microspectrophotometric results from the eyes of seven persons. Proceedings of the Royal Society of London, 220, 115-130.

Davson H (1990). Physiology of the Eye, 5th edition. Macmillan: Basingstoke.

Deeley RJ, & Drasdo N (1987). The effect of optical degradation on the contrast sensitivity function measured at the fovea and in the periphery. Vision Research, 27, 1179-1186.

Della Valle L, Andrews TG, & Ross S (1956). Perceptual thresholds of curvilinearity and angularity as functions of line length. Journal of Experimental Psychology, 51, 343-347.

Derefeldt G, Lennerstrand G, & Lundh B (1979). Age variations in normal human contrast sensitivity. Acta Ophthalmologica, 57, 679-690.

Derrington AM, & Lennie P (1984). Spatial and temporal contrast sensitivities of neurones in lateral geniculate nucleus of macaque. Journal of Physiology, 357, 219-240.

DeYoe EA, & Van Essen DC (1988). Concurrent processing streams in monkey visual cortex. Trends in Neuroscience, 11, 219-226.

Dixon J, & Mood AM (1948). A method for obtaining and analyzing sensitivity data. Journal of the American Statistical Association, 43, 109-126.

Dobbins A, Zucker SW, & Cynader MS (1987). Endstopped neurons in the visual cortex as a substrate for calculating curvature. Nature, 329, 438-441.

Dobelle WM, Turkel J, Henderson DC, & Evans JR (1979). Mapping the representation of the visual field by electrical stimulation of human visual cortex. American Journal of Ophthalmology, 88, 727-735.

Dow BM, Snyder AZ, Vautin RG, & Bauer R (1981). Magnification factor and receptive field size in foveal striate cortex of the monkey. Experimental Brain Research, 44, 213-228.

Dow BM, Vautin RG, & Bauer R (1985). The mapping of visual space onto foveal striate cortex in the macaque monkey. Journal of Neuroscience, 5, 890-902.

Drance SM, Berry V, & Hughes A (1967). Studies on the effects of age on the central and peripheral isopters of the visual field in normal subjects. American Journal of Ophthalmology, 63, 1667-1672.

Drasdo N (1977). The neural representation of visual space. Nature, 266, 554-556.

Drasdo N (1989). Receptive field densities of the ganglion cells of the human retina. Vision Research, 29, 985-988.

Drasdo N (1991). Neural substrates and threshold gradients in peripheral vision. In: Vision and Visual Dysfunction, Vol 5, Limits of Vision. Eds: Kulikowski JJ, Walsh V, & Murray IJ. Chapter 19, pp 251-265. Macmillan: Basingstoke.

Drasdo N, & Fowler CW (1974). Non-linear projection of the retinal image in a wide-angle schematic eye. British Journal of Ophthalmology, 58, 709-714.

Drasdo N, & Thompson CM (1989). Do visibility and colour recognition isopters relate to the distribution of Pα and Pβ ganglion cells of the human retina? Ophthalmic and Physiological Optics, 9, 447-450.

Drasdo N, Thompson CM, & Deeley RJ (1991). Psychophysical evidence of two gradients of neural sampling in peripheral vision. In: From Pigments to Perception: advances in understanding visual processes. Eds: Valberg A, & Lee BB. pp 189-192. Plenum Press: New York.

Drum B, Armaly MF, & Huppert W (1986). Scotopic sensitivity loss in glaucoma. Archives of Ophthalmology, 104, 712-717.

Dunn PM, & Lakowski R (1981). Fully-photopic and -scotopic spatial summation in chromatic perimetry. In: Documenta Ophthalmologica Proceedings Series, Vol 26. Eds: Greve EL, & Verriest G. pp 199-206. Junk: The Hague.

Egge K (1984). The visual field in normal subjects. Acta Ophthalmologica supplement, 169, 1-64.

Elliott DB (1987). Contrast sensitivity with ageing: a neural or optical phenomenon? Ophthalmic and Physiological Optics, 7, 415-419.

Elliott DB, & Bullimore MA (1993). Assessing the reliability, discriminative ability, and validity of disability glare tests. Investigative Ophthalmology and Visual Science, 34, 108-119.

Elliott DB, Whitaker D, & MacVeigh D (1990). Neural contribution to spatiotemporal contrast sensitivity decline in healthy ageing eyes. Vision Research, 30, 541-547.

Enoch J (1961). Nature of the transmission of energy in the retinal receptors. Journal of the Optical Society of America, 51, 122-1126.

Enroth-Cugell C, & Robson JG (1966). The contrast sensitivity of retinal ganglion cells of the cat. Journal of Physiology, 341, 279-307.

van Esch JA, Koldenhof EE, van Doorn AJ, & Koenderink JJ (1984). Spectral sensitivity and wavelength discrimination of the human peripheral visual field. Journal of the Optical Society of America A, 1, 443-450.

Fahle M (1986). Curvature detection in the visual field and a possible physiological correlate. Experimental Brain Research, 63, 113-124.

Fahle M, & Schmidt M (1988). Naso-temporal asymmetry of visual perception and of the visual cortex. Vision Research, 28, 293-300.

Fankhauser F, & Enoch JM (1962). The effects of blur on perimetric thresholds. Archives of Ophthalmology, 68, 120-131.

Fankhauser F, & Schmidt T (1958). Die Unterschung der raümlichen Summation mit stehender und bewegter Reizmarke nach der Methode der quantitativen Lichtsinnperimetrie. Ophthalmologica, 135, 660-666.

Fankhauser F, & Schmidt T (1960). Die optimalen Bedingungen für die Untersuchung der raümlichen Summation mit stehender Reizmarke nach der Methode der quantitativen Lichtsinnperimetrie. Ophthalmologica, 139, 409-423.

Farrell JE, & Desmarais M (1990). Equating character identification performance across the visual field. Journal of the Optical Society of America A, 7, 152-159.

Fechner GT (1860). Elemente der Psychophysik. Breitkopf and Härtel: Leipzig (Translation by Adler HE (1966). Elements of Psychophysics. Holt, Rinehart and Newman: New York).

Felleman DJ, & Van Essen DC (1991). Distributed hierarchical processing in the primate cerebral cortex. Cerebral Cortex, 1, 1-47.

Fendick M, & Westheimer G (1983). Effects of practice and the separation of test targets on foveal and peripheral stereoacuity. Vision Research, 23, 145-150.

Findlay JM (1978). Estimates on probability functions: a more virulent PEST. Perception and Psychophysics, 23, 181-185.

Finney DJ (1971). Probit analysis. The University Press: Cambridge.

Flom MC (1991). Contour interaction and the crowding effect. Problems in Optometry, 3, 237-257.

Flom MC, Heath GG, & Takahashi E (1963a). Contour interaction and visual resolution: contralateral effects. Science, 142, 979-980.

Flom MC, Weymouth FWW, & Kahneman D (1963b). Visual resolution and contour interaction. Journal of the Optical Society of America, 53, 1026-1032.

Foos RY, & Trese MT (1982). Chorioretinal juncture. Vascularisation of Bruch's membrane in peripheral fundus. Archives of Ophthalmology, 100, 1492-1503.

Forster KI (1970). Visual perception of rapidly presented word sequences of varying complexity. Perception and Psychophysics, 8, 215-221.

Foster DH, Thorson J, McIllwain JT, & Biederman-Thorson (1981). The fine-grain movement illusion: a perceptual probe of neuronal circuitry in the human visual system. Vision Research, 21, 1123-1128.

Fox PT, Miezin FM, Allman JM, Van Essen DC, & Raichle ME (1987). Retinotopic organisation of human visual cortex mapped with positron emission tomography. Journal of Neuroscience, 7, 913-922.

Gao H, & Hollyfield JG (1992). Aging of the human retina. Investigative Ophthalmology and Visual Science, 33, 1-17.

Genter CR, Kandel GL, & Bedell HE (1981). The minimum angle of resolution vs angle of regard function as measured with different targets. Ophthalmic and Physiological Optics, 1, 3-13.

Glezer VD (1965). The receptive fields of the retina. Vision Research, 5, 497-525.

Gordon J, & Abramov I. (1977) Color vision in the peripheral retina. II. Hue and saturation. Journal of the Optical Society of America, 67, 202-207.

Gorrand JM (1979). Diffusion of the human retina and quality of the optics of the eye on the fovea and peripheral retina. Vision Research, 19, 907-912.

Green DG (1970). Regional variations in the visual acuity for interference fringes on the retina. Journal of Physiology, 207, 351-356.

Green DM, & Swets JA (1966). Signal detection theory and psychophysics. Wiley: New York.

Greve EL (1973). Single and multiple stimulus static perimetry in glaucoma; the two phases of perimetry. Documenta Ophthalmologica, 36, 1-355.

van de Grind WA, van Doorn AJ, & Koenderink JJ (1983). Detection of coherent movement in peripherally viewed random-dot patterns. Journal of the Optical Society of America, 73, 1674-1683.

Haas A, Flammer J, & Schneider U (1986). Influence of age on the visual fields of normal subjects. American Journal of Ophthalmology, 101, 199-203.

Haber RN, & Hershenson M (1980). The psychology of visual perception, 2nd edition. Holt, Rinehart and Wilson: New York.

Hallett PE, Marriott FHC, & Rodger FC (1962). The relationship of visual threshold to retinal position and area. Journal of Physiology, 160, 364-373.

Hampton DR, & Kertesz AE (1983a). The extent of Panum's area and the human cortical magnification factor. Perception, 12, 161-165.

Hampton DR, & Kertesz AE (1983b). Fusional vergence response to local peripheral stimulation. Journal of the Optical Society of America, 73, 7-10.

Hartline HK (1940). The receptive fields of optic nerve fibers. American Journal of Physiology, 30, 690-699.

Harvey LO, & Pöppel E (1973). Contrast sensitivity of the human retina. American Journal of Optometry, 49, 748-753.

Harwerth RS, & Levi DM (1978). Reaction time as a measure of suprathreshold grating detection. Vision Research, 18, 1579-1586.

Hecht S, & Mintz EU (1939). The visibility of single lines at various illuminations and the retinal basis of visual resolution. Journal of General Physiology, 22, 593-612.

Hecht S, Schlaer S, & Pirenne MH (1942). Energy, quanta and vision. Journal of General Physiology, 25, 819-840.

Heijl A (1987). The implications of the results of computerised perimetry in normals for the statistical evaluation of glaucomatous visual fields. In: Glaucoma Update III. Ed: Kreiglstein GK. pp 115-123. Springer-Verlag: Berlin.

Herse PR (1992). Factors influencing normal perimetric thresholds obtained using the Humphrey field analyser. Investigative Ophthalmology and Visual Science, 33, 611-699.

Hess RF, & Hayes A (1993). Neural recruitment explains "Weber's law" of spatial position. Vision Research, 33, 1673-1684.

Hess RF, & Holliday IE (1992). The coding of spatial position by the human visual system: effects of spatial scale and contrast. Vision Research, 32, 1085-1097.

Hess RF, & McCarthy J (1994). Topological disorder in peripheral vision. Visual Neuroscience, 11, 1033-1036.

Hess RF, & Watt RJ (1990). Regional distribution of the mechanisms that underlie spatial localisation. Vision Research, 30, 1021-1031.

Higgins KE, Arditi A, & Knoblauch K (1992). Detection and discrimination of mirror-image letter pairs in central and peripheral vision. Investigative Ophthalmology and Visual Science, 33, 824.

Hirsch J, & Curcio CA (1989). The spatial resolution capacity of human foveal retina. Vision Research, 29, 1095-1101.

Hirsch J, & Miller WH (1987). Does cone positional disorder limit resolution? Journal of the Optical Society of America A, 4, 1481-1492.

Hubel DH, & Freeman DC (1977). Projection into the visual field of ocular dominance columns in macaque monkey. Brain Research, 122, 336-343.

Hubel DH, & Wiesel TN (1968). Receptive fields and functional architecture of monkey striate cortex. Journal of Physiology, 195, 215-243.

Hubel DH, & Wiesel TN (1974). Uniformity of monkey striate cortex: a parallel relationship between field size, scatter and magnification factor. Journal of Comparative Neurology, 158, 295-306.

Hubel DH, & Wiesel TN (1977). Functional architecture of macaque monkey visual cortex. Proceedings of the Royal Society of London, Series B, 198, 1-59.

Hudson C, & Wild JM (1992). Assessment of physiologic statokinetic dissociation by automated perimetry. Investigative Ophthalmology and Visual Science, 33, 3162-3168.

Inui T, Mimura O, & Kani K (1981). Retinal sensitivity and spatial summation in the foveal and parafoveal regions. Journal of the Optical Society of America, 71, 151-154.

Jacobs RA (1979). Visual resolution and contour interaction in the fovea and periphery. Vision Research, 19, 1187-1195.

Jaffe GJ, Alvarado JA, & Juster RP (1986). Age-related changes in the normal visual field. Archives of Ophthalmology, 104, 1021-1025.

Jamar JHT, Kwakman LFT, & Koenderink JJ (1984). The sensitivity of the peripheral visual system to amplitude-modulation and frequency-modulation of sine-wave patterns. Vision Research, 24, 243-249.

Jennings JAM, & Charman WM (1981). Off-axis image quality in the human eye. Vision Research, 21, 445-455.

Johnson CA, Adams AJ, & Lewis RA (1989). Evidence for a neural basis of age-related visual field loss in normal observers. Investigative Ophthalmology and Visual Science, 30, 2056-2064.

Johnson CA, & Keltner JL (1987). Optimal rates of movement for kinetic perimetry. Archives of Ophthalmology, 105, 73-75.

Johnson CA, Keltner JL, & Balestrery F (1978). Effects of target size and eccentricity on visual detection and resolution. Vision Research, 18, 1217-1222.

Johnson MA, & Choy D (1987). On the definition of age-related norms for visual function testing. Applied Optics, 26, 1449-1454.

Johnston A (1987). Spatial scaling of central and peripheral contrast sensitivity functions. Journal of the Optical Society of America A, 4, 1583-1593.

Johnston A (1989). The geometry of the topographic map in striate cortex. Vision Research, 29, 1493-1500.

Johnston A, & Wright MJ (1983). Visual motion and cortical velocity. Nature, 304, 436-438.

Johnston A, & Wright MJ (1985). Lower thresholds of motion for gratings as a function of eccentricity and contrast. Vision Research, 25, 179-185.

Johnston A, & Wright MJ (1986). Matching velocity in central and peripheral vision. Vision Research, 26, 1099-1109.

Jones WL, & Reidy RW (1985). Peripheral ocular fundus. Butterworths: London.

Kaplan E, & Shapley RM (1982). X and Y cells in the lateral geniculate nucleus of macaque monkeys. Journal of Physiology, 330, 125-143.

Katz J, & Sommer A (1986). Asymmetry and variation in the normal hill of vision. Archives of Ophthalmology, 104, 65-68.

Keele SW (1986). Motor control. In: Handbook of Perception and Human Performance, Vol 2, Cognitive processes and performance. Eds: KR Boff, L Kaufmann, & JP Thomas. Chap 30, pp 30-3 to 30-4. Wiley: New York.

Kelly DH (1984). Retinal inhomogeneity. I. Spatiotemporal contrast detection. Journal of the Optical Society of America A, 1, 107-113.

Kerr JL (1971). Visual resolution in the periphery. Perception and Psychophysics, 9, 375-378.

Klein SA, & Levi DM (1985). Hyperacuity thresholds of 1 sec: theoretical predictions and empirical validation. Journal of the Optical Society of America A, 2, 1170-1190.

Klein SA, & Levi DM (1987). Position sense of the peripheral retina. Journal of the Optical Society of America A, 4, 1543-1553.

Koenderink JJ (1977). Current models of contrast processing. In: Spatial contrast, report of a workshop. Eds: Spekreijse H., & Tweel LH. North Holland: Amsterdam.

Koenderink JJ, Bouman MA, Bueno de Mesquita AE, & Slappendel S (1978). Perimetry of contrast detection thresholds of moving spatial sine wave patterns. III. The target extent as a sensitivity controlling parameter. Journal of the Optical Society of America, 68, 854-860.

Kooi FL, Toet A, Tripathy SM, & Levi DM (1994). The effect of similarity and attention on contour interaction in peripheral vision. Spatial Vision, 8, 255-279.

Kuffler S (1953). Discharge patterns and functional organisation of mammalian retina. Journal of Neurophysiology, 16, 37-68.

Laming D (1991). On the limits of visual detection. In: Vision and visual dysfunction, Vol 5, Limits of vision. Eds: JJ Kulikowski, V Walsh and IJ Murray. Chapter 2, pp 6-14. Macmillan: Basingstoke.

Legge GE, & Gu Y (1989). Stereopsis and contrast. Vision Research, 29, 989-1004.

Legge GE, Pelli DG, Rubin GS, & Schleske MM (1985a). Psychophysics of reading-I. Normal vision. Vision Research, 25, 239-252.

Legge GE, Ross JA, Isenberg LM, & LaMay JM (1992). Psychophysics of reading: clinical predictors of low-vision reading speed. Investigative Ophthalmology and Visual Science, 33, 677-687.

Legge GE, Rubin GS, Pelli DG, & Schleske MM (1985b). Psychophysics of reading-II. Low vision. Vision Research, 25, 253-266.

Levi DM (1991). Sensory processing in strabismic and anisometropic amblyopia. In: Amblyopia: basic and clinical aspects. Eds: KJ Ciuffreda, DM Levi & A Selenow. Chap 3, pp 69-144. Butterworth-Heinemann: Boston.

Levi DM, & Klein SA (1985). Vernier acuity, crowding and amblyopia. Vision Research, 25, 979-991.

Levi DM, & Klein SA (1989). Both separation and eccentricity can limit precise position judgements: a reply to Morgan and Watt. Vision Research, 29, 1463-1469.

Levi DM, & Klein SA (1990a). The role of separation and eccentricity in encoding position. Vision Research, 30, 557-585.

Levi DM, & Klein SA (1990b). Equivalent intrinsic blur in spatial vision. Vision Research, 30, 1971-1993.

Levi DM, & Klein SA (1992). "Weber's law" for position: the role of spatial frequency and contrast. Vision Research, 32, 2235-2250.

Levi DM, Klein SA, & Aitsebaomo P (1984). Detection and discrimination of the direction of motion in central and peripheral vision of normal and amblyopic observers. Vision Research, 24, 789-800.

Levi DM, Klein SA, & Aitsebaomo AP (1985). Vernier acuity, crowding and cortical magnification. Vision Research, 25, 963-967.

Levi DM, Klein SA, & Yap YL (1988). "Weber's Law" for position: unconfounding the role of separation and eccentricity. Vision Research, 28, 597-603.

Levi DM, & Westheimer G (1987). Spatial-interval discrimination in the human fovea: what delimits the interval? Journal of the Optical Society of America A, 4, 1304-1313.

Levitt H (1970). Transformed up-down methods in psychoacoustics. Journal of the Acoustical Society of America, 49, 467-477.

Lie I (1980). Visual detection and resolution as a function of retinal locus. Vision Research, 20, 967-974.

Liebowitz HW, Johnson CA, & Isabelle E (1972). Peripheral motion detection and refractive error. Science, 177, 1207-1208.

Livingstone MS, & Hubel DH (1985). Spatial relationship and extrafoveal vision. Nature, 315, 285.

Livingstone M, & Hubel H (1988a). Do the relative mapping densities of the magno- and parvocellular systems vary with eccentricity? Journal of Neuroscience, 8, 4334-4339.

Livingstone M, & Hubel H (1988b). Segregation of form, color, movement and depth: anatomy, physiology and perception. Science, 240, 740-749.

Loomis JM (1978). Lateral masking in foveal and eccentric vision. Vision Research, 18, 335-338.

Low FN (1951). Peripheral visual acuity. Archives of Ophthalmology, 45, 80-99.

McKee SP (1991). The physical constraints on visual hyperacuity. In: Vision and Visual Dysfunction, Vol 5, Limits of Vision. Eds: JJ Kulikowski, V Walsh, & I Murray. Chap 17, pp 221-233. Macmillan: Basingstoke.

McKee SP, & Nakayama K (1984). The detection of motion in the peripheral visual field. Vision Research, 24, 25-32.

McKee SP, Welch L, Taylor DG, & Bowne SF (1990). Finding the common bond: stereoacuity and the other hyperacuities. Vision Research, 30, 879-891.

McKee SP, & Westheimer G (1978). Improvement in vernier acuity with practice. Perception and Psychophysics, 24, 258-262.

Maguire C (1971). Ametropia in the visual field. Transactions of the Ophthalmological Societies of the United Kingdom, 91, 663-678.

Mäkelä P, Whitaker D, & Rovamo J (1993). Modelling of orientation discrimination across the visual field. Vision Research, 33, 723-730.

Malpeli JG, & Baker FH (1975). The representation of the visual field in the lateral geniculate nucleus of *Macaca mulatta*. Journal of Comparative Neurology, 161, 569-594.

Mandelbaum J, & Sloan LL (1947). Peripheral visual acuity, with special reference to scotopic illumination. American Journal of Ophthalmology, 30, 581-588.

Meredith JT, & Celesia GG (1982). Pattern-reversal visual evoked potentials and retinal eccentricity. Electroencephalography and Clinical Neurophysiology, 53, 243-253.

Millodot M, Johnson CA, Lamont A, & Liebowitz HW (1975). Effect of dioptrics on peripheral visual acuity. Vision Research, 15, 1357-1362.

Millodot M, & Lamont A (1974). Peripheral visual acuity in the vertical plane. Vision Research, 14, 1497-1498.

de Monasterio FM (1978). Properties of concentrically organised X and Y ganglion cells of macaque retina. Journal of Neurophysiology, 41, 1394-1417.

Moreland JD (1972). Peripheral colour vision. In: Handbook of sensory physiology, Vol VII/4, Visual psychophysics. Eds: D Jameson, & LM Hurvich. Chapter 20, pp 517-536. Springer-Verlag: Berlin.

Moreland JD, & Cruz A (1959). Colour perception in the peripheral retina. Optica Acta, 6, 117-151.

Morgan MJ, & Regan D (1987). Opponent model for line interval discrimination: interval and vernier performance compared. Vision Research, 27, 107-118.

Morgan MJ, & Watt RJ (1989). The Weber relation for position is not an artefact of eccentricity. Vision Research, 29, 1457-1462.

Moriarty SE, & Scheiner EC (1984). A study of close-set text type. Journal of Applied Psychology, 69, 700-702.

Morrison JD, & McGrath C (1985). Assessment of the optical contributions to the age-related deterioration in vision. Quarterly Journal of Experimental Physiology, 70, 249-269.

Nazir TA (1992). Effects of lateral masking and spatial precueing on gap-resolution in central and peripheral vision. Vision Research, 32, 771-777.

Neale MD (1989). Neale analysis of reading ability, Revised British edition. NFER-Nelson: Windsor.

Noorlander C, Koenderink JJ, den Ouden RJ, & Edens BW (1983). Sensitivity to spatiotemporal colour contrast in the peripheral visual field. Vision Research, 23, 1-11.

Nothdurft HC (1985). Orientation sensitivity and texture segmentation in patterns with different line orientation. Vision Research, 25, 551-560.

Nyquist H (1919). Certain topics in telegraph transmission theory. Transactions of the AIEE, 47, 617-644.

Obstfeld H (1981). Spatial summation in static perimetry. The Ophthalmic Optician, (20 March), 214-229.

Ogilvie J, & Daicar E (1967). The perception of curvature. Canadian Journal of Psychology, 21, 521-525.

Ogle KN (1961a). Foveal contrast thresholds with blurring of the retinal image and increasing size of test stimulus. Journal of the Optical Society of America, 51, 862-869.

Ogle KN (1961b). Peripheral contrast thresholds and blurring of the retinal image for a point light source. Journal of the Optical Society of America, 51, 1265-1268.

Ordy JM, Brizzee KR, & Johnson HA (1982). Cellular alterations in visual pathways and the limbic system: implications for vision and short-term memory. In: Aging and Human Visual Function. Eds: Sekuler R, Kline D, & Dismukes K. pp 79-114. Liss: New York.

Østerberg G (1935). Topography of the layer of rods and cones in the human retina. Acta Ophthalmologica supplement, 65, 1-102.

Owsley C, & Burton KB (1991). Aging and spatial contrast sensitivity: underlying mechanisms and implications for everyday life. In: The changing visual system. Eds: P Bagnoli, & W Hodos. pp 119-136. Plenum Press: New York.

Owsley C, & Sekuler R (1982). Spatial summation, contrast threshold, and aging. Investigative Ophthalmology and Visual Science, 22, 130-133.

Owsley C, Sekuler R, & Siemsen D (1983). Contrast sensitivity throughout adulthood. Vision Research, 23, 689-699.

Paradiso MA, & Carney T (1988). Orientation discrimination as a function of stimulus eccentricity and size: nasal/temporal retinal asymmetry. Vision Research, 28, 867-874.

Pentland A (1980). Maximum likelihood estimation: the best PEST. Perception and Psychophysics, 28, 377-379.

Perry VH, & Cowey A (1981). The morphological correlates of X- and Y-like retinal ganglion cells in the retina of monkeys. Experimental Brain Research, 43, 226-228.

Perry VH, & Cowey A (1985). The ganglion cell and cone distributions in monkey's retina: implications for cortical magnification factors. Vision Research, 25, 1795-1810.

Perry VH, & Cowey A (1988). The lengths of the fibres of Henle in the retina of macaque monkeys: implications for vision. Neuroscience, 25, 225-236.

Perry VH, Oehler R, & Cowey A (1984). Retinal ganglion cells that project to the dorsal lateral geniculate nucleus in the macaque monkey. Neuroscience, 12, 1101-1123.

Perry VH, & Silveira LCL (1988). Functional lamination in the ganglion cell layer of the macaque's retina. Neuroscience, 25, 217-223.

Petersen SE, Fox PT, Snyder AZ, & Raichle ME (1990). Activation of extrastriate and frontal cortical areas by visual words and word-like stimuli. Science, 249, 1041-1044.

Pointer JS (1986). The cortical magnification factor and photopic vision. Biological Review, 61, 97-119.

Polyak S (1932). Localisation of function in the cerebral cortex, Vol 13, Association for Research into Nervous and Mental Disorders. Williams and Wilkins Company: Baltimore.

Polyak S (1941). The retina. University of Chicago press: Chicago.

Polyak S (1957). The vertebrate visual system. University of Chicago press: Chicago.

Posner MI, & Carr TH (1992). Lexical access and the brain: anatomical constraints on cognitive models of word recognition. American Journal of Psychology, 105, 1-26.

Posner MI, Petersen SE, Fox PT, & Raichle ME (1988). Localization of cognitive operations in the human brain. Science, 240, 1627-1631.

Potter MC (1984). Rapid Serial Visual Presentation (RSVP): a method for studying language processing. In: New methods of reading comprehension research. Eds: Kieras DE, & Just MA. Chap 5, pp.91-118. Lawrence Erlbaum Associates: New Jersey.

Rains JD (1963). Signal luminance and position effects in human reaction time. Vision Research, 3, 239-251.

Randall HG, Brown DJ, & Sloan LL (1966). Peripheral visual acuity. Archives of Ophthalmology, 75, 500-504.

Raninen A, & Rovamo J (1986). Perimetry of critical flicker frequency in human rod and cone vision. Vision Research, 26, 1249-1255.

Ransom-Hogg A, & Spillman L (1980). Perceptive field size in fovea and periphery of the light- and dark-adapted retina. Vision Research, 20, 221-228.

Regan D (1985). Masking of spatial-frequency discrimination. Journal of the Optical Society of America A, 2, 1153-1159.

Regan D, & Beverley KI (1985). Postadaptation orientation discrimination. Journal of the Optical Society of America A, 2, 147-155.

Rentschler I, & Treutwein B (1985). Loss of spatial phase relationships in extrafoveal vision. Nature, 313, 308-310.

Richards W (1971). The fortification illusions of migraines. Scientific American, 224, 89-96.

Rijsdijk JP, Kroon JN, & van der Wildt GJ (1980). Contrast sensitivity as a function of position on the retina. Vision Research, 20, 235-241.

Rodieck RW, Binmoeller KF, & Dineen J (1985). Parasol and midget ganglion cells of the human retina. Journal of Comparative Neurology, 223, 115-132.

Rolls ET, & Cowey A (1970). Topography of the retina and striate cortex and its relationship to visual acuity in rhesus monkeys and squirrel monkeys. Experimental Brain Research, 10, 298-310.

Rovamo J, Leinonen L, Laurinen P, & Virsu V (1984). Temporal integration and contrast sensitivity in foveal and peripheral vision. Perception, 13, 665-674.

Rovamo J, Mäkelä P, & Whitaker D (1993). Models of the visual cortex on the basis of psychophysical observations. In: Functional organisation of the human visual cortex. Eds: Gulyas B, Ottoson D, & Roland PE. Macmillan: Basingstoke.

Rovamo J, & Raninen A (1984). Critical flicker frequency and M-scaling of stimulus size and retinal illuminance. Vision Research, 24, 1127-1131.

Rovamo J, Raninen A, & Virsu V (1985). The role of retinal ganglion cell density and receptive-field size in photopic perimetry. In: Proceedings of 6th International Visual Field Symposium. Eds: Heijl A, & Greve EL. pp 589-594. Dr W Junk: Dortrecht.

Rovamo J, & Virsu V (1979). An estimation and application of the human cortical magnification factor. Experimental Brain Research, 37, 495-510.

Rovamo J, Virsu V, Laurinen P, & Hyvärinen L (1982). Resolution of gratings oriented along and across meridians in peripheral vision. Investigative Ophthalmology and Visual Science, 23, 666-670.

Rovamo J, Virsu V, & Näsänen R (1978). Cortical magnification factor predicts the photopic contrast sensitivity of peripheral vision. Nature, 271, 54-56.

Rowe MH (1991). Functional organisation of the retina. In: Vision and Visual Dysfunction, Vol 3, Neuroanatomy of the visual pathways and their development. Eds: Dreher B, & Robinson SR. Chapter 1, pp 1-68. Macmillan: Basingstoke.

Rubin GS (1993). Peripheral reading and spatial scaling. Investigative Ophthalmology and Visual Science, 34, 820.

Rubin GS, & Legge GE (1989). Psychophysics of reading-VI. The role of contrast in low vision. Vision Research, 29, 79-91.

Rubin GS, & Turano K (1992). Reading without saccadic eye movements. Vision Research, 32, 895-902.

Rubin GS, & Turano K (1994). Low vision reading with sequential word presentation. Vision Research, 34, 1723-1733.

Saarinen J (1988). Detection of mirror symmetry in random dot patterns at different eccentricities. Vision Research, 28, 755-759.

Saarinen J, Rovamo J, & Virsu V (1987). Texture discrimination at different eccentricities. Journal of the Optical Society of America A, 4, 1699-1703.

Saarinen J, Rovamo J, & Virsu V (1989). Analysis of spatial structure in eccentric vision. Investigative Ophthalmology and Visual Science, 30, 293-296.

Schein SJ (1988). Anatomy of macaque fovea and spatial densities of neurons in foveal representation. Journal of Comparative Neurology, 269, 479-505.

Schein SJ, & de Monasterio FM (1987). Mapping of retinal and geniculate neurons onto striate cortex of macaque. Journal of Neuroscience, 7, 996-1009.

Schlaer S (1937). The relation between visual acuity and illumination. Journal of General Physiology, 21, 165-188.

Schoultes AMW, & Bouman MA (1977). Psychophysical experiments on spatial summation at threshold level of the human retina. Vision Research, 17, 867-873.

Scobey RP (1982). Human visual orientation discrimination. Journal of Neurophysiology, 48, 18-26.

Scobey RP, & van Kan PLE (1991). A horizontal stripe of displacement sensitivity in the human visual field. Vision Research, 31, 99-109.

Shapley R, & Perry VH (1986). Cat and monkey retinal ganglion cells and their visual functional roles. Trends in Neuroscience, 9, 229-235.

Silveira LCL, & Perry VH (1991). The topography of magnocellular projecting ganglion cells (M-ganglion cells) in the primate retina. Neuroscience, 40, 217-237.

Silveira LCL, Picanço-Diniz CW, Sampaio LFS, & Oswaldo-Cruz E (1989). Retinal ganglion cell distribution in the Cebus monkey: a comparison with the cortical magnification factors. Vision Research, 11, 1471-1483.

Sloan LL (1961). Area and luminance of test object as variables in examination of the visual field by projection perimetry. Vision Research, 1, 121-138.

Sloan LL (1968). The photopic acuity-luminance function with special reference to parafoveal vision. Vision Research, 8, 901-911.

Sloane ME, Owsley C, & Jackson CA (1988). Aging and luminance-adaptation effects on spatial contrast sensitivity. Journal of the Optical Society of America A, 5, 2181-2190.

Smith RA, & Cass PF (1987). Aliasing in the parafovea with incoherent light. Journal of the Optical Society of America A, 4, 1530-1534.

Spear PD (1993). Neural bases of visual deficits during aging. Vision Research, 33, 2589-2609.

Stephenson C, & Braddick O (1983). Discrimination of relative spatial phase in fovea and periphery. Investigative Ophthalmology and Visual Science, 24, 146.

Stephenson CME, Knapp AJ, & Braddick OJ (1991). Discrimination of spatial phase shows a qualitative difference between foveal and peripheral processing. Vision Research, 31, 1315-1326.

Stone J, & Johnston E (1981). The topography of primate retina: a study of the human, bushbaby, and New- and Old-World monkeys. Journal of Comparative Neurology, 196, 205-223.

Strasburger H, Harvey LO, & Rentschler I (1991). Contrast thresholds for identification of numeric characters in direct and eccentric view. Perception and Psychophysics, 49, 495-508.

Sullivan JD, Oatley K, & Sutherland NS (1972). Vernier acuity as affected by target length and separation. Perception and Psychophysics, 12, 438-444.

Swanson WH, & Wilson HR (1985). Eccentricity dependence of contrast matching and oblique masking. Vision Research, 25, 1285-1295.

Talbot SA, & Marshall WH (1941). Physiological studies on neural mechanisms of visual localisation and discrimination. American Journal of Ophthalmology, 24, 1255-1264.

Tate GW (1985). The physiological basis for perimetry. In: Automatic perimetry in glaucoma: a practical guide. Eds: Drance SM, & Anderson D. Chap 1, pp 1-28. Grune and Stratton: Orlando.

Tate GW, & Lynn JR (1977). Principles of quantitative perimetry: testing and interpreting the visual field. Grune and Stratton: New York.

Taylor MM, & Creelman CD (1967). PEST: Efficient estimates on probability functions. Journal of the Acoustical Society of America, 41, 782-787.

Taylor MM, Forbes SM, & Creelman CD (1983). PEST reduces bias in forced choice psychophysics. Journal of the Acoustical Society of America, 74, 1367-1374.

Teichner WH (1954). Recent studies of simple reaction time. Psychological Bulletin, 51, 128-149.

Thibos LN, Cheney FE and Walsh DJ (1987). Retinal limits to the detection and resolution of gratings. Journal of the Optical Society of America A, 4, 1524-1529.

Toet A, van Eekhout MP, Simons HL, & Koenderink JJ (1987). Scale invariant features of differential spatial displacement discrimination. Vision Research, 27, 441-451.

Toet A, & Koenderink JJ (1988). Differential spatial discrimination thresholds for Gabor patches. Vision Research, 28, 133-143.

Toet A, & Koenderink JJ (1989). Differential spatial displacement discrimination with interfering stimuli. Biological Cybernetics, 60, 231-237.

Toet A, & Levi DM (1992). The two-dimensional shape of spatial interaction zones in the parafovea. Vision Research, 32, 1349-1357.

Toet A, Snippe HP, & Koenderink JJ (1988a). Local spatial scale for three-dot alignment acuity. Biological Cybernetics, 59, 319-323.

Toet A, Snippe HP, & Koenderink JJ (1988b). Effects of blur and eccentricity on differential spatial displacement discrimination. Vision Research, 28, 535-553.

Tolhurst DJ, & Ling L (1988). Magnification factors and the organisation of the human striate cortex. Human Neurobiology, 6, 247-254.

Tootell RBH, Silverman MS, Switkes E, & De Valois RL (1982). Deoxyglucose analysis of retinotopic organisation in primate striate cortex. Science, 218, 902-904.

Tootell RBH, Switkes E, Silverman MS, & Hamilton SL (1988). Functional anatomy of macaque striate cortex. II. Retinotopic organisation. Journal of Neuroscience, 8, 1531-1568.

Traquair HM (1927). An introduction to clinical perimetry. Kimpton: London.

Turano K, & Rubin G (1988). Reading performance with peripheral viewing using rapid serial visual presentation. In: Digest of Topical Meeting on Noninvasive Assessment of the Visual System. Incline Village, NV. pp 192-195. Optical Society of America: Washington DC.

Tyler CW (1973). Periodic vernier acuity. Journal of Physiology, 228, 637-647.

Tyler CW (1989). Two processes control variations in flicker sensitivity over the life span. Journal of the Optical Society of America A, 6, 481-490.

Tynan PD, & Sekuler R (1982). Motion processing in peripheral vision: reaction time and perceived velocity. Vision Research, 22, 61-68.

Valeton JM, & Watson AB (1990). Contrast detection does not have a local spatial scale. Investigative Ophthalmology and Visual Science, 31, 428.

Van Essen DC, Newsome WT, & Maunsell JHR (1984). The visual field representation in striate cortex of the macaque monkey: asymmetries, anisotropies and individual variation. Vision Research, 24, 429-448.

Virsu V, Näsänen R, & Osmoviita K (1987). Cortical magnification and peripheral vision. Journal of the Optical Society of America A, 4, 1568-1578.

Virsu V, & Rovamo J (1979). Visual resolution, contrast sensitivity and the cortical magnification factor. Experimental Brain Research, 37, 475-494.

Virsu V, Rovamo J, Laurinen P, & Näsänen R (1982). Temporal contrast sensitivity and cortical magnification. Vision Research, 22, 1211-1217.

Walls GL (1942). The vertebrate eye. Hafner Publishing: New York.

Wässle H, Grünert U, Röhrenbeck J, & Boycott BB (1989). Cortical magnification factor and the ganglion cell density of the primate retina. Nature, 341, 643-646.

Wässle H, Grünert U, Röhrenbeck J, & Boycott BB (1990). Retinal ganglion cell density and cortical magnification factor in the primate. Vision Research, 30, 1897-1911.

Watson AB (1987). Estimation of local spatial scale. Journal of the Optical Society of America A, 4, 1579-1582.

Watt RJ (1984). Further evidence concerning the analysis of curvature in human foveal vision. Vision Research, 24, 251-253.

Watt RJ (1987). Scanning from coarse to fine spatial scales in the human visual system after the onset of a stimulus. Journal of the Optical Society of America A, 4, 2007-2021.

Watt RJ, & Andrews DP (1982). Contour curvature analysis: hyperacuities in the discrimination of the detailed shape. Vision Research, 22, 449-460.

Watt RJ, & Campbell FW (1985). Vernier acuity: Interactions between length effects and gaps when orientation cues are eliminated. Spatial Vision, 1, 31-38.

Watt RJ, & Morgan MJ (1983). The recognition and representation of edge blur: evidence for spatial primitives in human vision. Vision Research, 23, 1465-1477.

Watt RJ, Morgan MJ, & Ward RM (1983). The use of different cues in vernier acuity. Vision Research, 23, 991-995.

Waugh SJ, & Levi DM (1993a). Visibility, timing and vernier acuity. Vision Research, 33, 505-526.

Waugh SJ, & Levi DM (1993b). Visibility and vernier acuity for separated targets. Vision Research, 33, 539-552.

Weale RA (1975). Senile changes in visual acuity. Transactions of the Ophthalmological Societies of the United Kingdom, 95, 36-38.

Weber EHL (1834). De pulsu, resoptione, auditu et tactu. Annotationes anatomicae et physiologicae. Koehler: Leipzig (Translation by Ross HE, & Murray DJ (1978). The sense of touch. Academic Press: London.).

Wehrkahn C, & Westheimer G (1990). How vernier acuity depends on contrast. Experimental Brain Research, 80, 618-620.

Wertheim T (1891; translated by Dunsky IL, 1980). Peripheral visual acuity. American Journal of Ophthalmology and Physiological Optics, 57, 915-924.

Westheimer G (1965). Spatial interaction in the human retina during scotopic vision. Journal of Physiology, 181, 881-894.

Westheimer G (1975). Visual acuity and hyperacuity. Investigative Ophthalmology and Visual Science, 14, 570-571.

Westheimer G (1979a). Scaling of visual acuity measurements. Archives of Ophthalmology, 97, 327-330.

Westheimer G (1979b). The spatial sense of the eye, Proctor lecture. Investigative Ophthalmology and Visual Science, 18, 893-912.

Westheimer G (1981). Visual hyperacuity. In: Progress in sensory physiology, Vol 1, pp 1-30. Springer-Verlag: Berlin.

Westheimer G (1982). The spatial grain of the perifoveal visual field. Vision Research, 22, 157-162.

Westheimer G (1983). Temporal order detection for foveal and peripheral visual stimuli. Vision Research, 23, 759-763.

Westheimer G (1992). Visual acuity. In: Adler's Physiology of the eye, 9th edition. Ed: Hart WM Jr. Chap 17, pp 531-547. Mosby: St Louis.

Westheimer G, & Hauske G (1975). Temporal and spatial interference with vernier acuity. Vision Research, 15, 1137-1141.

Westheimer G, & McKee SP (1977a). Integration regions for visual hyperacuity. Vision Research, 17, 89-93.

Westheimer G, & McKee SP (1977b). Spatial configurations for hyperacuity. Vision Research, 17, 941-947.

Westheimer G, & Troung TT (1988). Target crowding in foveal and peripheral stereoacuity. American Journal of Optometry and Physiological Optics, 65, 395-399.

Wetherill GB, & Levitt H (1965). Sequential estimation of points on a psychometric function. British Journal of Mathematical and Statistical Psychology, 18, 1-10.

Weymouth FWW (1958). Visual sensory units and the minimal angle of resolution. American Journal of Ophthalmology, 46, 102-112.

Whitaker D, Mäkelä P, Rovamo J, & Latham K (1992a). The influence of eccentricity on position and movement acuities as revealed by spatial scaling. Vision Research, 32, 1913-1930.

Whitaker D, Rovamo J, MacVeigh D, & Mäkelä P (1992b). Spatial scaling of vernier acuity tasks. Vision Research, 32, 1481-1492.

Whittaker SG, & Cummings RW (1990). Foveating saccades. Vision Research, 30, 1363-1366.

Whittaker SG, & Lovie-Kitchen J (1993). Visual requirements for reading. Optometry and Vision Science, 70, 54-65.

Whittaker S, Rohrkaste F, & Higgins K (1989). Optimum letter spacing for word recognition in central and eccentric fields. In: Non Invasive Assessment of the Visual System. Sante Fe, NM. pp 56-59. Optical Society of America: Washington DC.

Wild JM, & Hussey MK (1985). Some statistical concepts in the analysis of vision and visual acuity. Ophthalmic and Physiological Optics, 5, 63-71.

Wild JM, Wood JM, & Barnes DA (1986). The cortical representation of gradient-adapted multiple-stimulus perimetry. Ophthalmic and Physiological Optics, 6, 401-405.

Wild JM, Wood JM, & Crews SJ (1988). Peripheral refractive correction and automated perimetric profiles. Acta Ophthalmologica, 66, 249-254.

Wild JM, Wood JM, & Flanagan JG (1987). Spatial summation and the cortical magnification of perimetric profiles. Ophthalmologica, 195, 88-96.

Williams DR (1985). Aliasing in human foveal vision. Vision Research 25, 195-205.

Williams RA, Enoch JM, & Essock EA (1984). The resistance of selected hyperacuity configurations to retinal image degradation. Investigative Ophthalmology and Visual Science, 25, 389-399.

Williams TD (1983). Aging and central visual field area. American Journal of Optometry and Physiological Optics, 60, 888-891.

Wilson HR (1985). Discrimination of contour curvature: data and theory. Journal of the Optical Society of America A, 2, 1191-1199.

Wilson HR (1986). Responses of spatial mechanisms can explain hyperacuity. Vision Research, 26, 453-469.

Wilson HR (1991a). Model of peripheral and amblyopic hyperacuity. Vision Research, 31, 967-982.

Wilson HR (1991b). Pattern discrimination, visual filters, and spatial sampling irregularity. In: Computational models of visual processing. Eds: Landy MS, & Movshon JA. pp 153-168. MIT press: Cambridge, Mass.

Wilson HR, & Richards WA (1989). Mechanisms of contour curvature discrimination. Journal of the Optical Society of America A, 6, 106-115.

Wilson ME (1970). Invariant features of spatial summation with changing locus in the visual field. Journal of Physiology, 207, 611-622.

Wolf E, & Nadroski AS (1971). Extent of the visual field - changes with age and oxygen tension. Archives of Ophthalmology, 86, 637-642.

Wolford G, & Chambers L (1983). Lateral masking as a function of spacing. Perception and Psychophysics, 33, 129-138.

Wood JM, Wild JM, & Crews SJ (1987). Induced intraocular light scatter and the sensitivity gradient of the normal visual field. Graefe's Archive of Clinical and Experimental Ophthalmology, 225, 369-373.

Wood JM, Wild JM, Drasdo N, & Crews S (1986). Perimetric profiles and cortical representation. Ophthalmic Research, 18, 301-308.

Wood JM, Wild JM, Smerdon DL, & Crews SJ (1989). Alterations in the shape of the automated perimetric profile arising from cataract. Graefe's Archive of Clinical and Experimental Ophthalmology, 227, 157-161.

Wooten BR, & Wald G (1973). Color-vision mechanisms in the peripheral retinas of normal and dichromatic observers. Journal of General Physiology, 61, 125-145.

Wright CE, & Drasdo N (1985). The influence of age on the spatial and temporal contrast sensitivity function. Documenta Ophthalmologica, 59, 385-395.

Wright MJ (1987). Spatiotemporal properties of grating motion detection in the center and periphery of the visual field. Journal of the Optical Society of America A, 4, 1627-1633.

Wright MJ, & Johnston A (1983). Spatiotemporal contrast sensitivity and visual field locus. Vision Research, 23, 983-989.

Wright MJ, & Johnston A (1985a). The relationship of displacement thresholds for oscillating gratings to cortical magnification, spatiotemporal frequency and contrast. Vision Research, 25, 187-193.

Wright MJ, & Johnston A (1985b). Invariant tuning of motion aftereffect. Vision Research, 25, 1947-1955.

Yap YL, Levi DM, & Klein SA (1989). Peripheral positional acuity: retinal and cortical constraints on 2-dot separation discrimination under photopic and scotopic conditions. Vision Research, 29, 789-802.

Yellott JI (1982). Spectral analysis of spatial sampling by photoreceptors: topological disorder prevents aliasing. Vision Research, 22, 1205-1210.

Zeki S, & Shipp S (1988). The functional logic of cortical connections. Nature, 335, 311-317.

Zuidema P, Verschuure H, Bouman MA, & Koenderink JJ (1981). Spatial and temporal summation in the human dark adapted retina. Journal of the Optical Society of America, 71, 1472-1480.